UNIVERSITÀ
DEGLI STUDI
DI PADOVA

Sede Amministrativa:
Università degli Studi di Padova, Dipartimento di Geoscienze

CORSO DI DOTTORATO DI RICERCA IN: Scienze della Terra
CICLO: XXXII

The Natural Background Level problem: A Hydro-geochemical study on the natural occurrence of Arsenic located in the Veneto region (NE Italy)

Coordinatore: Prof. Claudia Agnini
Supervisore: Prof. Paolo Fabbri
Co-Supervisori: Dr. Fabio Tateo, Dr. Daniele Pedretti

Dottorando: Nico Dalla Libera

To my girlfriend Alessandra and my family…

Hunc igitur terrorem animi tenebrasque necessest
non radii solis neque lucida tela diei discutiant,
sed naturae species ratioque.
(Lucrezio, De Rerum Natura, vv. 146-148)

Index

Foreword

During the last decades, the groundwater quality preservation became a central topic for the environmental management and the stakeholders' activities. On 23 October 2000, the Directive 2000/60/EC of the European Parliament and of the Council establishing a framework for the Community action in the field of water policy, the EU Water Framework Directive, was finally adopted. It introduced several guidelines to reach the right management of the water resources, with wide space for the evaluation and the preservation procedures to be adopted. Among them, the Natural Background Level definition was outlined. Nonetheless, the estimation of the NBL for a specific contaminant raised doubts, especially in heterogeneous contexts where the naturally occurring contaminants are "patchy" distributed, like within the alluvial plain environments.

This is the case of the Venetian Alluvial Plain, where high geogenic concentrations of arsenic occur. In this context the Environmental Protection Agency for the Veneto Region (ARPAV as Italian acronym) developed some characterization studies in order to understand the contaminant behavior, which could give detailed indications for defining a more accurate Natural Background Level.

To this aim, a partnership between the Environmental Protection Agency and the Department of Geosciences of the University of Padova took place, kicking off the presented PhD project. The aim was to perform a detailed study that could shed light on the arsenic behavior within the Venetian Alluvial Plain, so that the NBL definition could be as reliable as possible.

List of abbreviations

A	Clay
ANN	Artificial neural network
ARPAV	Environmental Protection Agency (Italian acronym)
AWA	Agricultural west areas
BC	Boundary condition
BDP	Bengal Delta Plain
BME	Bayesian Maximum Entropy
COK	Cokriging
CPU	Central Processing Unit
CSC	Acronym for CTV in Italian legislation
CTV	Contamination threshold value
DBVL	Drainage Basin that Supplies Venice Lagoon
DMAA	Dimethylarsinic acid
DO	Dissolved oxygen
DRN	Drain boundary condition
EC	Electrical conductivity
ECDF	Experimental density function
EDA	Exploratory Data Analysis
Eh	Oxy-reduction potential respect to the hydrogen standard electrode
ETP	Experimental Transitional probability
G	Gravel
GHB	General Head boundary condition
GHP	Great Hungarian Plain

GWD	Groundwater directive
HDPE	High-density polyethylene
HFO	Iron hydroxide
Hnorm	Standardized conditional entropy index
HPC	High-Performance Computing
ICK	Indicator cokriging
ICP-OES	Inductively Coupled Plasma Optical Emission Spectroscopy
IK	Indicator kriging
K	Hydraulic conductivity
KRME	Kriged reduced mean error
L	Silt
LGM	Last Glacial Maximum
LMC	Linear Model of Co-regionalization
LNBL	Local Natural Background Level
LOQ	Limit of Quantification
LS	Silty sand
MAE	Mean absolute error
MCP	Markovian-type Categorical Prediction
ME	Mean error
MMAA	Monomethylarsonic acid
NBL	Natural Background Level
nRMSE	Normalized root mean square error
OM	Organic Matter
ON	Oxidation number
ORP	Oxy-reduction potential

PZP	Piezometer
QE	Quantization error
RCH	Recharge boundary condition
RMSE	Root mean square error
S	Sand
SAL	Salinity
SCMs	Surface complexation models
SD	Standard deviation
SOC	Sediment organic carbon
SOM	Self-Organizing maps
SS	Specific storage
SY	Specific yield
T	Temperature
TEAs	Terminal electron acceptors
TOC	Total Organic Carbon
TP	Transitional probability
TV	Threshold value
VAP	Venetian Alluvial Plain
WAA	Western Agricultural Areas
WHO	World Health Organization
XRF	X-ray Fluorescence
XRPD	X-ray Powder Diffraction

General abstract

Excess of arsenic in groundwater is a worldwide problem threatening the health of the millions of people directly exposed to Arsenic-rich water intake. The problem is particularly acute in naturally occurring unconsolidated aquifers where Arsenic-rich groundwater is an easily accessible resource of drinking water, such arsenic in India, Bangladesh and Vietnam. In Italy, arsenic is found in aquifers from north to south and it is associated to different geological settings (i.e. volcanic areas and alluvial plains). The shallow aquifer of Venetian Alluvial Plain (VAP) is notoriously affected by arsenic contamination, characterized by a patchy distribution with variable extensions and concentrations. With concentrations exceeding the WHO limit of 10 μg/L, this metal poses a risk for locals, arsenic the aquifer is exploited for agricultural purposes. Although empirical evidences exist about the relationship between arsenic occurrence and other factors, several aspects regarding the physical and geochemical processes controlling arsenic in the VAP aquifers remain unclear. In this line, the present study aims to elucidate both the geochemical processes fostering arsenic mobility and their correlation with the subsurface heterogeneity, in order to improve the knowledge about arsenic-controlling processes and use them arsenic aid for the environmental management. To this end, we focused in detail on an agricultural zone nearby the Venice lagoon, affected by arsenic contamination (called "Western Agricultural Areas", WAA). The available data, collected by several hydrogeological surveys, show a spatial and temporal variability of arsenic concentration, which can be associated to a variety of hydro-geochemical processes such arsenic redox variations, sorption or reductive dissolution of Arsenic-rich iron oxy-hydroxides. In order to point out the consistency and the importance of these processes, we structured the study in two main phases: 1) evaluation of geochemical processes by means of a PHREEQC batch-like reactive model and 2) creation of a 3D reactive transport model based on previous results. The former allows us for testing whether the supposed geochemical processes are able to fit the geochemical conditions of the study system, identifying the main actors for arsenic mobility. The latter couples the obtained reactive processes with a 3D flow model, in order to evaluate the spatial and temporal distribution of dissolved arsenic as function of the subsurface heterogeneity. The results highlighted a strong effect of oxy-reductive potential on arsenic mobility, and it seems to be strictly correlated to organic matter degradation. The uprising of reduced condition, then, affects other mechanism such arsenic reductive dissolution of iron hydroxides, ion exchange and sorption processes, causing arsenic mobilization. Moreover, this study shaded light on the existence of oxygen ingress arsenic function of local water recharge

events, which seems to be responsible of space/time redox variation. The 3D reactive transport model showed a strong dependence between the aforementioned processes and subsurface heterogeneity. The material distribution, indeed, plays an import role affecting the arising of the main chemical reactions.

1. Introduction

High concentrations of arsenic in groundwater threaten the health of millions of people worldwide. Awareness of the problems associated with arsenic in drinking water and the environment has grown significantly over the last two decades and today a specific and detailed literature exists, documenting its occurrence, behavior and impacts in many places across the globe (Bhattacharya et al., 2004; Mandal et al., 2002, National Research Council, 1999; 2001; Smedley & Kinniburgh, 2002; 2013; Welch et al., 2000). Nowadays, at least 140 million people in 50 countries (Figure 1) have been drinking water containing arsenic at levels above the WHO provisional guideline value of 10 µg/L (Ravenscroft et al., 2009) and, often, above the pre-1993 WHO limit of 50 µg/L. This overall situation results in a diffuse public-health issue.

Figure 1 - Worldwide arsenic occurrence (Smedley & Kinniburgh, 2013).

The exposure to arsenic pollution, either in groundwater or in soil matrix, provokes adverse effects on human health that is strongly dependent by both the dose and the exposure time. Specific dermatological effects, such as melanosis and hyperkeratosis, are typical expressions of chronical exposure to arsenic. Chronical exposure may trigger reproductive, neurological, cardiovascular (i.e.: Blackfoot disease), respiratory, hepatic, hematological, and diabetic diseases in humans (Gorby, 1994; National Research Council, 1999). Furthermore, intake of water and foods rich of inorganic arsenic is established to cause skin, bladder, liver and lung

cancers (Anawar et al., 2001; Chowdhury et al. 1999, National Research Council, 1999; 2001; Smith et al., 1992; 1998; WHO, 2011). Human exposure to arsenic occurs through a number of pathways, including air, food, water and soil. The relative impacts of these vary depending on local circumstances but of the potential pathways, drinking water poses one of the greatest threats to human health as borne out by the large number of documented case histories from around the world (Smedley & Kinniburgh, 2013).

In the developing countries, where arsenic-related health problems exist, the problems have generally arisen over the last few years as a result of the increasing drinkable water demand. The groundwater exploitations were developed as a positive alternative to traditional surface-water sources, which suffer from bacteriological contamination and can trigger severe water-borne diseases. Groundwater has been highly successful in reducing the incidence of such bacterial diseases but problems from geogenic contamination by inorganic constituents has, until now, often gone uncontrolled. Arsenic and fluoride, in this sense, are the two most severe of these inorganic contaminants. In this direction, during the last decades, lots of research projects have been developed in order to understand the main hydro-chemical processes controlling the arsenic mobility, thus the more suitable and effective remediation technologies.

The arsenic mobility in the environment is due to a complex combination of natural biogeochemical reactions and human interactions, which can mutually change from place to place over space and time. Most recognized problems are generated by mobilization and transport under natural conditions, but mobilization has also been caused and promoted by human activities such as mining, fossil-fuel combustion, industrial manufacturing and agricultural practices (i.e.: use of pesticides, herbicides, crop desiccants and arsenic-based additives in livestock feed). Excepting localized sources of anthropogenic contamination, the highest aqueous arsenic concentrations are usually found in groundwater because of the high "solid - solution" ratio in aquifers.

High arsenic groundwater concentrations, potentially harmful to humans or with already detectable health impacts, have been documented in several countries such as Argentina, Bangladesh, Burkina Faso, Cambodia, Chile, China, India, Hungary, Laos, Mexico, Nepal, Romania, Spain, Taiwan, Thailand and Vietnam, and occasional problems are found in many others (Fendorf et al., 2010, McArthur et al., 2001; Nickson et al., 1998, 2000, Smedley and Kinniburgh, 2013, Sorg et al., 2014; Welch et al., 2000). The natural occurrence of arsenic in these countries is often linked to the alluvial plain systems, but high arsenic concentrations can

be found in volcanic environments or mining districts (e.g., Argentina, Chile, Brazil, Ethiopia, Greece and Italy) (Nordstrom, 2003; Rango et al., 2013, Table 1).

Table 1 - Global groundwater arsenic contamination: Concentration ranges, Potential exposed population, and Environments affected by arsenic (Modified from Nordstrom, 2003).

GLOBAL ARSENIC CONTAMINATION IN GROUNDWATER

Country/Region	Potential exposed population	Concentration [µg/L]	Environmental conditions
Bangladesh	30M	< 1 to 2500	Natural: alluvial/deltaic sediments with high phosphate, organics
West Bengal, India	6M	<10 to 3200	Similar to Bangladesh
Vietnam	> 1M	1 to 3050	Natural: alluvial sediments
Thailand	15K	1 to 5000	Anthropogenic: mining and dredged alluvium
Taiwan	100K to 200K	10 to 1820	Natural: coastal zones, black shales
Inner Mongolia	100K to 600K	< 1 to 2400	Natural: alluvial and lake sediments, high alkalinity
Xinjiang, Shaxi	> 500	40 to 750	Natural: alluvial sediments
Argentina	2M	< 1 to 9900	Natural: loess and volcanic rocks, thermal springs, high alkalinity
Chile	400K	100 to 1000	Natural and anthropogenic: volcanic sediments, closed basin lakes, thermal springs, mining
Bolivia	50K	-	Natural: similar to Chile and part of Argentina
Brazil	-	0.4 to 350	Gold mining
Mexico	400K	8 to 620	Natural and anthropogenic: volcanic sediments, mining
Germany	-	< 10 to 150	Natural: mineralized sandstone
Hungary, Romania	400K	< 2 to 176	Natural: alluvial sediments, organics
Spain	> 50K	< 1 to 100	Natural: alluvial sediments
Greece	150K	-	Natural and snthropogenic: thermal springs and mining
United Kingdom	-	< 1 to 80	Mining (southwest England)
Ghana	< 100K	< 1 to 175	Anthropogenic and natural: gold mining
USA, Canada	-	< 1 to 100000	Natural and anthropogenic: mining, pesticides, As_2O_3 stockpiles, thermal springs, alluvial, closed basin lakes, various rocks

Legend: M = millions, K = thousands

1.1 Arsenic in groundwater and the environment

1.1.1 Arsenic in minerals

Arsenic (As) in nature is present as organic and inorganic constituent. The latter is the most frequent and it exists, mainly, as mineral specie (Table 2). Elemental arsenic, arsenides, sulphides, oxides, arsenates and arsenites are the well-known phases, and they are typically found in mineralized and volcanic areas. Nonetheless, arsenic occurs in alluvial areas because it is associated to those minerals resulting from weathering processes. In the mineralized areas, As is commonly found in close association with the transition metals as well as Cd, Pb, Ag, Au,

Sb, P, W and Mo. The most abundant and widespread arsenic ore mineral is arsenopyrite, FeAsS. Arsenopyrite, together with the other dominant As-sulphide minerals realgar and orpiment, are only formed under high temperature conditions in the earth's crust. Arsenic is also present in varying concentrations in other common rock-forming minerals such as silicates and carbonates. As the chemistry of arsenic is similar to Sulphur, the greatest concentrations of the element tend to occur in sulphide minerals (i.e.: Pyrite). Concentrations of arsenic in pyrite (FeS_2), chalcopyrite ($CuFeS_2$) and galena (PbS) can be very variable, but in some cases reach up to several weight percent. Pyrite is an important component of ore bodies but it could be formed even in low-temperature sedimentary environments under anaerobic conditions. Sedimentary pyrite plays a very important role in present-day geochemical cycles and is present in the sediments of many rivers, lakes and oceans, as well as in many aquifers. Usually, pyrite occurrence is linked to the organic matter (i.e.: peat layers and peaty fine sediments), as the organic matter is a main driver for reduced conditions in sedimentary basins. In this context, organic matter (OM) not only leads to reduced condition, but it could also act as a source of arsenic. Arsenic, indeed, could be adsorbed onto OM through chemical adsorption processes and released during its degradation (Molinari et al., 2015; Rotiroti et al., 2014). High arsenic concentrations are also found in many oxide minerals and hydrous metal oxides, either as part of the mineral structure or as adsorbed species. Concentrations in iron oxides can also reach weight percent values, particularly where they form as the oxidation products of primary iron sulphide minerals, which have an abundant supply of arsenic. Sorption of arsenate to hydrous iron oxides is particularly strong (Goldberg, 1986; Manning and Goldberg, 1996). Other important minerals for arsenic geochemistry are the clays minerals. Arsenic may also be adsorbed to the edges of clays, and gradually released when the clays are involved in cation exchange processes (Appelo and Postma, 2005). These sorption reactions are responsible for the relatively low (and non-toxic) concentrations of arsenic found in most natural waters. Arsenic can also substitute Si^{4+}, Al^{3+}, Fe^{3+} and Ti^{4+} in many mineral structures and is therefore present in many other rock-forming minerals, albeit at much lower concentrations. Thus, the most important arsenic-bearing minerals are the sulphide and oxide minerals. These have strong controls on arsenic mobilization and retardation in the environment. On the other hand, those minerals containing arsenic as a major element may cause local environmental problems, but are quantitatively less significant.

Table 2 – arsenic concentration in the main rock-forming minerals (Smedley and Kinniburgh, 2002).

Mineral	As concentration range (mg/kg)	Mineral	As concentration range (mg/kg)
Sulphide minerals		*Silicates minerals*	
Pyrite	100 - 10000	Quartz	0.4 - 1.3
Pyrite (gold ores)	300 - 54000	Feldspar	< 0.1 - 2.1
Pyrrhotite	5 - 100	Biotite	1.4
Marcasite	20 - 600	Amphibolite	1.1 - 2.3
Galena	5 - 10000	Olivine	0.08 - 0.17
Sphalerite	5 - 17000	Pyroxene	0.05 - 0.8
Chalcopyrite	10 - 5000	*Carbonate minerals*	
Oxide minerals		Calcite	1 - 8
Haematite	up to 160	Dolomite	< 3
Fe oxide	up to 2000	Siderite	< 3
Fe(III) oxyhydroxide	up to 76000	*Other minerals*	
Magnetite	2.7 - 41	Apatite	< 1 - 1000
Ilmenite	< 1	Halite	< 3
Sulphate minerals		Fluorite	< 2
Gypsum/anhydrate	< 1 - 6		
Barite	< 1 - 12		
Jarosite	34 - 1000		

1.1.2 Hydrochemistry of arsenic

Arsenic is perhaps unique among the heavy metalloids in its capacity to mobilize at the pH values of natural groundwater and over a wide range of redox conditions. Arsenic can occur in the environment in several oxidation states (-3 to +5) but in natural waters is mostly found as an oxyanion, as arsenite As(III) or arsenate As(V). As it is visible from Figure 2, at circumneutral pH condition, dissolve arsenic could occur as $HAsO_4^{2-}$, $H_2AsO_4^-$ and H_3AsO_3, for As(V) and As(III) respectively.

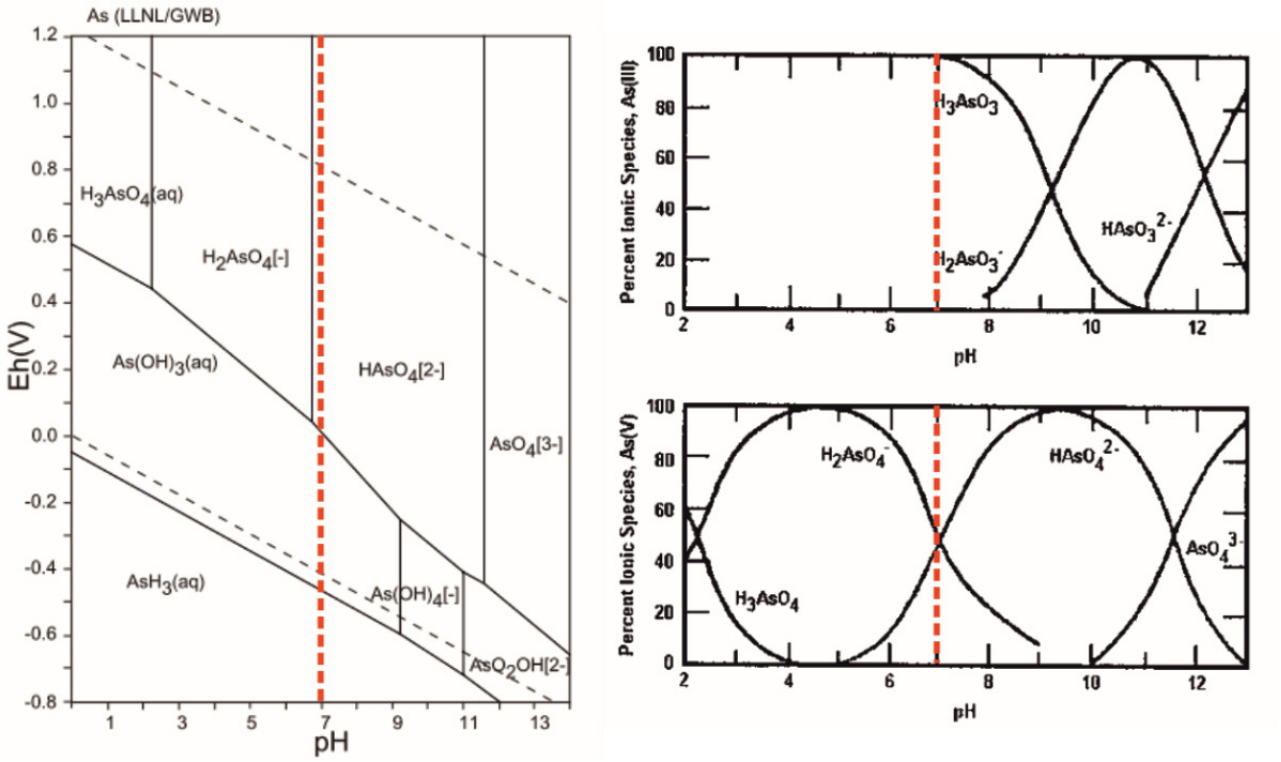

Figure 2 – Pourbaix diagram for As aqueous species (left side) and acid dissociation diagram for As(III) and As(V) (right side). The dashed red line emphasizes the neutral pH condition.

These factors, together with the high toxicity of As, render the element one of the most serious problems for potable groundwater quality. The arsenate form of arsenic is dominant in oxidizing conditions, whilst arsenite is more abundant in reducing conditions (Figure 2). The reduced form As(III) is more toxic and more mobile in soil than the oxidized As(V), thus it is the potentially detrimental species for human health. It is generally accepted that most of the arsenic in natural waters is present in inorganic form. Organic arsenicals (e.g. monomethylarsonic acid, MMAA, and dimethylarsinic acid, DMAA) are known to be produced by reactions involving bacteria and algae. These have been observed, albeit in small quantities, in some river waters and pore-water but are less significant in groundwater. However, the organic species are readily available for human metabolic processes (Bhattacharya et al., 2002).

As described in the section 1.1, mobility of As in water is limited principally by adsorption onto iron oxides and hydroxides, as well as possibly oxides of aluminium and manganese. Iron oxides in particular have long been recognized as effective arsenic scavengers and, indeed, precipitation of these is used as an effective water remediation technology (e.g. Wilkie and Hering, 1996). Adsorption is controlled strongly by both pH and As speciation (As(III) or As(V); Dzombak and Morel, 1990). Adsorption to iron oxides is less strong at high pH (>7) and As(V) is generally more strongly bound than As(III). The sorption capacity of the amorphous iron

oxides is greater than the more structured forms (goethite, hematite) due to the larger reactive surface area and, hence, increased availability of binding sites (Dzombak and Morel, 1990). Arsenic can also be mobilized under reducing conditions by the reductive dissolution of the iron oxides themselves. Binding efficiency may be affected by competition effects from other dissolved constituents. Presence of dissolved phosphate in particular has been shown to compete with arsenic (especially As(V)), for binding sites on iron oxides, hydroxides and clay minerals as well (e.g. Livesey and Huang, 1981; Manning and Goldberg, 1996).

1.2 Worldwide distribution of arsenic: Examples of arsenic-affected area similar to Venetian Alluvial Plain

In the previous part of this chapter, arsenic as global health issue has been introduced. Several literatures document the detrimental effects of a long-time exposure to groundwater arsenic contamination. A number of large aquifers worldwide have been identified with problems from arsenic occurring at concentrations above 50 μg/L, often significantly. The most noteworthy occurrences are in parts of West Bengal and Bangladesh, Taiwan, northern China, Argentina, Chile, Mexico, Hungary, and USA (Figure 1). The origin of arsenic in these regions are different, ranging from volcanic areas to alluvial environments. Nonetheless the interest is focused on alluvial environments as they are similar to Venetian Alluvial Plain. In this line, as follow, the main case studies located in this context are briefly presented, in order to get information about arsenic contamination in this geological/hydrogeological setting.

1.2.1 Bengal Delta Plain (Bangladesh and West Bengal, India)

The Bengal Delta Plain (BDP) area is perhaps the most known and studied area for arsenic contamination in groundwater. In terms of the population exposed, arsenic problems in groundwater from the alluvial and deltaic aquifers of BDP represent the most serious occurrences identified globally. Concentrations in groundwater from the affected areas have a very large range from < 0.5 μg/L to around 3200 μg/L (e.g. DPHE/BGS/MML, 1999; CGWB, 1999). Several health problems have been identified in affected populations. Skin disorders including pigmentation changes and keratosis are the most common manifestations, although skin cancer has also been identified. Several thousand patients have been identified with arsenic-related skin lesions. The affected aquifers are generally shallow (less than 100-150 m deep), of Holocene age and comprise mixed alluvial and deltaic sands, silts and clays associated with the Ganges, Hugli, Brahmaputra and Meghna river systems. According to the national data

set, based on the DPHE/UNICEF field kit results, the central and southeast regions in the delta plain are most affected (Figure 3). The most systematic laboratory study was conducted by DPHE/BGS (2000), and the most severely As-affected regions coincided with the area demarcated by the field kit survey. In addition, high As levels are also found in isolated ''hot spots'' at the southwestern, northwestern, north-eastern, and northcentral regions of the country. Interestingly, groundwater in the Hill Districts is mostly free from high-As concentrations for yet unknown reasons (DPHE/BGS, 2000). The high As concentration are typically associated to strongly reducing groundwater. Widespread mobilization of As from the BDP aquifers cannot be attributed to any anthropogenic activities in the region, and evidence indicates a predominantly geogenic source and mode for release of As into the groundwater (Bhattacharya et al., 1997; Naidu, 2000; Bhattacharya et al., 1996; 1998; 1999; Nickson et al., 1998). However, there exist many uncertainties in understanding the sources and mechanisms for As release in groundwater. BGS/MMI, 1998; Bhattacharya et al, 1999; Acharyya et al., 1999 identified several high-As geological domains in the Himalayas and adjoining highlands, which might be the source areas of As in the sedimentary aquifers. Two conflicting hypotheses have been widely suggested to explain the mechanisms of As mobilization in the sedimentary aquifers of the BDP. The first hypothesis suggests that As is released by the oxidation of pyrite (FeS_2) or arsenopyrite (FeAsS) following lowering of the water table during groundwater pumping (Saha and Chakraborty, 1995). The second hypothesis, that is widely accepted, suggests that As is released due to desorption from or reductive dissolution of Fe oxyhydroxides in a reducing aquifer environment (Bhattacharya et al., 2000; Smedley, 1996; von Bromssen, 1999; Nickson et al., 2000; Mukherjee and Bhattacharya, 2001). The second hypothesis is strongly linked to the wide occurrence of organic matter, which is well documented as reductant in aquifer systems (McArthur et al., 2004). On the other hand, deeper groundwater from the Holocene sediment sequence (> 100-150 m in depth, probably of Pleistocene age) have generally low arsenic concentrations (< 10 μg/L).

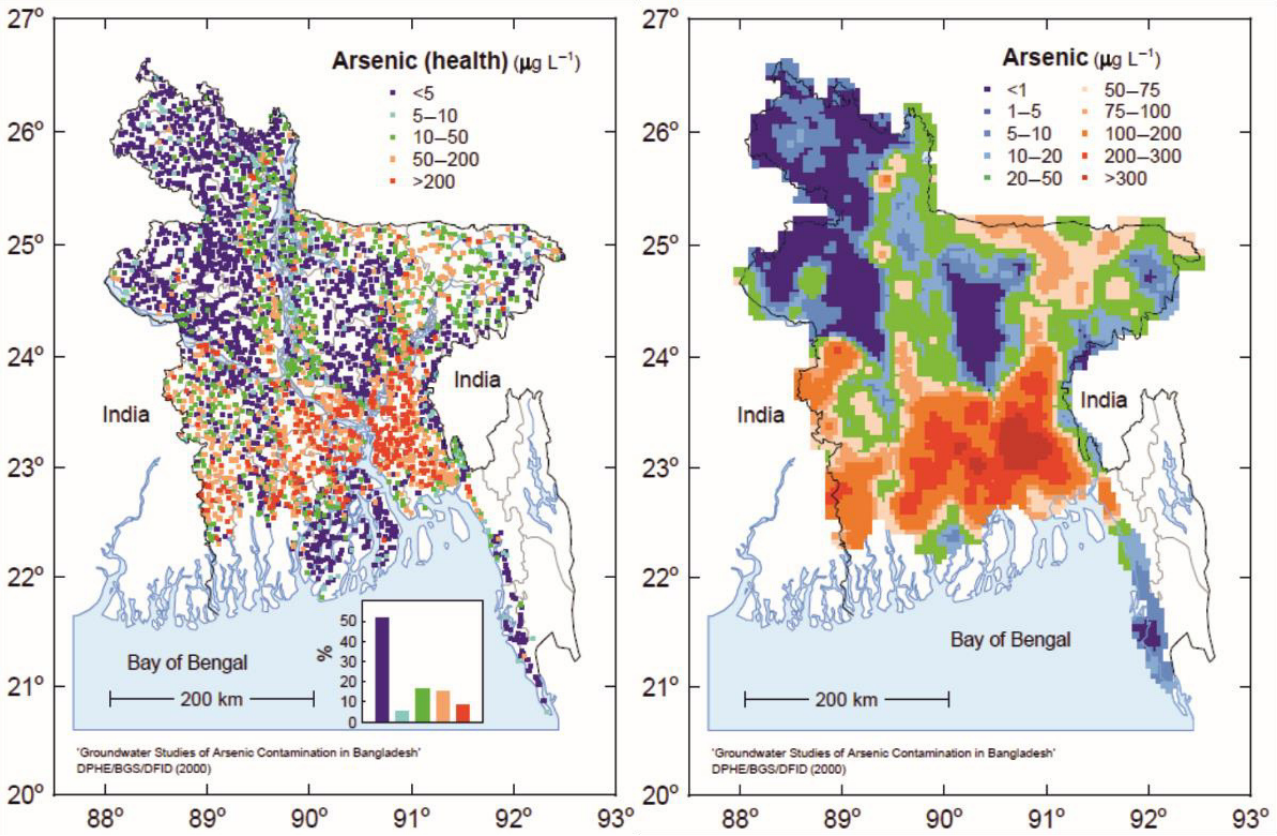

Figure 3 – Arsenic concentration in BDP groundwater. The left-side map represents the punctual distribution of As with respect to WHO threshold values (10 and 50 µg/L). The right-side map shows the interpolated data from the first map (DPHE/BGS National Hydrochemical Survey, 2000).

1.2.2 Hungary

In the southern part of the Great Hungarian Plain (GHP), in an area of 4263 km^2 with a population of nearly 456,500 in five towns and 54 villages, groundwater from the Pleistocene aquifers, containing As at levels about the national permissible limit of 50 µg/L, is used for public drinking water supplies. The aquifers comprise sediments deposited by the river Danube, while in the eastern part of the plains the sediments were brought by the Maros and Koros Rivers. The groundwater has highest arsenic concentrations in the lowest parts of the basin, where the sediment is fine-grained. Chemically, this groundwater was predominantly Ca-Mg-HCO_3 and Na-HCO_3 type. Typical As concentrations in the region vary between 25 and 150 µg/L, and it was concluded that the distribution of As in the GHP groundwater was controlled by the humic substances (Varsanáyi et al, 1991).

1.2.3 United States

Nearly 10% of groundwater resources in the United States indicate As concentrations exceeding the drinking water guideline of 10μg/L (Welch et al., 2000). In general, highest As concentrations are encountered in the western part and large areas of the Midwest and northeast exceeding the national and WHO drinking water guideline value of 10μg/L (WHO, 2017). However, in the southeastern part of the country, As concentrations are low (USGS, 2000; Focazio et al., 1999). The most prevalent mechanisms of widespread concentrations of As are desorption and reductive dissolution of iron oxides and oxidation of sulfide minerals, in addition to up flow of geothermal water and evaporative concentrations (Welch et al., 1998; Schreiber et al., 2000). During the last two decades, USGS developed a national-scale assessment for arsenic groundwater contamination. Using 18,850 wells from 595 counties, the study pointed out that 13.6% of these wells were over the 5 μg/L, 7.6% exceeded the WHO threshold limit (10 μg/L) and the others were lower than 5 μg/L (USGS, 2000; Focazio et al., 1999). The As is thought to derive from various sources, including natural dissolution/desorption reactions, geothermal water and mining activity. The main areas where naturally-high concentrations of As occur in groundwater in the USA are in the south-western states (e.g. Nevada, California, Arizona, Utah). These areas include some localized mining and geothermal-related As occurrences, but many of the affected groundwater are from alluvial basins which occur under a range of redox conditions (Figure 4). Welch and Lico (1998) reported high As concentrations (often exceeding 100 μg/L, but with extremes up 2600 μg/L) in shallow groundwater from the southern Carson Desert of Nevada. These are apparently largely present under reducing conditions, having low dissolved-oxygen concentrations and high concentrations of dissolved organic C, Mn and Fe. The high As concentrations were thought to be due to evaporative concentration of groundwater, together with the influence of redox and desorption processes involving metal oxides. In groundwater from the Tulare Basin of the San Joaquin Valley, California, redox conditions in the aquifers are highly variable and increased arsenic concentrations are found in both reducing and oxidizing conditions. The proportion of As present as As(III) is also variable but increases in different wells with depth. The groundwater from the Basin are often strongly affected by evaporative concentration with resulting high concentrations of dissolved solids

(Fujii and Swain, 1995). High groundwater arsenic concentrations occur in alluvial aquifers under oxidizing conditions in the Basin & Range Province in Arizona (Robertson, 1989). Dissolved arsenic is present predominantly as As(V) and is observed to correlate well with Mo, Se, V, F and pH. Oxidizing conditions apparently persist in the aquifers down to significant depths (600 m) despite significant groundwater age (up to 10,000 years old; Robertson, 1989).

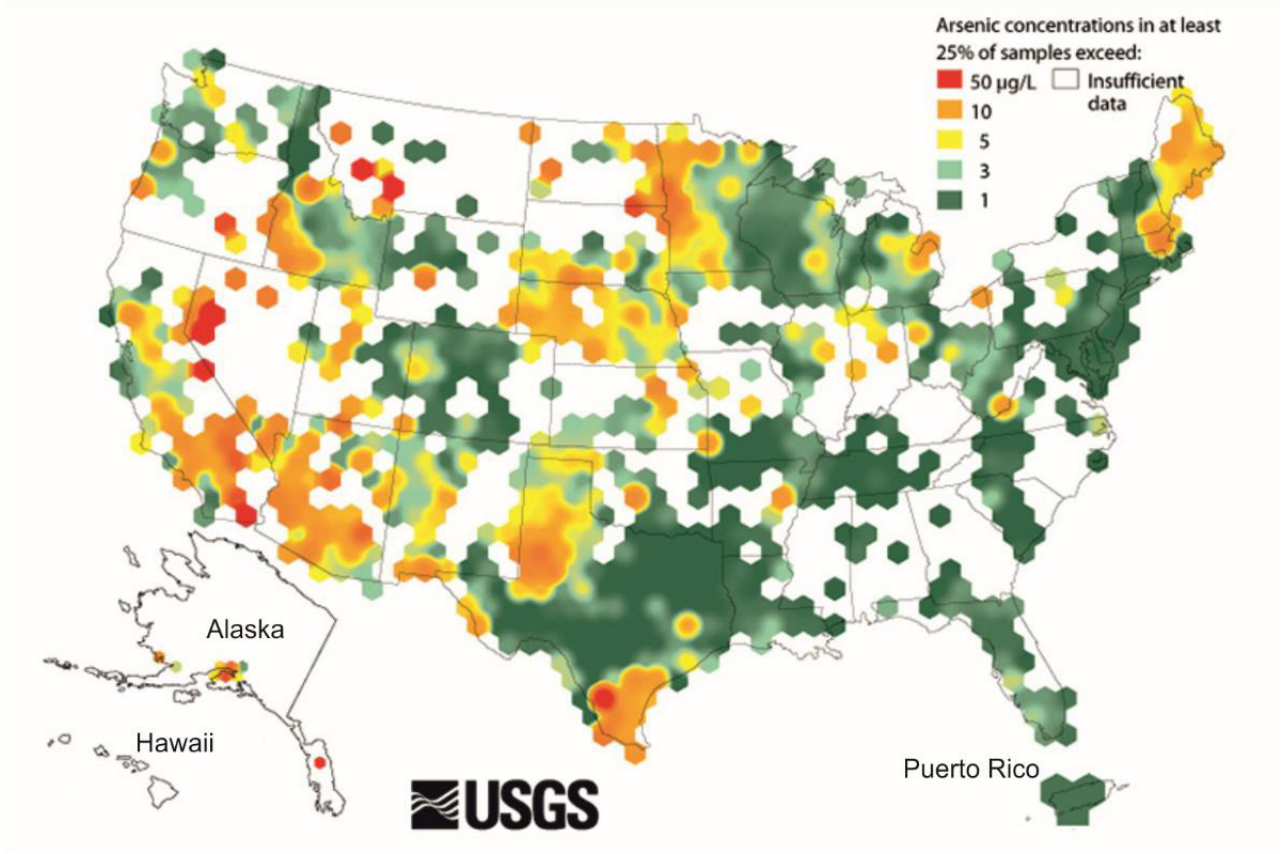

Figure 4 – Data-density-based map showing a moving 75th percentile of arsenic concentration in USA groundwater (updates from Welch et al., 2000).

1.3 Arsenic occurrence in Italy

Amongst the well-known countries around the world, Italy is affected by arsenic groundwater contamination as well. Even if Italy is not considered as one of the major countries for arsenic contamination, it has lot of areas characterized by high arsenic concentration. The origin of arsenic has different stories, due to a wide range of geological settings and anthropogenic activities. Keeping aside the events due to human activity, from the North to the South, high natural arsenic concentrations occur. These are linked to the variety of geological processes acting in Italy, either in the past or nowadays. The main contexts for arsenic contamination are

the alluvial plain deposits, mineralized areas and volcanic/geothermal areas. The former is typical of the northern part of Italy, where the main Italian rivers (Po, Adige; Brenta, etc.) are shaping the environment. The second scenarios are frequent in mineralized zones such as Sardinia, and the latter can find in the central and southern part of Italy, which are notoriously interested by volcanic and tectonic activities. In Italy, arsenic occurrence was well-known in the past, especially in volcanic/geothermal areas. By the way, the knowledges about its distribution got improved in the last decades with enhanced study on its natural background level and its impact on water quality and human health (Aiuppa et al. 2003; Carraro et al., 2013, 2015; Ducci et al., 2016; Dalla libera et al., 2016; 2017; 2018; Frau and Ardau, 2003, Molinari et al., 2012, 2015; Preziosi et al., 2010; Rotiroti et al., 2014; Tamasi and Cini, 2004; Ungaro et al., 2008).

1.3.1 North Italy

The northern part of Italy is typically interested by arsenic contamination associated to alluvial environments. The alluvial aquifers, composed of sedimentary materials coming from the river watersheds, are often rich of arsenic-bearing materials like silt, clay and organic matter layers. The fine sediments, in particular, could be rich of As-bearing oxides and hydroxides resulting from alteration of mineralized lithologies. The geological origins and the successive weathering process let these materials to be potential sources of As. The most frequent arsenic release mechanism occurring in the alluvial plains is the reductive dissolution of iron hydroxides (HFO). This mechanism, due to the uprising of reduced conditions, allows for desorption of arsenic bound on the reactive surfaces of HFO, which could result in high dissolved arsenic in groundwater (Carraro et al., 2013; 2015; Molinari et al., 2014; Rotiroti et al., 2014). In this context, organic matter (OM) gets an important role as its degradation (oxidation of OM) lead toward reduced groundwater (Appelo and Postma, 2005). In addition, the arsenic can also be strongly adsorbed onto organic matter, which could be a direct source of As in addition to its role of redox driver. Many studies (i.e.: Molinari et al., 2013; Redman et al., 2002; Smedley and Kinniburgh, 2002; Wang and Mulligan, 2006) highlighted the capacity of organic matter to release As under lower oxi-reduction potential values (ORP). The lower ORP values, however, are not always positive for arsenic release. Carraro et al. in 2015, indeed, demonstrated how, in the Brenta alluvial plain, (NE Italy) the occurrence of both lower ORP value (< -250mV) and Sulfur phases could scavenge As from reduced groundwater through pyrite precipitation. The alluvial plains in north Italy are characterized by a high subsurface heterogeneity (similar to

the Bengal Delta Plain), which affects the arsenic mobility by place to place and make its release mechanism very complex to understand.

1.3.2 Central Italy

Arsenic in central Italy is often associated to volcanic aquifers, in which the groundwater interacts with volcanic formations rich of arsenic-bearing minerals. The volcanic areas, moreover, are subjected to deep geothermal water circulation, which can transport arsenic and other trace minerals from the depth to the shallow portion of subsurface. The mixing process between mineralized deep water and shallow groundwater, often, results in groundwater enriched in trace elements over the drinkable water limits. These processes, even if geogenic, could affect the water quality and lead toward a health issue, especially when the reservoir is used for drinking water supply. An example of arsenic contamination due to volcanic environment is the Viterbo province (Latium; Central Italy), where high As concentration together with other trace elements (B, Rb, Co, Mo, U, Fe, Mn, etc) affected the drinkable water supply system, leading toward a harmful situation for the population (D'Ippoliti et al., 2015). In these areas several studies were performed to pointed out the hydro-geochemical mechanism involved in arsenic mobility. Angelone et al., 2009; Baiocchi et al., 2013 and Cinti et al., 2015 highlighted that arsenic distribution is linked to the structural setting of Cimino and Vicano volcanic complex. Relatively high As concentrations were measured in correspondence of fractured and faulted zones, i.e. in sectors characterized by reduced thickness of low-permeability cap units favoring the discharge of hydrothermal fluids and, consequently, enhancing mineral solubility during water–rock interaction processes. The same water-rock interaction processes pointed out by the hydro-geochemical analysis published by Sappa et al. in 2014. Other areas in central Italy, notoriously affect by arsenic contamination, exist. Larderello geothermal district and Monte Amiata are the main example. In the former arsenic is due to the deep geothermal fluids (Grassi et al., 2014), in the latter the interaction between the epithermal deposits and the surface/groundwater produced high arsenic concentrations (Baroni et al., 2004).

1.3.3 South Italy

As for the central part of Italy, even in the south Italy the arsenic occurrence is linked to the volcanic environment and its deposits. The study led by Aiuppa et al., 2003 resumes the As data obtained from volcanic groundwater in southern Italy and outlines the main factors controlling

As mobility and speciation. High As concentrations (up to about 7 mg/l) are characteristic of groundwaters of Vulcano Island and the Phlegrean Fields. These waters are high-T Cl-rich waters. Temperature exerts a major control on As mobilization enhancing mineral solubility during water–rock interaction. Arsenic–SO_4 positive correlation for these waters suggests the control of As-bearing sulfides in determining As mobility. These waters are interpreted as groundwaters heated by vapors boiled off from deep geothermal systems. The vapors are depleted in As because of it mainly partitions into the liquid phase. Relatively lower As values are found in the HCO_3^- waters of Etna and Vesuvius, where hydrothermal activity is minimal. A pH control on As speciation in these waters is recognized, whereas general inter-site pH–As correlation was poor. This trend of increasing As concentration in solution at higher pH might reflect the influence of Fe on As mobility. Thermodynamic calculations suggest that Fe oxy-hydroxides are the solid phases in equilibrium with most of the studied groundwaters. Under these conditions As mobility can be strongly controlled by adsorption on Fe oxy-hydroxides. Corniello and Ducci, 2014 and Ducci et al., 2016 pointed out the role of heated water for arsenic mobilization in the area of Volturno Plain-Regi Lagni'. The mechanism is the same suggested by Aiuppa et al., 2003 for Phlagrean fields, where the presence of steam-heated groundwater circulation enhanced the mobility of As. Even in the case study of Ischia Island (Naples, Italy), the hydrothermal fluids circulation was the main trigger for As release in groundwater as they encourage water rock interaction, especially along fractured and faulted zones due to volcano-tectonics activity (Daniele, 2004).

1.4 Implication on water management

Heavy metals and other chemical contaminant compounds (i.e. NO_3^-, NH_4^+, SO_4^{2-}, Hydrocarbons, etc.) have a great impact on environmental and life quality, requiring an occulated management. Among those chemicals, arsenic is one of the most known environmental issue worldwide (Bhattacharya et al., 2002; Smedley & Kinniburg, 2013; Nordstrom, 2003). The occurrence of As in soil and groundwater threatens the health of exposed population, being responsible for serious diseases. As described in the previous parts of the chapter, arsenic can be linked to different sources and different geochemical conditions. The high variability of As behavior within the environment leads toward a complicated management and definition of the right remediations to be adopted. In this direction, during the last decades several projects were conducted in order to enhance the knowledges on arsenic and its correlated chemicals. Furthermore, the emanation of updated laws and guidelines, about environmental quality

status and its management to rich the required quality standards, fed the awareness of both researcher and stakeholders in developing new methods and new strategies to tackle that issue. Nowadays, several knowledges have been got about arsenic mobility processes, and many related remediation procedures too. Nonetheless, in many countries the information on arsenic mobility, thus its behavior, is still fragmented and/or partially unclear. This situation, in some places like the Venetian Alluvial Plain (NE Italy), inhibits an effective management of the environment with controversial threshold values for dangerous chemicals and produce unresolved discussion about contamination origins as well (Dalla Libera et al., 2017; 2018; Ducci et al., 2016, Molinari et al., 2012; Rotiroti et al., 2014).

References

Acharyya, Chakraborty, Lahiri, Raymahashay, Guha, Bhowmik, 1999. Nature 401:545.

Aiuppa, A., D'Alessandro, W., Federico, C., Palumbo, B., Valenza, M., 2003. The aquatic geochemistry of arsenic in volcanic groundwaters from southern Italy. Appl. Geochemistry 18, 1283–1296. https://doi.org/10.1016/S0883-2927(03)00051-9

AK Saha and C Chakraborty, 1995. Geological and geochemical background of the arse- nic bearing groundwater occurrences of West Bengal. Proceedings, Int Conf on Arsenic in Groundwater, Calcutta, India.

Anawar, H.M., Akai, J., Mostofa, K.M.G., Safiullah, S., Tareq, S.M., 2001. Arsenic poisoning in groundwater: Health risk and geochemical sources in Bangladesh. Environ. Int. 27, 597–604. https://doi.org/10.1016/S0160-4120(01)00116-7

Angelone M, Cremisini C, Piscopo V, Proposito M, Spaziani F, 2009. Influence of hydrostratigraphy and structural setting on the arsenic occurrence in groundwater of the Cimino-Vico volcanic area (central Italy). Hydrogeol J 17:901–914

Appelo, C.A.J., Postma, D., 2005. Geochemistry, groundwater and pollution. 2nd. Ed. Balkema, Rotterdam.

Baiocchi, A., Coletta, A., Espositi, L., Lotti, F., Piscopo, V., 2013. Sustainable groundwater development in a naturally arsenic-contaminated aquifer: the case of the Cimino- Vico volcanic area (central Italy). Ital. J. Eng. Geol. Environ. http://dx.doi.org/10. 4408/IJEGE.2013-01.O-01.

Baroni, F., Boscagli, A., Di Lella, L.A., Protano, G., Riccobono, F., 2004. Arsenic in soil and vegetation of contaminated areas in southern Tuscany (Italy). J. Geochemical Explor. 81, 1–14. https://doi.org/10.1016/S0375-6742(03)00208-5

BGS/MMI, 1999. Groundwater Studies for Arsenic Contamination in Bangladesh, Vol S1, S2, and Main Report, British Geological Survey, Nottingham, England.

Bhattacharya, Ahmed, Hasan, Jacks, Khan, Akhter, Imam, Sracek, 1999. Groundwater arsenic in the Holocene alluvial aquifers of Bengal Delta Plains: petrological, geochemical and isotope geochemical studies. Int Conf on Arsenic in Bangladesh Ground Water: World's Greatest Arsenic Calamity. Wagner College, New York.

Bhattacharya, Chatterjee, Jacks, 1996. In: J Pickford, S House, D Miles, J Ockel- ford, J Parr, D Saywell, R Shaw, B Skinner, I Smout, R Stear, eds. Reaching the Unreached—Challenges for the 21st Century. Proc 22nd WEDC Conference, New Delhi, India. University of Loughborough, pp 258–261.

Bhattacharya, Jacks, 2000. Arsenic contamination in groundwater of the sedimentary aquifers in the Bengal Delta Plains: a review. In: P Bhattacharya, AH Welch, eds. Arsenic in Groundwater of Sedimentary Aquifers. Pre-Congress Workshop, 31st Int Geol Cong, Rio de Janeiro, Brazil, pp 18–21.

Bhattacharya, Larsson, Leiss, Jacks, Sracek, Chatterjee, 1998. Genesis of arseniferous groundwater in the alluvial aquifers of Bengal Delta Plains and strate- gies for low-cost remediation. Int Conf on Arsenic Pollution of Groundwater in Bangladesh: Causes, Effects and Remedies. Dhaka, Bangladesh, pp 120– 123. (http://bicn.com/acic/ infobank/dch98-02conf/bp1.htm).

Bhattacharya, P., Chatterjee, D., Jacks, G., 1997. Int J Wat Res Man 13(1):79–92.

Bhattacharya, P., Welch, A.H., Ahmed, K.M., Jacks, G., Naidu, R., 2004. Arsenic in groundwater of sedimentary aquifers. Appl. Geochemistry 19, 163–167. https://doi.org/10.1016/j.apgeochem.2003.09.004

Bhattacharya, Prosun, S. H. Frisbie, E. Smith, R. Naidu, G. Jacks, and B.S., 2002. Heavy Metals in the Environment edited by.

Carraro, A., Fabbri, P., Giaretta, A., Peruzzo, L., Tateo, F., Tellini, F., 2013. Arsenic anomalies in shallow Venetian Plain (Northeast Italy) groundwater. Environ. Earth Sci. 70, 3067–3084. https://doi.org/10.1007/s12665-013-2367-2

Carraro, A., Fabbri, P., Giaretta, A., Peruzzo, L., Tateo, F., Tellini, F., 2015. Effects of redox conditions on the control of arsenic mobility in shallow alluvial aquifers on the Venetian Plain (Italy). Sci. Total Environ. 532, 581–594. https://doi.org/10.1016/j.scitotenv.2015.06.003

CGWB, 1999. High Incidence of Arsenic in Ground Water in West Bengal. Central Ground Water Board report, India, 142 pp.

Chowdhury, T.R., Basu, G.K., Mandal, B.K., Biswas, B.K., Samanta, G., Chowdhury, U.K., Chanda, C.R., Lodh, D., Roy, S.L., Saha, K.C., Roy, S., Kabir, S., Quamruzzaman, Q., Chakraborti, D., 1999. Arsenic poisoning in the Ganges delta. Nature 401, 545–546. https://doi.org/10.1038/44056

Cinti, D., Poncia, P.P., Brusca, L., Tassi, F., Quattrocchi, F., Vaselli, O., 2015. Spatial distribution of arsenic, uranium and vanadium in the volcanic-sedimentary aquifers of the Vicano-Cimino Volcanic District (Central Italy). J. Geochemical Explor. 152, 123–133. https://doi.org/10.1016/j.gexplo.2015.02.008

D'Ippoliti, D., Santelli, E., De Sario, M., Scortichini, M., Davoli, M., Michelozzi, P., 2015. Arsenic in Drinking Water and Mortality for Cancer and Chronic Diseases in Central Italy, 1990-2010. PLoS One 10, e0138182. https://doi.org/10.1371/journal.pone.0138182

Dalla Libera, N., Fabbri, P., Mason, L., Piccinini, L., Pola, M., 2017. Geostatistics as a tool to improve the natural background level definition: An application in groundwater. Sci. Total Environ. 598, 330–340. https://doi.org/10.1016/j.scitotenv.2017.04.018

Dalla Libera, N., Fabbri, P., Mason, L., Piccinini, L., Pola, M., 2018. A local natural background level concept to improve the natural background level: a case study on the drainage basin of the Venetian Lagoon in Northeastern Italy. Environ. Earth Sci. 77, 487. https://doi.org/10.1007/s12665-018-7672-3

Dalla Libera, N., Fabbri, P., Piccinini, L., Pola, M., Leonardo Mason, L., 2016. Natural Arsenic in groundwater in the drainage basin to the Venice lagoon (Brenta Plain, NE Italy): the organic matter's role. Rend. Online della Soc. Geol. Ital. 41, 30–33. https://doi.org/10.3301/ROL.2016.85

Daniele L., 2004. Distribution ofarsenic and other minor trace elements in the groundwater of Ischia Island (southern Italy). Environ Geol; 46:96-103.

DPHE/BGS, 2000. Groundwater studies for arsenic contamination in Bangladesh. Final Draft Report.

DPHE/BGS/MML, 1999. Groundwater Studies for Arsenic Contamination in Bangladesh. Phase I: Rapid Investigation Phase. BGS/MML Technical Report to Department for International Development, UK), 6 volumes.

Ducci, D., Condesso, M.T., Melo, D., Preziosi, E., Sellerino, M., Parrone, D., Ribeiro, L., 2016. Science of the Total Environment Combining natural background levels (NBLs) assessment with indicator kriging analysis to improve groundwater quality data interpretation and management. Sci. Total Environ. 569–570, 569–584. https://doi.org/10.1016/j.scitotenv.2016.06.184

Dzombak, D.A. and Morel, F.M., 1990. Surface complexation modeling: hydrous ferric oxide. John Wiley & Sons.

Fendorf, S., Michael, H.A., van Geen, A., 2010. Spatial and Temporal Variations of Groundwater Arsenic in South and Southeast Asia. Science (80-.). 328, 1123–1127. https://doi.org/10.1126/science.1172974

Focazio, MJ., Welch, AH,. Watkins, SA., Helsel, DR., Horn, MA, 1999. A retrospective analy- sis on the occurrence of arsenic in ground water resources of the United States and limitations in drinking water supply characterizations. U.S. Geological Survey Water Resources Investigations Report 99-4279, 21 pp. 214.

Frau, F., Ardau, C., 2003. Geochemical controls on arsenic distribution in the Baccu Locci stream catchment (Sardinia, Italy) affected by past mining. Appl. Geochemistry 18, 1373–1386. https://doi.org/10.1016/S0883-2927(03)00057-X

Fujii, R. and Swain, W. C., 1995. Areal distribution of selected trace elements, salinity, and major ions in shallow ground water, Tulare Basin, southern San Joaquin Valley, California. USGS Water- Resources Investigations Report 95-4048,67 pp.

Goldberg S (1986) Chemical modeling of arsenate adsorption on alu- minum and iron oxide minerals. Soil Sci Soc Am J 50:1154–1157

Gorby, M. S., 1994. Arsenic in human medicine. In: Arsenic in the Environment, Part 11: Human Health and Ecosystem Effects, ed: Nriagu, J. O., 1-16, Wiley, New York.

Grassi, S., Amadori, M., Pennisi, M., Cortecci, G., 2014. Identifying sources of B and As contamination in surface water and groundwater downstream of the Larderello geothermal - Industrial area (Tuscany-Central Italy). J. Hydrol. 509, 66–82. https://doi.org/10.1016/j.jhydrol.2013.11.003

I.Varsana´yi, F Zsofia, A Bartha, 1991. Environ Geochem Health 13:14–22.

Livesey, N. T. and Huang, P. M., 1981. Adsorption of arsenate by soils and its relation to selected chemical properties and anions. Soil Sci., 131,88-94.

M von Brömssen, 1999. Genesis of high arsenic groundwater in the Bengal Delta Plains, West Bengal and Bangladesh. MSc thesis, Division of Land and Water Resources, Dept. of Civil and Environ. Engineering, Royal Institute of Technology, Stockholm, Sweden, 49 pp.

Mandal, B., 2002. Arsenic round the world: a review. Talanta 58, 201–235. https://doi.org/10.1016/S0039-9140(02)00268-0

Manning BA, Goldberg S. Modeling arsenate competitive adsorption on kaolinite, montmorillonite and illite. Clay Clay Miner 1996; 44:609–23.

McArthur, J.M., Banerjee, D.M., Hudson-Edwards, K.A., Mishra, R., Purohit, R., Ravenscroft, P., Cronin, A., Howarth, R.J., Chatterjee, A., Talukder, T., Lowry, D., Houghton, S., Chadha, D.K., 2004. Natural organic matter in sedimentary basins and its relation to arsenic in anoxic ground water: The example of West Bengal and its worldwide implications. Appl. Geochemistry 19, 1255–1293. https://doi.org/10.1016/j.apgeochem.2004.02.001

McArthur, J.M., Ravenscroft, P., Safiulla, S., Thirlwall, M.F., 2001. Arsenic in groundwater: Testing pollution mechanisms for sedimentary aquifers in Bangladesh. Water Resour. Res. 37, 109–117. https://doi.org/10.1029/2000WR900270

Molinari, A., Ayora, C., Marcaccio, M., Guadagnini, L., Sanchez-Vila, X., Guadagnini, A., 2014. Geochemical modeling of arsenic release from a deep natural solid matrix under alternated redox conditions. Environ. Sci. Pollut. Res. 21, 1628–1637. https://doi.org/10.1007/s11356-013-2054-6

Molinari, A., Guadagnini, L., Marcaccio, M., Guadagnini, A., 2012. Natural background levels and threshold values of chemical species in three large-scale groundwater bodies in Northern Italy. Sci. Total Environ. 425, 9–19. https://doi.org/10.1016/j.scitotenv.2012.03.015

Molinari, A., Guadagnini, L., Marcaccio, M., Guadagnini, A., 2015. Arsenic fractioning in natural solid matrices sampled in a deep groundwater body. Geoderma 247–248, 88–96. https://doi.org/10.1016/j.geoderma.2015.02.011

Molinari, A., Guadagnini, L., Marcaccio, M., Guadagnini, A., 2015. Arsenic fractioning in natural solid matrices sampled in a deep groundwater body. Geoderma 247–248, 88–96. https://doi.org/10.1016/j.geoderma.2015.02.011

Molinari, A., Guadagnini, L., Marcaccio, M., Straface, S., Sanchez-Vila, X., Guadagnini, A., 2013. Arsenic release from deep natural solid matrices under experimentally controlled redox conditions. Sci. Total Environ. 444, 231–240. https://doi.org/10.1016/j.scitotenv.2012.11.093

Mukherjee and Bhattacharya, 2001. Environ Rev 9:1–32.

Naidu, R., 2000. Arsenic contamination of rural groundwater supplies in Bangladesh, India and Australia: implications for soil quality, animal and human health. In: P Bhatta- charya, AH Welch, eds. Arsenic in Groundwater of Sedimentary Aquifers. Pre- Congress Workshop, 31st Int Geol Cong, Rio de Janeiro, Brazil, pp 72– 74.

Nickson, R., McArthur, J., Burgess, W., Ahmed, K.M., Ravenscroft, P., Rahman, M., 1998. Arsenic poisoning of Bangladesh groundwater. Nature 395, 338. https://doi.org/10.1038/26387

Nickson, R.T., Mcarthur, J.M., Ravenscroft, P., Burgess, W.G., Ahmed, K.M., 2000. Mechanism of arsenic release to groundwater, Bangladesh and West Bengal. Appl. Geochemistry 15, 403–413. https://doi.org/10.1016/S0883-2927(99)00086-4

Nordstrom, D.K., 2003. Arsenic in Ground Water, Science Mag. Springer US, Boston, MA. https://doi.org/10.1007/b101867

Preziosi, E., Giuliano, G., Vivona, R., 2010. Natural background levels and threshold values derivation for naturally As, V and F rich groundwater bodies: a methodological case study in Central Italy. Environ. Earth Sci. 61, 885–897. https://doi.org/10.1007/s12665-009-0404-y

Rango, T., Vengosh, A., Dwyer, G., Bianchini, G., 2013. Mobilization of arsenic and other naturally occurring contaminants in groundwater of the main ethiopian rift aquifers. Water Res. 47, 5801–5818. https://doi.org/10.1016/j.watres.2013.07.002

Ravenscroft, P., Brammer, H., Richards, K., 2009. Arsenic Pollution: A Global Synthesis. Arsen. Pollut. A Glob. Synth. 1–588. https://doi.org/10.1002/9781444308785

Redman, A.D., Macalady, D.L., Ahmann, D., 2002. Natural organic matter affects arsenic speciation and sorption onto hematite. Environ. Sci. Technol. 36, 2889–2896.

Robertson, F. N., 1989. Arsenic in ground-water under oxidising conditions, south-west United States. Environ. Geochem. Health, 11, 171-185.

Rotiroti, M., Sacchi, E., Fumagalli, L., Bonomi, T., 2014. Origin of Arsenic in Groundwater from the Multilayer Aquifer in Cremona (Northern Italy). Environ. Sci. Technol. 48, 5395–5403. https://doi.org/10.1021/es405805v

Schreiber, ME., Simo, JA., Freiberg, PG., 2000. Hydrogeol J 8(2):161–176.

Smedley, P. 1996. J Afr Earth Sci 22(4):459–470.

Smedley, P., Kinniburgh, D., 2002. A review of the source, behaviour and distribution of arsenic in natural waters. Appl. Geochemistry 17, 517–568. https://doi.org/10.1016/S0883-2927(02)00018-5

Smedley, P.L., Kinniburgh, D.G., 2013. Arsenic in Groundwater and the Environment, in: Essentials of Medical Geology. Springer Netherlands, Dordrecht, pp. 279–310. https://doi.org/10.1007/978-94-007-4375-5_12

Smith, A. H., Hopenhayn-Rich, C., Bates, M. N., Goeden, H. M., Hertz-Picciotto, I., Duggan, H. M., Wood, R., Kosnett, M. J. and Smith, M. T. 1992. Cancer risks from arsenic in drinking water. Environ. Health Persp., 97, 259-267.

Smith, A., Goycolea, M., Haque, R. and Biggs, M. L. 1998. Marked increase in bladder and lung cancer mortality in a region of Northern Chile due to arsenic in drinking water. Am. J. Epidemiol., 147,660-669

Sorg, T.J., Chen, A.S.C., Wang, L., 2014. Arsenic species in drinking water wells in the USA with high arsenic concentrations. Water Res. 48, 156–169. https://doi.org/10.1016/j.watres.2013.09.016

Tamasi, G., Cini, R., 2004. Heavy metals in drinking waters from Mount Amiata (Tuscany, Italy). Possible risks from arsenic for public health in the Province of Siena. Sci. Total Environ. 327, 41–51. https://doi.org/10.1016/J.SCITOTENV.2003.10.011

Ungaro, F., Ragazzi, F., Cappellin, R., Giandon, P., 2008. Arsenic concentration in the soils of the Brenta Plain (Northern Italy): Mapping the probability of exceeding contamination thresholds. J. Geochemical Explor. 96, 117–131. https://doi.org/10.1016/j.gexplo.2007.03.006

USGS. 2000. Arsenic in ground-water resources of the United States. Fact Sheet #063-00. http://co.water.usgs.gov/trace/pubs/fs-063-00/index.html.

W.H.O., 2011. Guidelines for Drinking-water Quality. World Health 1, 104–8. https://doi.org/10.1016/S1462-0758(00)00006-6

Wang, S., Mulligan, C.N., 2006. Effect of natural organic matter on arsenic release from soils and sediments into groundwater. Environ. Geochem. Health 28, 197–214. https://doi.org/10.1007/s10653-005-9032-y

Welch, A.H., Westjohn, D.B., Helsel, D.R., Wanty, R.B., 2000. Arsenic in Ground Water of the United States: Occurrence and Geochemistry. Ground Water 38, 589–604. https://doi.org/10.1111/j.1745-6584.2000.tb00251.x

Welch, Lico, 1998. Appl Geochem 13(4):521–539.

WHO, 2017. Guidelines for drinking-water quality, 4th edition, incorporating the 1st addendum.

Wilkie JA, Hering JG. Adsorption ofarsenic onto hydrous ferric oxide: effects of adsorbate/adsorbent ratios and co-occurring solutes. Colloids and Surfaces A 1996;107:97–110.

2. The project

2.1 Aims and structure of the project

As describe in the introduction (see Section 1.3), groundwater arsenic contamination is threatening the DBVL (approximately the VAP), decreasing the groundwater quality and so the environmental one. In this context, the PhD project aims to understand the main hydro-chemical processes that can control arsenic mobility within the aquifer system. This kind of study poses attention on improving the knowledge on arsenic mobility, going over what was pointed out by ARPAV in the last decade (ARPAV, 2011, 2014). To reach the aim, a multi-disciplinary approach was considered, combining hydrogeological and geochemical methods with machine learning and numerical modeling techniques. The study was structured in order to complete three main phases, being necessary to reach the aforementioned aim. These phases could be resumed as follows (see also Figure 2.1 below):

- Reconstruction of the study area subsurface heterogeneity through geostatistical methods. This first phase is important to spatialize the distribution of materials that compose the subsurface, as they can geochemically affects the reaction involved in arsenic release.

- Assembling a monitoring network for gathering chemical and physical data for groundwater and soil matrix. Subsequently, on those data, an advance machine learning-based exploratory data analysis (EDA) were performed to elucidate the main processes driving arsenic mobility.

- The third phase concerns the implementation of a reactive transport model able to simulate the system behavior described by both the field data and the EDA. The idea is of getting an effective model as tool for environmental and water management purposes, which could help in clarifying the controversial aspects on As NBL definition.

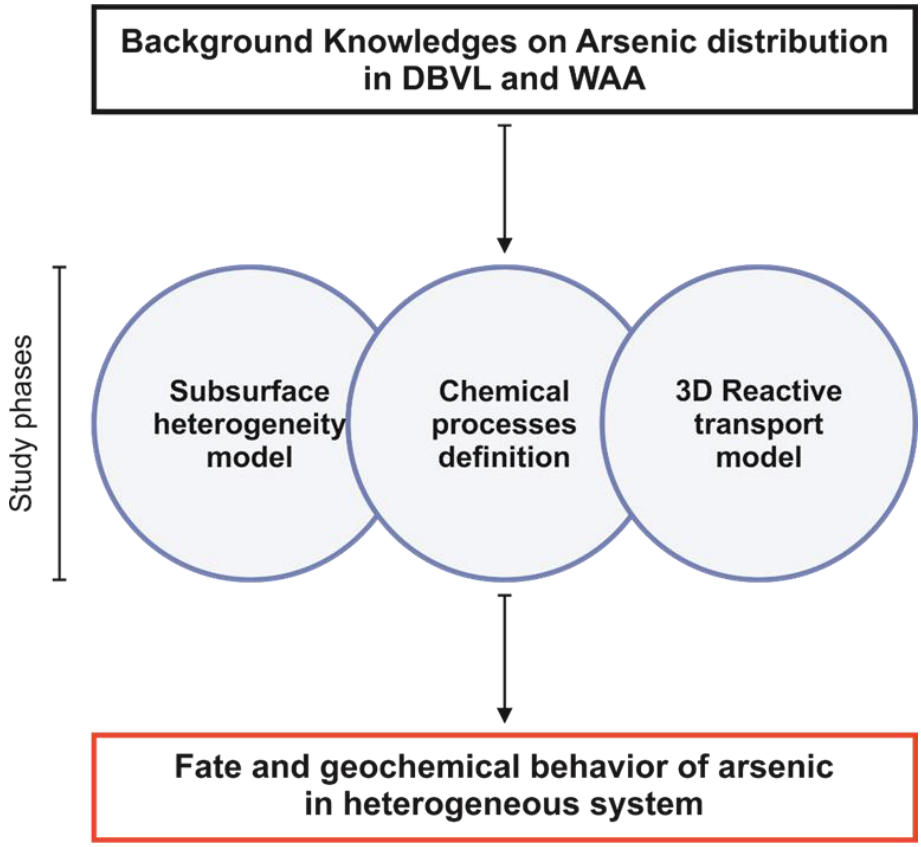

Figure 2.1 - General workflow explaining the principal phases of the PhD project. The described workflow was applied on a local scale area named "Western Agricultural Areas".

The described workflow was applied on a local scale area named "Western Agricultural Areas" (WAA). The study site is located inside the DBVL and was chosen because it has an existing and easily accessible monitoring network. Furthermore, the WAA shows the main geological and hydrogeological features observed around the DBVL, allowing for a possible upscaling of the main hydo-chemical processes linked to arsenic mobility. A detailed description of both the DBVL and WAA will be reported in the next paragraph (Section 2.2). As starting point, the PhD project takes advantage from the recent studies about the definition of the Natural Background Level of arsenic into DBVL (Dalla Libera et al., 2016, 2017, 2018). Thanks to the detailed reconstruction of the arsenic spatial distribution and the preliminary investigation on the chemical relations affecting arsenic mobility, these works provide a good basis for developing considerations about the plausible arsenic release mechanisms.

The development of this research project, following the aforementioned phases, produced several results, which are the topics of some published papers and unpublished text. As one can see from the table 2.1, these works are spilt into several sections and they make up the main

body of the thesis. All the main features of the PhD project will be addressed in each section respecting the structure of the workflow in figure 2.1.

Table 1.1 – List of the papers and the unpublished results produced during the PhD project. The results are devided as function of the main phases (topic) that composed the thesis workflow.

Topic	Sections
Background Knowledge on arsenic contamination in DVBL and WAA	• Section 2.3.1 (Paper 1) • Section 2.3.2 (Paper 2) • Section 2.3.3 (Paper 3)
Subsurface heterogeneity model	• Section 2.4.1 (Paper 4) • Section 2.4.2 (unpublished)
Chemical processes definition	• Section 2.5.1 (Paper 5)
3D reactive transport model	• Section 2.6 (unpublished)

References

ARPAV, 2011. INDAGINE AMBIENTALE "AREE AGRICOLE" - macroisola aree agricole – zona ovest, macroisola fusina – aree lungo naviglio brenta - sintesi dei risultati del piano di investigazione iniziale. Report data presentation.

ARPAV, 2014. ALiNa – Analysis of the Natural Background Level for Some Compounds Within the Groundwater of the Shallow Aquifer in the Drainage Basin to the Venice Lagoon (Brenta River Alluvial System) – Report and Data Presentation.

Dalla Libera, N., Fabbri, P., Mason, L., Piccinini, L., Pola, M., 2017. Geostatistics as a tool to improve the natural background level definition: An application in groundwater. Sci. Total Environ. 598, 330–340. https://doi.org/10.1016/j.scitotenv.2017.04.018

Dalla Libera, N., Fabbri, P., Mason, L., Piccinini, L., Pola, M., 2018. A local natural background level concept to improve the natural background level: a case study on the drainage basin of the Venetian Lagoon in Northeastern Italy. Environ. Earth Sci. 77, 487. https://doi.org/10.1007/s12665-018-7672-3

Dalla Libera, N., Fabbri, P., Piccinini, L., Pola, M., Leonardo Mason, L., 2016. Natural Arsenic in groundwater in the drainage basin to the Venice lagoon (Brenta Plain, NE Italy): the organic

matter's role. Rend. Online della Soc. Geol. Ital. 41, 30–33. https://doi.org/10.3301/ROL.2016.85

2.2 Study area

The DBVL constitutes a portion of the middle–low Venetian Plain, which includes Padua, Treviso and Venice provinces (PD, TV and VE, respectively, in Figure 2.2). It covers approximately 2038 km^2, with a topographic gradient ranging from 6 to 1‰ near the Venetian Lagoon.

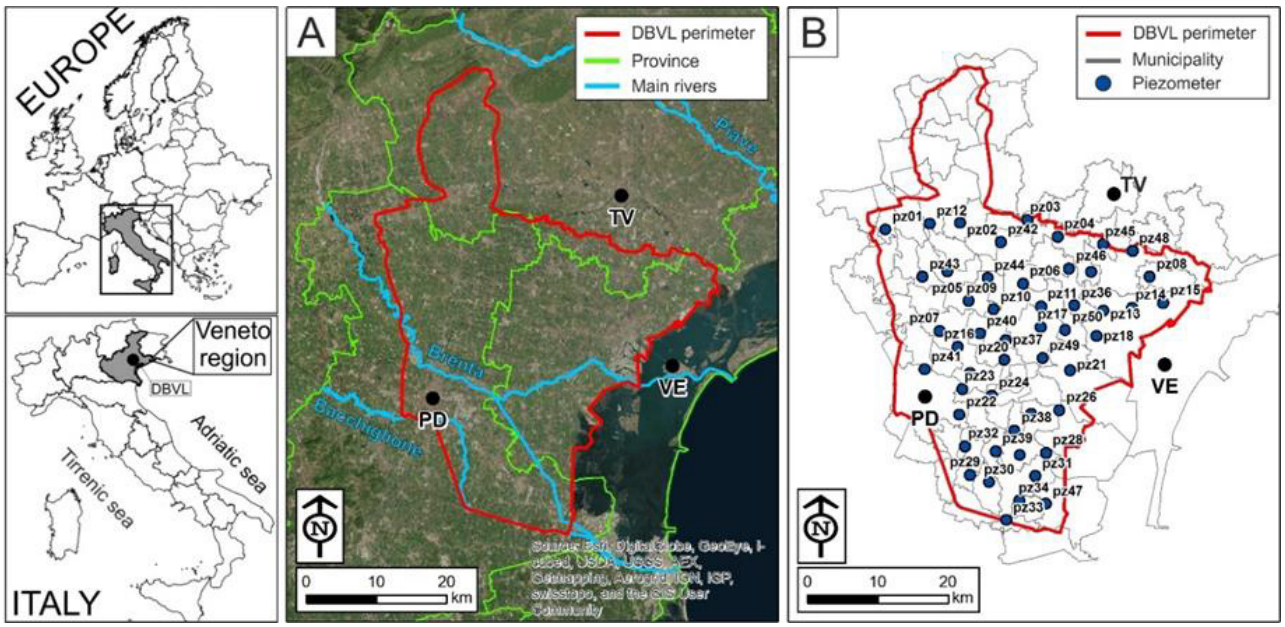

Figure 2.2 - Geographical description of the DBVL: A box shows the extension of DBVL, and B box the monitoring network used for getting information on it (Dalla Libera et al., 2018).

From a geological perspective, Pleistocene–Holocene deposits fill the Venetian alluvial plain, which result from sediments supplied by the Brenta River. In particular, the shallower portion of the plain [from 5 to 30 m below ground level (m b.g.l.)] is composed of sediments from the Last Glacial Maximum (LGM), with an age younger than 30,000 years (Fontana et al. 2004, 2008). In the upper part of the DBVL, gravelly and sandy alluvial deposits are present, whereas in the distal region, silty–clayey deposits prevail in the alluvial system, according to the typical structure of Brenta River's megafan (Mozzi et al. 2003; Bondesan and Meneghel 2004). These fine sediments are typical of a floodplain environment, and they often contain several peat layers, with a thickness up to several decimeters and a lateral extension up to several kilometers. The subsoil structure of the DBVL is heterogeneous due to complex and multiple alluvial sedimentation processes (Trevisani and Fabbri, 2010) that may influence the spatial

distribution of As-bearing materials. This is important because Arsenic may be concentrated in sulfide-minerals, such as pyrite (FeS_2), or adsorbed onto oxides or hydroxides composing the fine portion of the alluvial sediments (Baviskar et al., 2015; Rowland et al., 2007). Peat layers play an important role in the arsenic release mechanism because the degradation of organic matter controls the redox conditions of the aquifer (Carraro et al., 2013, 2015; Rotiroti et al., 2014). From a hydrogeological point of view, two main alluvial hydrogeological units occur in the Venetian Plain: a large unconfined aquifer extending for 15–20 km in the upper part of the plain from the Prealps, and a multi-layered-confined aquifer system in the lower part of the plain towards the Adriatic Sea. These two units correspond, respectively, to the upper and middle–lower plain environments. The plain springs belt (named the "Fontanili" belt) shows the transition zone from the upper plain to the lower plain, where the water table is very shallow and locally intersects the topographic surface. Excluding the northernmost region, the study area is characterized by a succession of silty layers (i.e., low permeability) and sandy layers (i.e., high/medium permeability), where the main aquifers are located (Dal Prà et al. 1992; Fabbri et al. 1993, 2011, 2016; Vorlicek et al. 2004; Cambruzzi et al. 2009; Trevisani and Fabbri 2010; Fabbri and Piccinini 2013; Piccinini et al. 2015, 2016; 2017; Figure 2.3).

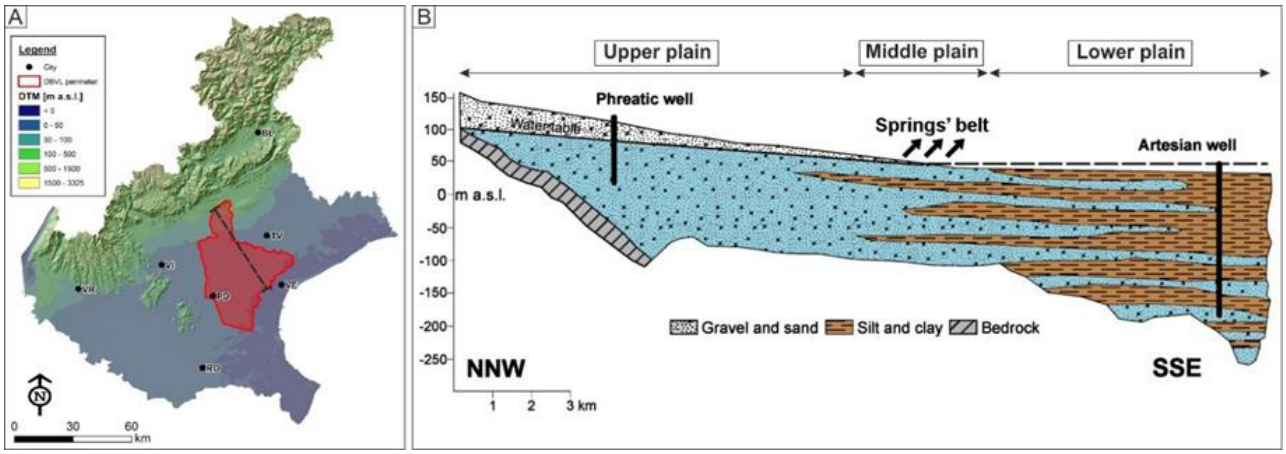

Figure 2.3 - Hydrogeological setting of Venetian alluvial plain (Dalla Libera et al., 2018).

The study area named "Western Agricultural Areas" (WAA, approximately 3.8 km^2, Figure 2.4), used for better understanding and modeling the As hydro-chemical processes, includes all the main geological and hydrogeological features of DBVL. Specifically, it is composed by deposits of the "Mestre's Unit", rich of fine sand, silt and clay (Bondesan et al., 2008; Fontana et al., 2008). The local hydrogeological features are quite similar to the regional scale area, even if the sandy aquifers are locally connected to each other (Fabbri et al., 2013). The WAA are also characterized by the presence of peat layers with lateral extension until some kilometers and

thickness of about some centimeters, in line with peat layers setting of DVBL. The described setting confirmed the fact that those areas are good example of the main geological setting acting within the Venetian alluvial plain.

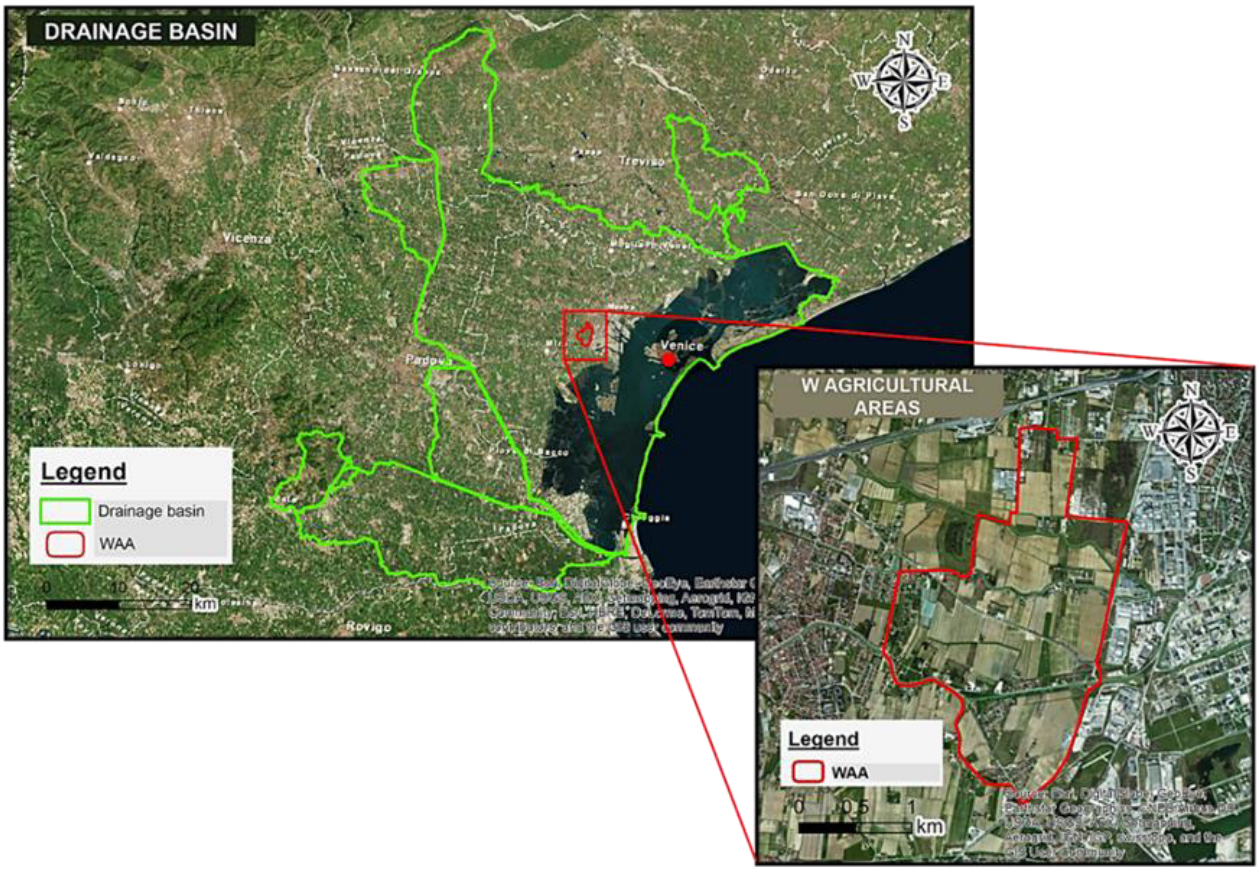

Figure 2.4 - Location and extension of WAA within the DBVL (Dalla Libera MSc thesis)

References

Baviskar, S., Choudhury, R., Mahanta, C., 2015. Dissolved and solid-phase arsenic fate in an arsenic-enriched aquifer in the river Brahmaputra alluvial plain. Environ. Monit. Assess. 187, 93. https://doi.org/10.1007/s10661-015-4277-0

Baviskar, S., Choudhury, R., Mahanta, C., 2015. Dissolved and solid-phase arsenic fate in an arsenic-enriched aquifer in the river Brahmaputra alluvial plain. Environ. Monit. Assess. 187, 93. https://doi.org/10.1007/s10661-015-4277-0

Bondesan A, Meneghel M (2004) Geomorphology of the Venice Prov- ince (in Italian). Esedra, Padova.

Bondesan, A., Primon, S., Bassan, V., Vitturi, A., 2008. Le unità geologiche della provincia di Venezia. Provincia di Venezia, Servizio Geologico e Difesa del Suolo.

Cambruzzi T, Conchetto E, Fabbri P, Marcolongo E, Rosignoli A, Zangheri P (2009) Underground water resources in the Venetian central plains. Rend Online della Soc Geol Ital 6:127–128

Carraro, A., Fabbri, P., Giaretta, A., Peruzzo, L., Tateo, F., Tellini, F., 2013. Arsenic anomalies in shallow Venetian Plain (Northeast Italy) groundwater. Environ. Earth Sci. 70, 3067–3084. https://doi.org/10.1007/s12665-013-2367-2

Carraro, A., Fabbri, P., Giaretta, A., Peruzzo, L., Tateo, F., Tellini, F., 2015. Effects of redox conditions on the control of arsenic mobility in shallow alluvial aquifers on the Venetian Plain (Italy). Sci. Total Environ. 532, 581–594. https://doi.org/10.1016/j.scitotenv.2015.06.003

Dal Prà A, Fabbri P, Bortoletto C (1992) The artesian hydrogeologi- cal system in the central Venetian plain between Treviso and the River Piave and its exploitation. Memorie Sci Geol 44:152–170

Dalla Libera, N., Fabbri, P., Mason, L., Piccinini, L., Pola, M., 2018. A local natural background level concept to improve the natural background level: a case study on the drainage basin of the Venetian Lagoon in Northeastern Italy. Environ. Earth Sci. 77, 487. https://doi.org/10.1007/s12665-018-7672-3

Fabbri P, Ferronato A, Zangheri P (1993) A case of groundwater contamination by organo-chlorine compounds. Hydrogeologie 3:207–215

Fabbri P, Gaetan C, Zangheri P (2011) Transfer function-noise model- ling of an aquifer system in NE Italy. Hydrol Process 25:194–206. https ://doi.org/10.1002/hyp.7832

Fabbri P, Piccinini L (2013) Assessing transmissivity from specific capacity in an alluvial aquifer in the middle Venetian plain (NE Italy). Water Sci Technol 67:2000–2008. https ://doi.org/10.2166/ wst.2013.074

Fabbri P, Piccinini L, Marcolongo E, Pola M, Conchetto E, Zangheri P (2016) Does a change of irrigation technique impact on ground- water resources? A case study in Northeastern Italy. Environ Sci Policy 63:63–75

Fabbri, P., Piccinini, L., 2013. Assessing transmissivity from specific capacity in an alluvial aquifer in the middle Venetian plain (NE Italy). Water Sci. Technol. 67, 2000–2008. https://doi.org/10.2166/wst.2013.074

Fontana, A., Mozzi, P., Bondesan, A., 2004. The geomorphological evolution of the Venetian-Friulian plain. Geomorphol. Venice Prov. Esedra, Padova 113–138.

Fontana, A., Mozzi, P., Bondesan, A., 2008. Alluvial megafans in the Venetian–Friulian Plain (north-eastern Italy): Evidence of sedimentary and erosive phases during Late Pleistocene and Holocene. Quat. Int. 189, 71–90. https://doi.org/10.1016/J.QUAINT.2007.08.044

Mozzi, P., Bini, C., Zilocchi, L., Beccatini, R., Mariotti, Lippi M., 2003. Stratigraphy, palaeopedology and palynology of late Pleistocene and Holocene deposits in the landward sector of the lagoon of Venice (Italy), in relation to Caranto level. Il Quaternario 16 (1 bis), 193–210.

Piccinini L, Fabbri P, Pola M, 2016. Point dilution tests to calculate groundwater velocity, an example in a porous aquifer in NE Italy. Hydrol Sci J. https ://doi.org/10.1080/02626 667.2015.10367 56

Piccinini L, Fabbri P, Pola M, Marcolongo E, 2017. An example of aquifer heterogeneity simulation to modeling well- head protec- tion areas. Ital J Eng Geol Environ Special Issue 103–115

Piccinini L, Fabbri P, Pola M, Marcolongo E, Rossignoli A, 2015. Numerical modeling to well-head protection area delineation, an example in Veneto Region (NE Italy). Rend Online Della Soc Geol Italy 35:232–235. https ://doi.org/10.3301/ROL.2015.108

Rotiroti, M., Sacchi, E., Fumagalli, L., Bonomi, T., 2014. Origin of Arsenic in Groundwater from the Multilayer Aquifer in Cremona (Northern Italy). Environ. Sci. Technol. 48, 5395–5403. https://doi.org/10.1021/es405805v

Trevisani, S., Fabbri, P., 2010. Geostatistical modeling of a heterogeneous site bordering the Venice lagoon, Italy. Ground Water 48, 614–623. https://doi.org/10.1111/j.1745-6584.2009.00632.x

Vorlicek, P.A., Antonelli, R., Fabbri, P., Rausch, R., 2004. Quantitative hydrogeological studies of the Treviso alluvial plain, NE Italy. Q. J. Eng. Geol. Hydrogeol. 37, 23–29. https://doi.org/10.1144/0036-9276/02-006

2.3 Background knowledge on arsenic contamination in DVBL and WAA

The DBVL was fully investigated during the last decades. That area was notoriously affected by groundwater and soil matrix contamination, requiring continuous efforts for understanding the causes and the linked effects. The lower part of DBVL, especially close to the national contaminated site named "SIN di Porto Marghera" (VE), shows several exceeding for different chemicals in both soil and groundwater (i.e.: heavy metals, organic compounds, chlorinated species, etc.). Among them, arsenic (As), iron (Fe) and manganese (Mn) concentrations were carefully investigated, in order to understand their real origin. The origin of these elements is dual as they come from either geogenic background (due to geological processes) or anthropogenic activities (i.e. depressed zone filling, industrial manufacturing and uncontrolled pollution events). The Environmental Protection Agency of Veneto Region (ARPAV) performed several studies on arsenic issue, in order to get knowledges on arsenic distribution and processes that could be involved in its mobility. In this direction, during the 2009, a project named Mo.Sp.As was carried out, and it was one of the first attempts to spatialize the arsenic distribution in groundwater of Mid-Low Venetian Alluvial Plain. This project did not reach the expected results due to the high heterogeneity of the subsurface (ARPAV, 2009). Some years later, several projects were developed in the DBVL area. Thanks to the environmental characterization of SIN of Porto Marghera (ARPAV, 2011) and A.Li.Na project (ARPAV, 2014), new data were gathered to estimate the distribution of As and the main associated elements like Fe, Mn and Ammonic ion (NH_4^+), thus elucidating the origin of their high amount. The results pointed out a patchy distribution of arsenic in the DBVL, occuring even at local scale (e.g.: WAA). This heterogeneous distribution impacts on the environmental management procedures, especially on the Natural Background Level (NBL) definition, requiring new understanding to align themselves with the European Council regulations (GDW, 2006). A patchy distribution of arsenic gets the Authorities in trouble when there are dealing with the NBL definition, since a unique value could be loyally misleading, especially, in those areas with background concentrations constantly above the adopted NBL. In this context some advanced methodologies such as non-linear statistical and geostatistical analyses were applied, which

allowed to enhance the knowledges about groundwater arsenic distribution and to carry out relationships able to explain geochemical mechanisms involved in arsenic mobility. Moreover, the information coupling allowed us to define a new concept named Local NBL (LNBL), keeping into account for geochemical relationships and spatial heterogeneity (Dalla Libera et al., 2017, 2018).

References

ARPAV, 2009. Progetto Mo.Sp.As – Monitoraggio sperimentale dello ione arsenico nelle acque sotterranee della media e bassa pianura veneta. Technical report, n. 17/2009.

ARPAV, 2011. INDAGINE AMBIENTALE "AREE AGRICOLE" - macroisola aree agricole – zona ovest, macroisola fusina – aree lungo naviglio brenta - sintesi dei risultati del piano di investigazione iniziale. Report data presentation.

ARPAV, 2014. ALiNa – Analysis of the Natural Background Level for Some Compounds Within the Groundwater of the Shallow Aquifer in the Drainage Basin to the Venice Lagoon (Brenta River Alluvial System) – Report and Data Presentation.

Dalla Libera, N., Fabbri, P., Mason, L., Piccinini, L., Pola, M., 2017. Geostatistics as a tool to improve the natural background level definition: An application in groundwater. Sci. Total Environ. 598, 330–340. https://doi.org/10.1016/j.scitotenv.2017.04.018

Dalla Libera, N., Fabbri, P., Mason, L., Piccinini, L., Pola, M., 2018. A local natural background level concept to improve the natural background level: a case study on the drainage basin of the Venetian Lagoon in Northeastern Italy. Environ. Earth Sci. 77, 487. https://doi.org/10.1007/s12665-018-7672-3

GWD (2006) Groundwater Directive 2006/118/CE, Directive of the European Parliament and of the Council on the protection of groundwater against pollution and deterioration, OJ L372, 27/12/ 2006, pp 19–31

2.3.1 Paper 1

Natural Arsenic in groundwater in the drainage basin to the Venice lagoon (Brenta Plain, NE Italy): the organic matter's role

Authors: Nico Dalla Libera[a], Paolo Fabbri[a], Leonardo Piccinini[a], Marco Pola[a], Leonardo Mason[b]

a) Dipartimento di Geoscienze, Università di Padova, Via G. Gradenigo, 6 - 35131 Padova, Italy.

b) SCA - U.O. Sito Interesse Nazionale, ARPAV Dipartimento di Venezia, Via Lissa 6 - 30171 Venezia, Mestre – Italy.

Status: Published in "Rendiconti Online della Società Geologica Italiana" (ROL - Vol. 41 (2016), pp. 30-33, 2 figs., doi: 10.3301/ROL.2016.85).

Abstract

The aim of the article is to show the role of the redox potential and of the ammonium ion concerning the release of arsenic into groundwater from naturally occurring sources. The study is carried out on both regional and local scale. The former is performed on the area of the drainage basin to the Venice lagoon (DBVL), while the latter interests a sub-area near the Porto Marghera contaminated sites of national interest, named "Agricultural west areas" (AWA). The results of the work will elucidate the processes continuity at different scales.

Key words: Arsenic, groundwater pollution, Veneto Region (NE, Italy), redox potential, ammonium ion.

Introduction

The arsenic groundwater pollution is a worldwide problem affecting many countries located in alluvial plains (e.g., USA, Vietnam, Hungary, Spain, Bangladesh and India), and it is object of many studies. The rising demand of drinkable water cannot be accomplished by surface-water, increasing the exploitation of groundwater. For instance, the demand for drinking water in Bangladesh and Bengal Delta (India) caused the increment of arsenic water contamination, producing some health issues due to arsenic poisoning (Nordstrom, 2002). Arsenic is not widespread in the Earth's continental crust. It is commonly concentrated in sulphide-bearing mineral deposits associated with Pyrite (FeS_2), Arsenopyrite (FeAsS), Realgar (AsS), Orpiment (As_2S_3) or Fe-Mn oxyhydroxides (i.e.: goethite, ferrihydrite, hematite) Furthermore, many geothermal waters can exceed the contamination threshold of 10 µg/l suggested by the Drinking Water Directive (DWD, 98/83/CE). Arsenic is a metalloid that has two form: the first one is oxidized with an oxidation number (ON) equal to +5, whereas the second one is reduced with ON equal to +3. The reduced form seems to be more mobile than the oxidized one in aqueous medium, even if both species have a good mobility. The arsenic toxicity is due to its affinity with Phosphorus, because As can replace P into metabolic processes like RNA and DNA

synthesis. The pollution of As is also diffused in the middle-low Venetian plain, where arsenic represents one of the most problematic contaminants. In particular, some zones of the middle-low Venetian plain across the Brenta River show As contents exceeding the Contamination Thresholds Values (CTVs), corresponding to CSC (10 μg/l) in the Italian legislation (D.Lgs. 152/06). Locally, an excess of the natural background levels (NBLs = 74 μg/l), suggested by the "A.Li.Na" study (ARPAV, 2014), occurs. This work is focused on the possible geochemical relationships that can influence arsenic release in the shallower aquifers (5-20 m below ground level). As pointed out by many studies (Carraro et al., 2013; Carraro et al., 2015), As often is adsorbed into both the Fe-Mn oxides or hydroxides and the organic matter. The dissolution of these minerals in acid-reduced environment causes arsenic desorption processes, exceeding its CTVs. Moreover, the organic matter could be a source of As contamination in addition to its role of redox potential (Eh) driver (Rotiroti et al., 2014; Molinari et al., 2015). As a matter of fact, a batch experiment made on an area around Bologna (Po Plain) showed the organic matter capacity to release arsenic under reducing conditions (low values of Eh; Molinari et al., 2013). Therefore, arsenic release in groundwater is influenced by the variation of both physical and chemical parameter like Eh and pH, as well as by the presence of elements and compounds such as phosphate anions, that can promote the desorption processes. The DBVL area is located in the Brenta alluvial system, in the low Venetian plain, extending on the provinces of Padua, Treviso and Venice. It covers about 2038 km2, with a topographic gradient ranging from 0.6% to 0.1% close to the Venice lagoon. From the geological point of view, the area is composed by sandy alluvial deposits in the upper part, near the springs belt, whereas in the distal part it is formed by silty clayey deposits (e.g., Vorlicek et al., 2004 Fabbri et al., 2011; Fabbri & Piccinini, 2013; Piccinini et al., 2015; Piccinini et al., 2016.). About the hydrogeological background, the drainage basin to the Venice lagoon is characterized by the presence of many silty clay layers with lower conductivity alternated to sandy permeable ones, containing the main aquifers (Fig. 1). The local scale area named "Agricultural west areas" (approximately 3,8 km2) is composed by deposits of the "Mestre's Unit", rich of fine sand, silt and clay. The local hydrogeological features are quite similar to the regional scale area, even if the sandy aquifers are locally connected to each other (Fabbri et al., 2013). Furthermore, both areas are characterized by the presence of peat layers with lateral extension until some kilometers and thickness of about some centimeters.

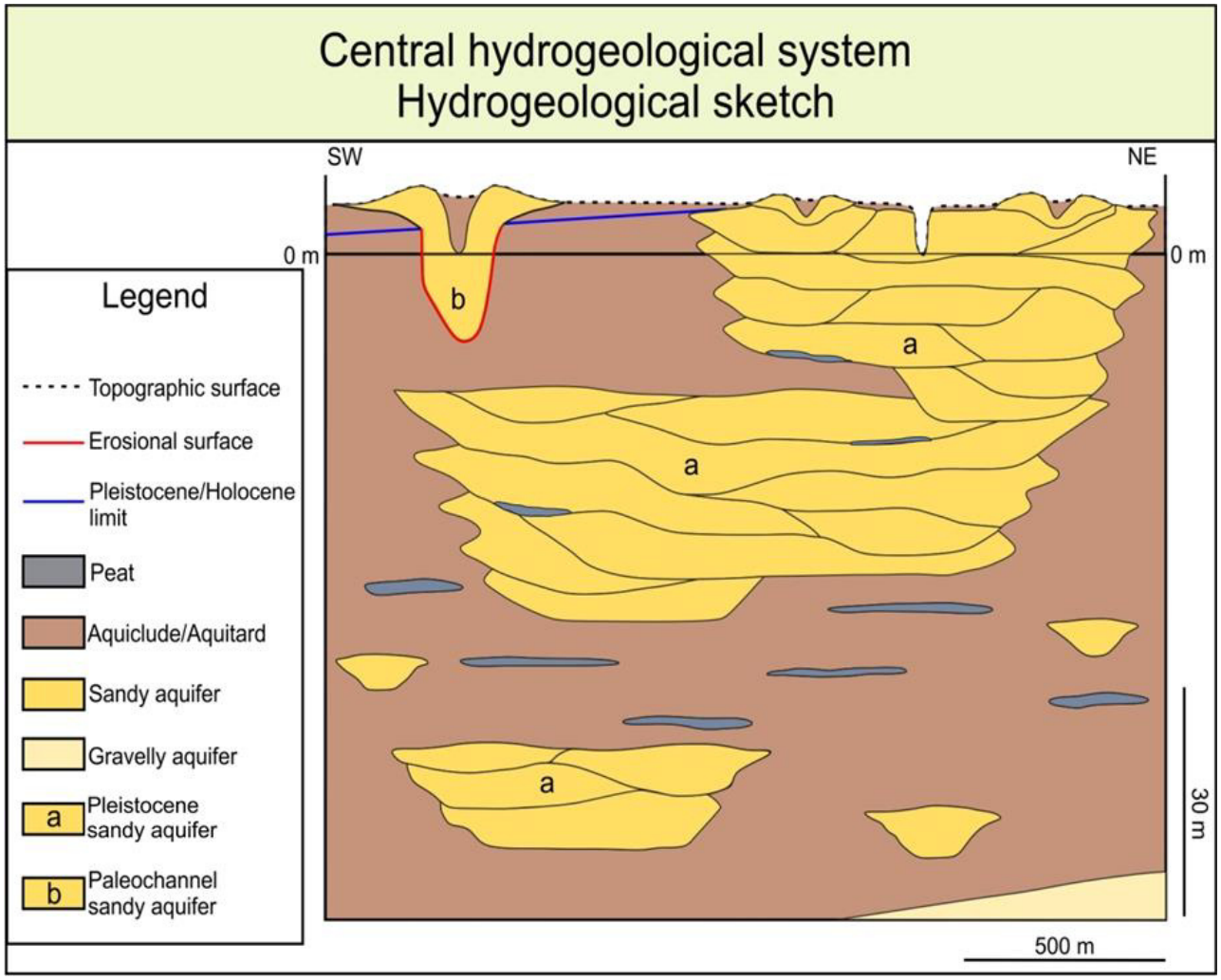

Fig. 1 -Hydrogeological sketch section that explains the structure of the aquifers in the studied area (Fabbri et al., 2013).

Materials and Methods

The dataset

Two datasets were used in this work, the first referred to the DBVL and the second one referred to AWA. These datasets report chemical composition of the shallow aquifer groundwater (5-20 m b.g.l.) and the related geographical information. The two datasets were processed apart because the data were collected in different periods. The regional dataset, named "A.Li.Na", was made by Regional Environmental Agency (ARPAV) during the period 2013-2014 to define the natural background values of As, Fe, Mn and Ammonium (NH_4^+). The samples come from 50 piezometers located into the drainage basin to the Venice lagoon (DBVL). The sampling was done during four seasonal surveys. The Eh was collected in-situ by multi-parametric probes (mod. YSI 556 MPS), whereas the element's concentrations were determined in laboratory (for

As UNI EN ISO 17294-2:2005 and for NH4+ APAT-IRSA CNR 4030 A1). The original dataset was homogenized coding the values below the Limit of Quantification (LOQ) by a number equal to half of LOQ, and if necessary estimating physical-chemical missing values by statistical methods. The second dataset, named "Agricultural West Areas", was made by ARPAV from 2009 to 2011 for a local characterization study. The sampling network is composed by 40 piezometers, but only 34 piezometers that reach the shallow aquifer were used in this work. This dataset was homogenized as the first one.

Data processing

The applied methodology involves: i) exploration of As-Eh relationship for the two areas through the use of correlation scatterplots; ii) exploration of As-NH_4^+ relationship by the use of the same scatterplots; iii) collection of information about the presence of peat layers into the aquifer or around it from stratigraphic logs.

Result

Looking at the arsenic Pourbaix diagram in Fig. 2A, we can note that the major part of the As data correspond to reducing Eh values. Reduction of As(V) to As(III) contributes to enhance its mobilization.. The As release interval comes from 0 mV to -200 mV for "A.Li.Na" dataset (Fig. 2B), whereas the Eh release interval ranges from +50 mV to -150 mV for "Agricultural West Areas" dataset (Fig. 2C). Both areas show, more or less, the same behavior. As already pointed out, the arsenic concentration decreases significantly below the Eh threshold of -200 mV, probably linked to the co-precipitation of As such as As-sulphides (Carraro et al., 2015). In these conditions, the presence of Sulphur is strictly connected with the organic matter (OM) availability (i.e., peat layers) coming from degradation processes. The relationship between As and NH_4^+ concentrations (Pola & Fabbri, 2009; semi-log type, Fig.2D) shows that the increase of ammonium concentrations seems to be associate to the As presence. Ammonium ion is a compound that derives from the degradation of OM in reduced conditions (Molinari et al., 2012). In addition, it is a good marker to show the presence of peat in/or around the investigated aquifer and to confirm the reduced conditions. The Eh and NH_4^+ seem to be related to the As, although they are not the only involved hydro-geochemical parameters (i.e. Sulphate; Carraro et al., 2015). Moreover, peat not only drives the redox condition, but it also acts as a source of arsenic. Arsenic could be adsorbed onto OM through chemical adsorption processes (Molinari et al., 2015).

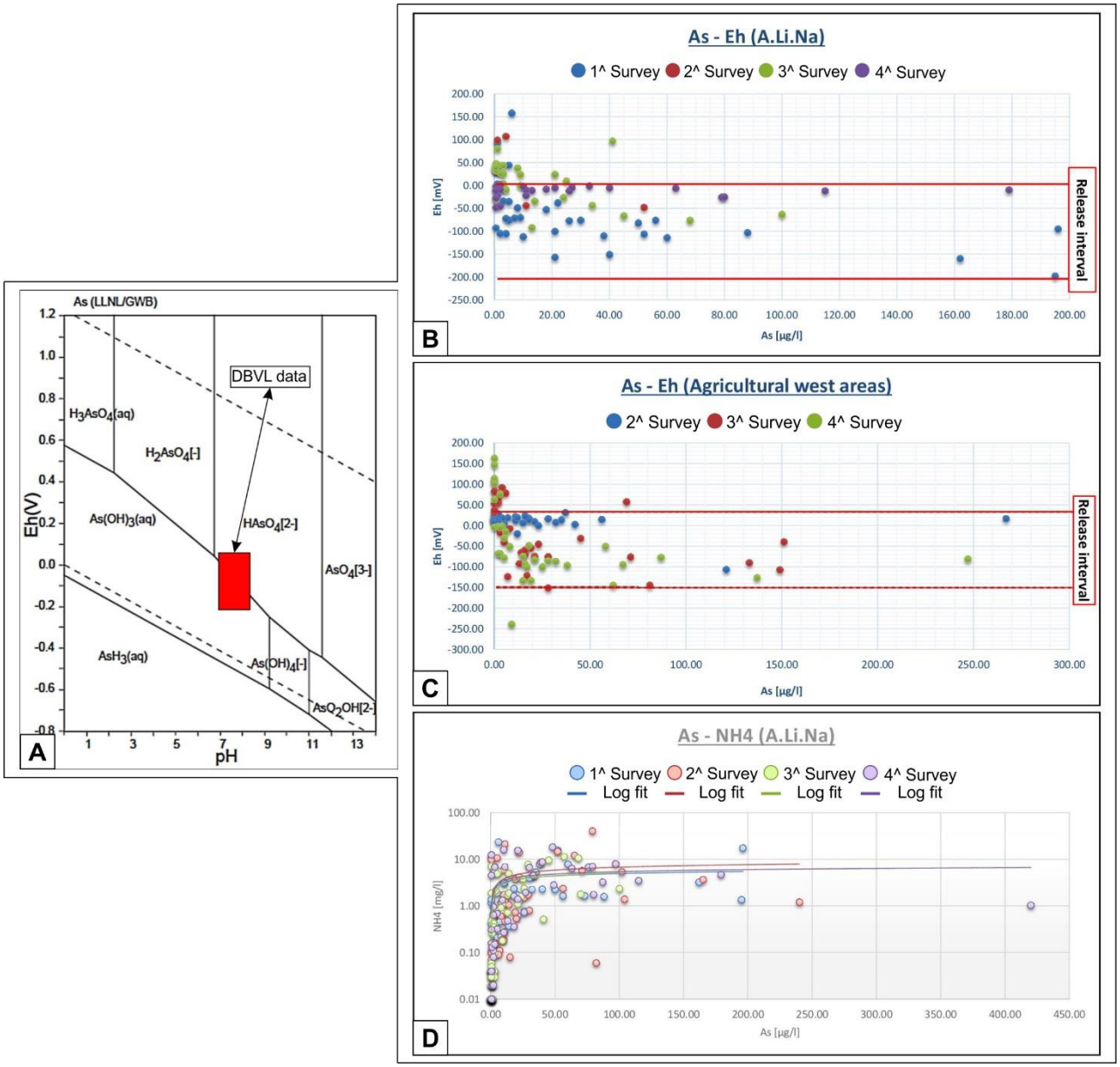

Fig. 5 - Geochemical relationships: A) Theoretical Eh-pH diagram for Arsenic, the red box represents the Eh-pH interval of the considered data. B) Scatterplot that show the relationship between arsenic (As) and Eh, it's referred to DBVL area. C) Scatterplot for the relationship As-Eh referred to the "Agricultural West Areas". D) Scatterplot that denotes the relationship between arsenic and ammonium ion; the increase of ammonium confirms the degradation of the organic matter under reduced condition, producing arsenic release.

Conclusion

The natural release of arsenic in the groundwater is linked to the presence of reducing conditions into aquifers. In fact, the arsenic reduced species is more soluble than the oxidized one in acidic and reducing environmental conditions (Fig. 2A). The primary process that drives the natural As concentrations in the studied areas is the degradation of the organic matter (peat layers), which can occur into or around the investigated shallow aquifer. In particular, Arsenic

is released from Fe-Mn oxides or hydroxides, composing the aquifer reservoir sediments, via redox processes that interest peat degradation. This degradation can be depicted by the increase of ammonium produced by the degradation of peat organic nitrogen. The relationships found by this study confirm the arsenic behavior in presence of organic matter and in reducing environment, as already shown in previous studies focused on this environmental problem. Therefore, these processes can produce an arsenic enrichment in groundwater of the great alluvial plains like the Venetian plain, exceeding the contamination threshold of 10 μg/l. In conclusion, these correlations could be used to improve the decisional processes related to environmental management, decontamination procedures and/or drinking water management.

Acknowledgements

We thank the ARPAV agency to have shared their data about arsenic groundwater contamination into the DBVL and Porto Marghera area.

References

ARPAV (2014) - Progetto A.Li.Na. – Analisi dei Livelli di fondo Naturale per alcune sostanze presenti nelle acque sotterranee della falda superficiale dell'acquifero differenziato del bacino scolante in laguna di Venezia (bacino deposizionale del Brenta) – presentazione dei dati e determinazione dei livelli di fondo. Servizio Osservatorio Acque interne, Padova, 31 pp.

Carraro A., Fabbri P., Giaretta A., Peruzzo L., Tateo F. & Tellini F. (2015) - Effects of redox conditions on the control of arsenic mobility in shallow alluvial aquifers on the Venetian Plain (Italy). Sci. Total Environ. 532, 581-594. DOI: 10.1016/j.scitotenv.2015.06.003

Carraro A., Fabbri P., Giaretta A., Peruzzo L., Tateo F. & Tellini F. (2013) - Arsenic anomalies in shallow Venetian Plain (Northeast Italy) groundwater. Environ. Earth Sci. 70, 3067-3084. DOI: 10.1007/s12665-013-2367-2

Fabbri P. & Piccinini L. (2013) - Assessing Transmissivity from Specific Capacity in an Alluvial Aquifer in the Middle Venetian Plain (NE, Italy). Water Sci. Technol., 67, 9, 2000-2008. DOI: 10.2166/wst2013.074

Fabbri P., Gaetan C. & Zangheri P. (2011) - Transfer functionnoise modelling of an aquifer system in NE Italy. Hydrol. Process., 25, 194-206. DOI: 10.1002/hyp.7832

Fabbri P., Zangheri P., Bassan V., Fagarazzi E., Mazzucato A., Primon S. & Zogno C. (2013) - Sistemi idrogeologici della Provincia di Venezia: Acquiferi superficiali. Cierre Grafica, Verona, 288 pp.

Molinari A., Guadagnini L., Marcaccio M. & Guadagnini A. (2015) - Arsenic fractioning in natural solid matrices sampled in a deep groundwater body. Geoderma, 247–248, 88-96. DOI: 10.1016/j.geoderma.2015.02.011

Molinari A., Guadagnini L., Marcaccio M., Starface S., Sanchez-Vila X. & Guadagnini A. (2013) - Arsenic release from deep natural solid matrices under experimentally controlled redox conditions. Sci. Total Environ. 444, 231-240. DOI: 10.1016/j.scitotenv.2012.11.093

Molinari A., Guadagnini L., Marcaccio M. & Guadagnini A. (2012) - Natural background levels and threshold values of chemical species in three large-scale groundwater bodies in Northern Italy. Sci. Total Environ. 425, 9-19. DOI: 10.1016/j.scitotenv.2012.03.015

Nordstrom D.K. (2002) - Worldwide occurrences of arsenic in groundwater. Science, 296, 5576, 2143-2145. DOI: 10.1126/science.1072375

Piccinini L., Fabbri P. & Pola M. (2016) - Point dilution tests to calculate groundwater velocity: an example in a porous aquifer in NE Italy. Hydrolog. Sci. J., DOI: 10.1080/02626667.2015.1036756

Piccinini L., Fabbri P., Pola M., Marcolongo E. & Rosignoli A. (2015) - Numerical modeling to well-head protection area delineation, an example in Veneto Region (NE Italy). Rend. On-line Soc. Geol. It., 35, 232-235, DOI: 10.3301/ROL.2015.108.

Pola M. & Fabbri P. (2009) - Studio geostatistico sulla distribuzione dell'ammoniaca nella pianura veneziana. Rend. Online Soc. Geol. It., 6, 382-383.

Rotiroti M., Sacchi E., Fumagalli L. & Bonomi T. (2014) - Origin of Arsenic in groundwater from the multilayer aquifer in Cremona (Northern Italy). Environ. Sci. Technol., 48, 5395-5403. DOI: 10.1021/es405805v.

Vorlicek P.A., Antonelli R., Fabbri P. & Rausch R. (2004) - Quantitative hydrogeological studies of Treviso alluvial plain (north east of Italy). Q. J. Eng. Geol. Hydroge., 37, 23-29. DOI: 10.1144/0036-9276/02-006.

2.3.2 Paper 2

Geostatistics as a tool to improve the natural background level definition: An application in groundwater

Authors: Nico Dalla Libera[a], Paolo Fabbri[a], Leonardo Mason[b], Leonardo Piccinini[a], Marco Pola[a]

a) Dipartimento di Geoscienze, Università di Padova, Via G. Gradenigo, 6 - 35131 Padova, Italy.

b) SCA - U.O. Sito Interesse Nazionale, ARPAV Dipartimento di Venezia, Via Lissa 6 - 30171 Venezia, Mestre – Italy.

Status: Published in "Science of the Total Environment" 598 (2017) 330 – 340 (http://dx.doi.org/10.1016/j.scitotenv.2017.04.018)

Abstract

The Natural Background Level (NBL), suggested by UE BRIDGE project, is suited for spatially distributed datasets providing a regional value that could be higher than the Threshold Value (TV) set by every country. In hydro-geochemically dis-homogeneous areas, the use of a unique regional NBL, higher than TV, could arise problems to distinguish between natural occurrences and anthropogenic contaminant sources. Hence, the goal of this study is to improve the NBL definition employing a geostatistical approach, which reconstructs the contaminant spatial structure accounting geochemical and hydrogeological relationships. This integrated mapping is fundamental to evaluate the contaminant's distribution impact on the NBL, giving indications to improve it. We decided to test this method on the Drainage Basin of Venice Lagoon (DBVL, NE Italy), where the existing NBL is seven times higher than the TV. This area is notoriously affected by naturally occurring arsenic contamination. An available geochemical dataset collected by 50 piezometers was used to reconstruct the spatial distribution of arsenic in the densely populated area of the DBVL. A cokriging approach was applied exploiting the geochemical relationships among As, Fe and NH_4^+. The obtained spatial predictions of arsenic concentrations were divided into three different zones: i) areas with an As concentration lower than the TV, ii) areas with an As concentration between the TV and the median of the values higher than the TV, and iii) areas with an As concentration higher than the median. Following the BRIDGE suggestions, where enough samples were available, the 90th percentile for each zone was calculated to obtain a local NBL (LNBL). Differently from the original NBL, this local value gives more detailed water quality information accounting the hydrogeological and

geochemical setting, and contaminant spatial variation. Hence, the LNBL could give more indications about the distinction between natural occurrence and anthropogenic contamination.

Keywords: Local Natural Background Level (LNBL), cokriging (COK), Arsenic and Drainage Basin to the Venice Lagoon (DBVL).

Introduction

The assessment of the groundwater quality and the impact of the human activities are important worldwide challenges. Actually, the assessment of groundwater body qualitative status is related to the definition of Natural Background levels (NBLs) and Threshold values (TVs). The first one is mainly linked to the hydro-geochemical settings of the aquifer, while the second is associated to the public health issue. The NBL definition is a well-known problem due to its complexity, its challenging estimation and the delicate consequences on the environmental protection. The NBL of an element or compound in groundwater represents the range of concentrations resulting from the interaction of different natural atmospheric, geological, chemical and biological process during the hydrological cycle, and it could be influenced by human activities (Edmunds and Shand, 2008; Hinsby et al., 2008a; Reimann and Garrett, 2005). By defining the NBL, it is necessary to know the extension and the hydro-geochemical characteristics of the examined groundwater body, paying attention to collect pristine water samples of the same aquifer body far from anthropogenic sources of contamination (Coetsier et al., 2009; Hinsby et al., 2008; Wendland et al., 2008). Many studies treat the problem of the NBL definition testing different approaches for its estimation (Coetsier et al., 2009; Ducci et al., 2016; Molinari et al., 2012; Preziosi et al., 2010; Rotiroti et al., 2013, 2015), since the NBL assumes importance discriminating the anthropogenic contamination from the natural occurrence. A first approach to estimate the NBL value into European groundwater bodies was suggested by Edmunds and Shand (2008), and it was based on a geochemical prospective rather than a statistical one. Actually, the European Community in accordance with the European "BRIDGE" project (Background cRiteria for the Identification of Groundwater thrEsholds; Müller et al., 2006) suggests two main statistical method to estimate the NBL. The first approach, the "Component Separation" method (CP), is based on the distinguishable data distributions produced by the natural and anthropogenic sources that can be unraveled by a statistical analysis. In this approach, the observed concentration frequency distribution is fitted by the superimposition of two different distributions that represent the

natural and the anthropogenic concentrations. Once the distribution (shape and statistical parameters) of the natural component is assessed, the related data are used to estimate the NBL. On the other hand, the second method suggests a pre-selection of the data basing on some markers' concentrations that point an anthropogenic contamination out (e.g. nitrate, salinity, etc.). The basic idea of this method is that there is a correlation between the markers' concentrations and the presence of an anthropogenic pressure. Thus, where the markers show concentration values over the pre-defined limits, the groundwater samples are excluded from the NBL estimation. Subsequently, the NBL is estimated as the 90th or 97th percentile of the modified distribution of the concentration data for both methods (Coetsiers et al., 2009; Müller et al., 2006; Wendland et al., 2008b). These approaches give a unique NBL value for the entire area, which seems to be not capable to represent the local variation of the geochemical and environmental conditions. The definition of a unique NBL value for a large area, in fact, could make a considerable uncertainty defining the contaminant's natural occurrence against an anthropogenic source. Considering both the importance of the health problem related to the contaminant natural occurrence and the complexity to define an exhaustive NBL value, this study aims to improve the NBL concept by using geostatistical methodology such as cokriging predictor (COK). This method, like other types of kriging, allows redefining the NBL as function of the spatial distribution of contaminant concentration. However, the COK keeps also in consideration the relationships among the target contaminant and other, geochemically related, dissolved species in groundwater. This methodology is applied on the case of the Drainage Basin of the Venice lagoon (DBVL) notoriously affected by both high natural and anthropic concentrations of arsenic. Furthermore, the Regional Agency for Environmental Protection and Prevention of Veneto (ARPAV) through the "A.Li.Na" project (ARPAV, 2014) estimated an arsenic NBL of 74 μg/L that is seven times higher than the Threshold Value (TV=10 μg/L) defined by the annex III in the Commission Staff Working report of the EU's Groundwater Directive (GWD 2006/118/EC). However, the results of this project pointed out the importance of a detailed and local NBL accounting the complex and laterally variable geological and hydro-chemical settings. The results of our study could be useful to improve the definition of the NBL because it exploits the knowledge about the spatial structure and uncertainty of the naturally occurring contaminant into groundwater, giving a local detail that considers the environmental background. In addition, they could be used by the stakeholders to perform a completer and more explanatory plan for the environmental management.

Knowledge about arsenic contamination

High arsenic concentrations in groundwater have been documented in several countries, such as Bangladesh, India (McArthur et al., 2001; Nickson et al., 1998, 2000), Vietnam (Fendorf et al., 2010), Hungary and the USA (Sorg et al., 2014; Welch et al., 2000). The natural occurrence of arsenic in these countries is often linked to the alluvial plain systems, but high arsenic concentrations can be found in volcanic environments or mining districts (e.g., Argentina, Chile, Brazil, Ethiopia, Greece and Italy) (Nordstrom, 2003; Rango et al., 2013). In Italy, high natural concentrations of arsenic in groundwater have been documented in volcanic aquifers of the central and southern Italy related to the uprising of geothermal fluids (Baiocchi et al., 2011; Ducci et al., 2016; Preziosi et al., 2010). Furthermore, in northern Italy, a high arsenic concentration can be found in the alluvial aquifers of the Po Plain (Molinari et al., 2013; Rotiroti and Fumagalli, 2013; Rotiroti et al., 2014; Zavatti et al., 1995) and the Venetian Plain (Carraro et al., 2013; Ungaro et al., 2008). Few materials (e.g., gold or sulfide mineral deposits, volcanogenic sources, alluvial sediments and organic matter) are currently recognized as significant sources of arsenic or drivers for its mobilization in groundwater. Nevertheless, the occurrence of arsenic in groundwater could be caused by anthropic activities, such as mineral extraction, industrial processes or fertilizer use. Arsenic is a metalloid that has three oxidation states nevertheless the most common forms in groundwater are the followings: the first is oxidized with an oxidation number (ON) equal to + 5, whereas the second is reduced with an ON equal to + 3. The reduced form appears to be more movable than the oxidized form in an aqueous medium, although both species have good mobility. The arsenic toxicity is due to its affinity to Phosphorus (P) that could be replaced by arsenic (As) in the metabolic processes of RNA and DNA synthesis. Arsenic is not widespread in the Earth's continental crust but is commonly concentrated in sulfide-bearing mineral deposits associated with Pyrite or Fe-hydroxides. Furthermore, many geothermal waters naturally exceed the TV of 10 μg/L. As determined in many studies, arsenic often is adsorbed onto Fe-Mn oxides or hydroxides, as well as into the organic matter (Baviskar et al., 2015; Carraro et al., 2015; McArthur et al., 2004, 2001, Molinari et al., 2015, 2013; Nickson et al., 2000; Rowland et al., 2007). Dissolution of these minerals in an acid-reducing environment causes the desorption processes that enable the release of As in an aqueous medium, exceeding its threshold value (McArthur et al., 2016; Smedley and Kinniburgh, 2002). Therefore, the organic matter could be a source of As, in addition to its role as a redox driver (Rotiroti et al., 2014). In particular, the release of As in groundwater is influenced by the variation of physical and chemical parameters, such as the Oxidation-Reduction Potential (ORP) and pH (Smedley and Kinniburgh, 2002; Sorg et al., 2014),

as well as the presence of elements and compounds that can promote its release (e.g., NO_3^-, NH_4^+, HCO_3^-, SO_4^{2-}, PO_4^{3-}) (Biswas et al., 2014).

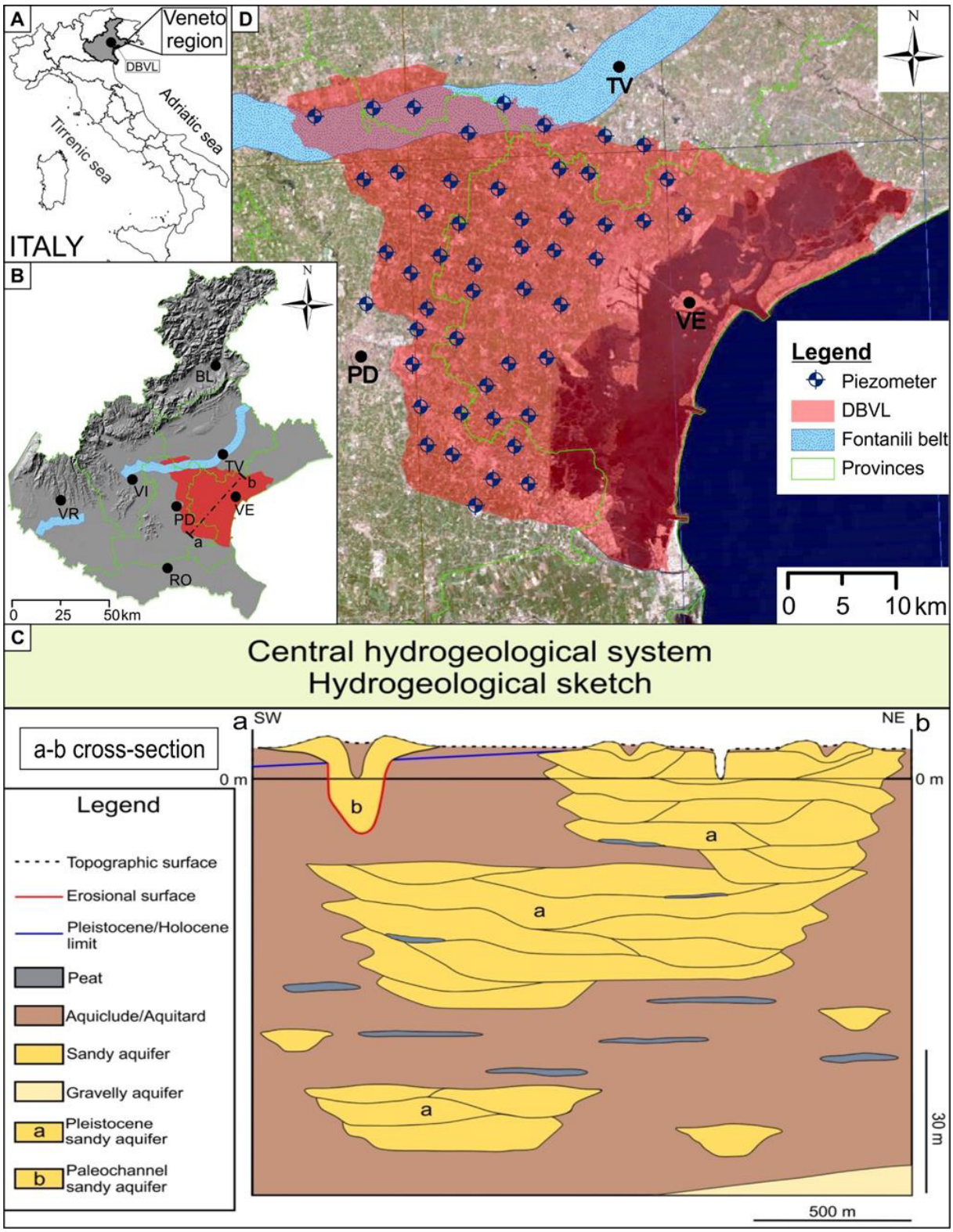

Figure 1 - A) The location of the Veneto region in Italy; B) The location of the study area in the Veneto region. The main municipalities of the Region are also reported (PD: Padua; RO: Rovigo; TV: Treviso; VE: Venice; VI: Vicenza; VR: Verona) C) A hydrogeological sketch of the low Venetian Plain along the "a-b cross-section"; D) The piezometer

locations in the DBVL. All of the piezometers are in the shallow aquifer, between 10 and 20 meters below ground level (BGL).

Geological and hydrogeological settings

The study area is located in the middle-low Venetian Plain, including the Padua, Treviso and Venice provinces. The area covers approximately 2038 km^2 with a topographic gradient ranging from 0.6% to 0.1% near the Venice lagoon (Figure 1A, B). Two primary alluvial hydrogeological units occur in the Venetian plain: a large unconfined aquifer extending 15-20 km in the upper region of the plain from the foot of Prealps, and a multi-layered confined aquifer system in the lower region of the plain towards the Adriatic Sea. These two units correspond, respectively, to the upper and middle-lower plain environments. The plain spring's belt (named the "Fontanili" belt) shows the transition from the upper plain to the lower plain, where the water table is very shallow and locally intersects the topographic surface. From a geological perspective, the Venetian plain comprises gravelly and sandy alluvial deposits in the upper region near the "Fontanili" belt and silty-clayey deposits in the distal region (upper Pleistocene – Holocene) (Bondesan et al., 2004; Fontana et al., 2004, 2008; Mozzi et al., 2003). These fine sediments often contain peat layers formed in a floodplain environment, with a thickness of decimeters and a lateral extension of kilometers. The Drainage Basin to the Venice Lagoon (DBVL) extends to the lower plain environment, alternating silty layers with low permeability and sandy permeable layers, where the primary aquifers are located (Cambruzzi et al., 2009; Dal Prà et al., 1992; Fabbri and Piccinini, 2013; Fabbri et al., 2011, 2013, 2016; Piccinini et al., 2015, 2016; Vorlicek et al., 2004) (Figure 1C). The subsoil structure of the DBVL is heterogeneous due to complex and multiple alluvial sedimentation processes (Trevisani and Fabbri, 2010) that may influence the spatial distribution of As-bearing materials. This is important because Arsenic may be concentrated in sulfide-minerals, such as Pyrite (FeS_2), or adsorbed onto oxides or hydroxides composing the fine portion of the alluvial sediments (Baviskar et al., 2015; Rowland et al., 2007). Therefore, the peat layers play an important role in the arsenic release mechanism because the degradation of the organic matter controls the aquifer's redox conditions and the thus the dissolution of these As bearing minerals (Rotiroti et al., 2014).

Materials and methods

Dataset

The data used in this work was obtained from the "A.Li.Na" project, which was developed to estimate the natural background levels (NBLs) of As, Fe, Mn and NH_4^+ in the groundwater of the DBVL, according to the pre-selection method suggested by BRIDGE project. The hydro-geochemical sampling network (50 piezometers) was established with a variable spacing grid, covering all of the investigated area (Figure 1D). The sampled piezometers, used for NBL definition, are located far from the anthropogenic pollutant sources in order to obtain some pristine water samples. The piezometers tap the shallow aquifer at a depth of 10 – 20 meters below ground level (BGL). The hydro-geochemical parameters were collected during four seasonal surveys conducted from 2013 to 2014. The groundwater sampling was performed according to the standard protocols established by the Italian Environment Protection and Technical Services Agency (APAT, 2006). In addition, the physical parameters (e.g., pH, ORP, electric conductivity, temperature and dissolved oxygen) were measured by a multi-parametric probe YSI mod. 556 MPS. The chemical parameters were estimated in the laboratory through standardized methods. Arsenic and Manganese were estimated by the UNI EN ISO 17294-2:2005 (revised by ISO 17294-2:2016) method, Iron by the APAT CNR IRSA 3160 Man 29 2003 method and Ammonium by the APAT CNR IRSA 4030 A1 Man 29 2003 method (APAT, 2003). Furthermore, each sampling point was georeferenced in the Gauss-Boaga coordinate system (Roma 1940 datum, West zone). According to BRIDGE suggestions, the data were processed to estimate the average values from each available concentration time series, in order to create an average dataset that depicts the average system behavior. Afterwards, the concentration values below the limit of quantification (i.e., As < 1 μg/L) were changed to make the entire "A.Li.Na" dataset suitable for mapping purposes. In such a case, the As concentrations below this limit were set equal to 0.5 μg/L. The water samples show high concentrations of arsenic in reducing environments and often in association with rich organic matter reservoirs (Carraro et al., 2015; Molinari et al., 2015; Rotiroti et al., 2014), according with the geological genesis of the area. Looking at the Figure 2, the major part of the arsenic data shows an ORP values from 0 mV to -150 mV and a pH between 7 and 8 according with the releasing as reduced forms.

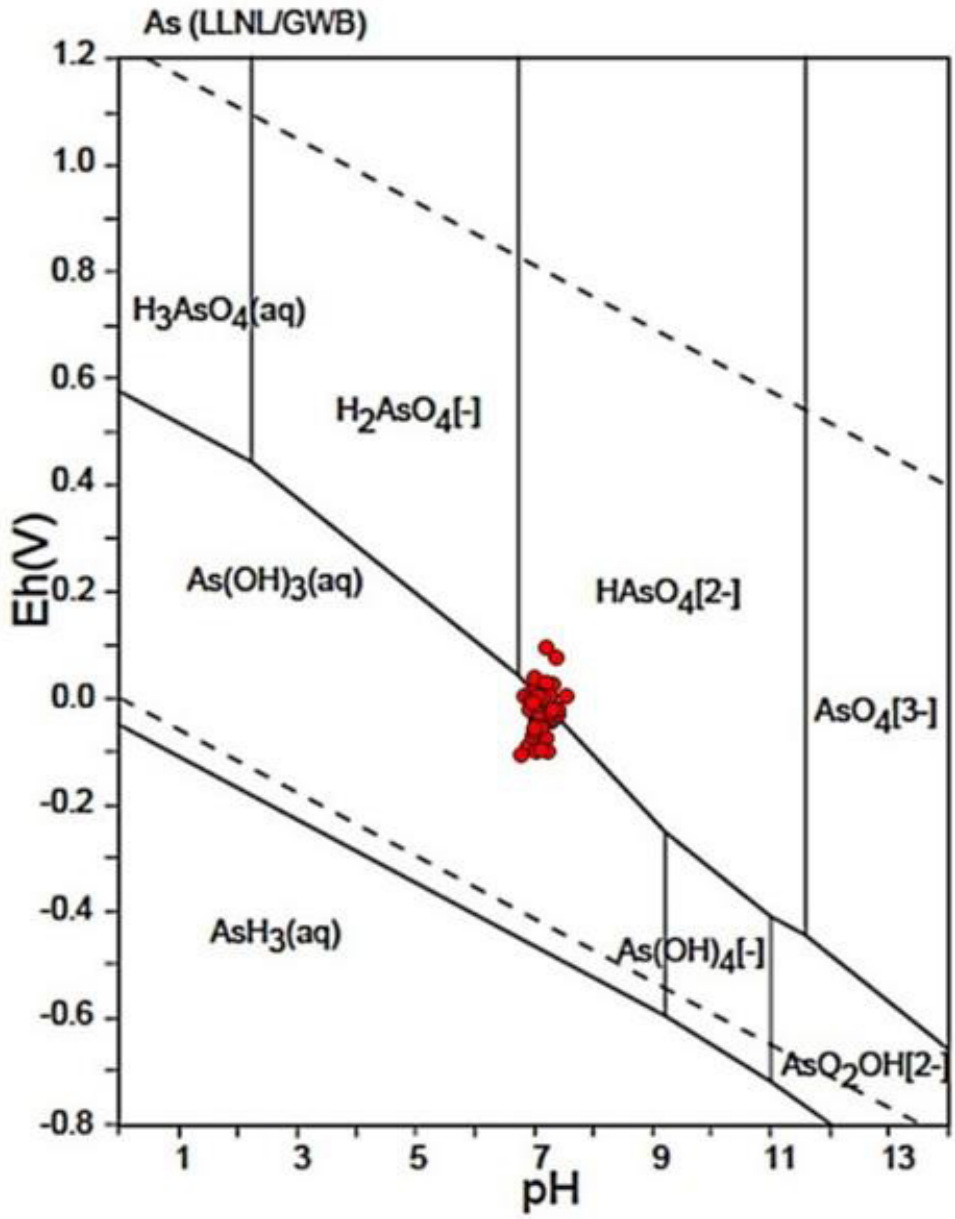

Figure 2 - A Pourbaix diagram of Arsenic species built under the conditions of T = 298.15 [°K] and P = 105 [Pa]. The red dots represent the experimental data used for this study. The majority of the sample data falls into the arsenic reduced species stability field (Takeno, 2005).

Geostatistical methods

The arsenic concentration in groundwater is linked to complex hydro-geochemical processes not yet well understood, hence its distribution in groundwater can be more usefully approached by geostatistical methods than by deterministic ones (e.g., Inverse Distance Weighting and Natural Neighbors). The geostatistical kriging predictor is based on a mixed model [1]:

$$\hat{Z}(\boldsymbol{u_i}) = R(\boldsymbol{u_i}) + m(\boldsymbol{u_i}) \quad [1].$$

Where the predicted concentration $\hat{Z}(\boldsymbol{u_i})$, at location $\boldsymbol{u_i}$, is composed of a residual component $R(\boldsymbol{u_i})$ plus the mean $m(\boldsymbol{u_i})$, representing, respectively, the stochastic component and the deterministic component of the predicted geostatistical concentration. Moreover, the kriging method needs to assume the stationary condition, considering the spatial correlation of the variable Z independent of their spatial position ($\boldsymbol{u_i}$) but dependent only on the separation distance (h) (Bivand et al., 2008; Isaak and Srivastava, 1989; Posa and De Iaco, 2009). Because the kriging predictor was built according to Equation [1], the problem is to define the mean m dependent on the position ($\boldsymbol{u_i}$). Depending on the mean characteristics, three types of predictors can be considered as follows: i) Simple (co)kriging ($m(\boldsymbol{u_i}) = m$, the mean is known and constant), ii) Ordinary (co)kriging ($m(\boldsymbol{u_i}) = m$, the mean is unknown but constant), and iii) Universal (co)kriging ($m(\boldsymbol{u_i})$, the mean is not constant but defined by a spatial function). In the context of this study, the more acceptable condition was a mean that was constant within a moving search neighborhood but unknown, and thus, the selected prediction was an ordinary kriging approximation of $\hat{Z}(\boldsymbol{u_o})$.

$$\hat{Z}(\boldsymbol{u_o}) = \sum_{i=1}^{n} \omega(\boldsymbol{u_i})\, Z(\boldsymbol{u_i}) \quad [2]$$

If auxiliary variables correlated to the primary variable are available, a cokriging approach can be considered. Theoretically, it gives a prediction enhancement respect to ordinary kriging application. Cokriging is based on the same principles of kriging but also uses correlated auxiliary variables (in our case Fe and NH_4^+) to predict the primary variable (in our case As).

$$\hat{Z}(\boldsymbol{u_o}) = \sum_{i=1}^{n} \omega(\boldsymbol{u_i})\, Z(\boldsymbol{u_i}) + \sum_{j=1}^{n} \tau\left(\boldsymbol{u_j}\right) V\left(\boldsymbol{u_j}\right) \quad [3].$$

As evidenced in Equation [3], the cokriging predictor uses a weighted linear combination of the principal variable $Z(\boldsymbol{u_i})$ and of the auxiliary variables $V(\boldsymbol{u_j})$ in the different position ($\boldsymbol{u_i}$) and ($\boldsymbol{u_j}$). In this manner, improving the principal variable prediction is possible. Using the matrix notation, the cokriging system is written as:

$$\boldsymbol{K_{CK}}\, \boldsymbol{L_{CK}}(\boldsymbol{u}) = \boldsymbol{k_{CK}} \quad [4].$$

Where $\boldsymbol{K_{CK}}$ is the $n(\boldsymbol{u})$ x $n(\boldsymbol{u})$ matrix of data covariances, $\boldsymbol{L_{CK}(u)}$ is the vector of the weights $\omega(\boldsymbol{u_i})$ and $\tau(\boldsymbol{u_j})$, $\boldsymbol{k_{CK}}$ represents the vector of data-to-unknown covariances. Basing on the [4], the

cokriging weights required by the COK estimator [3] are obtained by multiplying the inverse of the data covariance matrix by the vector of data-to-unknown covariances:

$$\boldsymbol{L_{CK}(u)} = \boldsymbol{K_{CK}^{-1}}\,\boldsymbol{k_{CK}} \quad [5].$$

Furthermore, to satisfy the stationary and unbiased conditions, the estimated weights from [5] have to undergo the following constrains:

$$\begin{cases} \sum_{i=1}^{n} \omega_i(u) = 1, \\ \sum_{j=1}^{n} \tau_j(u) = 0. \end{cases} \quad [6].$$

As reported in literature, cokriging method work better when the primary variable is less sampled respect to the auxiliary one. Furthermore, one could also use it when main and auxiliary variable are sampled in the same location (collocated cokriging) even if it gives lower prediction advantage than the classical application. The geostatistical analysis was conducted in the R environment (R Core Team, 2015), in particular with the gstat package (Pebesma, 2004). The logical process (Figure 3) to estimate the arsenic spatial distribution was composed of four primary steps: Exploratory Data Analysis, Variographic Analysis, Cross-validation, Ordinary cokriging.

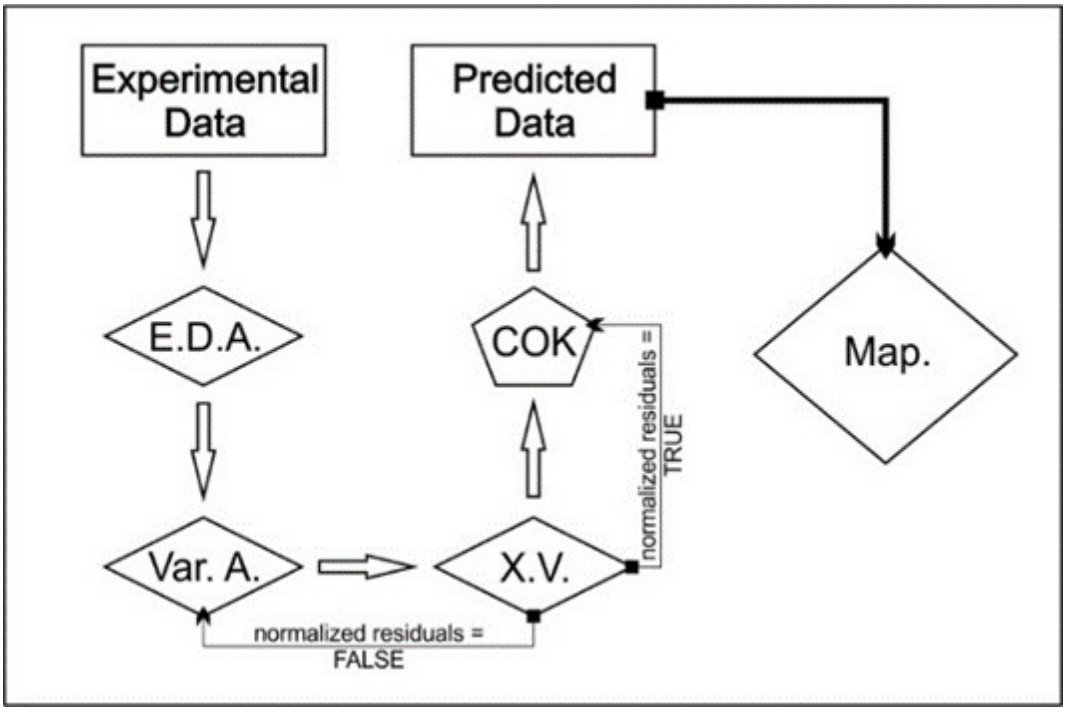

Figure 6 - The flow chart of the classical logical process implemented in the geostatistical analysis. E.D.A = Exploratory Data Analysis, Var.A. = Variographic Analysis, X.V. = Cross–Validation, COK = Ordinary cokriging, Map. = Mapping the predicted principal variable.

Results and discussion

Geostatistical analysis

According to the goal of this study, the average dataset was considered. Initially, a study of the correlations between arsenic and other related chemical components (i.e., iron and ammonium) was performed. The robust correlation among As and other parameters indicated that the cokriging (COK) approach might be appropriate. To evaluate the correlation, we used a Spearman's correlation test and scatterplots. The experimental data do not have a normal distribution and the relation among the variables is not linear. The Spearman's test, basing on ranks correlation, allows evaluating the strength of the correlation among the variables even if it is not linear. In addition, the most known Pearson's test could be less exhaustive because it is not able to evaluate a non-linear correlation (Isaak and Srivastava, 1989). The relationships among As, Fe and NH4+ are illustrated in Figure 4 in which the scatterplots show the poor linear correlation between two variables emphasized by the local regression function LOESS (Cleveland, 1979) (red line) and the numerical coefficients represent the Spearman's ρ. The juxtaposition of these elements allows showing again the poor relevance of the linear correlation on our data. The Spearman's ρ is greater than 0.5 and statistically meaningful (p-

value < 5% significance level). Based on these relationships, we decided to use Fe and NH4+ as the auxiliary variables in the COK prediction process of As.

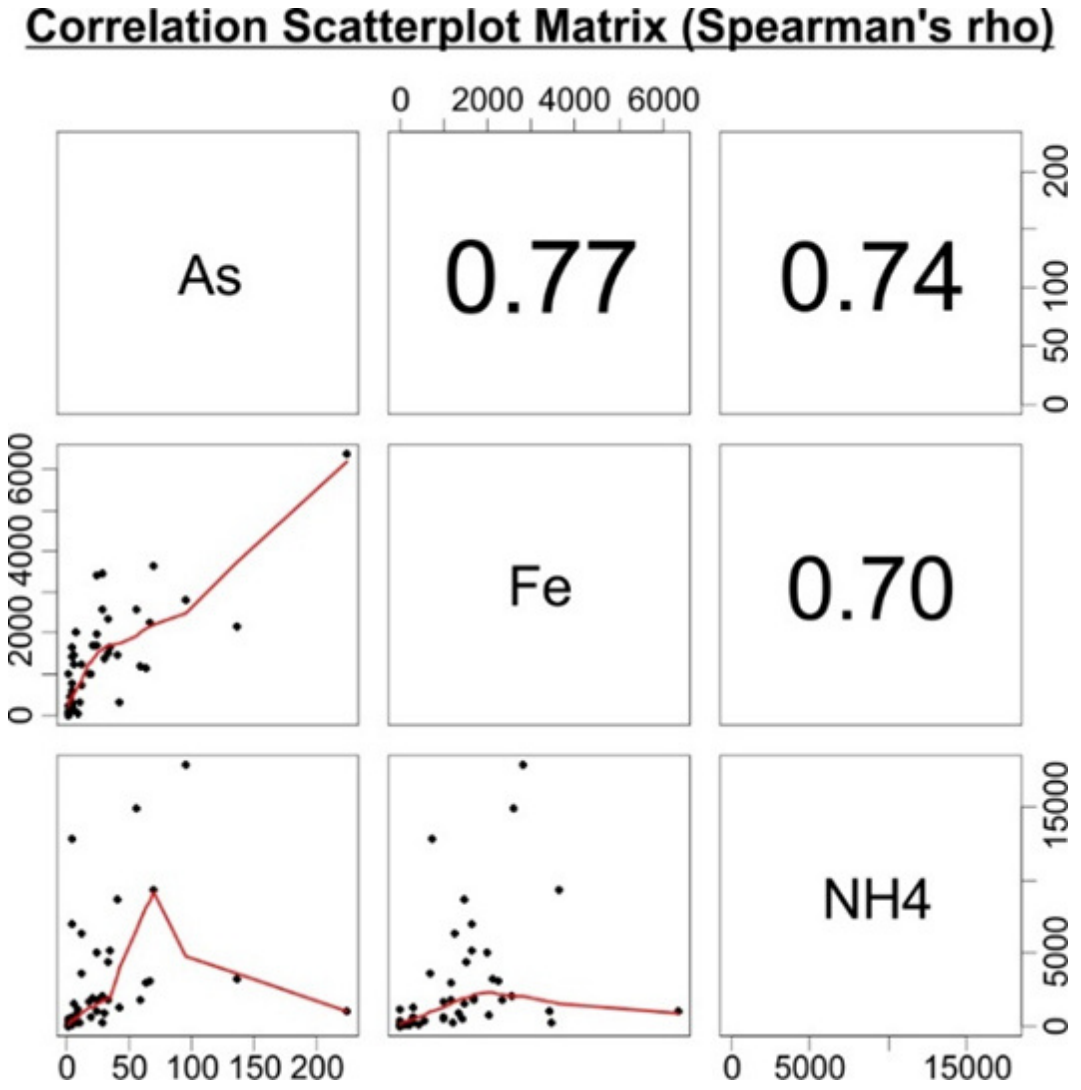

Figure 7 - A correlation scatterplot matrix based on Spearman's method, providing the ρ coefficients for the pairs As-Fe, As-NH4+ and Fe-NH4+. In the lower part of the matrix, the scatterplot related to the variable pairs are shown. They draw the poor linear correlation emphasized by the red line that represents the local regression function LOESS. The correlation coefficients ρ are shown in the upper part of the matrix. The used dataset is the average of the four surveys and the Spearman's correlation test was conducted with the experimental concentration variables.

Subsequently, histograms and scatterplots were used to explore the statistical structure of the raw data. In this manner, estimating the statistical parameters of the data (i.e., means, standard deviation, variance, skewness, etc.) was possible. Arsenic, iron and ammonium data followed a lognormal distribution with positive skewness coefficients (3.13, 2.20, 1.87, respectively; Figure 5). The raw data were transformed to a normal score in order to perform a COK prediction with lower error. Furthermore, the normal score transformation allows an easier

back-transformation of the processed data, giving lower error respect to the use of log-transformation.

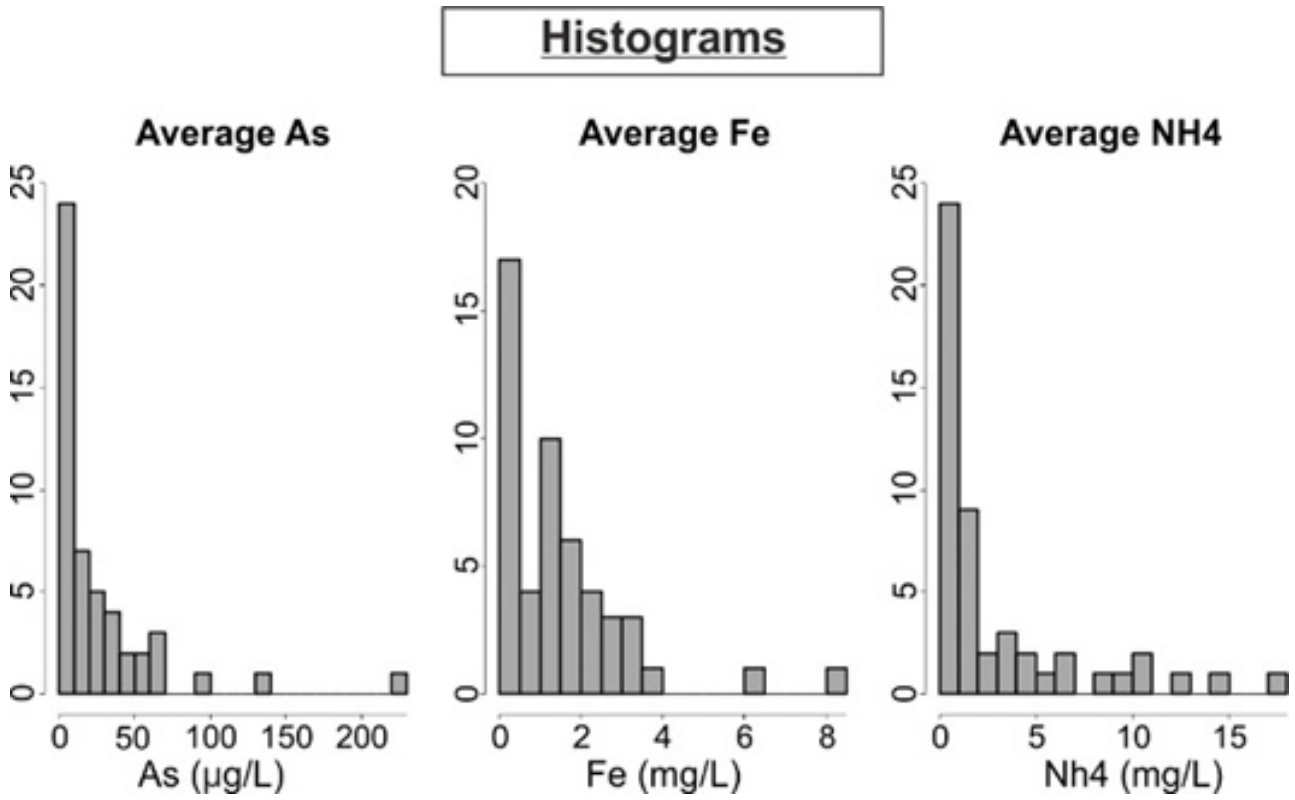

Figure 8 - The three histograms represent the distributions of the average data of As, Fe and NH_4^+, respectively.

The second step of the geostatistical process was the Variographic Analysis of the transformed data. The variogram g(h) describes how spatial continuity changes with the distance (h) and the direction. In addition, the cokriging approach requires the variogram and the cross-variogram analyses. An analysis of the surface variograms in Figure 6A did not reveal any anisotropy in the continuity structures of the studied variables. Considering this, only omnidirectional variograms and cross-variograms were considered (Figure 6B). A Linear Model of Co-regionalization (LMC) fits a theoretical variogram model with both experimental variograms and cross-variograms. The LMC provides authorized theoretical models of variograms and cross-variograms of two or more variables so that the variance of any possible linear combination of these variables is always positive (Isaak and Srivastava, 1989). The resulting theoretical variograms (Figure 6) were used during the cokriging prediction. The variogram model used in this study was spherical both for auto- and cross-variograms:

$$\gamma(h) = \begin{cases} c_0 + c; & |h| > a \\ c_0 + c\left[\frac{3}{2}\frac{|h|}{a} - \frac{1}{2}\left(\frac{|h|}{a}\right)^3\right]; & |h| \le a \end{cases} \quad [7].$$

Where c_0 is the nugget effect, c represents the partial sill and a represents the range. The variogram models referred to As, Fe and NH_4^+, and the three cross-variogram models of As-Fe, As-NH_4^+ and Fe-NH_4^+ are visible in Table 1.

Table 1 - The variogram and cross-variogram models used to predict the arsenic spatial distribution.

Variogram model	Parameter
$\gamma(h) = \begin{cases} 0.486 + 0.523; & \lvert h\rvert > 8000 \\ 0.486 + 0.523\left[\frac{3}{2}\frac{\lvert h\rvert}{8000} - \frac{1}{2}\left(\frac{\lvert h\rvert}{8000}\right)^3\right]; & \lvert h\rvert \le 8000 \end{cases}$	[As]
$\gamma(h) = \begin{cases} 0.730 + 0.260; & \lvert h\rvert > 8000 \\ 0.730 + 0.260\left[\frac{3}{2}\frac{\lvert h\rvert}{8000} - \frac{1}{2}\left(\frac{\lvert h\rvert}{8000}\right)^3\right]; & \lvert h\rvert \le 8000 \end{cases}$	[Fe]
$\gamma(h) = \begin{cases} 0.055 + 0.884; & \lvert h\rvert > 8000 \\ 0.055 + 0.884\left[\frac{3}{2}\frac{\lvert h\rvert}{8000} - \frac{1}{2}\left(\frac{\lvert h\rvert}{8000}\right)^3\right]; & \lvert h\rvert \le 8000 \end{cases}$	[NH_4^+]
$\gamma(h) = \begin{cases} 0.581 + 0.148; & \lvert h\rvert > 8000 \\ 0.581 + 0.148\left[\frac{3}{2}\frac{\lvert h\rvert}{8000} - \frac{1}{2}\left(\frac{\lvert h\rvert}{8000}\right)^3\right]; & \lvert h\rvert \le 8000 \end{cases}$	[As-Fe]
$\gamma(h) = \begin{cases} 0.034 + 0.521; & \lvert h\rvert > 8000 \\ 0.034 + 0.521\left[\frac{3}{2}\frac{\lvert h\rvert}{8000} - \frac{1}{2}\left(\frac{\lvert h\rvert}{8000}\right)^3\right]; & \lvert h\rvert \le 8000 \end{cases}$	[As-NH_4^+]
$\gamma(h) = \begin{cases} -0.004 + 0.429; & \lvert h\rvert > 8000 \\ -0.004 + 0.429\left[\frac{3}{2}\frac{\lvert h\rvert}{8000} - \frac{1}{2}\left(\frac{\lvert h\rvert}{8000}\right)^3\right]; & \lvert h\rvert \le 8000 \end{cases}$	[Fe-NH_4^+]

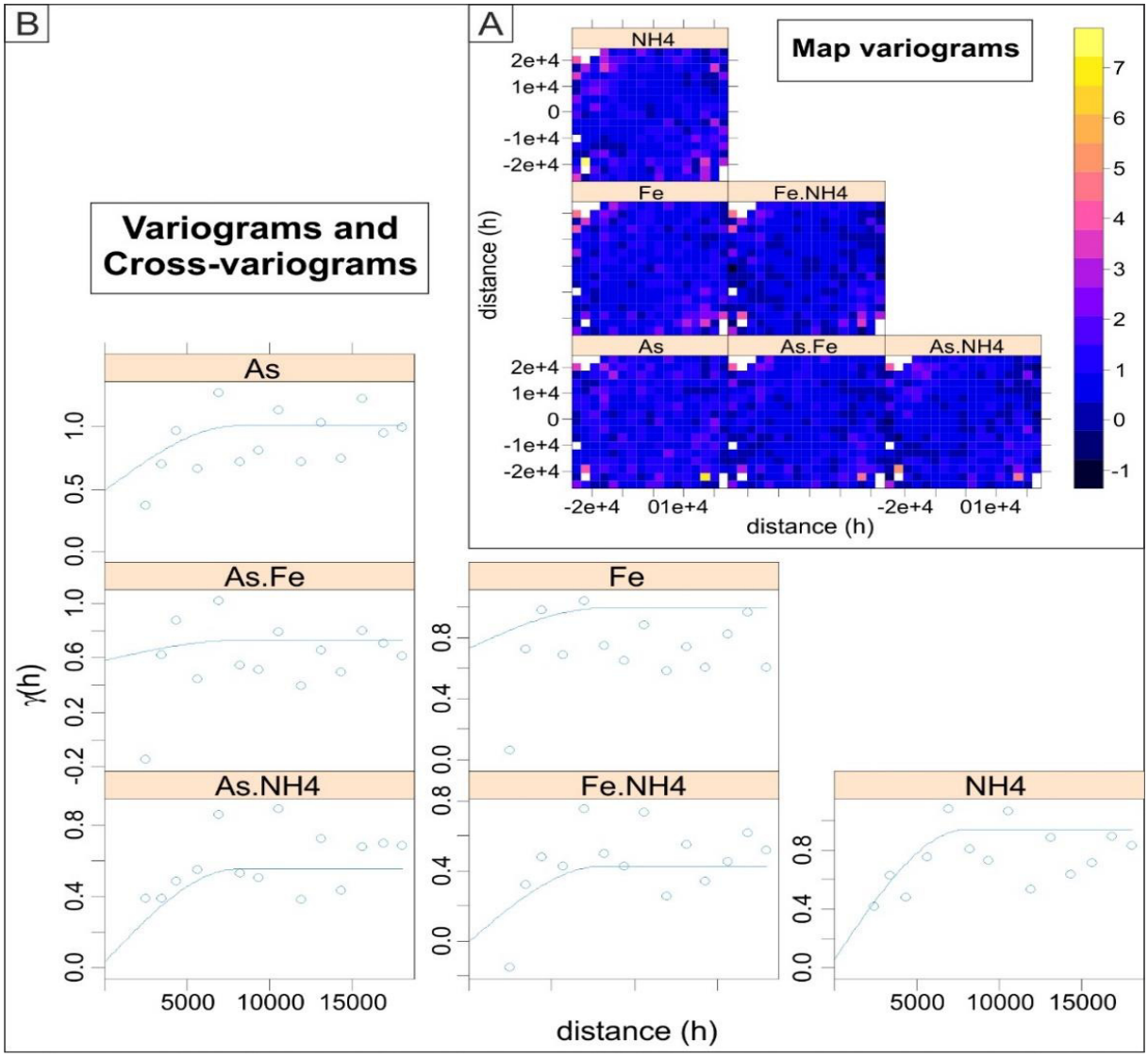

Figure 9 - A) The surface variograms and cross-variograms. The surface variograms are shown in the first column. B) The omnidirectional variogram and cross-variograms. The variograms are on the diagonal, and the associated cross-variograms (referred to the average values of surveys) are below the diagonal.

Following the above variogram analysis, a cross-validation procedure was applied. The cross-validation tests the ability of the model to reproduce the spatial continuity structure by the prediction of the used dataset. The cross-validation, applied on our data, gives a mean estimation error equal to 0.001 µg/L, confirming the good prediction given by the chosen variogram model (Isaak and Srivastava, 1989). The normality of the estimation errors and the good reproduction of the experimental data highlight the model's goodness (Figure 7). Furthermore, in our case, the cross-validation resulted in an acceptable normalized root mean square error (nRMSE) equal to 13.3%, which is around 10% lower than the nRMSE obtained by the ordinary kriging prediction on the same data. A similar nRMSE is likely linked to the

presence of punctual high values of arsenic (hot spots), influencing the prediction process. Generally, the problems linked to the hot spots are common in environmental datasets.

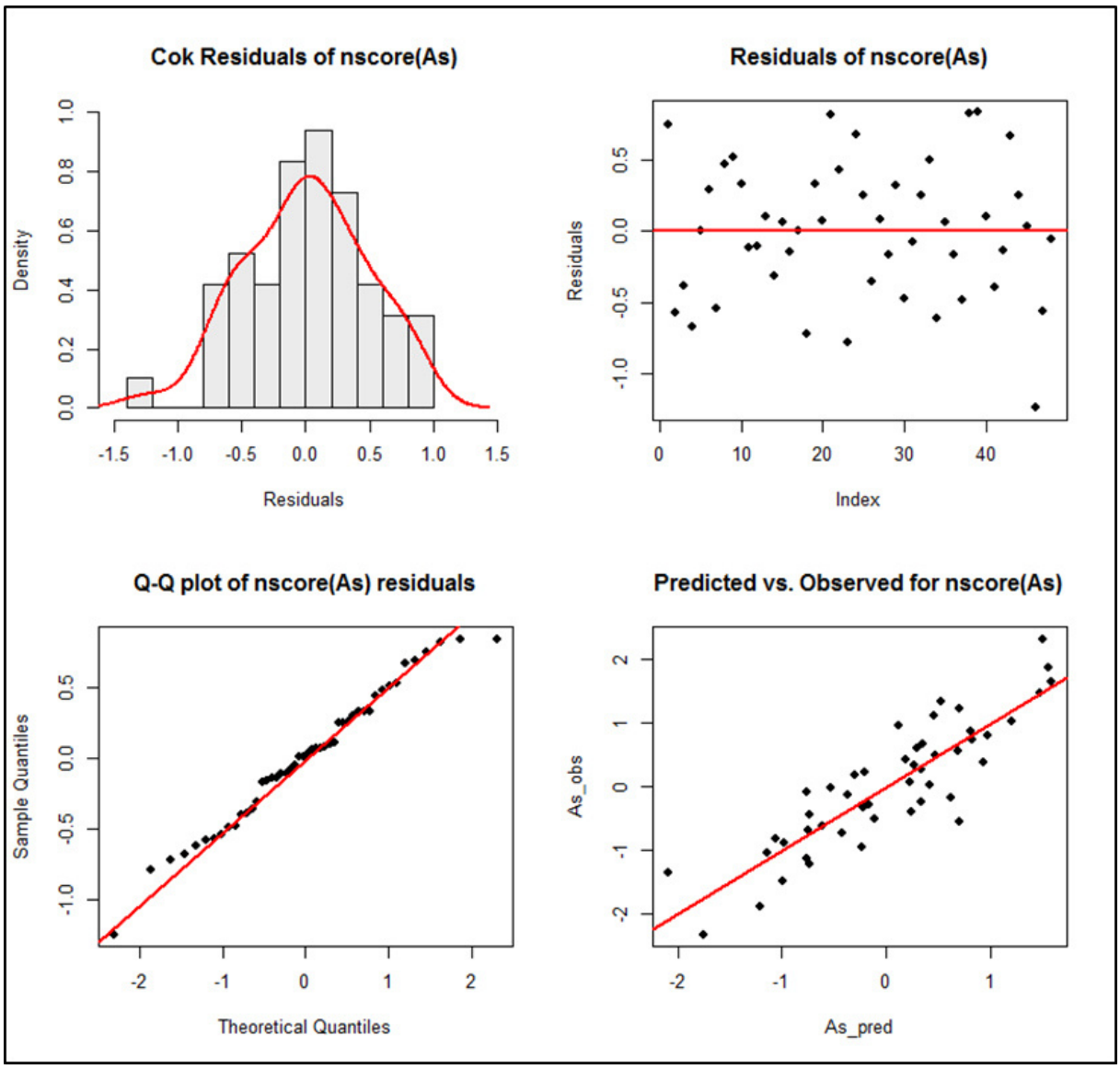

Figure 10 - Graphical representation of the arsenic residuals coming from the cross-validation process by assessing the goodness of the chosen spatial model. Moving from the upper left corner toward the lower right one, there are the probability density function of residuals, the distribution around the zero value, the QQ-norm plot and the scatterplot observed As vs predicted As. In the last diagram, the red line represents the linear trend line (correlation coeff. = 0.67).

Arsenic distribution

Following the previous geostatistical analysis, an ordinary cokriging predictor was applied. The prediction process allowed mapping the arsenic distribution on the shallow groundwater of the DBVL (Figure 8). By improving the NBL concept and getting a more detailed value, we decided to consider the TV and the median (M) of the original dataset as thresholds to reclassify the

distribution map. The reclassification process is necessary to identify the data that have similar arsenic values and then estimate some Local NBL following the 90th percentile method. In our case, the median was chosen because the "A.Li.Na" NBL value is several times higher than the TV and it seems adequate as intermediate threshold, separating the 50% of the data. However, the choice of the intermediate threshold is linked to both the dataset structure and the gap between the existing NBL and TV. In this way, we are able to define some sub-area in which estimate, effectively, some local NBL (LNBL) values (Table 2). A unique value of NBL does not seem to be realistic in regional environments with a large variation of concentrations.

Table 3 - Arsenic concentration classes used to evaluate the LNBLs.

1st	As ≤ 10 µg/L (TV)	Lower ($LNBL_L$)
2nd	10 < As ≤31.4 µg/L (M)	Intermediate ($LNBL_I$)
3rd	As > 31.4 µg/L	Higher ($LNBL_H$)

According to the above-described thresholds, the map in Figure 9 (related to the average values of the four surveys) shows that many zones (about 49% of the study area) exceeded the threshold value (TV) set in the Annex III of the Commission staff working document of the GWD 2006/118/EC. In some of these zones (9% of the domain), the predicted values also exceeded the natural background level (NBL) of 74 µg/L suggested by the "A.Li.Na" project. In particular, in the central-western region of the area between the Padua and Venice provinces (including Piezometers 9, 10, 20, 37, 40 and 44), the predicted arsenic concentrations were greater than the TV, ranging from 33.75 to 224 µg/L. Similarly, arsenic concentrations reached the maximum value of 95 µg/L in the eastern region of the study area, near the Venice airport (Piezometer 15). Examining the ORP overlaid post-map, the ORP values denoted a reducing environment in these areas, in agreement with the results of several studies on the role of ORP in As release (Carraro et al., 2015, 2013; Dalla Libera et al., 2016; McArthur et al., 2001; Molinari et al., 2015; Nickson et al., 2000; Rotiroti et al., 2014). These reducing conditions occur also in some "green" and "yellow" zones but in this case arsenic is low cause the As-bearing material are missing in the subsoil. Otherwise, analyzing the available stratigraphic logs (Figure 9), the presence of peat layers is evident in the areas with high concentrations, confirming the role of organic matter as a redox driver of As release (Dalla Libera et al., 2016; Molinari et al., 2013; Nickson et al., 2000;

Rotiroti and Fumagalli, 2013; Rotiroti et al., 2014; Ungaro et al., 2008). From a hydrogeological perspective, a map analysis suggested that the arsenic contamination disagreed with the groundwater natural drainage and did not spread in accordance with the groundwater flow directions (NW-SE) (Fabbri et al., 2013). The main cause should be the geological heterogeneity that influences the hydro-geochemical conditions driving the sorption processes.

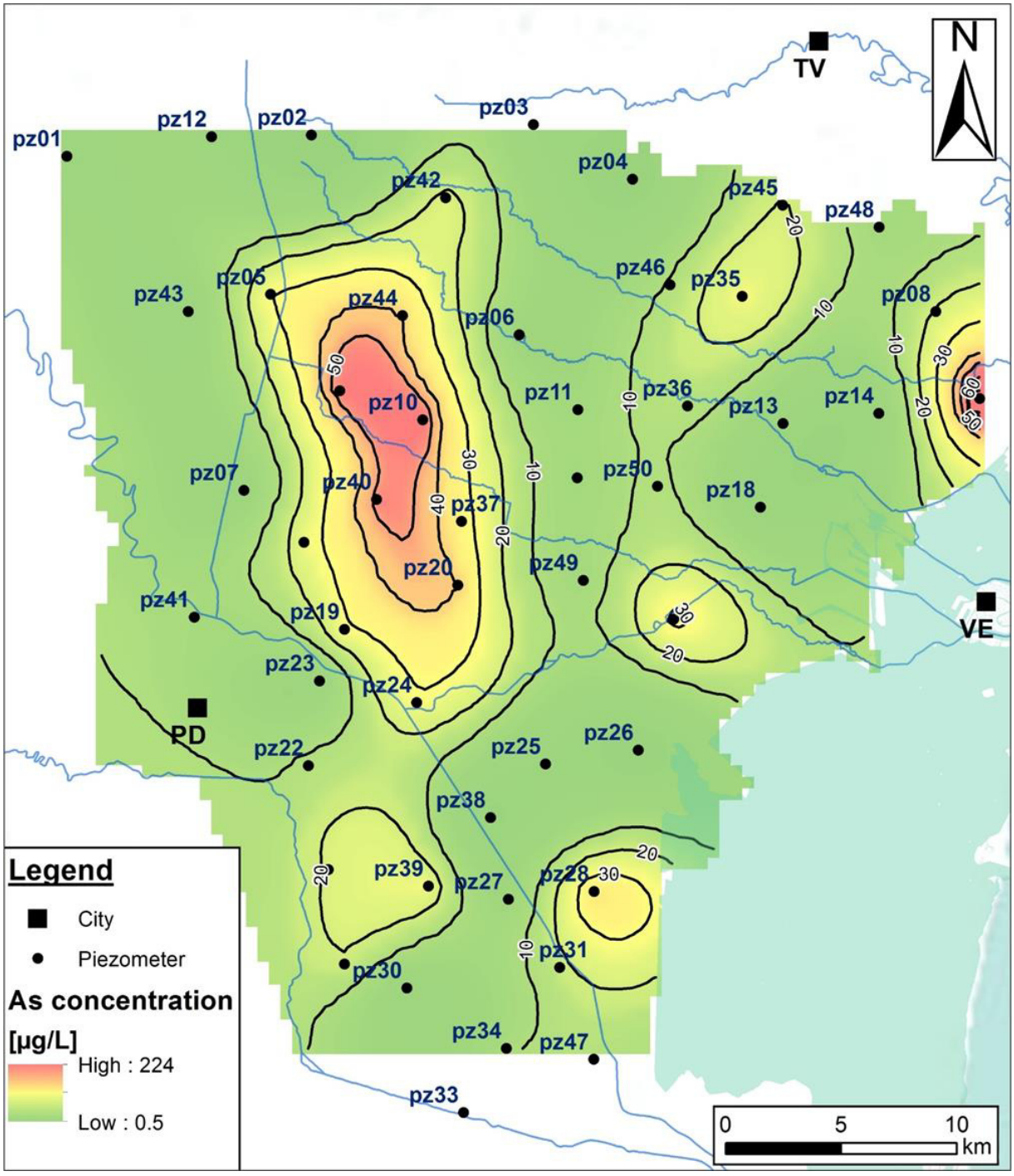

Figure 11 - The raw prediction of arsenic concentration within the DBVL obtained by the COK method. The contour lines represent the arsenic concentration values basing on the COK prediction with an interval of 10 µg/L. The bold labels PD, TV and VE represent the cities of Padua, Treviso and Venice, respectively.

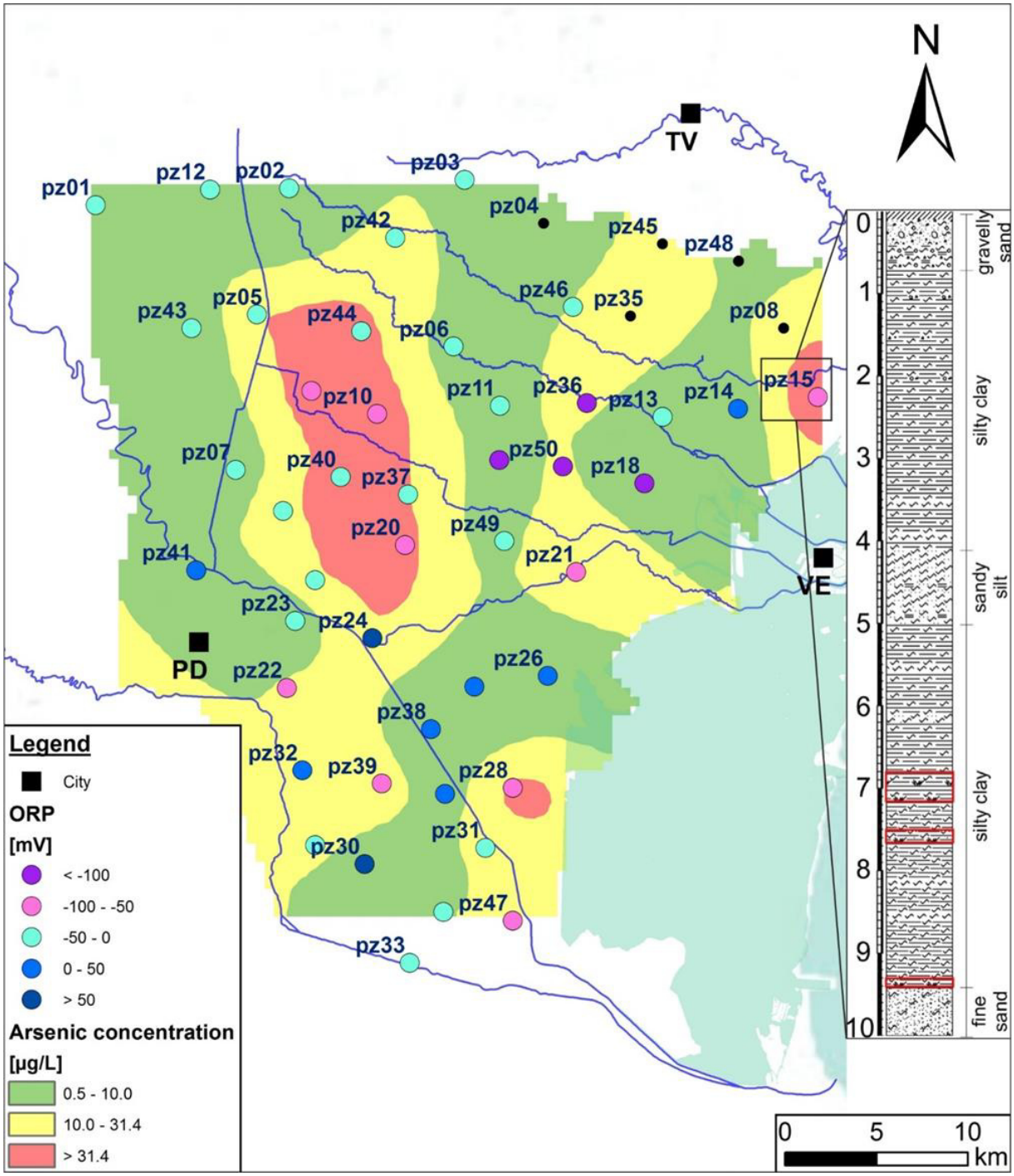

Figure 12 - The reclassified arsenic prediction, obtained from the raw prediction in figure 8, and the ORP post-map. The stratigraphic log shows some peat layers corresponding to the zones with high arsenic values. The red boxes highlight the peat layers. The bold labels PD, TV and VE represent the cities of Padua, Treviso and Venice.

Implications for water and environmental management

Groundwater arsenic pollution in alluvial systems can result from natural processes, such as weathering, the interaction between groundwater and mineral deposits or the degradation of organic matter deposits (e.g., peat layers). The distinction between anthropogenic and natural

sources of contamination is important for approaching the contamination issues. Therefore, the evaluation of an NBL value plays an important role in highlighting anthropogenic pollution. The methods, suggested by the EU BRIDGE project, provide a statistically representative value for the entire study area but does not take into consideration the spatial distribution of the data. Our approach suggests a Local Natural Background Levels (LNBLs), combining the 90th percentile concept and the spatial data distribution and defining an adequate number of classes (depending to the difference between TV and NBL), in which we can estimate the LNBLs. In this way, the errors between the natural occurrence and the anthropogenic pollution are minimized. By considering a unique NBL value for the entire area, an incorrect distinction between natural occurrence and pollution could occur. For example, in zones with a concentration lower than the NBL, we risk accepting an external pollution as a natural occurrence. However, in an area belonging to a higher class, we risk misinterpreting a natural occurrence as pollution. Therefore, we suggest calculating a local NBL using only the data inside the areas, defined by concentration classes established using a geostatistical prediction (e.g., the green areas in Figure 9 with predicted values between 0.5 and 10 µg/L). This step could be easily conducted if the number of available data is significantly adequate in each class ($n \geq 30$) (Müller et al., 2006). If the number of data is lower than 30, the sampling network should be enhanced. Referring to the DBVL area, all three identified zones have a number of piezometers fewer than 30 in the "A.Li.Na" sampling network. Therefore, a significant calculation of the LNBL was not performed. However, in the green areas (about 51% of the study area, Figure 9) with a predicted arsenic concentration between 0.5 to 10 µg/L (TV), 24 piezometers are available. For example, in these areas, the LNBL was estimated to be equal to 6.68 µg/L, according to the 90th percentile method. Such a result shows that the LNBL value is not only much lower than the "A.Li.Na" NBL value (74 µg/L) but is also lower than the TV (10 µg/L). In this case, the application of the "A.Li.Na" NBL is clearly misleading because it means considering anthropogenic pollution as naturally occurring contamination. The inadequate treating of this potential anthropogenic pollution could represent a serious environmental issue affecting the public health.

Conclusion

The results presented in this paper show how a geostatistical spatial approach allows for the application of the 90th percentile method (NBL) in a more critical way. The map of the natural distribution of arsenic allows for the identification of critical areas, highlighting where the As values exceed the TV. In particular, this result illustrates the usefulness of calculating a local

NBL (LNBL) related to the different defined areas. Using the cokriging approach, the definition of LNBLs takes advantage of the arsenic spatial distribution and the geochemical relationships among arsenic and other related parameters. In fact, the correlations between arsenic and auxiliary variables, such as Fe and NH_4^+, are taken into consideration for cokriging prediction. The results of this study highlight the critical issues related to the application of a single NBL value at the regional scale. Through the BRIDGE suggestions, the European GWD proposes a NBL value without considering the spatial distribution of the parameter concentration or the geochemical relations among the correlated parameters. The LNBL concept aims to reduce the error associated with the distinction between the natural occurrence of arsenic and anthropogenic pollution. By defining a LNBL for every class of concentration, the anthropogenic pollution events can be easily depicted, particularly in the classes with low threshold values. The suggested approach is easily applicable to estimate the LNBL of any kind of elements or compound deriving from natural processes, both in groundwater and soil. In addition, the proposed approach might be applied to obtain a global view of the study area, informing decisions about water and environmental management and improving the characterization plan necessary to evaluate potentially contaminated sites.

Acknowledgment

This work was founded by the Venice Province, project "IDRO", grant to P. Fabbri. We thank the ARPAV agency, in particular the internal water observatory, to share their data concerning the arsenic groundwater contamination into the DBVL.

References

APAT, 2003. Analytical methods for chemical water analysis, vol. 1. Handbooks and guidelines, 29, I.G.E.R. srl, Roma.

APAT, 2006. Handbook for environmental investigation upon contaminated sites. Handbooks and guidelines, I.G.E.R. srl, Roma.

ARPA, 2014. ALiNa – Analysis of the Natural Background Level for some compounds within the groundwater of the shallow aquifer in the Drainage Basin to the Venice Lagoon (Brenta river alluvial system) – Report and data presentation.

Baiocchi, A., Lotti, F., Piscopo, V., 2011. Influence of hydrogeological setting on the arsenic occurrence in groundwater of the volcanic areas of central and southern Italy. AQUA mundi 2, 131–142. doi:10.4409/Am-035-11-0035

Baviskar, S., Choudhury, R., Mahanta, C., 2015. Dissolved and solid-phase arsenic fate in an arsenic-enriched aquifer in the river Brahmaputra alluvial plain. Environ. Monit. Assess. 187, 93. doi:10.1007/s10661-015-4277-0

Biswas, A., Gustafsson, J.P., Neidhardt, H., Halder, D., Kundu, A.K., Chatterjee, D., Berner, Z., Bhattacharya, P., 2014. Role of competing ions in the mobilization of arsenic in groundwater of Bengal Basin: Insight from surface complexation modeling. Water Res. 55, 30–39. doi:10.1016/j.watres.2014.02.002

Bivand R.S., Pebesma E.J., Gomez-Rubio V., 2009. Applied spatial data analysis wit R; Springer, ISBN 978-0-387-78170-9, DOI: 10.1007/978-0-387-78171-6

Bondesan, A., Meneghel, M., 2004. Geomorphology of the Venice Province (in Italian). Esedra, Padova.

Cambruzzi T., Conchetto E., Fabbri P., Marcolongo E., Rosignoli A., Zangheri P., 2009. Groundwater resources in the middle Venetian plain. Rend. Online Soc. Geol. It., 6, 127-128.

Carraro, A., Fabbri, P., Giaretta, A., Peruzzo, L., Tateo, F., Tellini, F., 2015. Effects of redox conditions on the control of arsenic mobility in shallow alluvial aquifers on the Venetian Plain (Italy). Sci. Total Environ. 532, 581–594. doi:10.1016/j.scitotenv.2015.06.003

Carraro, A., Fabbri, P., Giaretta, A., Peruzzo, L., Tateo, F., Tellini, F., 2013. Arsenic anomalies in shallow Venetian Plain (Northeast Italy) groundwater. Environ. Earth Sci. 70, 3067–3084. doi:10.1007/s12665-013-2367-2

Cleveland W.S., 1979. Robust Locally Weighted Regression and Smoothing Scatterplots. Journal of the American statistical association, Vol. 74, No. 368, pp. 829 – 836.

Coetsiers, M., Blaser, P., Martens, K., Walraevens, K., 2009. Natural background levels and threshold values for groundwater in fluvial Pleistocene and Tertiary marine aquifers in Flanders, Belgium. Environ. Geol. 57, 1155–1168. doi:10.1007/s00254-008-1412-z

Dalla Libera, N., Fabbri, P., Mason, L., Piccinini, L., Pola, M. 2016. Natural Arsenic in groundwater in the drainage basin to the Venice lagoon (Brenta Plain, NE Italy): the organic matter's role. Rend. Online della Soc. Geol. Ital. 41, 30–33. doi:10.3301/ROL.2016.85

Dal Prà, A., Fabbri, P., Bortoletto, C., 1992. The artesian hydrogeological system and its exploitation in the area between the Treviso City and the Piave River (in Italian). Memorie di Scienze Geologiche, 44, 151-170.

D. Lgs. 152/06, 2006. Legislative Decree on environmental regulations.

D. Lgs. 30/09, 2009. Legislative Decree on the implementation of Directive 2006/118/EC on the protection of groundwater from contamination and degradation.

Edmunds, W.M., Shand, P., 2008. Natural Groundwater Quality.Wiley-Blackwell (488 pp., ISBN 978-14051- 5675-2).

Fabbri, P., Piccinini, L., Marcolongo, E., Pola, M., Conchetto, E., Zangheri, P., 2016. Does a change of irrigation technique impact on groundwater resources? A case study in Northeastern Italy. Environ. Sci & Policy. 63, 63.75. doi: 10.1016/j.envsci.2016.05.009

Fabbri, P., Gaetan, C., Zangheri, P., 2011. Transfer function-noise modelling of an aquifer system in NE Italy. Hydrol. Process. 25, 194–206. doi:10.1002/hyp.7832

Fabbri, P., Piccinini, L., 2013. Assessing transmissivity from specific capacity in an alluvial aquifer in the middle Venetian plain (NE Italy). Water Sci. Technol. 67, 2000–2008. doi:10.2166/wst.2013.074

Fabbri, P., Zangheri, P., Bassan, V., Fagarazzi, E., Mazzucato, A., Primon, S., Zogno, C., 2013. Hydrogeology of the Venice Province – The shallow aquifers (in Italian). Venice Province – University of Padova.

Fendorf, S., Michael, H.A., van Geen, A., 2010. Spatial and Temporal Variations of Groundwater Arsenic in South and Southeast Asia. Science (80-.). 328, 1123–1127. doi:10.1126/science.1172974

Fontana, A., Mozzi, P., Bondesan, A., 2004. The geomorphological evolution of the Venetian-Friulian plain (in Italian). Whitin the: Bondesan, A., Meneghel, M., 2004. Geomorphology of the Venice Province. Esedra, Padova. 113-138.

Fontana, A., Mozzi, P., Bondesan, A., 2008. Alluvial megafans in the Venetian–Friulian Plain (northeastern Italy): Evidence of sedimentary and erosive phases during Late Pleistocene and Holocene. Quaternary International, 189, 71-90.

GWD, 2006. Groundwater Directive 2006/118/CE, Directive of the European Parliament and of the Council on the protection of groundwater against pollution and deterioration, OJ L372, 27/12/ 2006, pp 19–31.

Hinsby, K., Condesso de Melo, M.T., Dahl, M., 2008. European case studies supporting the derivation of natural background levels and groundwater threshold values for the protection of dependent ecosystems and human health☆. Sci. Total Environ. 401, 1–20. doi:10.1016/j.scitotenv.2008.03.018

Isaaks E.H., Srivastava R.M. An introduction to Applied Geostattistics; Oxford University Press: New York, 1989.

McArthur, J.M., Banerjee, D.M., Hudson-Edwards, K.A., Mishra, R., Purohit, R., Ravenscroft, P., Cronin, A., Howarth, R.J., Chatterjee, A., Talukder, T., Lowry, D., Houghton, S., Chadha, D.K., 2004. Natural organic matter in sedimentary basins and its relation to arsenic in anoxic ground water: The example of West Bengal and its worldwide implications. Appl. Geochemistry 19, 1255–1293. doi:10.1016/j.apgeochem.2004.02.001

McArthur, J.M., Ghosal, U., Sikdar, P.K., Ball, J.D., 2016. Arsenic in Groundwater: The Deep Late Pleistocene Aquifers of the Western Bengal Basin. Environ. Sci. Technol. 50, 3469–3476. doi:10.1021/acs.est.5b02477

McArthur, J.M., Ravenscroft, P., Safiulla, S., Thirlwall, M.F., 2001. Arsenic in groundwater: Testing pollution mechanisms for sedimentary aquifers in Bangladesh. Water Resour. Res. 37, 109–117. doi:10.1029/2000WR900270

Molinari, A., Guadagnini, L., Marcaccio, M., Guadagnini, A., 2015. Arsenic fractioning in natural solid matrices sampled in a deep groundwater body. Geoderma 247-248, 88–96. doi:10.1016/j.geoderma.2015.02.011

Molinari, A., Guadagnini, L., Marcaccio, M., Guadagnini, A., 2012. Natural background levels and threshold values of chemical species in three large-scale groundwater bodies in Northern Italy. Sci. Total Environ. 425, 9–19. doi: 10.1016/j.scitotenv.2012.03.015

Molinari, A., Guadagnini, L., Marcaccio, M., Straface, S., Sanchez-Vila, X., Guadagnini, A., 2013. Arsenic release from deep natural solid matrices under experimentally controlled redox conditions. Sci. Total Environ. 444, 231–240. doi: 10.1016/j.scitotenv.2012.11.093

Mozzi P., Bini C., Zilocchi L., Beccatini R., Mariotti Lippi M., 2003. Stratigraphy, palaeopedology and palynology of late Pleistocene and Holocene deposits in the landward sector of the lagoon of Venice (Italy), in relation to Caranto level. Il Quaternario, 16 (1 bis), pag. 193 – 210.

Müller D., Blum A., Hart A., Hookey J., Kunkel R., Scheidleder A., Tomlin C., Wendland F., 2006. BRIDGE Project: Background criteria for identification of groundwater thresholds, D18: Final proposal for a methodology to set up groundwater threshold values in Europe.

Nickson, R., McArthur, J., Burgess, W., Ahmed, K.M., Ravenscroft, P., Rahman, M., 1998. Arsenic poisoning of Bangladesh groundwater. Nature 395, 338. doi:10.1038/26387

Nickson, R.T., Mcarthur, J.M., Ravenscroft, P., Burgess, W.G., Ahmed, K.M., 2000. Mechanism of arsenic release to groundwater, Bangladesh and West Bengal. Appl. Geochemistry 15, 403–413. doi:10.1016/S0883-2927(99)00086-4

Nordstrom, D.K., 2003. Arsenic in Ground Water, Science Mag. Springer US, Boston, MA. doi:10.1007/b101867

Pebesma, E.J., 2004. Multivariable geostatistics in S: the gstat package. Comput. Geosci. 30, 683–691. doi: 10.1016/j.cageo.2004.03.012

Piccinini, L., Fabbri, P., Pola, M., 2016. Point dilution tests to calculate groundwater velocity, an example in a porous aquifer in NE Italy. Hydrol. Sci. J. 61(8), 1512-1523. doi:10.1080/02626667.2015.1036756

Piccinini, L., Fabbri, P., Pola, M., Marcolongo, E., Rosignoli, A., 2015. Numerical modeling to well-head protection area delineation, an example in Veneto Region (NE Italy). Rend. Online Soc. Geol. It. 35, 232-235. doi: 10.3301/ROL.2015.108

Preziosi, E., Giuliano, G., Vivona, R., 2010. Natural background levels and threshold values derivation for naturally As, V and F rich groundwater bodies: a methodological case study in Central Italy. Environ. Earth Sci. 61, 885–897. doi:10.1007/s12665-009-0404-y

Posa D., De Iaco S., 2009. Geostatistics, theory and applications. G. Giappichelli Editore, Turin, Italy, ISBN 978-88-348-9744-7

R Core Team, 2015. R: A language and environment for statistical computing, R Foundation for Statistical Computing, Vienna, Austria. URL: http://www.R-project.org/

Rango, T., Vengosh, A., Dwyer, G., Bianchini, G., 2013. Mobilization of arsenic and other naturally occurring contaminants in groundwater of the main ethiopian rift aquifers. Water Res. 47, 5801–5818. doi:10.1016/j.watres.2013.07.002

Rotiroti, M., Fumagalli, L., 2013. Derivation of preliminary natural background levels for naturally Mn, Fe, As and NH4+ rich groundwater: The case study of Cremona area (Northern Italy). Rend. Online Soc. Geol. Ital. 24, 284–286.

Rotiroti, M., Sacchi, E., Fumagalli, L., Bonomi, T., 2014. Origin of Arsenic in Groundwater from the Multilayer Aquifer in Cremona (Northern Italy). Environ. Sci. Technol. 48, 5395–5403. doi:10.1021/es405805v

Rowland, H.A.L., Pederick, R.L., Polya, D.A., Pancost, R.D., Van Dongen, B.E., Gault, A.G., Vaughan, D.J., Bryant, C., Anderson, B., Lloyd, J.R., 2007. The control of organic matter on microbially mediated iron reduction and arsenic release in shallow alluvial aquifers, Cambodia. Geobiology 5, 281–292. doi:10.1111/j.1472-4669.2007.00100.x

Smedley, P.L., Kinniburgh, D.G., 2002. A review of the source, behaviour and distribution of arsenic in natural waters. Appl. Geochemistry 17, 517–568. doi:10.1016/S0883-2927(02)00018-5

Sorg, T.J., Chen, A.S.C., Wang, L., 2014. Arsenic species in drinking water wells in the USA with high arsenic concentrations. Water Res. 48, 156–169. doi:10.1016/j.watres.2013.09.016

Takeno, N., 2005. Atlas of Eh-pH diagrams Intercomparison of thermodynamic databases. Natl. Inst. Adv. Ind. Sci. Technol. Tokyo 285.

Trevisani, S., Fabbri, P., 2010. Geostatistical modeling of a heterogeneous site bordering the Venice lagoon, Italy. Ground Water 48, 614–623. doi:10.1111/j.1745-6584.2009.00632.x

Ungaro, F., Ragazzi, F., Cappellin, R., Giandon, P., 2008. Arsenic concentration in the soils of the Brenta Plain (Northern Italy): Mapping the probability of exceeding contamination thresholds. J. Geochemical Explor. 96, 117–131. doi:10.1016/j.gexplo.2007.03.006

Vorlicek, P.A., Antonelli, R., Fabbri, P., Rausch, R., 2004. Quantitative hydrogeological studies of the Treviso alluvial plain, NE Italy. Q. J. Eng. Geol. Hydrogeol. 37, 23–29. doi:10.1144/0036-9276/02-006

Welch, A.H., Westjohn, D.B., Helsel, D.R., Wanty, R.B., 2000. Arsenic in Ground Water of the United States: Occurrence and Geochemistry. Ground Water 38, 589–604. doi:10.1111/j.1745-6584.2000.tb00251.x

Wendland, F., Berthold, G., Blum, A., Elsass, P., Fritsche, J.-G., Kunkel, R., Wolter, R., 2008a. Derivation of natural background levels and threshold values for groundwater bodies in the Upper Rhine Valley (France, Switzerland and Germany). Desalination 226, 160–168. doi:10.1016/j.desal.2007.01.240

Wendland, F., Blum, A., Coetsiers, M., Gorova, R., Griffioen, J., Grima, J., Hinsby, K., Kunkel, R., Marandi, A., Melo, T., Panagopoulos, A., Pauwels, H., Ruisi, M., Traversa, P., Vermooten, J.S.A., Walraevens, K., 2008b. European aquifer typology: A practical framework for an overview of major groundwater composition at European scale. Environ. Geol. 55, 77–85. doi:10.1007/s00254-007-0966-5

Zavatti, A.; Attramini, D.; Bonazzi, A.; Boraldi, V.; Malagò, R.; Martinelli, G.; Naldi, S.; Patrizi, G.; Pezzera, G.; Vandini, W.; Venturini, L.; Zuppi, G. M., 1995. Occurrence of groundwater arsenic in the Po Plain: Environmental evidences and geochemical hypothesis. Quad. Geol. Appl., S2, 2.301–2.326.

2.3.3 Paper 3

A local natural background level concept to improve the natural background level: a case study on the drainage basin of the Venetian Lagoon in Northeastern Italy

Authors: Nico Dalla Libera[a], Paolo Fabbri[a], Leonardo Mason[b], Leonardo Piccinini[a], Marco Pola[a]

a) Dipartimento di Geoscienze, Università di Padova, Via G. Gradenigo, 6 - 35131 Padova, Italy.

b) SCA - U.O. Sito Interesse Nazionale, ARPAV Dipartimento di Venezia, Via Lissa 6 - 30171 Venezia, Mestre – Italy.

Status: Published in "Environmental Earth Sciences" (2018) 77:487 (https://doi.org/10.1007/s12665-018-7672-3).

Abstract

This study analyzes a problem related to the definition of a natural background level (NBL) for naturally occurring contaminants. Specifically, it considers the definition of an arsenic NBL in groundwater because arsenic in alluvial aquifers is a worldwide problem that causes issues in human health. Currently, the European Union (through the BRIDGE project) has suggested several methods to estimate NBLs based on the quantity and quality of the available data, providing a unique NBL value for an investigated study area. This study suggests an improvement of the NBL concept by introducing the local NBL (LNBL). LNBLs are estimated considering an indicator geostatistical approach, which considers both the spatial distribution of arsenic and the geochemical relationships occurring inside the aquifer. The LNBL concept aims to provide detailed spatial information of the natural background level and prevents one from defining uncontaminated water sources as contaminated water sources, and vice versa. In this study, an application of the LNBL in the drainage basin of the Venetian Lagoon is proposed.

Keywords: Natural background level (NBL), Local NBL (LNBL), Indicator cokriging (ICK), Water management, Drainage basin of the Venetian Lagoon (DBVL).

Introduction

The definition of a contaminant's natural background level (NBL), from an environmental management point of view, is an important problem that needs to be solved carefully. The NBL of an element or compound in groundwater represents the range of concentrations resulting from the interaction of different natural processes (e.g., atmospheric, geological, chemical and biological) during the hydrological cycle, and it could be influenced by human activities (Reimann and Garrett 2005; Shand et al. 2007; Hinsby et al. 2008). Therefore, its definition is complex, and it is an ongoing challenge for stakeholders. NBL identification requires knowledge of geological and hydro-geochemical characteristics of the considered aquifer, being careful to collect pristine water samples from the same water body, and far from anthropogenic sources of contamination (Coetsiers et al. 2009; Preziosi et al. 2010; Molinari et al. 2012; Rotiroti and

Fumagalli 2013; Rotiroti et al. 2015; Ducci et al. 2016). The European Union Water Framework Directive provides the standards of quality in order to guarantee a healthy status and define the starting points for reversing contamination trends, both for surface water and groundwater (WFD 2000/60/EC, article 17). The Groundwater Daughter Directive (GWD2006/118/EC) supplies the procedures and criteria to achieve these objectives. To define the groundwater status, the BRIDGE project was developed. It provides a method for the evaluation of threshold values (TVs) and natural background levels of pollutants in groundwater bodies (Müller et al. 2006; Pauwels et al. 2007; Wendland et al. 2008a; Wendland et al. 2008b). Principally, BRIDGE methods are based on a purely statistical approach, suggesting that the definition of NBLs can either be determined by the separation method or the preselection method (Müller et al., 2006; Pauwels et al. 2007; Molinari et al. 2013). The first method expresses observed concentrations by a frequency distribution function that allows the separation of two different distributions, which represents the natural and anthropogenic components. The second method excludes all groundwater samples with indicator substances (e.g., nitrate and potassium) over a certain threshold in order to avoid polluted samples due to human activity. Once the users select the samples, the NBL represents the 90^{th} or 97^{th} percentile of the data distribution. These methods are simple and "user friendly" (particularly the preselection method) in providing a NBL value for an entire region. However, they do not evaluate the spatial distribution of the considered parameter due to the variation in the physio-chemical characteristics of the subsoil. This study suggests an integrated analysis that combines both the spatial distribution of the contaminant concentrations (i.e., the geostatistical approach) and the classic BRIDGE approach. The application of kriging methods for environmental problems has been widely present in the literature (Pebesma et al. 1997; Critto et al. 2003; Fabbri & Trevisani 2005; Baalousha 2010; Sollitto et al. 2010; Elumalai et al. 2017), particularly regarding the indicator approach (Fabbri 2001; Ducci et al. 2016). One of the advantages of indicator (co)kriging is modeling local uncertainties evaluating the risk involved in any decision-making process (e.g., the delimitation of contaminated areas where remedial actions should be performed). Therefore, the proposed approach assumes indicator cokriging (ICK) or kriging (IK) to define different subareas where the classic 90^{th} percentile method proposed by the BRIDGE project is taken into account. This approach does not estimate a singular NBL, but it estimates different local NBLs in every subarea defined by the ICK estimation. The ICK results show portions of the study area where contaminants have a high exceedance probability with respect to the defined cutoffs. These cutoffs can be based on the GWD quality thresholds and the statistical parameters of the dataset. There are other procedures that spatialize this type of information (Dalla Libera et al.

2017), but ICK seems the most useful as it focuses on several thresholds and their related probability of exceedance. The study area is located in the drainage basin of the Venetian Lagoon (DBVL), where high concentrations of arsenic are present. This area allows us to compare a classic NBL result (ARPAV, 2014) with the LNBL results. The NBL value of the DBVL, obtained by the preselection method, is 74 μg/L, which is seven times higher than the threshold value (TV; GWD, 2006/118/EC). Considering the geochemical setting of the study area, the procedure applied by the Regional Environmental Protection Agency (ARPAV) and the obtained NBL do not seem to be adequate. As matter of fact, several subzones in the DBVL show very low naturally occurring arsenic concentrations that the BRIDGE approach is not able to discriminate about a possible anthropogenic contamination. Vice-versa, when analyzing subareas with high natural arsenic concentrations, the BRIDGE approach represents them as contaminated subzones.

Materials and methods

Geological setting of the DBVL

The DBVL constitutes a portion of the middle-low Venetian Plain, which includes the Padua, Treviso and Venice provinces (PD, TV and VE, respectively, in Fig. 1-A). It covers approximately 2,038 km2, with a topographic gradient ranging from 6‰ to 1‰ near the Venetian Lagoon. From a geological perspective, Pleistocene–Holocene deposits fill the Venetian alluvial plain, which results from sediments supplied by the Brenta River. In particular, the shallower portion of the plain (from 5 to 30 meters below ground level (m b.g.l.)) is composed of sediments from the Last Glacial Maximum (LGM), with an age younger than 30,000 years (Fontana et al. 2004, 2008). In the upper part of the DBVL, gravelly and sandy alluvial deposits are present, whereas in the distal region, silty-clayey deposits prevail in the alluvial system, according to the typical structure of Brenta River's megafan (Mozzi et al. 2003; Bondesan et al. 2004). These fine sediments are typical of a floodplain environment, and they often contain several peat layers, with a thickness up to several decimeters and a lateral extension up to several kilometers. Peat layers have an important role in the arsenic release mechanism, because the degradation of organic matter controls the redox conditions of the aquifer (Carraro et al. 2013; Rotiroti et al. 2014; Carraro et al. 2015).

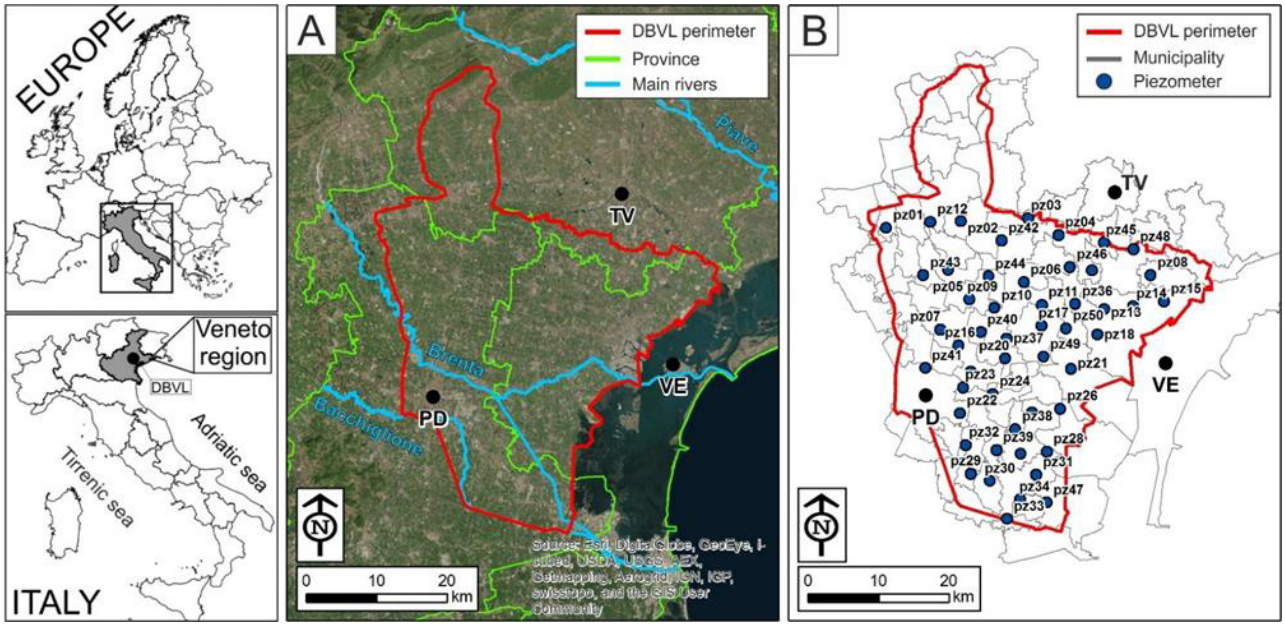

Fig. 1 - The DBVL (Drainage Basin of the Venetian Lagoon) in the alluvial Venetian Plain (A); water sampling network in the study area (B). The main cities of the study area (i.e., Padua, PD, Treviso, TV, and Venice, VE) and their provinces are also reported.

From a hydrogeological point of view, two main alluvial hydrogeological units occur in the Venetian Plain: a large unconfined aquifer extending for 15-20 km in the upper part of the plain from the Prealps, and a multi-layered confined aquifer system in the lower part of the plain towards the Adriatic Sea. These two units correspond respectively to the upper and middle-lower plain environments. The plain springs belt (named the "Fontanili" belt) shows the transition zone from the upper plain to the lower plain, where the water table is very shallow and locally intersects the topographic surface. Excluding the northernmost region, the study area is characterized by a succession of silty layers (i.e., low permeability) and sandy layers (i.e., high permeability), which is where the main aquifers are located (Dal Prà et al. 1992; Fabbri et al. 1993; Vorlicek et al. 2004; Cambruzzi et al. 2009; Trevisani and Fabbri 2010; Fabbri et al. 2011; Fabbri and Piccinini 2013; Piccinini et al. 2015; Fabbri et al. 2016; Piccinini et al. 2016; Piccini et al. 2017; Fig. 2).

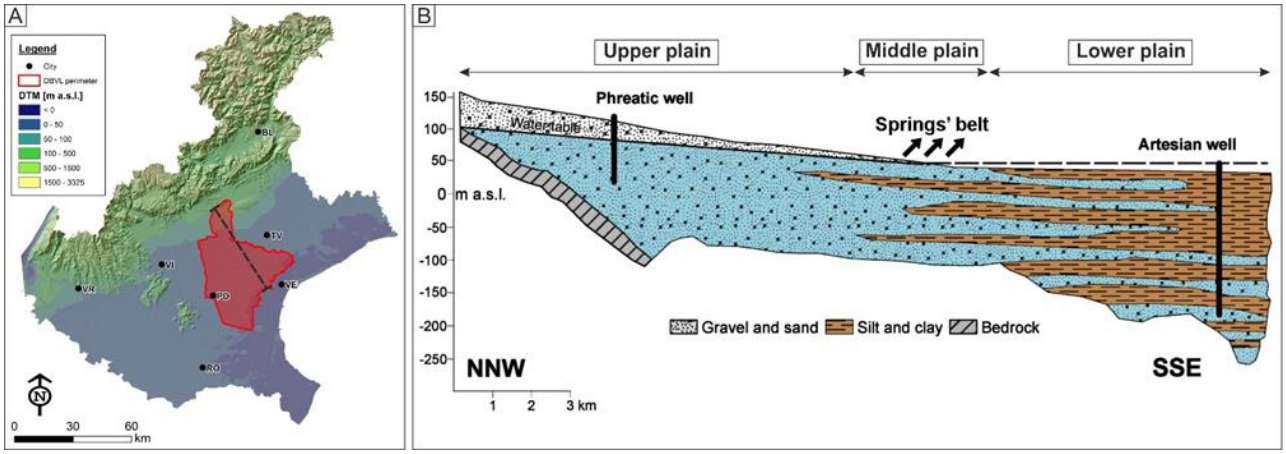

Fig. 2 - The DBVL in the Veneto Region (red area in A); schematic cross-section through the DBVL (modified from Fabbri et al. 2016). The trace of the cross-section is the dashed line in the sketch A.

Available dataset

The "A.Li.Na" project from the Regional Agency for Environmental Protection and Prevention of Veneto (ARPAV) provided the dataset used in this work and estimated the natural background levels (NBLs) of arsenic (As), iron (Fe), manganese (Mn) and ammonic ion (NH_4^+) in groundwater in the DBVL. The sampling network, composed by 50 piezometers, covered the entire investigated area (Fig. 1-B) taking care to avoid zones in which relevant anthropogenic activities could affect the natural status of groundwater (ARPAV, 2014). These piezometers mainly tapped the shallower confined aquifer 10 to 20 m below ground level, which was where the arsenic contamination in the main aquifer occurred. Hydrogeochemical parameters were collected during four seasonal surveys from 2013 to 2014. Groundwater sampling was performed according to the standard protocols suggested by the Italian National Environmental Agency (APAT, 2006). The physical parameters (i.e., pH, Eh, electric conductivity, temperature and dissolved oxygen) were measured by a multiparametric probe (YSI 556 MPS); on the other hand, the chemical parameters were estimated in a laboratory through standardized methods. Arsenic and manganese were estimated by the UNI EN ISO 17294-2:2005 method, iron was estimated by the APAT CNR IRSA 3160 Man 29 2003 method, ammonium was estimated by the APAT CNR IRSA 4030 A1 Man 29 2003 method, and total organic carbon (TOC) was estimated through the APHA 5310-B Ed 21st 2005 method. Furthermore, every sampling point was georeferenced in the Gauss-Boaga coordinate system (Roma 1940 datum, west zone). The concentration values below the limit of detection (i.e., As < 1 µg/L) were changed; this value was set equal to 0.5 µg/L to make all "A.Li.Na" dataset suitable for mapping purposes. Afterwards, based on the BRIDGE suggestions, the average

values of each available variable were considered. The main characteristics of this "averaged" dataset are reported in Table 1. All variables showed a positively-skewed distribution, except for electrical conductivity (EC), redox potential (Eh) and pH, which resembled a normal distribution. In particular, As had a skewness equal to 3.03, indicating a lognormal distribution (Fig. 3).

Table 1 - Descriptive statistics of the average "A.Li.Na" dataset. The "N. obs" and "SD" abbreviations indicate the number of observation points and the standard deviation, respectively.

Variable	N. obs	Mean	SD	Median	Min	Max	Range	Skewness	Kurtosis
As [µg/L]	50	25.69	39.61	10.75	0.50	224.00	223.50	3.03	11.07
Fe [µg/L]	50	1,477.2006	1,619.96	1,198.50	4.88	8,464.75	8,459.87	2.14	5.96
Mn [µg/L]	50	227.57	208.07	180.50	0.88	1,131	1,130.12	2.13	5.88
NH4 [µg/L]	50	2,968.5	4,217.36	1,063.75	12.50	17,797.5	17,785	1.81	2.58
SO4 [µg/L]	50	40,312.5	43,225.41	28,000	1,500	231,000	229,500	2.24	6.09
EC [µS/cm]	50	817.80	206.37	807.74	435.83	1,338.30	902.48	0.24	-0.30
Eh [mV]	45	-28.89	43.53	-26.50	-112.00	90.95	202.95	0.28	0.24
pH [-]	50	7.16	0.16	7.15	6.82	7.56	0.75	0.23	-0.29
TOC [mg/L]	50	2.75	1.88	2.11	0.24	10.15	9.91	1.60	3.09

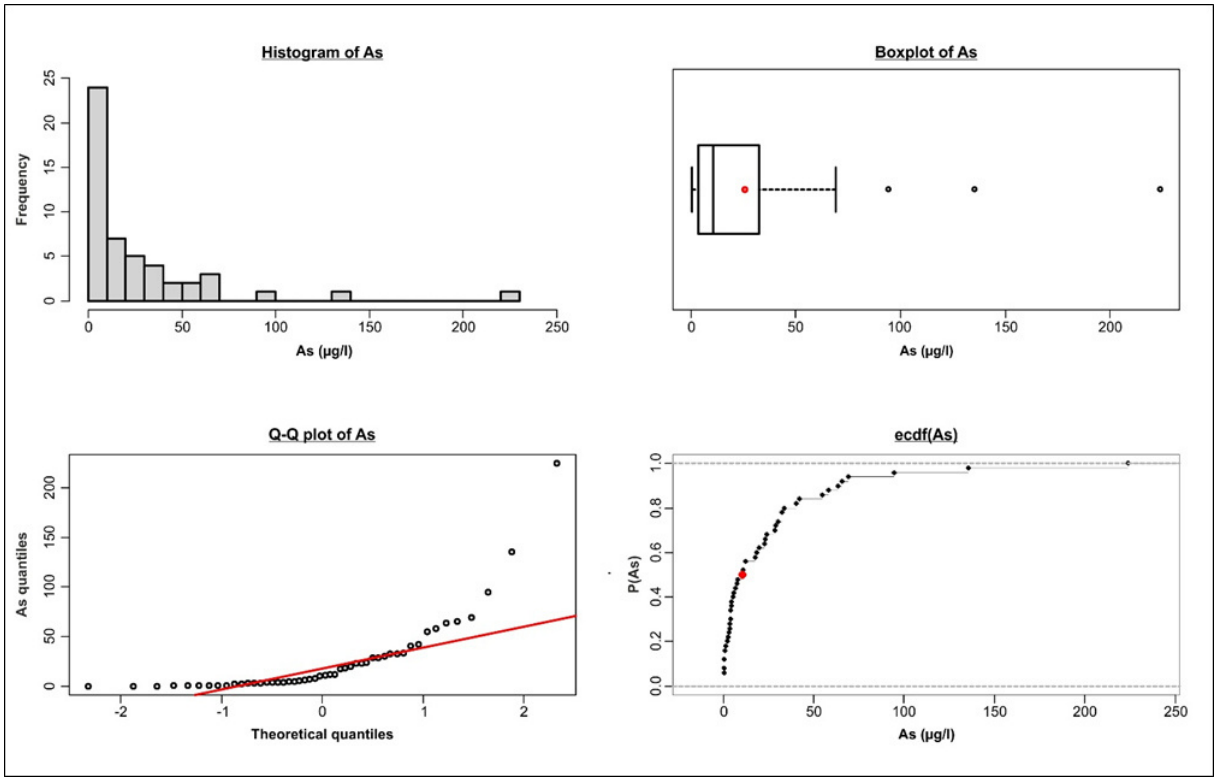

Fig. 3 - Exploratory data analysis of arsenic values. The red point in the boxplot diagram and the experimental cumulative density function (ECDF) represent the mean value of arsenic, whereas the red line in the Q-Q plot represents the theoretical normal distribution.

Arsenic occurrence in groundwater

Arsenic is not widespread in the Earth's continental crust. It is present in both igneous and sedimentary rocks at an average concentration of 2–3 mg/kg (Mandal 2002; Herath et al. 2016), but the highest concentrations are in alluvial sediments rather than in rocks. Arsenic exists in minerals such as arsenate, arsenite, sulfide, sulfosalt and Fe-Mn hydroxides (Mandal 2002), which form soil and aquifer sediments. Furthermore, arsenic may be adsorbed by clay minerals, organic matter and Fe-Mn (hydro)oxides (Nickson et al. 2000; McArthur et al. 2001; Rowland et al. 2007; Carraro et al. 2013; Molinari et al. 2013; Baviskar et al. 2015; Carraro et al. 2015; Molinari et al. 2015). The interactions among groundwater and these minerals allow several geochemical triggers for arsenic mobilization. There are four release processes that are the most important and clearly depend on the geochemical condition of the subsoil. The first one is the reductive dissolution of Fe-Mn hydroxides, which requires anoxic conditions (Eh < 0) and a pH ranging from 6.5 to 7.5. The second one concerns the alkali desorption process under oxic condition (Eh > 0) and a pH ~ 8. The ion exchange between soluble alkali species and adsorbed arsenic allows the release of metalloid into groundwater. The third one is sulfide oxidation, which represents an important cause of arsenic groundwater contamination due to the production of acid drainage that is rich in toxic inorganic pollutants at high concentrations. This type of process is available when there are As-bearing sulfides in an oxic and acid environment (Eh > 0; pH < 7). The last one is the interaction between groundwater and organic matter within aquifer sediments (Herath et al. 2016). Organic matter may be a source of arsenic in addition to its role as a redox driver (Rotiroti et al. 2014). Therefore, reductive dissolution, sulfide oxidation and organic matter decomposition are thought to be the most significant geochemical triggers that release arsenic into groundwater at a large scale (Bauer and Blodau 2006; Herath et al. 2016). Arsenic may exist in several valence states (-3, 0, +3, and +5), but in groundwater, its valence is either +3 or +5. Looking at the Eh-pH diagram in Fig. 4, both As(III) and As(V) form oxyanions in aqueous solutions (Lu and Zhu 2011). In an oxygenated water system with a pH < 2, arsenious acid (H_3AsO_4) is predominant, whereas in a pH range from 2 to 11, arsenic exists as $H_2AsO_4^-$ and $HAsO_4^{2-}$, respectively. In a reducing environment, uncharged $As(OH)_3$ is the main species at a pH < 9; however, if the pH is greater than 11, AsO_2OH^{2-} exists. Fully dissociated arsenic is rare because it requires strongly reducing conditions and pH values over 11.5. Taking into account the "A.Li.Na" dataset, we can note that the samples (red dots in Fig. 4) fall mainly within the stability field of $As(OH)_3$ formed by the reduced As(III).

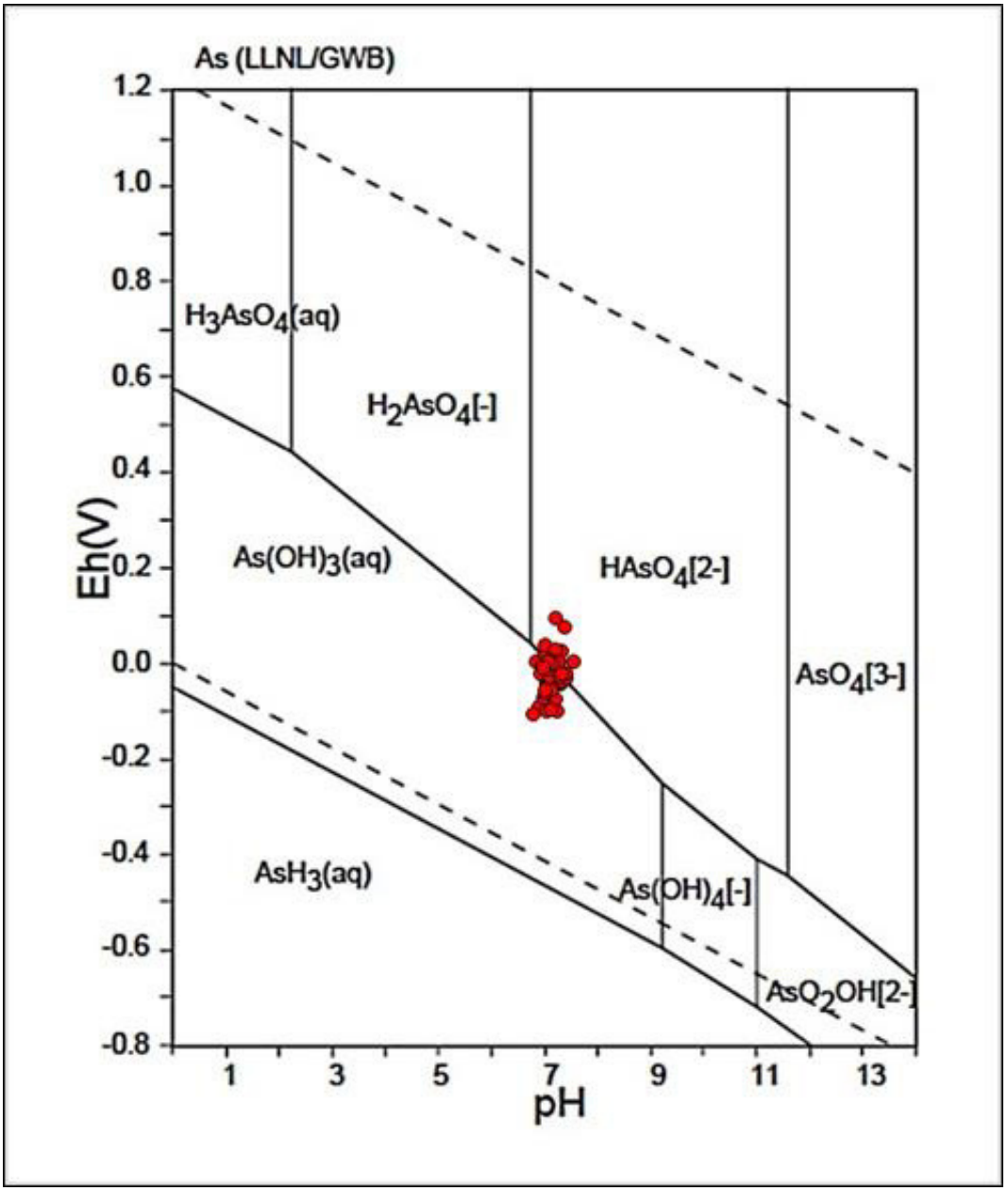

Fig. 4 - Eh-pH diagram of arsenic species built under the conditions of T=298.15 [°K] and P=105 [Pa] (Takeno 2005). The red dots represent the experimental data used for this study. The majority of the sample data falls into the arsenic-reduced species stability field (modified from Dalla Libera et al. 2017).

Some geochemical studies of the DBVL (Ungaro et al. 2008; Dalla Libera et al. 2016; Dalla Libera et al. 2017) demonstrated that Eh, NH_4^+ and Fe are related to As concentrations, although they are not the only geochemical parameters involved (Biswas et al. 2014; Carraro et al. 2015). These correlations are visible in the correlogram in Fig. 5, where the correlation coefficients are respectively equal to -0.39, 0.64 and 0.67 for redox potential, ammonic ion and iron. Analyzing the "A.Li.Na" data, the As release interval ranges from 0 mV to -100 mV (Fig. 5), whereas the arsenic concentration decreases significantly below the Eh threshold of -200 mV

due to the co-precipitation of As-bearing sulfides (Carraro et al. 2015). Under these conditions, the presence of sulfur is strictly connected with organic matter (OM) availability (i.e., peat layers) during the degradation processes. The occurrence of organic matter may be evaluated by the relation between As and NH_4^+ concentrations (Fig. 5), where the ammonium ion is derived from the degradation of OM under reduced conditions (Molinari et al. 2012; Molinari et al. 2014; Molinari et al. 2015). Indeed, NH_4^+ could be considered an adequate marker of peat presence in or around the investigated aquifer, which confirms reducing conditions.

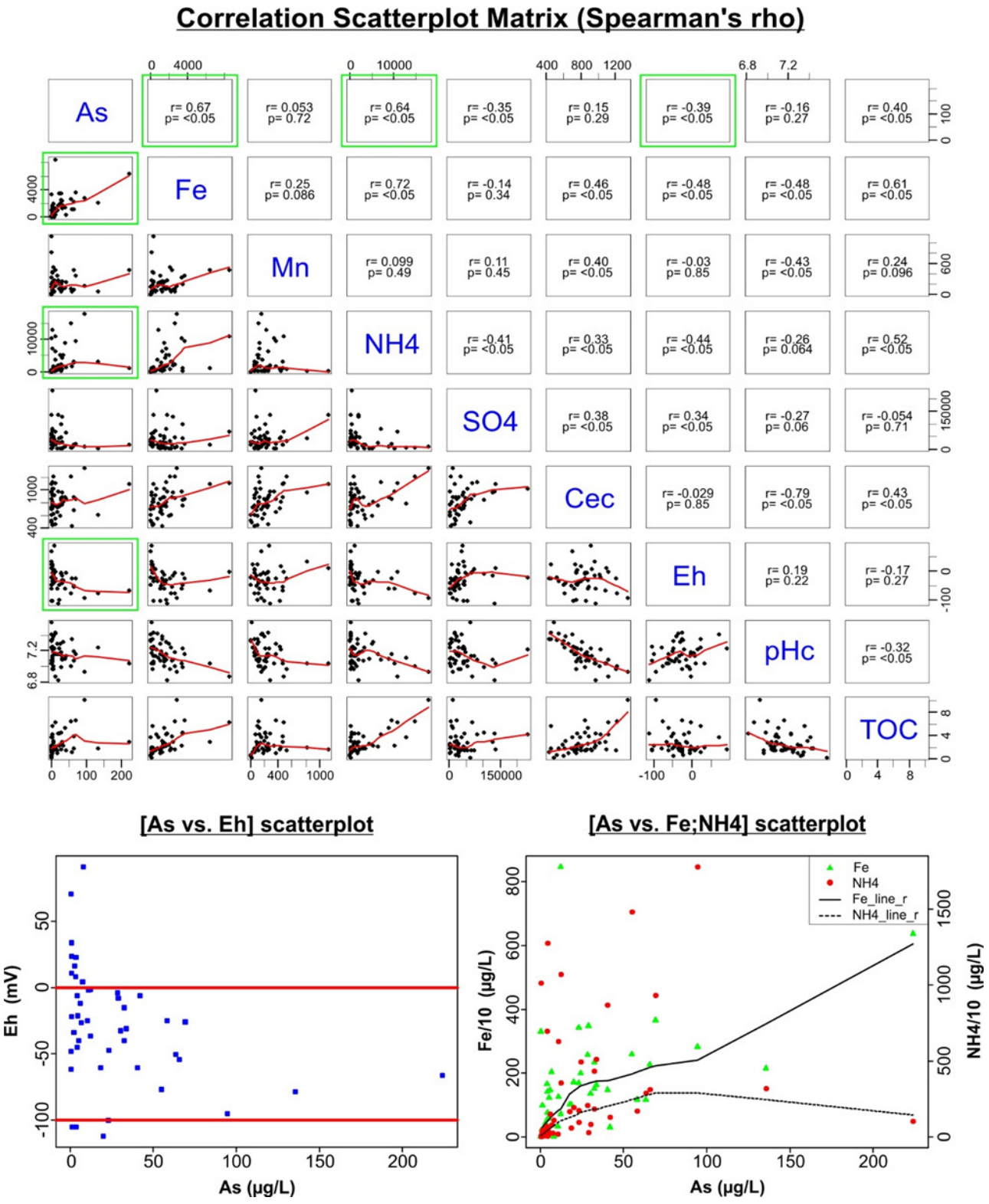

Fig. 5 - Correlation scatterplot matrix among several elements or compounds dissolved in groundwater. The acronyms "r" and "p" specify the Spearman's correlation index and its associated p-value, respectively. The most important relations are As vs. Eh, As vs. Fe and As vs. NH_4^+, which are highlighted by green squares. The horizontal red lines in the As vs. Eh scatterplot highlight the Eh release interval, whereas on the right side of the scatterplot, the solid and dashed lines represent the locally weighted polynomial regression line (LOWESS smoother, Cleveland 1979, Cleveland

and McGill 1985, Gotway et al. 2002) for Fe and NH_4^+, respectively. LOWESS lines are represented in the upper correlation matrix by red lines.

Geostatistical indicator approach

The indicator kriging method (IK) is one of the best methods for defining spatial (non)exceedance probabilities with respect to a threshold value. Indicator kriging (Journel 1982, 1983) is a non-parametric technique that estimates the probability of (non)exceedance of a regionalized random variable, *Z(u)*, with respect to an established threshold (t) at an unsampled location (u). The probability of (non)exceedance is defined by the value of the cumulative distribution function, *F(u;t)*:

$$F(u;t) = P[Z(u) \leq t] \qquad [1]$$

IK is based on an indicator variable, *i(u; t)*, depending on the spatial location, u, and the predefined threshold value, t, from a given continuous random variable.

$$i(u_i;t) = \begin{cases} 1, z(u_i) \leq t \\ 0, otherwise \end{cases} \qquad [2]$$

As visible from equation [2], $i(u_i;t)$ represents a binary variable that assumes either 1 or 0 depending on the value of *z(u)* with respect to t (Fig. 6).

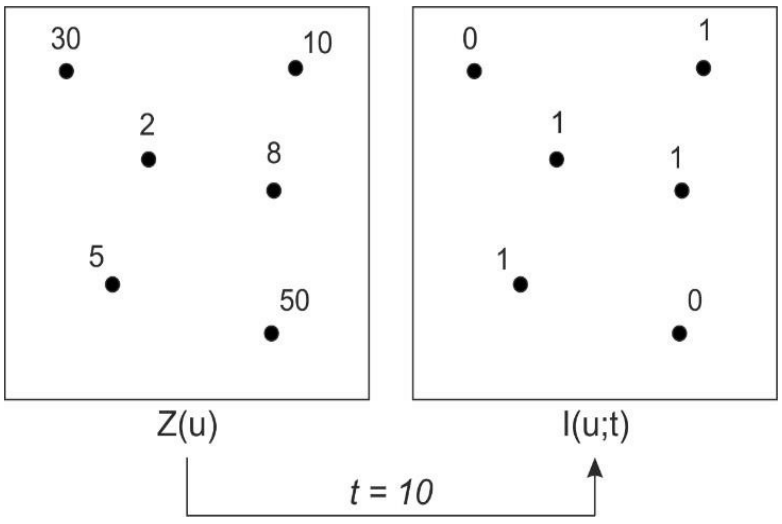

Fig. 6 - Conversion of a continuous random variable, z(ui), into an indicator variable, i(ui; t). This is an essential step in IK prediction.

The expected value (E) and the variance (Var) of the indicator variable are:

$$E[I(u;t)] = 1 \cdot P[Z(u) \leq t] + 0 \cdot P[Z(u) > t] = P[Z(u) \leq t] = F(u;t) \quad [3]$$

$$Var[I(u;t)] = F(u;t) - F^2(u;t) \qquad [4]$$

Taking into account equation [3], the inference of the expected value (*E[I(u; t)]*) is equal to the value of the cumulative distribution function at position u with respect the threshold t (i.e., *F(u;t)*). Therefore, equation [3] represents the essence of the IK method. The prevision of the indicator variable, $\hat{I}(u_0;t)_{IK}$, in unknown position u_0 is the expected value of the indicator variable, $\hat{E}[I(u;t)]$, that corresponds to the value of the cumulative distribution function, $\hat{F}(u_0;t)_{IK}$, with respect to threshold t. Indicator kriging is an estimation technique that is defined as follows:

$$\hat{I}(u_0;t)_{IK} \cong \sum_{i=1}^{n} \omega_i{}^{IK}(u;t) i(u_i;t) \qquad [5]$$

$$\hat{I}(u_0;t)_{IK} = \hat{F}(u_0;t)_{IK} \qquad [6]$$

IK results in a linear combination of indicator variable $i(u_i;t)$ at different locations (u_i) with respect to threshold t, and $\omega_i{}^{IK}(u;t)$, which represents the related weights. In this way, where $\hat{I}(u_0;t)_{IK}$ represents the estimated value (i.e., expected value $E[I(u_0;t)]$ in [3]), the value of the cumulative distribution function in location u_0 with respect to threshold t results in the probability of (non)exceedance with respect to defined threshold t ($\hat{F}(u_0;t)_{IK}$ in [6]).

The weights, derived by indicator variograms at the thresholds, are:

$$\gamma(h) = \frac{1}{2N(h)} \sum_{i=1}^{n} [i(u_i;t) - i(u_i + h;t)]^2 \qquad [7]$$

Nevertheless, because indicator kriging (IK) considers thresholds separately, a more correct approach is indicator cokriging (ICK), which considers different thresholds together and is able to take into account the relationships among indicator variables at different thresholds. The ICK formalism takes into account all indicator variograms and cross-variograms in the definition of weights. The indicator cokriging estimator can be written as follows:

$$\hat{F}(u_0, t_j)_{ICK} \cong \sum_{j=1}^{T} \sum_{i=1}^{n} \omega_{i_j}^{ICK}(u;t_j) i(u_{i_j};t_j) \qquad [8]$$

where *j* represents the number of defined t thresholds, and *i* represents the number of spatial locations at position u. Thus, in order to obtain an accurate and theoretically correct prediction for the (non)exceedance probabilities of arsenic in groundwater, this work considers an ICK estimator.

Geostatistical analysis

The geostatistical analysis was performed through the gstat package (Pebesma 2004) available in the R software (R Core Team 2017). The use of the R environment allows us to have more control on the geostatistical process and more freedom during variogram modeling. First, several threshold values (t) were defined in order to source the indicator variables used for exceedance probability prediction. Then, we set up the indicators in Table 2 based on the statistical structure of the dataset and the TV suggested by Annex III of the European GWD.

Table 2 - Summary of the indicator variables and their associated threshold values.

Name of Indicator variable	Indicator variable	Associated threshold value
As_TV	i(As ≤ 10)	10 µg/L
As_int	i(10 < As ≤ 31.4)	Range 10 – 31.4 µg/L
As_median	i(As > 31.4)	31.4 µg/L

The values used to define the indicator variables represent the TV (10 µg/L) and the median (31.4 µg/L) of our dataset. Once the indicator variables have been determined, a variogram analysis can be performed. In this phase, we are interested in thoroughly evaluating the spatial structure of the indicator variables by the variogram (γ(h)) analysis, which describes how spatial continuities change with distance (h) and direction. This analysis did not reveal any kind of anisotropy (Fig. 7).

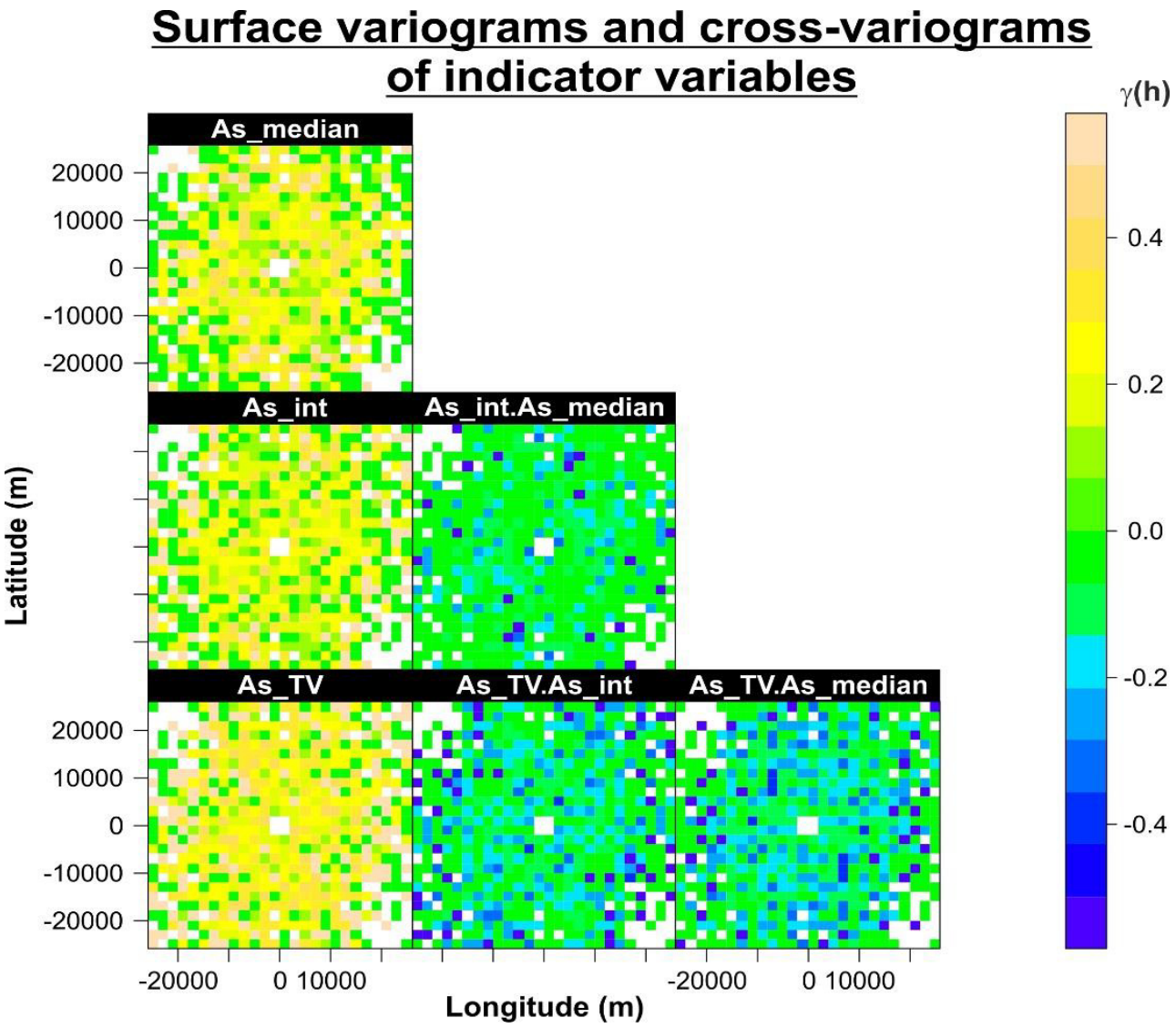

Fig. 7 - Indicator surface variograms (1st column) and cross-variograms (2nd and 3rd columns). The blank pixels represent regions where there are not pairs for the estimation of variograms and cross-variograms γ(h).

We analyzed only the omnidirectional variograms (Fig. 8) characterized by a spatial lag (h) of 2,000 m and a cutoff value equal to 25,000 m. These parameters approximate the smallest distance between two sampling points and the average distance at which the data lose their spatial relationship.

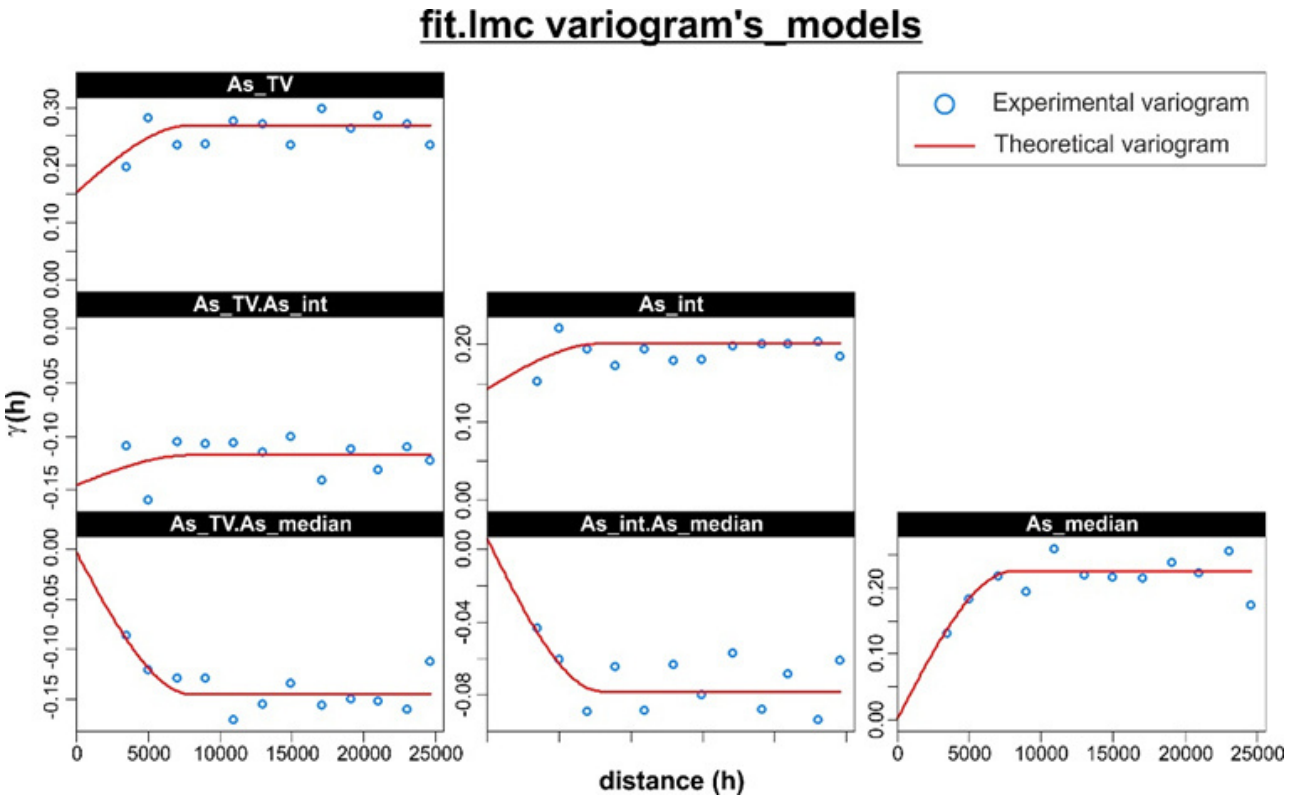

Fig. 8 - Omnidirectional, experimental direct and cross-variograms (blue circles) and their theoretical models (red lines). The diagonal plots represent the direct indicator variograms. The theoretical models are estimated by means of an automatic fitting function, "fit.lmc", which is in the gstat package.

Analyzing the experimental variograms (Fig. 8), a "spherical" theoretical model [9] approximates the spatial continuity structure of I(u,t) adequately. The spherical model is defined as follows:

$$\gamma(h) = \begin{cases} c_0 + c; & h > a \\ c_0 + c\left[\frac{3}{2}\frac{|h|}{a} - \frac{1}{2}\left(\frac{|h|}{a}\right)^3\right]; & h \le a \end{cases} \qquad [9];$$

where c_0 represents the nugget effect, c represents the partial sill (psill) and a represents the range. Because we decided to use the cokriging algorithm, variogram modeling was quite complex because the models needed to satisfy the co-regionalization rules (Journel and Huijbregts 1978; Goovaerts 1997). Thus, an automatic fitting process was used with the "fit.lmc" command in the gstat package. This command allows us to fit several variogram models with respect to the linear model of co-regionalization for both direct and cross-variograms. In particular, the fitted spherical models are shown in Table 3.

Table 4 - The direct and cross-variogram models used to predict the exceedance probabilities of arsenic in the DBVL. These models satisfy the linear model of co-regionalization.

Variogram model	Indicator variable
$\gamma(h) = \begin{cases} 0.153 + 0.117; & h > 8000 \\ 0.153 + 0.117\left[\frac{3}{2}\frac{\lvert h\rvert}{8000} - \frac{1}{2}\left(\frac{\lvert h\rvert}{8000}\right)^3\right]; & h \leq 8000 \end{cases}$	[As_TV]
$\gamma(h) = \begin{cases} 0.143 + 0.058; & h > 8000 \\ 0.143 + 0.058\left[\frac{3}{2}\frac{\lvert h\rvert}{8000} - \frac{1}{2}\left(\frac{\lvert h\rvert}{8000}\right)^3\right]; & h \leq 8000 \end{cases}$	[As_int]
$\gamma(h) = \begin{cases} 0.002 + 0.223; & h > 8000 \\ 0.002 + 0.223\left[\frac{3}{2}\frac{\lvert h\rvert}{8000} - \frac{1}{2}\left(\frac{\lvert h\rvert}{8000}\right)^3\right]; & h \leq 8000 \end{cases}$	[As_median]
$\gamma(h) = \begin{cases} -0.145 + 0.028; & h > 8000 \\ -0.145 + 0.028\left[\frac{3}{2}\frac{\lvert h\rvert}{8000} - \frac{1}{2}\left(\frac{\lvert h\rvert}{8000}\right)^3\right]; & h \leq 8000 \end{cases}$	[As_TV – As_int]
$\gamma(h) = \begin{cases} -0.004 - 0.141; & h > 8000 \\ -0.004 - 0.141\left[\frac{3}{2}\frac{\lvert h\rvert}{8000} - \frac{1}{2}\left(\frac{\lvert h\rvert}{8000}\right)^3\right]; & h \leq 8000 \end{cases}$	[As_TV – As_median]
$\gamma(h) = \begin{cases} 0.006 - 0.084; & h > 8000 \\ 0.006 - 0.084\left[\frac{3}{2}\frac{\lvert h\rvert}{8000} - \frac{1}{2}\left(\frac{\lvert h\rvert}{8000}\right)^3\right]; & h \leq 8000 \end{cases}$	[As_int – As_median]

Based on the above variogram analysis, a cross-validation procedure was performed. Cross-validation tested the ability of the model to reproduce the spatial continuity structure by a prediction of the known indicator variable. The results of the cross-validation suggested the adequacy of the chosen theoretical model and resulted in a mean absolute error (MAE) equal to 0.016 and a root mean squared error (RMSE) of 0.018. The low values of these parameters express the adequate prediction capacity of the model, giving an average magnitude of the errors in a set of predictions (Bivand et al. 2008). In the literature, two other parameters are used to evaluate the kriging accuracy: the mean error (ME) and the kriged reduced mean error (KRME; Adhikary et al. 2011; Ohmer et al. 2017). These error indexes should be close to zero, and they were 1.55E-05 and 8.50E-06 in our model, respectively. For these results, our prediction can be considered an adequate inference process that well reproduces both the spatial structure of the indicator variables and the exceedance probabilities.

Results and discussion

The distributions of the exceedance probabilities of arsenic are displayed as 2D maps with respect to the predefined concentration thresholds. In this way, the spatial information is more suitable and easier to achieve for future environmental management.

Exceedance probability mapping

As mentioned above, the exceedance probability estimation requires one or more thresholds values (t). Based on both the statistical analysis of dataset and European normative, we used thresholds of 10 μg/L and 31.4 μg/L, as shown in Table 2. The former represents the arsenic TV established by the EU, and the latter is the median of our dataset. We choose the median because it represents 50% of the experimental data and defines an intermediate class. Looking at the probability maps in Fig. 9, the study area shows different probabilities varying with the threshold (e.g., As ≤ 10 μg/L). The red tones indicate high probability values, and the blue tones display zones with low probability. The green zones highlight local areas with exceedance probabilities of approximately 50%, indicating maximum uncertainty. The A map in Fig. 9 represents arsenic probabilities lower than 10 μg/L (As_TV). We note a large part of the area with probabilities from 60% to 80%, showing how probabilities with higher arsenic concentrations are localized and limited. Considering the probabilities related to a threshold of 10 μg/L < As ≤ 31.4 μg/L (As_int), the B map in Fig. 9 shows low probabilities linked to a medium level of arsenic in the same areas with low probabilities when using the previous threshold. This result is important and highlights the abrupt spatial change from a low arsenic level to a high arsenic level. According to the previous scenarios, the C map gets on light the presence of some local areas where the probability of exceeding the arsenic threshold of 31.4 μg/L (As_median) is higher, reaching probabilities from 70% to 100%. The three described scenarios are linked to the geological and hydrogeological characteristics of the study area. In these zones (i.e., where arsenic has high probabilities to be greater than the median value), there are specific geochemical conditions linked to the occurrence of both peat layers and silty-clayey deposits (Dalla Libera et al. 2016; Dalla Libera et al. 2017).

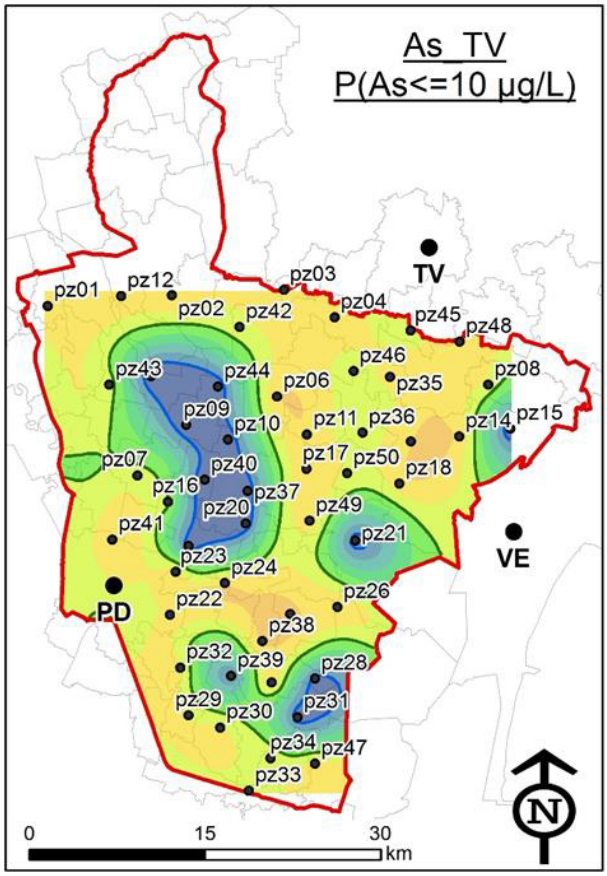
As_TV
P(As<=10 µg/L)
TV
VE
PD
pz01
pz12
pz03
pz02
pz42
pz04
pz45
pz48
pz46
pz43
pz44
pz06
pz35
pz08
pz09
pz10
pz11
pz36
pz14
pz15
pz07
pz40
pz17
pz50
pz18
pz16
pz37
pz20
pz49
pz41
pz21
pz23
pz24
pz22
pz26
pz38
pz32
pz39
pz28
pz29
pz30
pz31
pz34
pz47
pz33
0
15
30
km
N

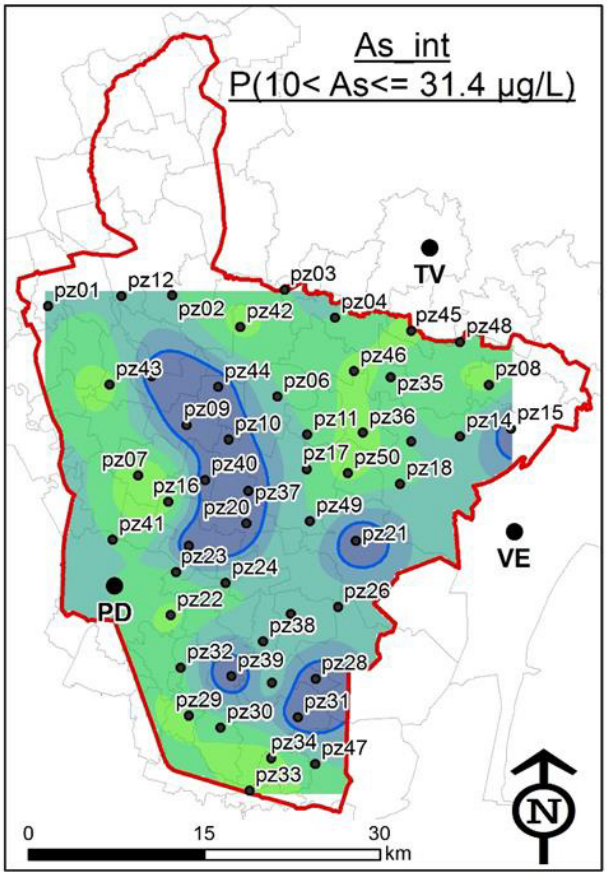
As_int
P(10< As<= 31.4 µg/L)
TV
VE
PD
pz01
pz12
pz03
pz02
pz42
pz04
pz45
pz48
pz46
pz43
pz44
pz06
pz35
pz08
pz09
pz10
pz11
pz36
pz14
pz15
pz07
pz40
pz17
pz50
pz18
pz16
pz37
pz20
pz49
pz41
pz21
pz23
pz24
pz22
pz26
pz38
pz32
pz39
pz28
pz29
pz30
pz31
pz34
pz47
pz33
0
15
30
km
N

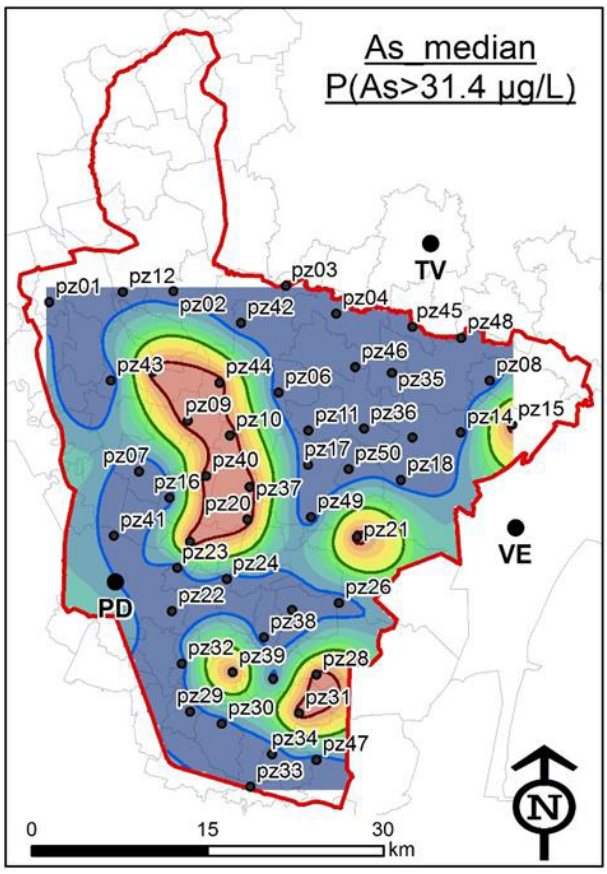
As_median
P(As>31.4 µg/L)
TV
VE
PD
pz01
pz12
pz03
pz02
pz42
pz04
pz45
pz48
pz46
pz43
pz44
pz06
pz35
pz08
pz09
pz10
pz11
pz36
pz14
pz15
pz07
pz40
pz17
pz50
pz18
pz16
pz37
pz20
pz49
pz41
pz21
pz23
pz24
pz22
pz26
pz38
pz32
pz39
pz28
pz29
pz30
pz31
pz34
pz47
pz33
0
15
30
km
N

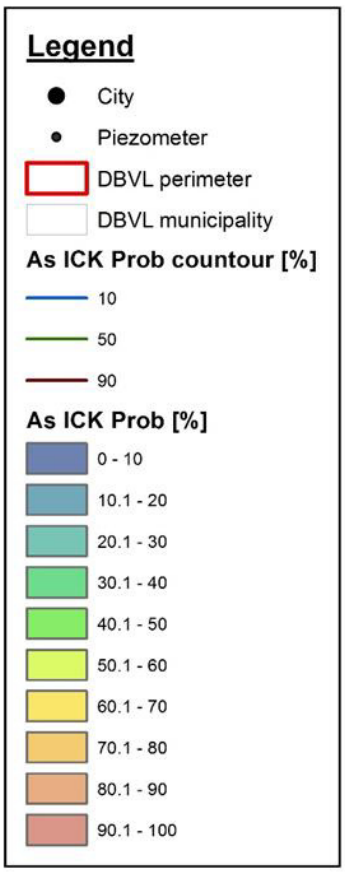
Legend
City
Piezometer
DBVL perimeter
DBVL municipality
As ICK Prob countour [%]
10
50
90
As ICK Prob [%]
0 - 10
10.1 - 20
20.1 - 30
30.1 - 40
40.1 - 50
50.1 - 60
60.1 - 70
70.1 - 80
80.1 - 90
90.1 - 100

Fig. 9 - Probability maps of arsenic in the DBVL. Each map shows the probabilities referred to each logical condition depicted in Table 2. Insets A, B and C concern the indicator variables As_TV (P ≤ 10 μg/L), As_int (10 < P ≤ 31.4 μg/L) and As_median (P > 31.4 μg/L), respectively. The cities of Padua (PD), Treviso (TV) and Venice (VE) are also shown.

To evaluate the uncertainty related to the prediction process, the standardized conditional entropy index (Hnorm) is calculated (Goovaerts 1997). This index allows one to get information about the lack of data for a study variable, and its spatial distribution. In this work, it represents the uncertainty of the spatial information linked to the predicted exceedance probabilities. In other words, the Hnorm map suggests both zones where the information is accurate and suitable for environmental management purposes and where the sampling network should be improved. As visible in Fig. 10, the maximum entropy (i.e., Hnorm ≥ 90%) is located in zones with a lack of sampling points and high concentration variability. As matter of fact, these regions are the same where ICK pointed out a probability of 50% for both the As_TV (P ≤ 10 μg/L) and As_median (P > 31.4 μg/L) indicators. Low values of Hnorm, instead, cover the zones where the data are well distributed and quite similar. Where the data are present, even if sparse, the Hnorm index does not exceed 60% - 70% and it usually ranges from 0% to 20% (blue colors in Fig. 10). The conditional entropy map depicts a good reliability in the zones where the data are well distributed, and a rough result where data are missing or sparse. In this sense, the normalize entropy map gives us an important hint for a possible enhancement of sampling network, showing where new data should be acquired (i.e., zones with Hnorm ≥ 90%). Anyway, the applied method (ICK) reproduces quite well the exceedance probabilities getting a good trade-off between the available data and the prediction accuracy.

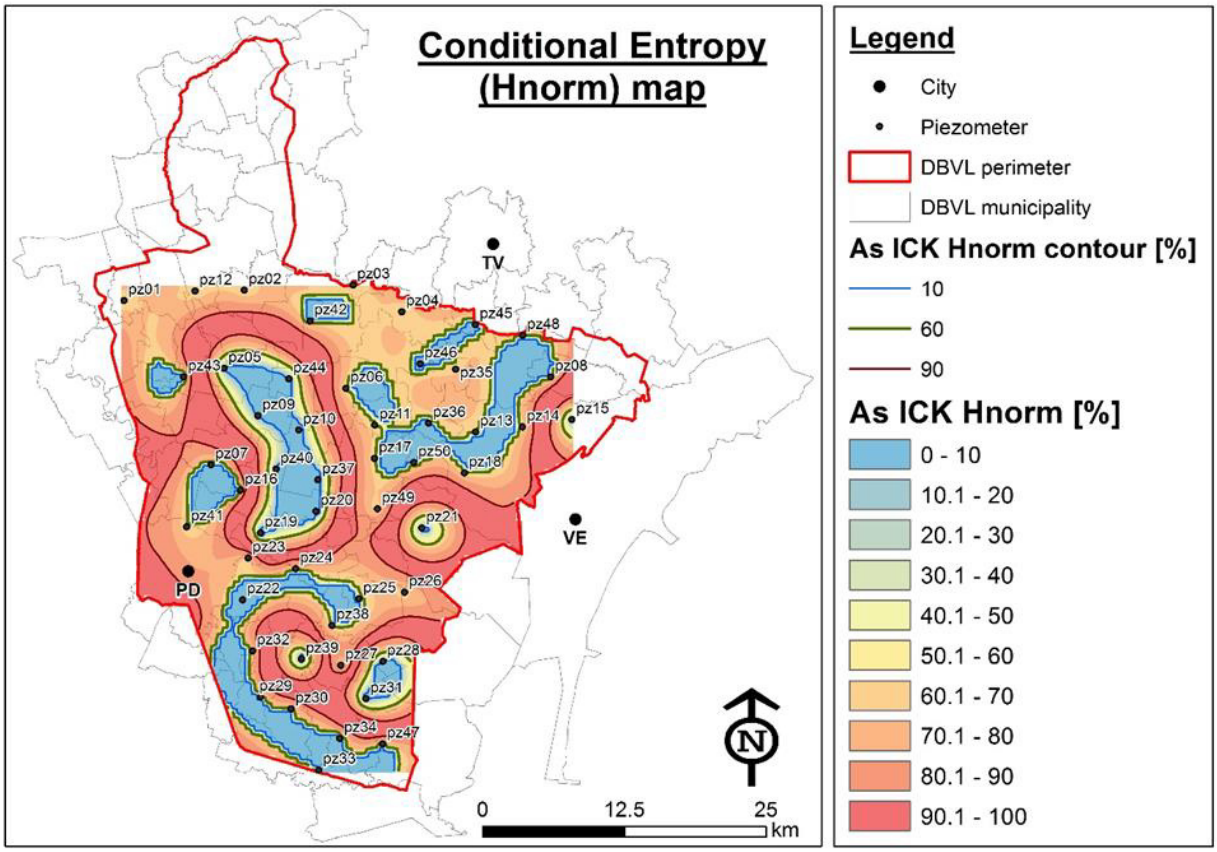

Fig. 13 - Conditional entropy (Hnorm) map obtained considering the probabilities calculated through the ICK. The map shows the location of the main cities of Padua (PD), Treviso (TV) and Venice (VE) in the study area.

Implication in groundwater management

The results obtained by the ICK, and its reduced uncertainty, demonstrate the potential of this approach for enhancing the NBL estimation and its usefulness for the decision process of stakeholders. The use of ICK, through exceedance probability mapping, improves the approach suggested in Dalla Libera et al. 2017. It introduces a probability approach in the LNBL definition that is suggested to evaluate the risk involved in any decision-making process (Goovaerts 1997). Considering the results in the study area, it is evident that a unique NBL value is inadequate for environmental management purposes. The exceedance probability maps highlight heterogeneous probability distributions resulting in high arsenic concentration in the DBVL groundwater enclosed by areas with low arsenic content. As matter of fact, a large region of the study area presents high probabilities that do not exceed the TV (10 µg/L) with respect to limited zones with high probabilities that exceed the threshold median (31.4 µg/L). In a similar context, a patchy distribution of arsenic requires the definition of several local NBLs rather than a single one. This supports the usefulness of this kind of approach when

discriminating potentially contaminated zones from uncontaminated ones. Actually, the results show how the applied geostatistical method gives good information even when the data are sparse. From the economical perspective, ICK allows experts and stakeholders to get a good trade-off between investing for the sampling network enhancement and getting reliable information. Furthermore, the normalized entropy analysis lets to highlight the specific zones in which a further investigation is needed, reducing the costs for a possible sampling network improvement. To test the feasible enhancement revealed by the combination of the ICK and the 90th percentile method, we estimated several local NBLs in areas depicted by the As_TV and As_median indicators. Due to the definition of several local areas with different exceedance probabilities, we are able to divide the experimental dataset into several subsets, including samples that fall inside areas with high probabilities of non-exceedance (As≤10 μg/L) or exceedance (As>31.4 μg/L) with respect to the considered threshold. By applying the 90th percentile method on every subset, we can estimate the LNBL. For instance, considering a probability equal to 60%, the maps described in the previous chapter allow for the definition of two main LNBLs as shown in the following table.

Table 5 - LNBLs estimated from previous probability maps. Every LNBL is estimated through a number of samples inside the areas associated with the probability classes. The red numbers indicate a non-exhaustive number of samples from a statistical point of view.

Name of Indicator variable	Probability class	90th Percentile [μg/L]	No. samples
As_TV	P(As ≤ 10 μg/L)	6.53	24
As_median	P(As > 31.4 μg/L)	127.30	13

From a statistical perspective, the LNBL estimation process would require at least 30 samples (Bortolucci et al. 2009); therefore, the obtained values are rough but meaningful for explaining the advantages brought by this approach. At this stage, we are getting on light the aids that ICK can give to the NBL definition, even if a relative small amount of data is available. As mentioned before, the "A.Li.Na" project calculated a NBL equal to 74 μg/L; compared with the LNBL values (Tab. 4) the difference is huge. A unique NBL value for the DBVL is too high for areas with low arsenic concentrations and too low for those with high values. These situations could make no sense, especially when one wants to discriminate polluted areas from naturally contaminated ones.

Conclusions

The results presented in this paper show how a geostatistical approach combined with a 90th percentile method allows for the application of the NBL concept in a more critical way. The map of exceedance probabilities of arsenic allows for the identification of critical areas and highlights where arsenic values do not exceed the TV of the EU. In particular, these results elucidate the importance of calculating a local NBL related to different geostatistically defined areas. Using the indicator cokriging approach, the definition of LNBLs takes advantage of the arsenic spatial distribution related to the geochemical relationships occurring in the aquifer. Through BRIDGE suggestions, the European GWD proposes a NBL value without considering the spatial distribution of contaminants. The LNBL concept aims to reduce errors associated with a unique NBL definition by improving, spatially, the distinguishing between the natural occurrence of arsenic and anthropogenic pollution. By defining a LNBL for every (non-) exceedance probability class, the monitoring of anthropogenic pollution events can be enhanced; above all, as in our case, the monitoring of areas with high probabilities that do not exceed the threshold value of the EU can be improved. Although the sampling network of the specific local areas should be enhanced, the suggested approach proves the improvements given by LNBLs with respect to a unique NBL value. In addition, the proposed approach allows for a global view of the study area, which forms decisions regarding water and environmental management and improves the characterization plan necessary for the evaluation of potentially contaminated sites.

Acknowledgment

This work was funded by the Venice Province (project “IDRO”, grant given to P. Fabbri). We thank the ARPAV agency, in particular the internal water observatory, for sharing their data concerning arsenic groundwater contamination in the DBVL.

References

Adhikary PP, Dash CJ, Bej R, Chandrasekharan H (2011) Indicator and probability kriging methods for delineating Cu, Fe, and Mn contamination in groundwater of Najafgarh Block, Delhi, India. Environ Monit Assess 176:663–676. doi: 10.1007/s10661-010-1611-4

APAT (2006) Handbook for environmental investigation upon contaminated sites. Handbooks and guidelines (in Italian), I.G.E.R. srl, Roma

APHA (2005) Standard Methods for the Examination of Water and Wastewater. 21st Edition, American Public Health Association/American Water Works Association/Water Environment Federation, Washington DC

ARPA (2014) ALiNa – Analysis of the Natural Background Level for some compounds within the groundwater of the shallow aquifer in the Drainage Basin to the Venice Lagoon (Brenta river alluvial system) – Report and data presentation (in Italian)

Baalousha H (2010) Assessment of a groundwater quality monitoring network using vulnerability mapping and geostatistics: A case study from Heretaunga Plains, New Zealand. Agric Water Manag 97:240–246. doi: 10.1016/j.agwat.2009.09.013

Bauer M, Blodau C (2006) Mobilization of arsenic by dissolved organic matter from iron oxides, soils and sediments. Sci Total Environ 354:179–190. doi: 10.1016/j.scitotenv.2005.01.027

Baviskar S, Choudhury R, Mahanta C (2015) Dissolved and solid-phase arsenic fate in an arsenic-enriched aquifer in the river Brahmaputra alluvial plain. Environ Monit Assess 187:93. doi: 10.1007/s10661-015-4277-0

Biswas A, Gustafsson JP, Neidhardt H, et al (2014) Role of competing ions in the mobilization ofarsenic in groundwater of Bengal Basin: Insight from surface complexation modeling. Water Res 55:30–39. doi: 10.1016/j.watres.2014.02.002

Bivand R.S, Pebesma E.J, Gomez-Rubio V (2009) Applied spatial data analysis wit R; Springer, ISBN 978-0-387-78170-9, DOI: 10.1007/978-0-387-78171-6

Bondesan A, Meneghel M (2004) Geomorphology of the Venice Province (in Italian). Esedra, Padova

Bartolucci E, Bussettini M, Calace N, D'Aprile L, Fratini M, Guerra M, Marangio L, Pirani G (2009) Guidelines for defining the Natural Background Values of inorganic substances in groundwater, ISPRA report (in Italian)

Cambruzzi T, Conchetto E, Fabbri P, Marcolongo E, Rosignoli A, Zangheri P (2009) Underground water resources in the Venetian central plains. Rend Online della Soc Geol Ital 6:127–128

Carraro A, Fabbri P, Giaretta A, et al (2013) Arsenic anomalies in shallow Venetian Plain (Northeast Italy) groundwater. Environ Earth Sci 70:3067–3084. doi: 10.1007/s12665-013-2367-2

Carraro A, Fabbri P, Giaretta A, et al (2015) Effects of redox conditions on the control of arsenic mobility in shallow alluvial aquifers on the Venetian Plain (Italy). Sci Total Environ 532:581–594. doi: 10.1016/j.scitotenv.2015.06.003

Cleveland WS (1979) Robust Locally Weighted Regression and Smoothing Scatterplots. J Am Stat Assoc 74:829–836. doi: 10.2307/2286407

Cleveland WS, Mcgill R (1985) We have studied the elementary Graphical Perception and Graphical Methods for Analyzing Scientific Data. Am Assoc Adv Sci 229:828–833. doi: 10.1126/science.229.4716.828

Coetsiers M, Blaser P, Martens K, Walraevens K (2009) Natural background levels and threshold values for groundwater in fluvial Pleistocene and Tertiary marine aquifers in Flanders, Belgium. Environ Geol 57:1155–1168. doi: 10.1007/s00254-008-1412-z

Critto A, Carlon C, Marcomini A (2003) Characterization of contaminated soil and groundwater surrounding an illegal landfill (S. Giuliano, Venice, Italy) by principal component analysis and kriging. Environ Pollut 122:235–244. doi: 10.1016/S0269-7491(02)00296-8

Dalla Libera N, Fabbri P, Mason L, et al (2017) Geostatistics as a tool to improve the natural background level definition: An application in groundwater. Sci Total Environ 598:330–340. doi: 10.1016/j.scitotenv.2017.04.018

Dalla Libera N, Fabbri P, Piccinini L, et al (2016) Natural Arsenic in groundwater in the drainage basin to the Venice lagoon (Brenta Plain, NE Italy): the organic matter's role. Rend Online della Soc Geol Ital 41:30–33. doi: 10.3301/ROL.2016.85

Dal Prà A, Fabbri P, Bortoletto C (1992) The artesian hydrogeological system in the central Venetian plain between Treviso and the River Piave and its exploitation. Memorie di Scienze Geologiche, Vol. 44, 152-170

Ducci D, Condesso MT, Melo D, et al (2016) Science of the Total Environment Combining natural background levels (NBLs) assessment with indicator kriging analysis to improve groundwater

quality data interpretation and management. Sci Total Environ 569–570:569–584. doi: 10.1016/j.scitotenv.2016.06.184

Elumalai V, Brindha K, Sithole B, Lakshmanan E (2017) Spatial interpolation methods and geostatistics for mapping groundwater contamination in a coastal area. Environ Sci Pollut Res 24:11601–11617. doi: 10.1007/s11356-017-8681-6

Fabbri P (2001) Probabilistic assessment of temperature in the Euganean geothermal area (Veneto Region, NE Italy). Mathematical Geology 6:745-760

Fabbri P, Ferronato A, Zangheri P (1993) A case of groundwater contamination by organo-chlorine compounds. Hydrogeologie 3:207-215

Fabbri P, Gaetan C, Zangheri P (2011) Transfer function-noise modelling of an aquifer system in NE Italy. Hydrol Process 25:194–206. doi: 10.1002/hyp.7832

Fabbri P, Piccinini L (2013) Assessing transmissivity from specific capacity in an alluvial aquifer in the middle Venetian plain (NE Italy). Water Sci Technol 67:2000–2008. doi: 10.2166/wst.2013.074

Fabbri P, Piccinini L, Marcolongo E, Pola M, Conchetto E, Zangheri P (2016) Does a change of irrigation technique impact on groundwater resources? A case study in Northeastern Italy. Environ. Sci. Policy 63: 63–75.

Fabbri P, Trevisani S (2005) A geostatistical simulation approach to a pollution case in Northeastern Italy. Math Geol 37:569–586. doi: 10.1007/s11004-005-7307-6

Fontana A, Mozzi P, Bondesan A (2004) The geomorphological evolution of the Venetian-Friulian plain (in Italian). Whitin the: Bondesan, A., Meneghel, M., 2004. Geomorphology of the Venice Province. Esedra, Padova. 113-138

Fontana A, Mozzi P, Bondesan A (2008) Alluvial megafans in the Venetian–Friulian Plain (northeastern Italy): Evidence of sedimentary and erosive phases during Late Pleistocene and Holocene. Quaternary International, 189, 71-90

Goovaerts, P. (1997) Geostatistics for natural resource evaluation: Oxford University Press, New York, 483 pp

Gotway C, Helsel DR, Hirsch RM (2002) Statistical Methods in Water Resources. Hydrol Anal Interpret 4:1–524. doi: 10.2307/1269385

GWD (2006) Groundwater Directive 2006/118/CE, Directive of the European Parliament and of the Council on the protection of groundwater against pollution and deterioration, OJ L372, 27/12/ 2006, pp 19–31

Herath I, Vithanage M, Bundschuh J, et al (2016) Natural Arsenic in Global Groundwater: Distribution and Geochemical Triggers for Mobilization. Curr Pollut Reports 2:68–89. doi: 10.1007/s40726-016-0028-2

Hinsby K, Condesso de Melo MT, Dahl M (2008) European case studies supporting the derivation of natural background levels and groundwater threshold values for the protection of dependent ecosystems and human health☆. Sci Total Environ 401:1–20. doi: 10.1016/j.scitotenv.2008.03.018

Journel, A. G. (1982) The indicator approach to estimation of spatial distributions, in Johnson, T. B. et al (eds.), Proceedings of the 17th. APCOM symposium.

Journel A. G. (1983) Nonparametric estimation of spatial distri- bution. Mathematical Geology 15, no. 3: 445–468

Journel A.G., Huijbregts Ch.J. (1978) Mining Geostatistics. Academic Press, London 600pp.

Lu P, Zhu C (2011) Arsenic Eh-pH diagrams at 25??C and 1 bar. Environ Earth Sci 62:1673–1683. doi: 10.1007/s12665-010-0652-x

Mandal B (2002) Arsenic round the world: a review. Talanta 58:201–235. doi: 10.1016/S0039-9140(02)00268-0

McArthur JM, Ravenscroft P, Safiulla S, Thirlwall MF (2001) Arsenic in groundwater: Testing pollution mechanisms for sedimentary aquifers in Bangladesh. Water Resour Res 37:109–117. doi: 10.1029/2000WR900270

Molinari A, Ayora C, Marcaccio M, et al (2014) Geochemical modeling of arsenic release from a deep natural solid matrix under alternated redox conditions. Environ Sci Pollut Res 21:1628–1637. doi: 10.1007/s11356-013-2054-6

Molinari A, Guadagnini L, Marcaccio M, et al (2013) Arsenic release from deep natural solid matrices under experimentally controlled redox conditions. Sci Total Environ 444:231–240. doi: 10.1016/j.scitotenv.2012.11.093

Molinari A, Guadagnini L, Marcaccio M, Guadagnini A (2015) Arsenic fractioning in natural solid matrices sampled in a deep groundwater body. Geoderma 247–248:88–96. doi: 10.1016/j.geoderma.2015.02.011

Molinari A, Guadagnini L, Marcaccio M, Guadagnini A (2012) Natural background levels and threshold values of chemical species in three large-scale groundwater bodies in Northern Italy. Sci Total Environ 425:9–19. doi: 10.1016/j.scitotenv.2012.03.015

Mozzi P, Bini C, Zilocchi L, Beccatini R, Mariotti Lippi M (2003) Stratigraphy, palaeopedology and palynology of late Pleistocene and Holocene deposits in the landward sector of the lagoon of Venice (Italy), in relation to Caranto level. Il Quaternario, 16 (1 bis), pag. 193 – 210

Muller D, Blum A, Hart A, Hookey J, Kunkel R, Scheidleder A, Tomlin C, Wendland F (2006) Final Proposal for methodology to setup groundwater treshold values in Europe, Deliverable D18. BRIDGE project, 63 p., www.wfd-bridge.net

Nickson RT, Mcarthur JM, Ravenscroft P, et al (2000) Mechanism of arsenic release to groundwater, Bangladesh and West Bengal. Appl Geochemistry 15:403–413. doi: 10.1016/S0883-2927(99)00086-4

Ohmer M, Liesch T, Goeppert N, Goldscheider N (2017) On the optimal selection of interpolation methods for groundwater contouring: An example of propagation of uncertainty regarding inter-aquifer exchange. Adv Water Resour 109:121–132. doi: 10.1016/j.advwatres.2017.08.016

Pauwels H, Muller D, Griffioen J, et al (2007) BRIDGE - Background criteria for the identification of groundwater.

Pebesma EJ (2004) Multivariable geostatistics in S: the gstat package. Comput Geosci 30:683–691. doi: 10.1016/j.cageo.2004.03.012

Pebesma EJ, de Kwaadsteniet JW (1997) Mapping groundwater quality in the Netherlands. J Hydrol 200:364–386. doi: 10.1016/S0022-1694(97)00027-9

Piccinini L, Fabbri P, Pola M (2016) Point dilution tests to calculate groundwater velocity, an example in a porous aquifer in NE Italy. Hydrol Sci J. doi: 10.1080/02626667.2015.1036756

Piccinini L, Fabbri P, Pola M, Marcolongo E (2017) An example of aquifer heterogeneity simulation to modeling well- head protection areas. Ital. J. Eng. Geol. Environ. Special Is: 103–115.

Piccinini L, Fabbri P, Pola M, et al (2015) Numerical modeling to well-head protection area delineation, an example in Veneto Region (NE Italy). Rend online della Soc Geol Ital 35:232–235. doi: 10.3301/ROL.2015.108

Preziosi E, Giuliano G, Vivona R (2010) Natural background levels and threshold values derivation for naturally As, V and F rich groundwater bodies: a methodological case study in Central Italy. Environ Earth Sci 61:885–897. doi: 10.1007/s12665-009-0404-y

R Core Team (2017) R: A language and environment for statistical computing, R Foundation for Statistical Computing, Vienna, Austria. URL: http://www.R-project.org/

Reimann C, Garrett RG (2005) Geochemical background - Concept and reality. Sci Total Environ 350:12–27. doi: 10.1016/j.scitotenv.2005.01.047

Rotiroti M, Fumagalli L (2013) Derivation of preliminary natural background levels for naturally Mn, Fe, As and NH4+ rich groundwater: The case study of Cremona area (Northern Italy). Rend Online Soc Geol Ital 24:284–286.

Rotiroti M, Fumagalli L, Frigerio MC, et al (2015) Natural background levels and threshold values of selected species in the alluvial aquifers in the Aosta Valley Region (N Italy). Rend online della Soc Geol Ital 35:256–259. doi: 10.3301/ROL.2015.114

Rotiroti M, Sacchi E, Fumagalli L, Bonomi T (2014) Origin of Arsenic in Groundwater from the Multilayer Aquifer in Cremona (Northern Italy). Environ Sci Technol 48:5395–5403. doi: 10.1021/es405805v

Rowland HAL, Pederick RL, Polya DA, et al (2007) The control of organic matter on microbially mediated iron reduction and arsenic release in shallow alluvial aquifers, Cambodia. Geobiology 5:281–292. doi: 10.1111/j.1472-4669.2007.00100.x

Shand P, Edmunds WM, Lawrence AR, et al (2007) The natural (baseline) quality of groundwater in England and Wales. BGS Res Rep RR/07/06 72

Sollitto D, Romic M, Castrignanò A, et al (2010) Assessing heavy metal contamination in soils of the Zagreb region (Northwest Croatia) using multivariate geostatistics. CATENA 80:182–194. doi: 10.1016/j.catena.2009.11.005

Takeno N (2005) Atlas of Eh-pH diagrams Intercomparison of thermodynamic databases. Natl Inst Adv Ind Sci Technol Tokyo 285.

Trevisani S, Fabbri P (2010) Geostatistical modeling of a heterogeneous site bordering the Venice lagoon, Italy. Ground Water 48:614–623. doi: 10.1111/j.1745-6584.2009.00632.x

Ungaro F, Ragazzi F, Cappellin R, Giandon P (2008) Arsenic concentration in the soils of the Brenta Plain (Northern Italy): Mapping the probability of exceeding contamination thresholds. J Geochemical Explor 96:117–131. doi: 10.1016/j.gexplo.2007.03.006

Vorlicek PA, Antonelli R, Fabbri P, Rausch R (2004) Quantitative hydrogeological studies of the Treviso alluvial plain, NE Italy. Q J Eng Geol Hydrogeol 37:23–29. doi: 10.1144/0036-9276/02-006

Wendland F, Berthold G, Blum A, et al (2008a) Derivation of natural background levels and threshold values for groundwater bodies in the Upper Rhine Valley (France, Switzerland and Germany). Desalination 226:160–168. doi: 10.1016/j.desal.2007.01.240

Wendland F, Blum A, Coetsiers M, et al (2008b) European aquifer typology: a practical framework for an overview of major groundwater composition at European scale. Environ Geol 55:77–85. doi: 10.1007/s00254-007-0966-5

WFD (2000) European Parliament and Council, 2000. Directive 2000/60/EC establishing a framework for community action in the field of water policy, Brussels, Belgium, October 23, 2000

2.4 Subsurface heterogeneity model

2.4.1 Paper 4

Subsoil reconstruction in geostatistics beyond the kriging: a case study in Veneto Region (NE, Italy)

Authors: Paolo Fabbri[1], Carlo Gaetan[2], Luca Sartore[3], Nico Dalla Libera[1]

1) Dipartimento di Geoscienze, Università di Padova, Via G. Gradenigo, 6 - 35131 Padova, Italy.

2) University of Venice "Ca' Foscari", Department of Environmental Sciences, Informatics and Statistics, Via Torino 155, 30172, Venice Mestre, Italy.

3) National Institute of Statistical Science, 19 T.W. Alexander Drive, P.O. Box 14006, Research Triangle Park, NC 27709-4006, U.S.A.

Status: Under review (2019).

Abstract

Reconstruction of hydro-stratigraphic units in subsoil plays an important role in the assessment of soil heterogeneity, which is a keystone in groundwater flow and transport modeling. A geostatistic approach appears to be a good way to reconstruct subsoil, and now other methods besides the classical indicator (co)kriging are available as alternative approximations of the conditional probabilities. Some of these techniques specifically consider categorical variables as lithologies, but they are computationally prohibitive. Moreover, the stage before subsoil prediction/simulation can be very informative from a hydro-stratigraphic point of view, as the detailed transiogram analysis of this paper demonstrates. In this context, an application of the spMC package for the R software is presented by using a test site located within the Venetian Alluvial Plain (NE Italy). First, a detailed transiogram analysis was conducted, and then a maximum entropy approach based on transition probabilities, named Markovian-type Categorical Prediction (MCP), was applied in order to approximate the posterior conditional probabilities. The study does not compare prediction versus simulation methods hereafter mentioned, but it does highlight some advantages of the presented approach in term of hydrogeological knowledge and computational efficiency. spMC couples a transiogram analysis with a maximum entropy approach by taking advantage of High-Performance Computing (HPC) techniques. These characteristics make the spMC package useful for simulating hydro-stratigraphic units in subsoil, despite the use of a large number of lithologies (categories).

Keywords: Subsoil reconstruction; heterogeneity assessment, hydrofacies distribution, categorical variables; transiograms; Markovian-type Categorical Prediction; parallel computation; Venetian Plain NE Italy.

Introduction

Approaching predictions/simulations with geostatistical methods in hydro-statigraphy is still an open question (Koltermann and Gorelick, 1996; de Marsily et al., 1998, 2005; Al-Khalifa et al., 2007; Comunian et al., 2011; dell'Arciprete et al., 2012; Pyrcz, 2014; Marini et al., 2018) since the subsoil heterogeneity assessment is one of the keystones in groundwater flow and transport modeling. Different approaches were proposed, e.g. the Boolean (Haldorsen and Chang, 1986; Viseur, 1999; Vargas-Guzmán and Al-Qassab, 2006), the truncated Gaussian (Matheron et al., 1987) and the pluri-gaussian simulation methods (Armstrong, 2011). However, the most known lithological prediction/simulation in classical geostatistics is based on indicator kriging (Journel AG, 1983; Bierkens and Burrough, 1993a, 1993b; Journel and Gomez-Hernandez, 1993; Johnson, 1995; Journel et al., 1998; Seifert and Jensen, 1999; Falivene et al., 2007; De Iaco et al., 2010; Trevisani and Fabbri, 2010; Dalla Libera et al., 2018). Although this approach appears frequently in literature due to the availability of open source programs, there are some intrinsic probabilistic inconsistencies typical of indicator kriging:

- The sum of occurrence is not exactly 1;
- The probabilities are not guaranteed to be between 0 and 1;
- The cumulative distribution functions may not increase monotonically.

These issues are well known in literature as the "order relation problem" (Pyrcz, 2014). Thus, a post-processing of the conditional probabilities is frequently needed (Fabbri, 2001). In the classical indicator approach, spatial variability is modeled by indicator (cross)variograms, which capture only some spatial peculiarities of geological facies. However, the approach based on indicator kriging predictions/simulations is computationally expensive because of the need to solve a large system of linear equations. Therefore, the lithological categories accounted for are rarely more than four or five. The concepts of transition probability in geostatistics and their graphical representations as probability-lag diagrams ("transiogram") appeared in earlier articles, such as (Schwarzacher, 1969; Luo, 1996). This concept depends on the distance between two locations and is able to account for more stratigraphic information than classical

variogram (Carle and Fogg, 1996, 1997; Weissmann and Fogg, 1999; Weissmann et al., 1999; Lee et al., 2007). This concept combines juxtapositions modeled through embedded Markov chains, which are already known and used in sedimentary geology (Miall, 1973; Hattori, 1976). In this context, transiograms replace indicator (cross)variograms within prediction/simulation procedures. These consider some important stratigraphic information not considered by indicator variograms such as the mean thickness and volumetric proportions of materials, and produce information about lithology juxtapositional tendencies. The empirical estimates of the transitional probabilities are modeled by continuous Markov-chains to obtain a theoretical transition probability function depending to the distance. However, (Carle and Fogg, 1996) maintained an indicator kriging-based approach in their prediction/simulation procedure, thus approximating the posterior probabilities via least-squares and taking over the related computational load. A multiple-point geostatistics approach was also introduced (Strebelle, 2002; Jef Caers, 2004; Chugunova and Hu, 2008; Mariethoz and Renard, 2010; Comunian et al., 2012), mainly by considering a better reproduction of a specific conceptual geological model, such as modeling a meandering channel system. Principal strengths and weaknesses of this geostatistical approach are summarized in (Chugunova and Hu, 2008). The lack of specifications for an underlying categorical random field improves its flexibility and efficiency, but on the other hand, further inference is difficult to carry out since the underlying model (i.e. the training image) is hard to parameterize efficiently and may be difficult to acquire. The use of spatially correlated latent variables is a statistical solution to overcome the problem of setting down a parsimonious parameterization under a more general framework of generalized linear mixed models (Breslow and Clayton, 1993). Under this approach, the probability of an occurrence of a category in one site depends on the latent process itself (usually Gaussian). A main drawback of this method is that the posterior probability of the introduced latent variables is not available in a closed form owing to the non-Gaussian response variables. Thus, Markov chain Monte Carlo sampling is often used for the inference with latent variables. Alternatively, a spatial multinomial logistic mixed model (Cao et al., 2011) was proposed for spatially correlated categorical variables with several categorical outcomes. In hydro-stratigraphic predictions/simulations where probability values are restricted (i.e. the different lithologies) and constrained to sum up to one, a maximum entropy selection rule should be preferred to the least-squares when dealing with a categorical variable (Csiszar, 1991). The Bayesian Maximum Entropy principle (BME) (Christakos, 1990) has been applied in spatial statistics to categorical variables stored in soil data sets(D'Or et al., 2001; Bogaert, 2002; Bogaert and D'Or, 2002; D'Or and Bogaert, 2004), but it faces the same computational

limitations as the indicator kriging approach due to the number of lithologies. In Allard et al., 2011, the maximum entropy principle is revisited and its solution presents a closed-form expression that depends only on bivariate probabilities. Thus, the posterior conditional probabilities are approximated only by the use of univariate and bivariate probabilities. This approach was named Markovian type Categorical Prediction (MCP). Transition probabilities can be aggregated using a Bayesian updating formulation, and interpreted as expert opinions for updating the prior marginal probabilities of categorical variables (Huang et al., 2016). The aim of this paper is to apply the MCP approach to study the subsoil composition in a small test area and produce consistent simulations of the subsoil heterogeneity. In doing this we exploit a recent implementation of MCP approach available in the spMC package (Sartore et al., 2016) for the R environment (R Development Core Team, 2018). The spMC package provides graphical tools for a better understanding of the data, and several options for parameter estimation, lithological simulations, and predictions. It allows the user to account for a non-kriging-based approach on the approximation of the conditional probabilities among lithologies and all the hydrogeological information coming from a transiograms analysis. The package provides several functions to deal with categorical spatial data whose coordinates are either regularly or irregularly located over a multidimensional space. The main model used in the package is based on continuous-lag Markov chains, and allows for a formal representation of the conditional probabilities of lithological occurrences between two sites. These probabilities depend on a multidimensional continuous-lag defined as the difference between two spatial positions. The spMC package was partially implemented by exploiting High Performance Computing (HPC) techniques in order to improve its computational efficiency and allow for the processing of a larger number of the lithological categories. Since this package was designed for intensive geostatistical computations, part of the code deals with parallel computing via the OpenMP constructs (OpenMP Architecture Review Board, 2008).

Materials and methods

Traditionally, Markov chains are stochastic processes described by a probabilistic model along a single dimension (usually time) subdivided into discrete lags. The extension of this concept arises by the definition of a Markov process involving continuous lags in a *d* dimensional space (Carle and Fogg, 1997).

When considering a stationary process, the transition probability between two lithologies (categories), *i* and *j*, in two locations, $\mathbf{s}$ and $\mathbf{s} + \mathbf{h}$ is defined as:

$$t_{ij}(\boldsymbol{h}) = Pr[Z(\boldsymbol{s}+\boldsymbol{h}) = j \cap Z(\boldsymbol{s}) = i],\ \forall i,j = 1,\dots,K \quad (1)$$

where K is the total number of lithologies (1, …, K) that the categorical random variable Z can assume as outcomes and **h** is a multidimensional lag from any observed location **s**. The transition probability $t_{ij}(\boldsymbol{h})$ is the element in the *i* th row and in the *j* th column of the matrix **T(h)** such that:

$$\boldsymbol{T}(\boldsymbol{h}) = exp(\|\boldsymbol{h}\|\boldsymbol{R_h}) \quad (2)$$

where the transition rate matrix $\boldsymbol{R_h}$depends both on the length of the lag **h** and its direction. Carle and Fogg, 1997 formulated the transition rate matrix $\boldsymbol{R_h}$ for the direction **h** by an ellipsoidal approximation, which combines the matrix $\boldsymbol{R_{e_k}}$ derived from the main axial directions. The vector $\boldsymbol{e_k}$ indicates the standard basis vector of dimension *d*, whose *k* th component (corresponding to the *k* th axial direction) is one and the others are zeros. For the scope of our study, the first problem consists of the estimation of the transition rate matrix components $r_{ij,\boldsymbol{h}}$, and the second arises from the choice of the conditional probability approximation adopted for simulating/predicting the lithologies. Different methods address the first problem and are implemented in spMC. These include the mean lengths and the maximum entropy method suggested by Carle and Fogg, 1997. The lithological simulation and prediction algorithms implemented in spMC are based on attempts proposed to solve the second problem, and consider different approximations of the conditional probability

$$Pr[Z(s_0) = j \mid \cap_{l=1}^{n} Z(s_l) = z(s_l)], \forall j = 1,\dots,K \quad (3)$$

Where s_0 denotes the simulation/prediction spatial location without lithological information,s_l represents the *l* th spatial position of the available data, and $z(s_l)$ corresponds to the observed lithology of the random variable $Z(s_l)$. The classical approximation of (3) is based on cokriging or kriging approach, while other formulations bypass the kriging formalism and its related issues. For instance, Bogaert, 2002 introduced a Bayesian procedure that exploits the maximum entropy principle, but requires a computationally intensive entropy optimization. Allard *et al.*, 2011 avoided the entropy optimization by aggregating the transition probabilities (Markovian type Categorical Prediction; MCP) to approximate the optimal solution of the maximum entropy approach. The approximation of the conditional probability proposed by Allard *et al.*, 2011 is formulated as follow:

$$Pr[Z(s_0) = z_i | \cap_{l=1}^{n} Z(s_l) = z(s_l)] \approx \frac{p_i \prod_{l=1}^{n} t_{ik_l}(s_0 - s_l)}{\sum_{i=1}^{K} p_i \prod_{l=1}^{n} t_{ik_l}(s_0 - s_l)} \quad (4)$$

where p_i denotes the proportion of the *i* th lithology considered for the location s_0, and t_{ik_l} is the transition probability to the *i* th lithology in $s_0$from the *k* th lithology observed in the location s_l.

Case study

The analyses center around a hydrogeological study in an experimental site of 1.5 ha placed inside the drinking water supply area of ACEGAS APS, which supplies the city of Padua. This site is located in the Venetian plain (NE, Italy) (Fig. 1). The Venetian Plain is delimited in the north by the Pre Alps, in the east by the Livenza river, in the west by Lessini mountains, Berici and Euganei hills, in the south by the Adige river and Adriatic Sea. The alpine limit of the plain is on 150-200 m a.s.l. diminishing towards SSE until the coast. From the West to the East, we can observe the hydrographical system of Leogra Timonchio, Astico Bacchiglione, Brenta and Piave; these rivers have deposited a huge amount of loose materials, forming the subsoil of the Venetian Plain. Therefore, the Venetian plain consists of several large alluvial fans (Plio Quaternary deposits) called "megafans" whose width increases towards the SSE (Fontana et al., 2008). The hydrogeological features of the Venetian plain depend principally on depositional sequences of rivers and on the granulometric characteristics. In the upper part of the alluvial plain, near the Pre Alps, where the subsoil is composed almost totally by gravel, there is only a thick unconfined aquifer with high hydraulic conductivity. Towards the south east and closer to the Adriatic Sea, the alluvial sediments move into a multi-layered system where cohesive and incohesive sediments alternate. Thus, the unconfined aquifer gradually evolves into a system of stratified, confined (or semiconfined), often artesian aquifers, which represent the lower plain (Vorlicek et al., 2004; Fabbri et al., 2011; Carraro et al., 2013, 2015; Fabbri and Piccinini, 2013). Between the upper and the lower plain, there is the middle plain that consists of progressively finer materials than the high plain. The middle plain is formed by gravelly and sandy horizons alternating with clayey and silty levels, where the latest become more frequent from upstream to downstream (Fabbri et al., 2016). This area is characterized by a high quantity of plain springs (arising from the intersection between the topography surface and the water table) (Fig. 1). This natural drainage system supplies numerous perennial stream flows (Fig. 1), e.g. the Sile River (5–6 m^3/s). This regional context affects our area of study, contributing to its heterogeneity.

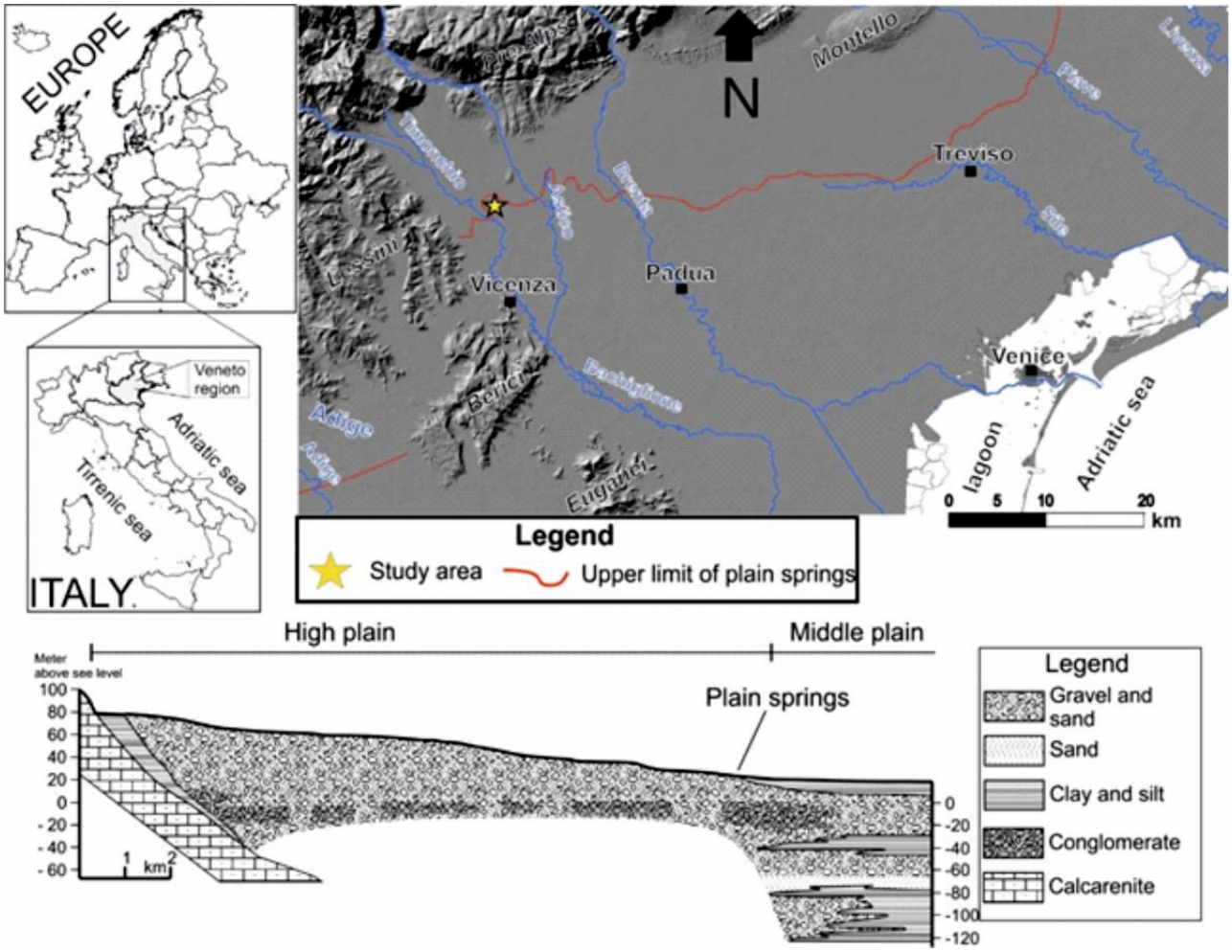

Fig. 1 - Geographical location of studied area and cross section of Venetian plain (Fabbri et al., 2011, modified).

In the considered area, 39 piezometers are present with a depth ranging from 1.6 to 22 m and a diameter ranging from 50 to 90 mm. The structural characteristics of 29 piezometers are available. The subsurface composition, and consequently the hydrogeological features, shows high heterogeneity with gravel horizons alternating with sandy, silty and clayey levels (Fig. 2b, 2c). The shallow unconfined aquifer of this area is essentially recharged by rainfall, as studied by Fabbri et al., 2012 and Piccinini et al., 2016. Fig. 2a shows the red rectangle of the simulation area with the location of 13 available borehole logs that are 5 m deep and have data every 2 cm. An example of stratigraphy (Ps3) is given in Fig. 2b.

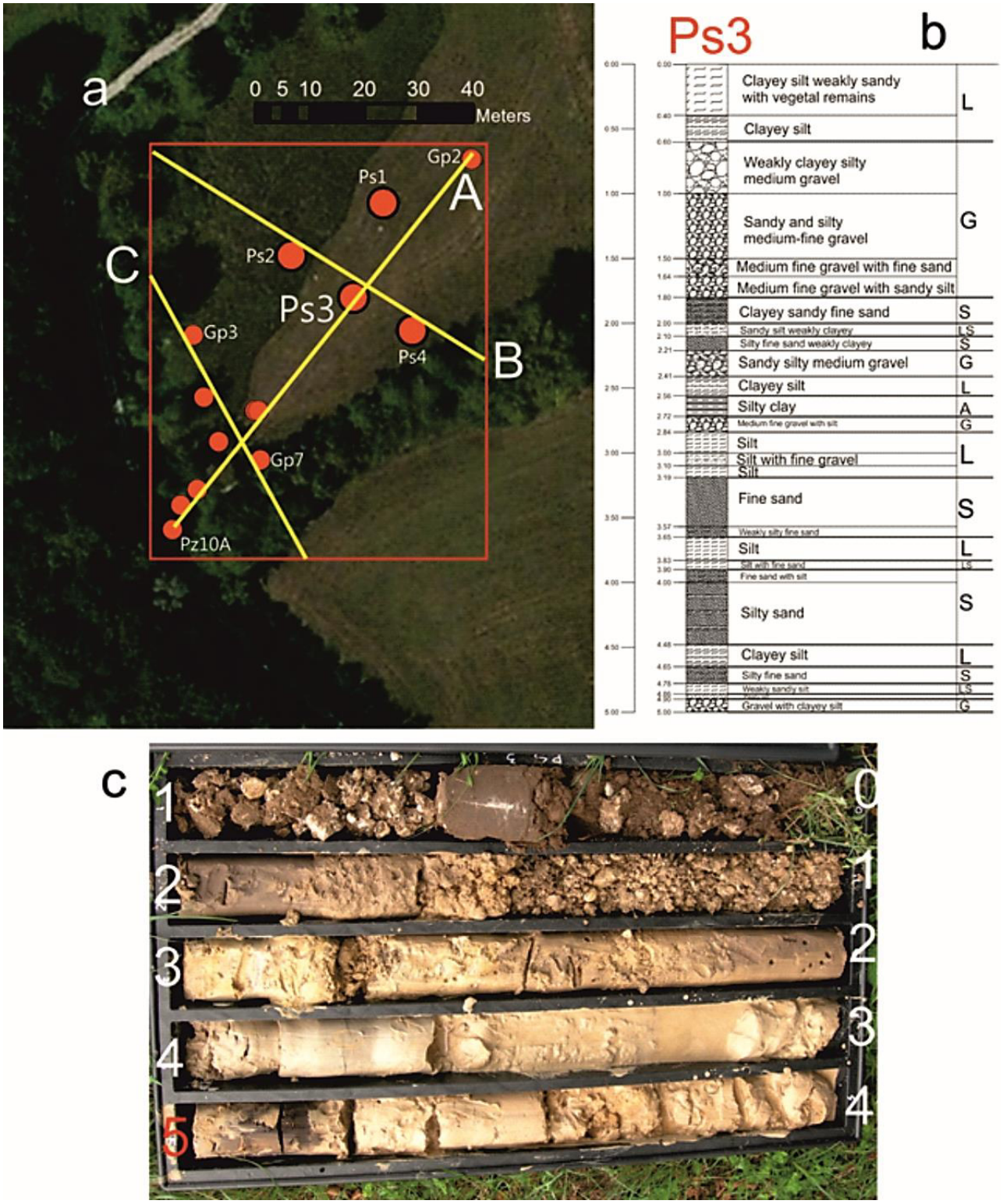

Fig. 2 - Location of 13 piezometers (red dots); simulated area (red rectangle); traces of cross sections (yellow lines); stratigraphy of Ps3 with example of lithologic reduction to 5 materials; core box of Ps3 piezometer

Data analysis

The first step simplifies the local complex heterogeneity of the available 13 stratigraphic logs into five lithologies: A = clay, G = gravel, L = silt, LS = silty sand and S = sand. All analyses were

performed by the package spMC (Sartore et al., 2016) implemented in R, which is a free software environment for statistical computing and graphics. Fig.3a shows the sediments distribution indicated in the subsoil G (0.34%), S (0.28%) and L (0.22%) as more frequent than A (0.09%) and LS (0.07%).

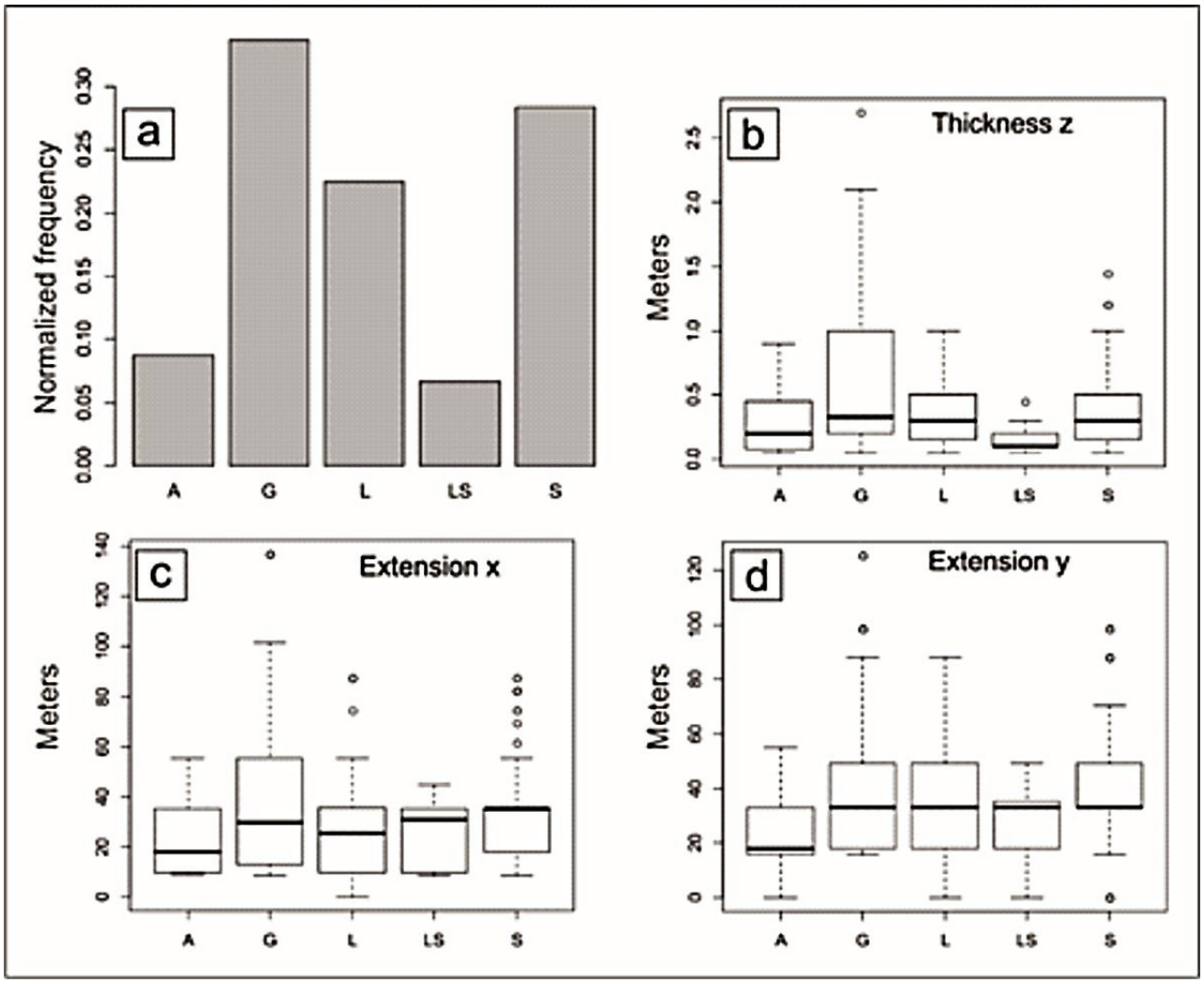

*Fig. 3 - Normalized frequency distribution of lithologies (a); boxplot thickness for every lithology along direction Z (depth) (b); extension of the lithologies along the directions X (c) and Y (d).*14

The boxplots of Fig. 3b, 3c, 3d show the thickness/extension distribution of the lithologies along the directions Z (depth), X (longitude), and Y (latitude), and their mean values are exposed in Table 1.

Table 1 - Mean of thickness along Z, and its extension along the directions X and Y for the considered lithologies.

Lithology	Thickness Z (m)	Extension X (m)	Extension Y (m)
Clay (A)	*0.27*	*21.15*	*20.67*
Gravel (G)	*0.70*	*32.99*	*37.74*
Silt (L)	*0.35*	*26.55*	*33.13*
Silty Sand (LS)	*0.14*	*23.73*	*31.83*
Sand (S)	*0.38*	*31.31*	*37.33*

As visible in Fig. 3b, layers made out of gravels (G) present more variation in thickness than the other four lithologies, while the variation of the lithological extension along the directions X and Y (Fig. 3c, 3d) are higher but comparable between them. The analysis of the embedded transition probabilities in 3D allows for a first rough juxtapositional investigation among the five considered materials, independently of their thickness or extension. For instance, the analysis of Table 2 along the direction Z (depth) highlights that, among all the five lithologies, it is more probable to find a layer of LS (sandy silt) above a layer of S (sand) (0.62) than a layer of S above a layer of LS (0.36), while the probability to find a layer of G (gravel) above a layer of L (silt) (0.36) is similar to its opposite condition (0.37). It is also evident that the probabilities seeing a layer of LS (silty sand) above a layer of A (clay) (0.07) or a layer of G (gravel) above a layer of LS (sandy silt) (0.11) are both low. The analysis of Tables 2 along the direction X (longitude) and Y (latitude) shows the estimated probability that one lithology is laterally neighboring to another. For instance, it is evident that there is a high probability to pass from A (clay) to G (gravel) (0.64 along direction X and 0.66 along Y). Moreover, similar probabilities to pass from L to G (0.70) and from G to L (0.69) were computed along Y, while the probability to pass from A to LS are the smallest (0.00 along Y and 0.05 along X).

Table 2 - Embedded Transition Probabilities (ETP) along the directions Z (depth), X (longitude) and Y (latitude).

Z	**A**	**G**	**L**	**LS**	**S**
A	-	0.29	0.12	0.18	0.41
G	0.14	-	0.36	0.11	0.39
L	0.14	0.37	-	0.20	0.26
LS	0.07	0.14	0.17	-	0.62
S	0.20	0.18	0.23	0.36	-
X	**A**	**G**	**L**	**LS**	**S**
A	-	0.64	0.14	0.05	0.18
G	0.24	-	0.31	0.10	0.36
L	0.20	0.40	-	0.10	0.30
LS	0.11	0.47	0.09	-	0.34
S	0.04	0.45	0.41	0.10	-
Y	**A**	**G**	**L**	**LS**	**S**
A	-	0.66	0.11	0.00	0.23
G	0.08	-	0.69	0.08	0.15
L	0.08	0.70	-	0.00	0.23
LS	0.06	0.47	0.26	-	0.21
S	0.15	0.42	0.40	0.03	-

Transiogram analysis

The lithological transition probabilities are analyzed along the directions Z (depth), X (longitude) and Y (latitude) in relationship with different distances (h). These probabilities are modeled through continuous lag Markov chains, and used in the next section for the lithological simulation. The theoretical transition probabilities were calculated by estimating transition rates with a maximum entropy approach that uses the trimmed mean of the lithological layers. The analysis of the diagonal transiogram (e.g. A vs A, G vs G, etc.) in Fig. 4 gives some information about the thickness of the layers by showing the probabilities of finding the same lithologies juxtaposed every 5 cm in depth (direction Z). Along the diagonal of auto transitions, a high empirical probability is visible in sand (S), and it reaches a sill of about 0.4 at a range of 1 m (Fig. 4a). At the same time, the empirical auto transition probability in gravel (G) regularly decreases in depth down to 0 (Fig. 4b). This could mean that sandy layers are thinner (sand thickness 0.38 m) and more frequent than the gravely ones (gravel thickness 0.70 m). This is

also visible in the boxplot of the length distribution for sand in Fig. 3b. The transiogram behavior (Fig. 4c) for silt (L) suggests that the thickness of silt layers is comparable to that of sand layers (S), but silty layers are more frequent than the sandy ones (cfr Fig 4c vs Fig 4a). The probabilities of auto transition for clay (A) and sandy silt (LS) (Fig. 4d, 4e) quickly achieve a very low sill value. This makes it less likely to find thick or frequent layers for those two lithologies. Off diagonal transiograms analysis of Fig. 4 gives some information about juxtapositional tendency of the materials at different distances h. The results are comparable with those of embedded transition probability in Table 2, but in this case, transition probabilities are plotted versus distances h. A high probability is notable to find sandy silt (LS) in contact and above sand (S) with a sill of approximately 0.5 and range of about 1 m (Fig. 4f).

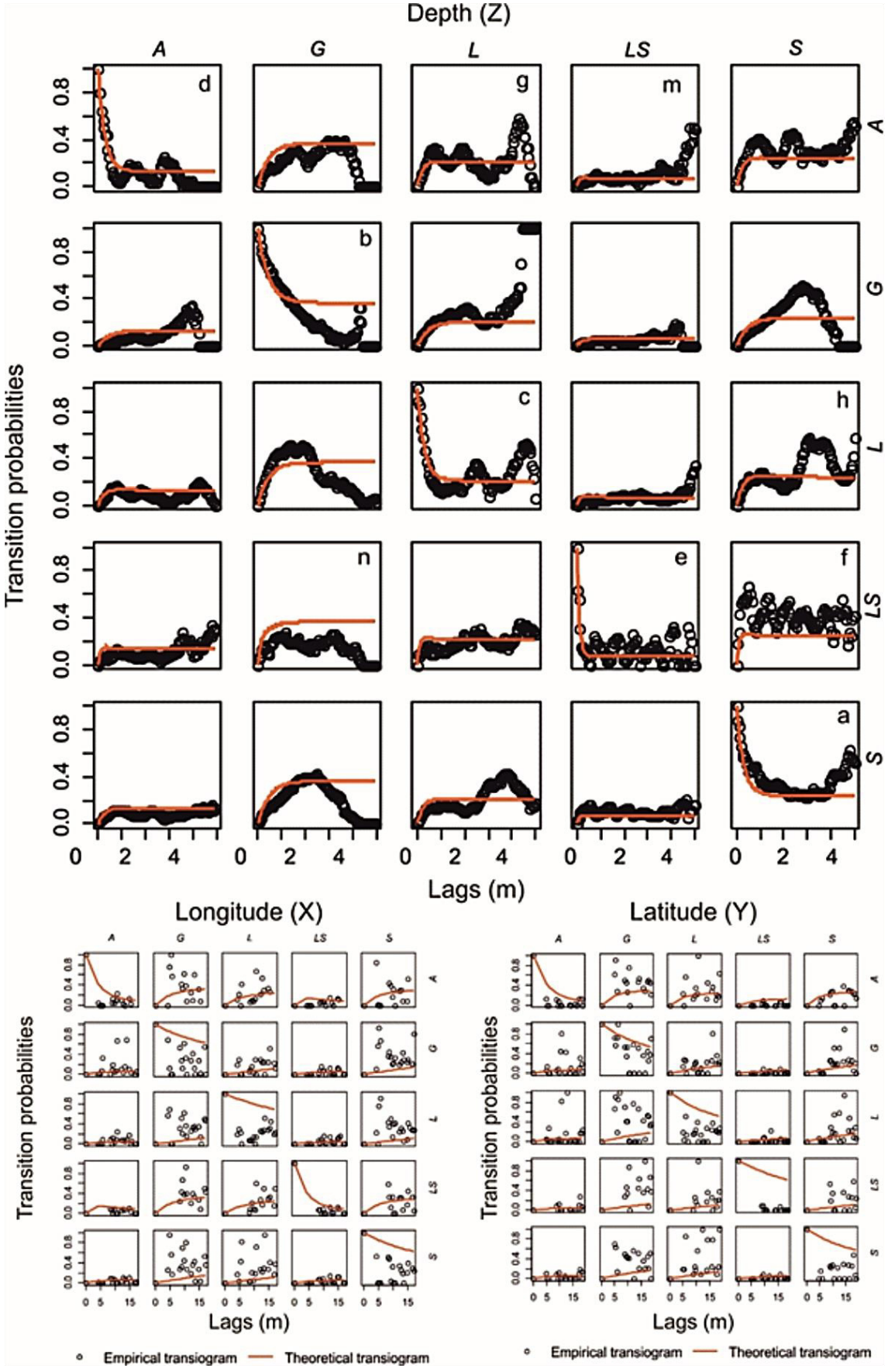

Fig. 4 - Experimental transition probabilities with respect to the distance (h) (black circles) and theoretical transition probabilities modeled by Markov chains (red lines) along the directions Z, X and Y).

A “hole effect” is also visible in transition diagram from clay (A) above silt (L) (Fig. 4g), but also from silt (A) above sand (S) (Fig. 4h), indicating an irregular alternate occurrence in those couples of lithologies. Transiogram along the directions X and Y are calculated without considering Walther's law of facies stating that the vertical (along Z, i.e. depth) succession of facies reflects their lateral changes. This probably produces less interpretable experimental transiograms, but they are based on the information available from real data. After analyzing transiograms, the surface theoretical transiograms are studied with (Fig. 5b) or without (Fig. 5a) ellipsoidal interpolation calculated by experimental data. These diagrams highlight the anisotropies of the modeled transiograms in the X-Y plain. The auto transition in L (silt) and G (gravel) show an anisotropy along the latitude. It is more probable to find silt and gravel along the direction Y (latitude) than in X (longitude). This is also confirmed from the lengths in Y and X (Table 1), while the visible anisotropy along X related to silty sand (LS) it is not visible in Table 1.

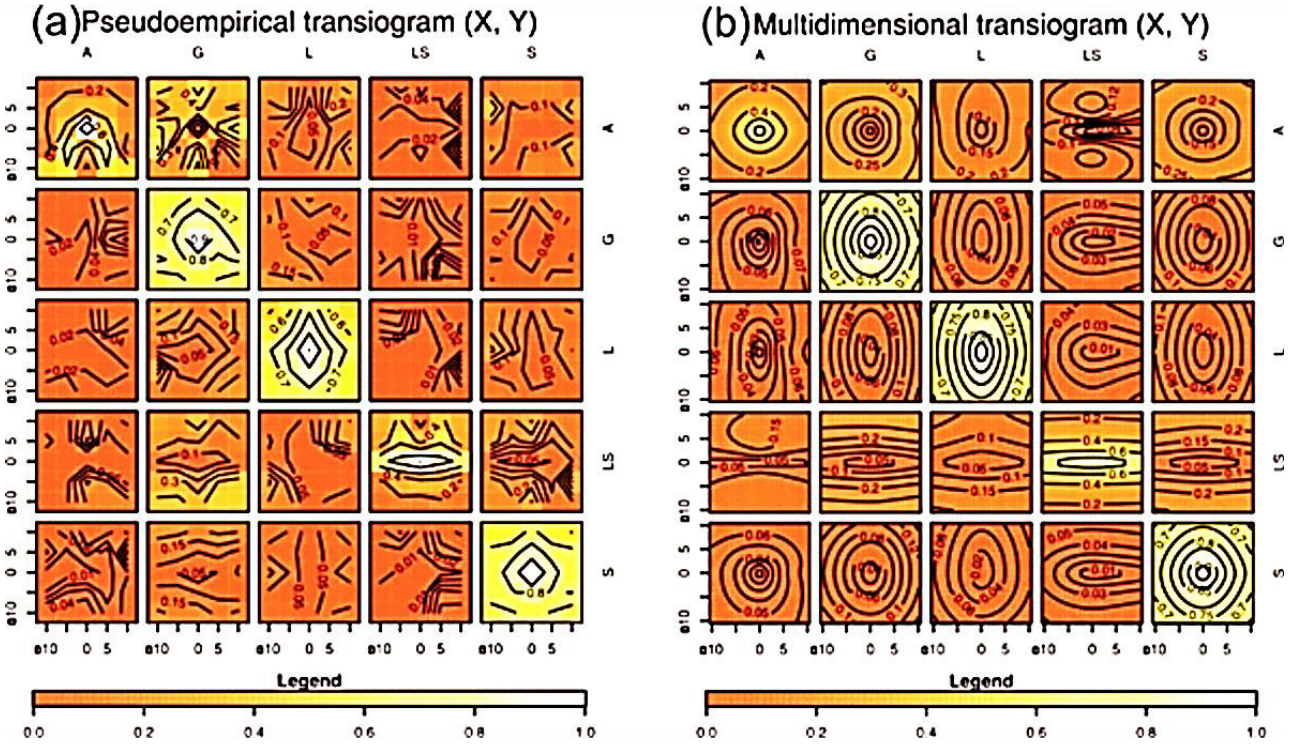

Fig. 5 - Surface theoretical transiograms without (a) and with (b) ellipsoidal interpolation.

Simulation results

After the transiogram analysis and modeling, a 3D simulation of lithologies was performed by means of the MCP algorithm. This algorithm is implemented in the spMC package and uses a maximum entropy approach in order to approximate the posterior conditional probabilities. A

small portion (70 m x 60 m x 5m) of the hydrogeological zone described before was converted into a discrete 3D grid of 56 x 69 x 91cells [1m x 1m x 0,05m] (Fig. 2). An example of lithological heterogeneity in the studied area is visible in the core box of the 5 m deep borehole Ps3 exposed in the same Fig. 2c. The aim of the geostatistical simulation performed by the MCP algorithm is to reproduce such a heterogeneity. In Fig. 6, the results of lithologic simulation are visible in 3D and in 3 cross sections (A, B, C) from 48.5 m to 53 m a.s.l., while the latitude and longitude are expressed according to the "Monte Mario Italy 1" coordinate system. The simulation obtained by MCP algorithm is plotted through ParaView code (Ahrens et al., 2005; Ayachit et al., 2014). ParaView is an open source, multiplatform data analysis and visualization application. The traces of those cross sections are also visible as yellow lines in Fig. 2a. The first cross section (A) (Fig. 6) is a diagonal obtained from the simulated area and starts from borehole Gp2 to Pz10A. The second (B) is almost perpendicular to the first one and passes through borehole Ps2 and Ps4. The third (C) passes through borehole Gp3 and Gp7. The analysis of these simulated cross sections confirms (cfr. Table 2, Fig.4f) as LS (sandy silt) layers are often located above S (sand) layers rather than vice versa. Moreover, LS (sandy silt) layers are rarely below A (clay) layers as visible in Fig. 4m and Table 2. A more probable situation occurs with regard to G (gravel) layers located below LS (sandy silt) layers as shown in Fig. 4n and Table 2.

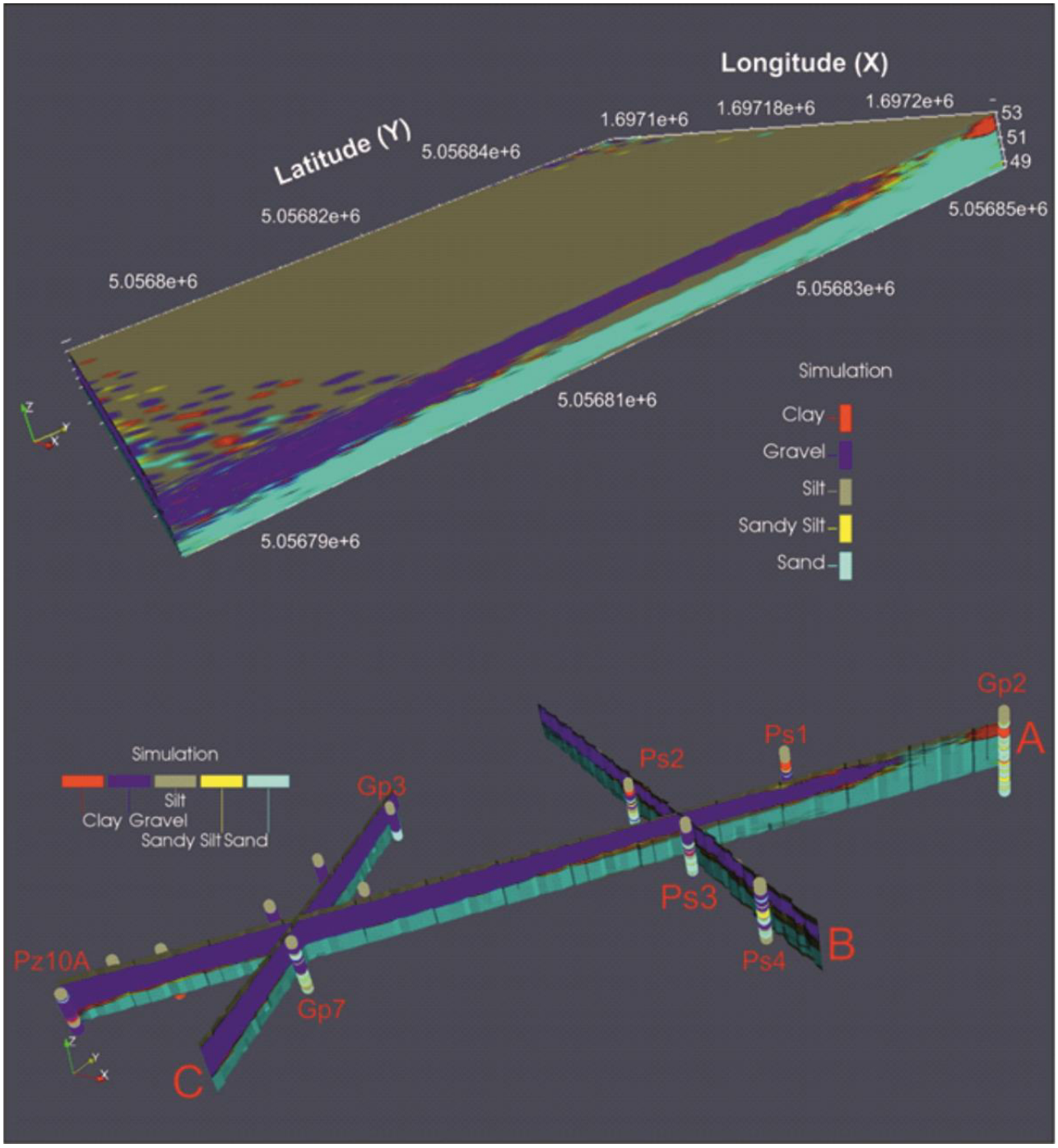

Fig. 6 - MCP 3D simulation on 91 layers every 5 cm in depth from 53 m to 48.5 m a.s.l.; cross sections A, B, C of MCP 3D simulation and simplified stratigraphy of the 13 boreholes.

Conclusions

In this paper, a simulation of lithological distribution in a small area located in NE Italy was carried out. Geostatistical reconstruction of subsoil, considering compositional data, is frequently made by indicator kriging approach being affected by the aforementioned conceptual issues. A Markovian type Categorical Prediction (MCP) by the R package spMC was

applied in order to show the code's potentialities and the advantages of applying this geostatistical approach (i.e.: MCP). The main results of this study revealed important aspects to consider, both for application purposes and computational perspective. From the geological perspective, the juxtapositional tendencies by pairs of lithologies (especially in depth), regardless of their distances, provide information about depositional correlation amongst materials. These tendencieselucidate the spatial probability of finding material changes. Furthermore, the inspection of the diagonal transiogram (i.e. auto transiograms) supplies the associated probability to find thickness of lithologies. These two pieces of information play an important role for sedimentological and hydrogeological perspectives, as they could dig out depositional cycles and related hydrogeological structures controlling flow direction. The MCP simulation effectively reproduces the heterogeneity of the studied area, and the observable juxtaposition tendencies are comparable with the estimated ETP and the transiogram results. From the computational point of view, the simulation performed by MCP only accounts for the sums and products of univariate and bivariate probabilities in agreement with the maximum entropy approach, and produces consistent results with the lithological heterogeneity of the simulated area, by avoiding the well-known "order relation problem" of the indicator kriging. The simulation avoids high computational costs, which are typical of the indicator kriging approach, and HPC techniques further improve the computational efficiency. This computational setting also allows for an increased number of lithological categories considered during the simulation. In conclusion, when dealing with lithological variables (categorical variables), the results obtained by spMC package suggest that this software should be considered to be a good candidate for simulating subsoil lithological distributions especially in limited areas. The computational capabilities and efficacy in modeling heterogeneity allow for a wide application of spMC in hydrogeological modeling.

Acknowledgment

The authors would like to thank Arthur Rosales for proofreading the manuscript and providing useful comments.

References

Ahrens J, Geveci B, Law C. 2005. Paraview: An end-user tool for large data visualization. The visualization handbook 717

Al-Khalifa MA, Payenberg THD, Lang S. 2007. Overcoming the Challenges of Building 3D Stochastic Reservoir Models Using Conceptual Geological Models: A Case Study. In SPE Middle East Oil and Gas Show and ConferenceSociety of Petroleum Engineers. DOI: 10.2118/104496-MS

Allard D, D'Or D, Froidevaux R. 2011. An efficient maximum entropy approach for categorical variable prediction. European Journal of Soil Science 62 (3): 381–393 DOI: 10.1111/j.1365-2389.2011.01362.x

Armstrong M. 2011. Plurigaussian simulations in geosciences. Springer.

Ayachit, U., Bauer, A., Chaudhary, A, DeMarle, D., Geveci, B., Jourdain, S., Lutz, K., Marion, P., Maynard, R., Nikhil, S., Yuan, Y., Azgaris, G., Scott, A., Moreland, K., Brandon, M., 2014. ParaView Manual - A Parallell Visualization Application - Version 4.0.

Bierkens MFP, Burrough PA. 1993a. The indicator approach to categorical soil data. Journal of Soil Science 44 (2): 369–381 DOI: 10.1111/j.1365-2389.1993.tb00459.x

Bierkens MFP, Burrough PA. 1993b. The indicator approach to categorical soil data. Journal of Soil Science 44 (2): 361–368 DOI: 10.1111/j.1365-2389.1993.tb00458.x

Bogaert P. 2002. Spatial prediction of categorical variables: the Bayesian maximum entropy approach. Stochastic Environmental Research and Risk Assessment (SERRA) 16 (6): 425–448 DOI: 10.1007/s00477-002-0114-4

Bogaert P, D'Or D. 2002. Estimating Soil Properties from Thematic Soil Maps. Soil Science Society of America Journal 66 (5): 1492 DOI: 10.2136/sssaj2002.1492

Breslow NE, Clayton DG. 1993. Approximate Inference in Generalized Linear Mixed Models. Journal of the American Statistical Association 88 (421): 9–25 DOI: 10.1080/01621459.1993.10594284

Cao G, Kyriakidis PC, Goodchild MF. 2011. A multinomial logistic mixed model for the prediction of categorical spatial data. International Journal of Geographical Information Science 25 (12): 2071–2086 DOI: 10.1080/13658816.2011.600253

Carle SF, Fogg GE. 1996. Transition probability-based indicator geostatistics. Mathematical Geology 28 (4): 453–476 DOI: 10.1007/BF02083656

Carle SF, Fogg GE. 1997. Modeling Spatial Variability with One and Multidimensional Continuous-Lag Markov Chains. Mathematical Geology 29 (7): 891–918 DOI: 10.1023/A:1022303706942

Carraro A, Fabbri P, Giaretta A, Peruzzo L, Tateo F, Tellini F. 2013. Arsenic anomalies in shallow Venetian Plain (Northeast Italy) groundwater. Environmental Earth Sciences 70 (7): 3067–3084 DOI: 10.1007/s12665-013-2367-2

Carraro A, Fabbri P, Giaretta A, Peruzzo L, Tateo F, Tellini F. 2015. Effects of redox conditions on the control of arsenic mobility in shallow alluvial aquifers on the Venetian Plain (Italy). Science of The Total Environment 532: 581–594 DOI: 10.1016/j.scitotenv.2015.06.003

Christakos G. 1990. A Bayesian/maximum-entropy view to the spatial estimation problem. Mathematical Geology 22 (7): 763–777 DOI: 10.1007/BF00890661

Chugunova TL, Hu LY. 2008. Multiple-Point Simulations Constrained by Continuous Auxiliary Data. Mathematical Geosciences 40 (2): 133–146 DOI: 10.1007/s11004-007-9142-4

Comunian A, Renard P, Straubhaar J. 2012. 3D multiple-point statistics simulation using 2D training images. Computers & Geosciences 40: 49–65 DOI: 10.1016/J.CAGEO.2011.07.009

Comunian A, Renard P, Straubhaar J, Bayer P. 2011. Three-dimensional high resolution fluvio-glacial aquifer analog – Part 2: Geostatistical modeling. Journal of Hydrology 405 (1–2): 10–23 DOI: 10.1016/J.JHYDROL.2011.03.037

Csiszar I. 1991. Why Least Squares and Maximum Entropy? An Axiomatic Approach to Inference for Linear Inverse Problems. The Annals of Statistics 19 (4): 2032–2066 DOI: 10.1214/aos/1176348385

D'Or D, Bogaert P. 2004. Spatial prediction of categorical variables with the Bayesian Maximum Entropy approach: the Ooypolder case study. European Journal of Soil Science 55 (4): 763–775 DOI: 10.1111/j.1365-2389.2004.00628.x

D'Or D, Bogaert P, Christakos G. 2001. Application of the BME approach to soil texture mapping. Stochastic Environmental Research and Risk Assessment 15 (1): 87–100 DOI: 10.1007/s004770000057

Dalla Libera N, Fabbri P, Mason L, Piccinini L, Pola M. 2018. A local natural background level concept to improve the natural background level: a case study on the drainage basin of the Venetian Lagoon in Northeastern Italy. Environmental Earth Sciences 77 (13): 487 DOI: 10.1007/s12665-018-7672-3

dell'Arciprete D, Bersezio R, Felletti F, Giudici M, Comunian A, Renard P. 2012. Comparison of three geostatistical methods for hydrofacies simulation: A test on alluvial sediments. Hydrogeology Journal 20 (2): 299–311 DOI: 10.1007/s10040-011-0808-0

Fabbri P. 2001. Probabilistic Assessment of Temperature in the Euganean Geothermal Area (Veneto Region, NE Italy). Mathematical Geology 33 (6): 745–760 DOI: 10.1023/A:1011030900322

Fabbri P, Piccinini L. 2013. Assessing transmissivity from specific capacity in an alluvial aquifer in the middle Venetian plain (NE Italy). Water Science and Technology 67 (9): 2000–2008 DOI: 10.2166/wst.2013.074

Fabbri P, Gaetan C, Zangheri P. 2011. Transfer function-noise modelling of an aquifer system in NE Italy. Hydrological Processes 25 (2): 194–206 DOI: 10.1002/hyp.7832

Fabbri P, Ortombina M, Piccinini L. 2012. Estimation of Hydraulic Conductivity Using the Slug Test Method in a Shallow Aquifer in the Venetian Plain (NE, Italy). Aqua Mundi 3 (April): 125–133 DOI: 10.4409/Am-045-12-0048

Fabbri P, Piccinini L, Marcolongo E, Pola M, Conchetto E, Zangheri P. 2016. Does a change of irrigation technique impact on groundwater resources? A case study in Northeastern Italy. Environmental Science & Policy 63: 63–75 DOI: 10.1016/J.ENVSCI.2016.05.009

Falivene O, Cabrera L, Muñoz JA, Cazo PA, Fernández Ó, Sáez A. 2007. Statistical grid-based facies reconstruction and modelling for sedimentary bodies. Alluvial-palustrine and turbiditic examples. Geologica Acta 5 (3): 199–230 DOI: 10.1344/105.000000295

Fontana A, Mozzi P, Bondesan A. 2008. Alluvial megafans in the Venetian–Friulian Plain (north-eastern Italy): Evidence of sedimentary and erosive phases during Late Pleistocene and Holocene. Quaternary International 189 (1): 71–90 DOI: 10.1016/J.QUAINT.2007.08.044

Haldorsen HH, Chang DM. 1986. Notes on stochastic shales; from outcrop to simulation model. In Reservoir CharacterizationElsevier; 445–485.

Hattori I. 1976. Entropy in Markov chains and discrimination of cyclic patterns in lithologic successions. Journal of the International Association for Mathematical Geology 8 (4): 477–497 DOI: 10.1007/BF01028983

Huang X, Wang Z, Guo J. 2016. Prediction of categorical spatial data via Bayesian updating. International Journal of Geographical Information Science 30 (7): 1426–1449 DOI: 10.1080/13658816.2015.1133819

De Iaco S, Myers DE, Palma M, Posa D. 2010. FORTRAN programs for space–time multivariate modeling and prediction. Computers & Geosciences 36 (5): 636–646 DOI: 10.1016/J.CAGEO.2009.10.004

Jef Caers TZ. 2004. Multiple-point Geostatistics: A Quantitative Vehicle for Integrating Geologic Analogs into Multiple Reservoir Models: 383–394 Available at: http://archives.datapages.com/data/specpubs/memoir80/CHAPTER18/CHAPTER18.HTM [Accessed 27 May 2019]

Johnson NM. 1995. Characterization of alluvial hydrostratigraphy with indicator semivariograms. Water Resources Research 31 (12): 3217–3227 DOI: 10.1029/95WR02571

Journel AG, 1983. Nonparametric estimation of spatial distributions. Math. Geol. 15, 445–468. https://doi.org/10.1007/BF01031292

Journel AG, Gomez-Hernandez JJ. 1993. Stochastic Imaging of the Wilmington Clastic Sequence. SPE Formation Evaluation 8 (01): 33–40 DOI: 10.2118/19857-PA

Journel AG, Gundeso R, Gringarten E, Yao T. 1998. Stochastic modelling of a fluvial reservoir: a comparative review of algorithms. Journal of Petroleum Science and Engineering 21 (1–2): 95–121 DOI: 10.1016/S0920-4105(98)00044-8

Koltermann CE, Gorelick SM. 1996. Heterogeneity in Sedimentary Deposits: A Review of Structure-Imitating, Process-Imitating, and Descriptive Approaches. Water Resources Research 32 (9): 2617–2658 DOI: 10.1029/96WR00025

Lee SY, Carle SF, Fogg GE. 2007. Geologic heterogeneity and a comparison of two geostatistical models: Sequential Gaussian and transition probability-based geostatistical simulation. Advances in Water Resources 30 (9): 1914–1932 DOI: 10.1016/j.advwatres.2007.03.005

Luo J. 1996. Transition Probability Approach to Statistical Analysis of Spatial Qualitative Variables in Geology.Springer, Boston, MA; 281–299. DOI: 10.1007/978-1-4613-0363-3_14

Mariethoz G, Renard P. 2010. Reconstruction of Incomplete Data Sets or Images Using Direct Sampling. Mathematical Geosciences 42 (3): 245–268 DOI: 10.1007/s11004-010-9270-0

Marini M, Felletti F, Beretta G, Terrenghi J, Marini M, Felletti F, Beretta G Pietro, Terrenghi J. 2018. Three Geostatistical Methods for Hydrofacies Simulation Ranked Using a Large Borehole Lithology Dataset from the Venice Hinterland (NE Italy). Water 10 (7): 844 DOI: 10.3390/w10070844

de Marsily G, Delay F, Gonçalvès J, Renard P, Teles V, Violette S. 2005. Dealing with spatial heterogeneity. Hydrogeology Journal 13 (1): 161–183 DOI: 10.1007/s10040-004-0432-3

de Marsily G, Delay F, Teles V, Schafmeister MT. 1998. Some current methods to represent the heterogeneity of natural media in hydrogeology. Hydrogeology Journal 6 (1): 115–130 DOI: 10.1007/s100400050138

Matheron G, Beucher H, de Fouquet C, Galli A, Guerillot D, Ravenne C. 1987. Conditional Simulation of the Geometry of Fluvio-Deltaic Reservoirs. In SPE Annual Technical Conference and ExhibitionSociety of Petroleum Engineers. DOI: 10.2118/16753-MS

Miall AD. 1973. Markov chain analysis applied to an ancient alluvial plain succession. Sedimentology 20 (3): 347–364 DOI: 10.1111/j.1365-3091.1973.tb01615.x

OpenMP Architecture Review Board, 2008. OpenMP Application Program Interface Version 3.0. Rev. Lit. Arts Am. https://doi.org/10.1080/08905769008604595

Piccinini L, Fabbri P, Pola M. 2016. Point dilution tests to calculate groundwater velocity: an example in a porous aquifer in northeast Italy. Hydrological Sciences Journal DOI: 10.1080/02626667.2015.1036756

Pyrcz M. 2014. Pyrcz, M.J., and Deutsch, C.V., Geostatistical Reservoir Modeling, 2nd Edition, Oxford University Press, New York, p. 448.

R Development Core Team, 2018. R: A Language and Environment for Statistical Computing, Web. https://doi.org/10.1016/0164-1212(87)90019-7

Sartore L, Fabbri P, Gaetan C. 2016. spMC: An R-package for 3D lithological reconstructions based on spatial Markov chains. Computers & Geosciences 94 (July): 40–47 DOI: 10.1016/j.cageo.2016.06.001

Schwarzacher W. 1969. The use of Markov chains in the study of sedimentary cycles. Journal of the International Association for Mathematical Geology 1 (1): 17–39 DOI: 10.1007/BF02047069

Seifert D, Jensen JL. 1999. Using Sequential Indicator Simulation as a Tool in Reservoir Description: Issues and Uncertainties. Mathematical Geology 31 (5): 527–550 DOI: 10.1023/A:1007563907124

Strebelle S. 2002. Conditional Simulation of Complex Geological Structures Using Multiple-Point Statistics. Mathematical Geology 34 (1): 1–21 DOI: 10.1023/A:1014009426274

Trevisani S, Fabbri P. 2010. Geostatistical modeling of a heterogeneous site bordering the Venice lagoon, Italy. Ground Water 48 (4): 614–623 DOI: 10.1111/j.1745-6584.2009.00632.x

Vargas-Guzmán JA, Al-Qassab H. 2006. Spatial conditional simulation of facies objects for modeling complex clastic reservoirs. Journal of Petroleum Science and Engineering 54 (1–2): 1–9 DOI: 10.1016/J.PETROL.2006.06.007

Viseur S. 1999. Stochastic Boolean Simulation of Fluvial Deposits : A New Approach Combining Accuracy with Efficiency. In SPE Annual Technical Conference and ExhibitionSociety of Petroleum Engineers. DOI: 10.2118/56688-MS

Vorlicek PA, Antonelli R, Fabbri P, Rausch R. 2004. Quantitative hydrogeological studies of the Treviso alluvial plain, NE Italy. Quarterly Journal of Engineering Geology and Hydrogeology 37 (1): 23–29 DOI: 10.1144/0036-9276/02-006

Weissmann GS, Fogg GE. 1999. Multi-scale alluvial fan heterogeneity modeled with transition probability geostatistics in a sequence stratigraphic framework. Journal of Hydrology 226 (1–2): 48–65 DOI: 10.1016/S0022-1694(99)00160-2

Weissmann GS, Carle SF, Fogg GE. 1999. Three-dimensional hydrofacies modeling based on soil surveys and transition probability geostatistics. Water Resources Research 35 (6): 1761–1770 DOI: 10.1029/1999WR900048

2.4.2 Application on Western Agricultural Areas (WAA)

The WAA, as described in section 2.2, is the result of complex sedimentological processes (i.e.: alluvial and tidal dynamics), working jointly during the last 30,000 years. These processes led toward a huge subsurface heterogeneity, thus to model the subsurface structure, a geostatistical approach was chosen. In this direction, we used the spMC package (Sartore et al., 2016) implemented in R environment (R Core Team, 2019). Specifically, we used the approach previously described in section 2.4.1 (Article 4). The MCP algorithm (Allard et al., 2011) allows for an efficient subsurface modeling, especially when one is dealing with lots of data and several materials.

Stratigraphic dataset

The first phase of the presented PhD project concerns the reconstruction of the subsurface heterogeneity, in order to get information about the spatial distribution of As-bearing materials within WAA and use them as base for the reactive transport modeling (third phase of the study). For the subsurface modeling we used the boreholes dataset developed by the Veneto Region, which records all the stratigraphic logs developed from geotechnical, environmental and research studies. The entire dataset was filtered to get only those logs falling within or around the WAA. Through this filtering process 119 boreholes were kept into account and used to build up the actual dataset for modeling purposes (Figure 1a). The stratigraphic logs reach a maximum depth of 20 meter below the ground level, the range of depth in which the targeted aquifer is located. The boreholes data were reclassified in four material classes (i.e.: Sand, Silt, Clay and Peat) and, then, discretized along depth direction with a Δz of 0.10 meter to make it suitable for 3D geostatistical modeling (Figure 1b, 1c). The discretization process was developed through a simple C++ code wrote “ad hoc” to recognize the materials along the depth direction and re-assign them to the new discretized depth information. The starting point for depth elaboration is always the ground level respect to the mean sea level. This information was originally included in Veneto Region’s boreholes dataset.

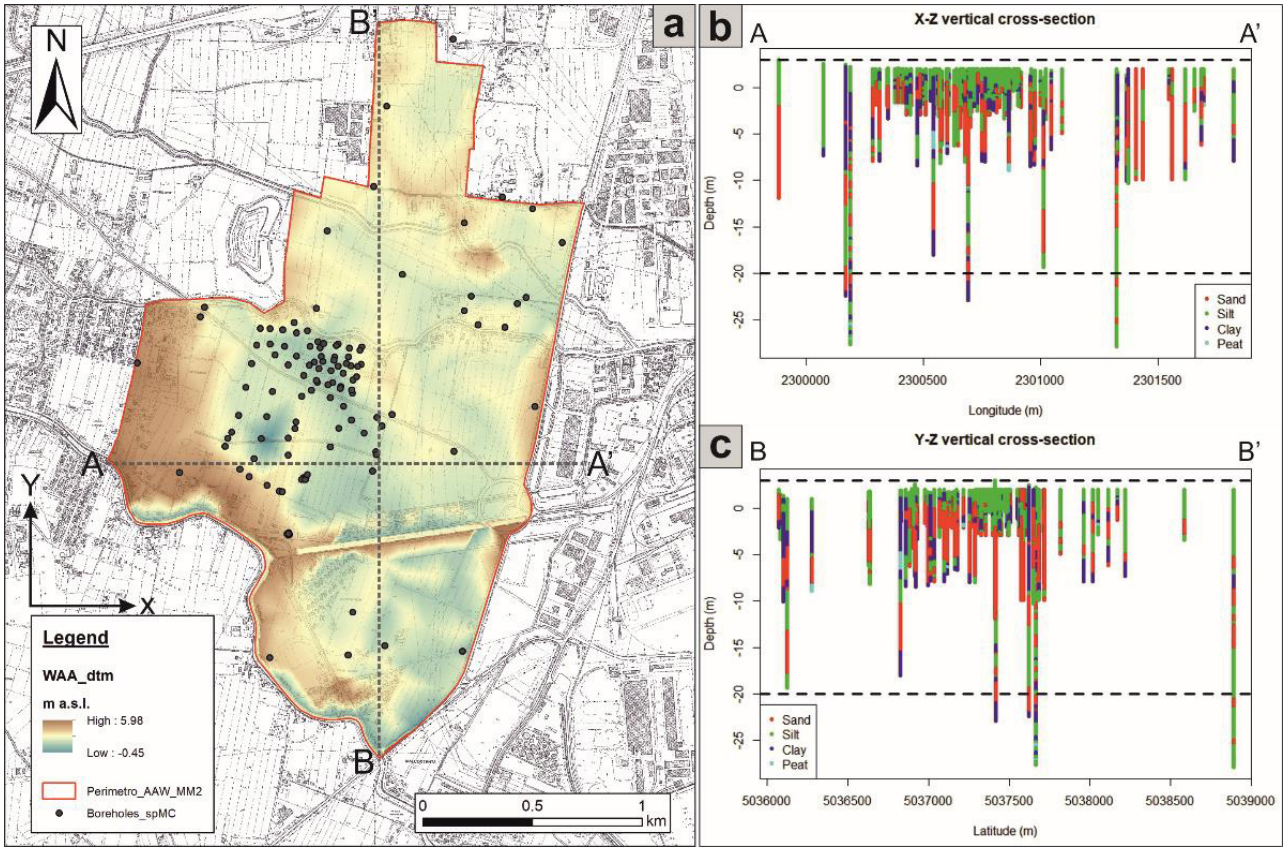

Figure 1 – a) Spatial distribution of boreholes used for subsurface heterogeneity modeling of WAA. b) and c) show two cross-sections along X and Y direction respectively with a depth (z) discretization of 0.1 m.

Results

The modeling of subsurface heterogeneity of WAA through spMC code (Sartore et al., 2013) highlighted the large variability of geological materials within WAA and, in general, in the DBVL. A first statistical analysis of the available borehole logs pointed out a sharp difference between materials' proportion and their spatial extension as well. The Figure 2A shows the main discrepancies in term of percentage of frequency with a 35% of sandy materials, 64% of fine sediments (46% silt and 18% clay) and only 1% of organic matter (expressed as peat). As first sight, these frequency values reflect the geological setting of the study area, in particular, the sedimentary characteristics of the Mestre depositional unit described by Bondesan et al., 2008. In this line, the analysis of the average extension (along x and y, Figure 2B, 2C) and the average thickness (in z, Figure 2D) of each material, confirm the high heterogeneity of the subsurface, which is typical of distal alluvial plain environment affected by tidal processes.

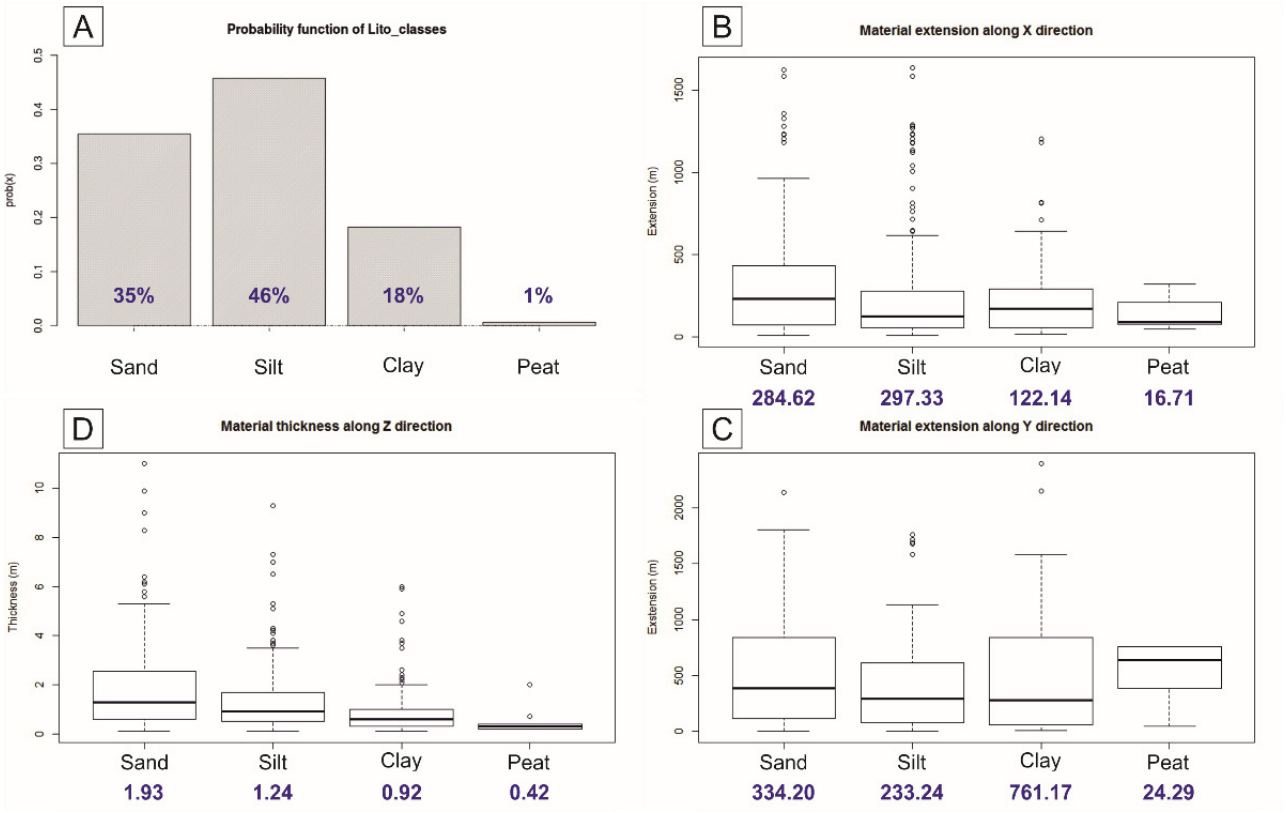

Figure 2 – Preliminary boreholes data analysis. A) percentage of material occurring in the WAA. B) Average material layers extension along x direction, C) average extension along Y and D) average thickness along depth (nella figure B e C mi fermerei ad 1 cifra decimale!).

The estimation of average thickness and lateral extension emphasizes the occurrence of thicker and more or less wide sandy deposits, which are overlapped or limited by wider silty - clayey layers. A similar stratigraphic setting recallsan environment formed by braided river paleo-canals and wide floodplain areas (silt and clay deposit, Bondesan et al., 2008; Mozzi et al. 2003). The geometry of peat deposit, instead, is very limited in space with short lateral extension and lowered thickness. The organic layers, indeed, are often associated to limited ponding zones developed during flood events or lagoon ingressions (Fontana et al., 2004). The spMC modeling gets light on other interesting sedimentological information such as the juxstapositional tendency among materials, thus their transitional probabilities (TP). The TP are the base for the transiogram-based geostatistics (Carle and Fogg, 1996; Weissmann, 1999) and, at the same time, they give important hints for evaluate the depositional processes.

Table 1 – Embedded transitional probabilities along x, y and z direction.

eMCx	Sand	Silt	Clay	Peat
Sand	NA	0.72	0.28	0.00
Silt	0.55	NA	0.42	0.03
Clay	0.46	0.54	NA	0.00
Peat	0.00	0.76	0.24	NA

eMCy	Sand	Silt	Clay	Peat
Sand	NA	0.67	0.32	0.01
Silt	0.58	NA	0.41	0.01
Clay	0.32	0.62	NA	0.06
Peat	0.61	0.30	0.09	NA

eMCz	Sand	Silt	Clay	Peat
Sand	NA	0.63	0.35	0.02
Silt	0.49	NA	0.50	0.01
Clay	0.22	0.74	NA	0.04
Peat	0.00	0.71	0.29	NA

Table 1 shows the embedded transitional probabilities for each material along the 3 main spatial direction (x, y, z). As one can see from those values, there is a clear transition tendency from silt to clay along x - y directions, emphasized on the associated transiogram map in Figure 3A. This evidence is in line with the depositional trend of a flood plain environment. On the contrary, the TPs associated to peaty materials are overall lower, suggesting a limited occurrence of that material and its local distribution within the study WAA. Looking the auto-transiogram map for peat in Figure 3A, it is evident that peaty deposits are limited in space with few meters of lateral extension. Figure 3B shows the transiograms along the depth direction, which are very useful to determine the scale at which the transition between two materials can occurs. In our study area, it is evident how the sand and silt have a transition lag wider than the other materials. Peat deposits, instead, have small transition lags repeated along the depth (oscillation of experimental transiogram), which means peat layers can be stack on top each other along the depth with small thickness. The information from the vertical experimental transiograms are useful for both heterogeneity reconstruction and studying the depositional cycles.

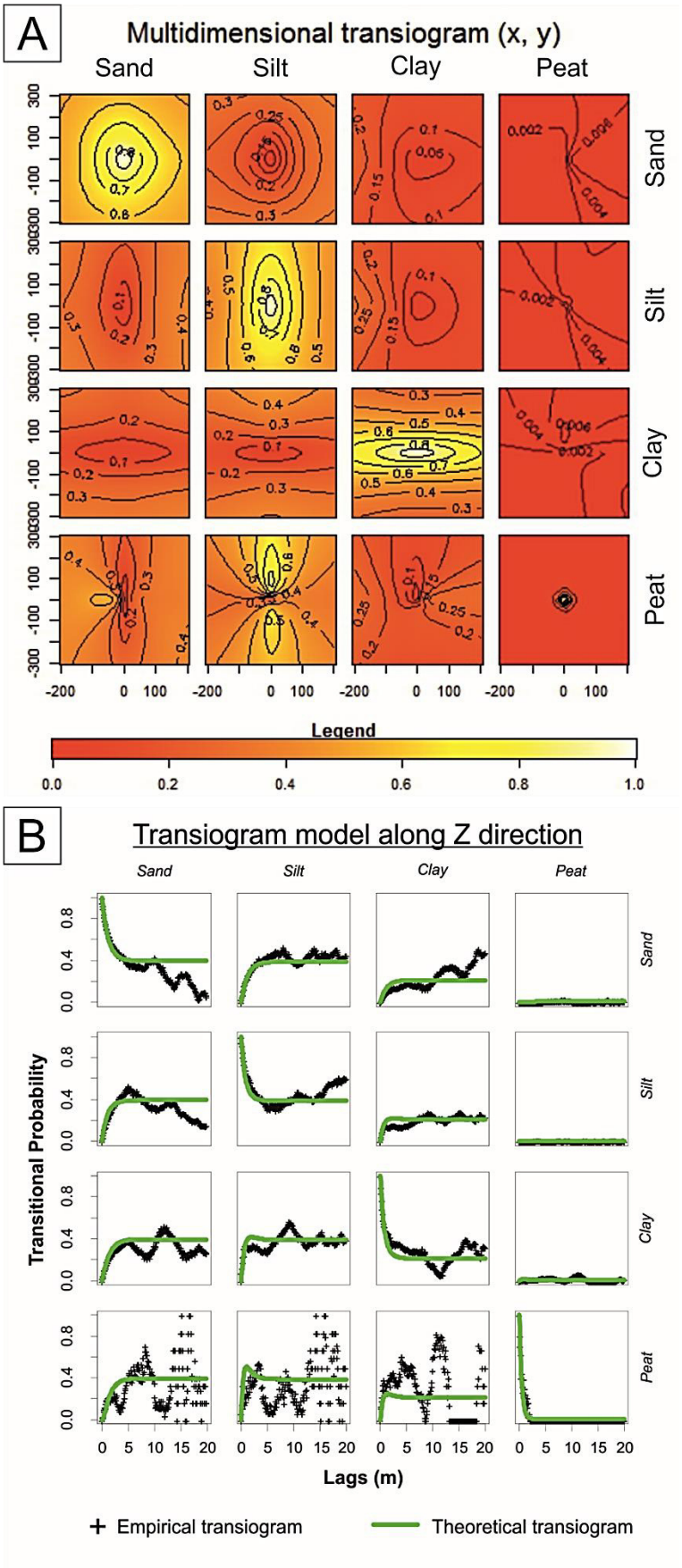

Figure 3 – A) Multidimensional transiograms along x and y direction. The color ramp describes the magnitude of the transitional probability. B) Transiogram along depth direction.

The modeling of the experimental transiograms obtained by the borehole's information and the information about the average extension of the material layers allowed to reconstruct the geostatistical-based distribution of subsurface materials in WAA in a grid X x Y x Z. The MCP algorithm was used. It is powerful and helpful due to its high computational performance and a more efficient way in managing large material dataset. The application of MCP results in the 3D material distribution shown in Figure 4.

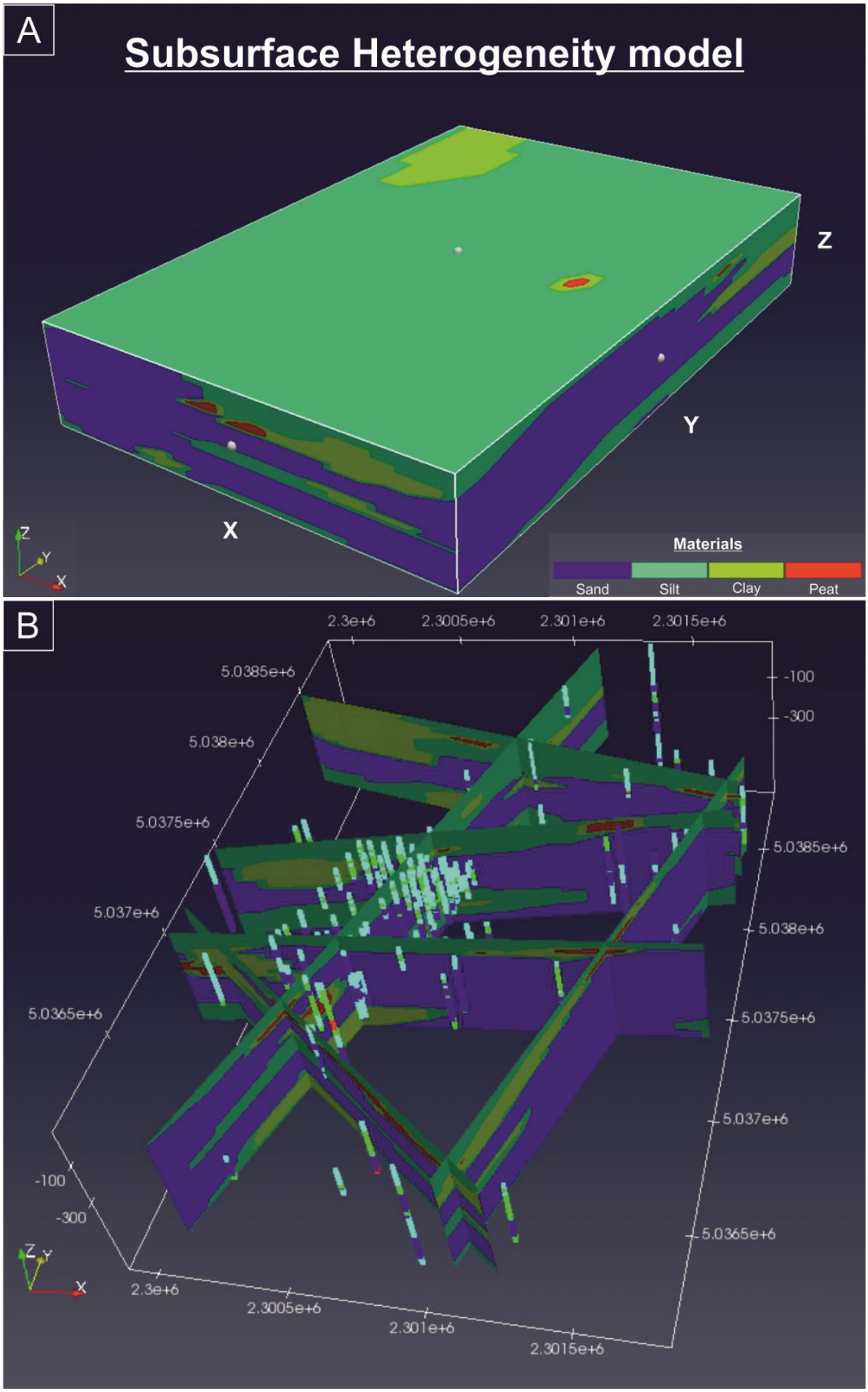

Figure 4 – Subsurface model of WAA: A) Volume material distribution, B) cross-section reproducing the available in ARPAV, 2011. The sparse columns represent the input boreholes.

The obtained subsurface model keeps the main geological characteristics of the WAA. The northern portion of the area is characterized by the presence of larger amount of fine materials, which enclose a thinner sandy layer, location of the studied shallow aquifer. This setting is in accordance with the information brought by the experimental boreholes. Moving toward the southern part of WAA, the spMC-model reconstructs a larger occurrence of sandy material, which form a wider and thicker aquifer than in the north. The central aquifer was modeled shallower than in the north being in accordance with the structure described by ARPAV 2011 and Beretta et al. in 2018. The southern WAA, instead, have a different geological and hydrogeological setting, because it shows a double aquifer system divided by impermeable materials (i.e.: clay and silt). In this area, a larger occurrence of organic matter deposits exists, typically associated to fine material deposits. The accuracy of the 3D subsurface model was evaluated comparing the experimental transiograms (Figure 2) with the transiograms of predicted data. Figure 5, for instance, shows the good fitting of synthetic transiograms (calculate on predicted data) with respect to the experimental ones. The best fitting was got along the depth direction (z dimension) due to the high resolution of the input data (boreholes). The availability of geological information every 0.10 meters along the depth allows for a detailed analysis of transitional tendency, which results in errors lower than 10%. The accuracy of the model slightly decreases considering the planar dimensions x and y. It is mainly due to the lower number of input data and their sparse distances along the planar directions, which results in lack of information, thus the accuracy. Anyway, visually comparing the model results with the experimental boreholes (Figure 5B), the model fits the main geological and geometrical characteristics of the WAA subsurface, making itself suitable for spatializing the hydraulic properties needed for a 3D reactive transport model (explained in section 2.6).

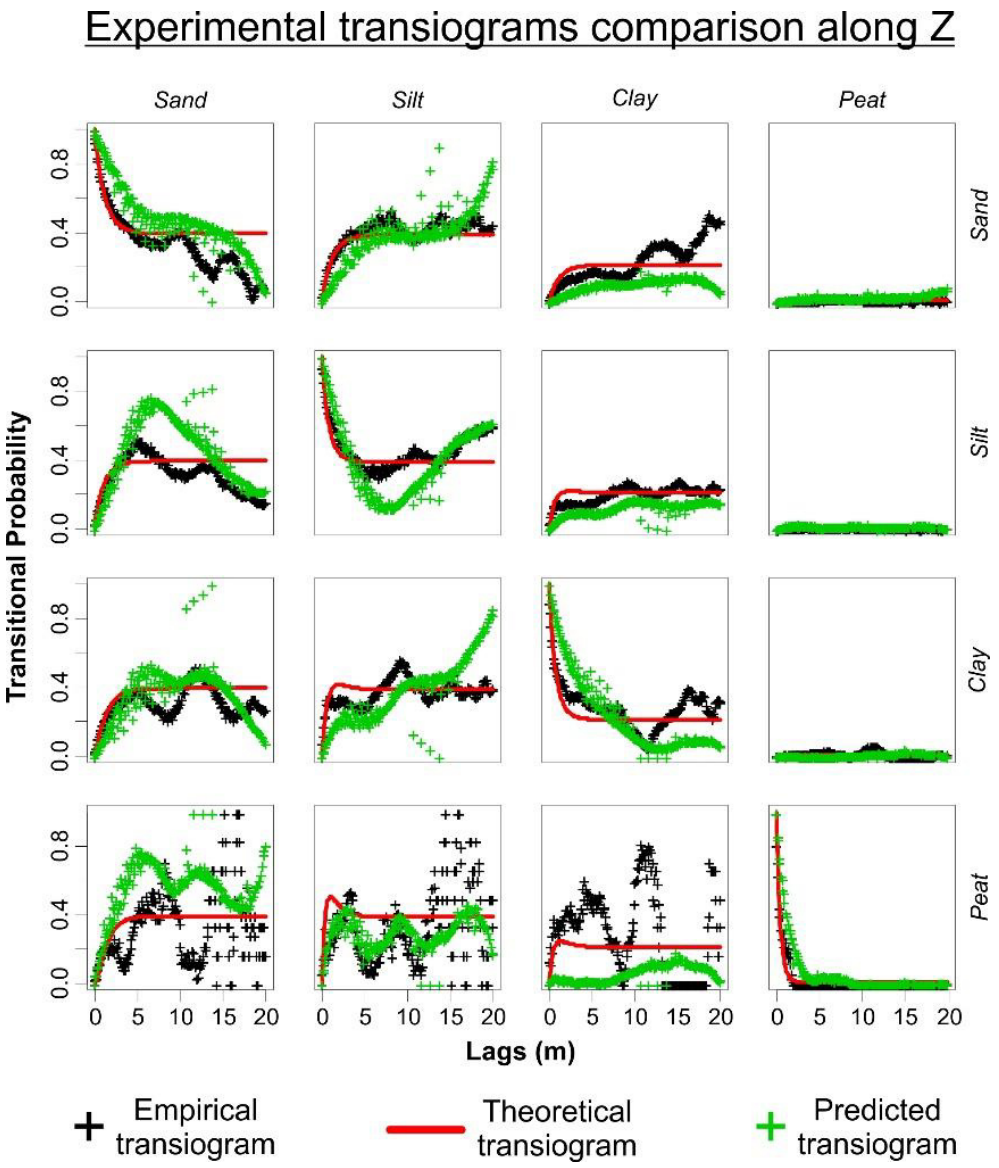

Figure 5 – Comparison between the experimental transiograms (black crosses) and the transiograms calculated on predicted data (green crosses). The red line represents the theoretical transiograms used for modeling the material transitional probabilities along z direction.

Conclusions

The boreholes data and their geostatistical analysis confirmed the huge heterogeneity of the WAA, and of the DBVL in a regional sense. The heterogeneous spatial distribution of materials beneath the ground level could impact the arsenic mobility somehow, as they are involved in geochemical interactions with groundwater. In this line, the subsurface heterogeneity study gets relevance because the better is knowledge of the subsurface structure the better will be the understanding of the involved geochemical mechanisms. With respect to the 3D reactive transport model, a detailed subsurface model could be useful for elucidating the role of subsurface heterogeneity on the chemical processes, thus on arsenic mobility. The obtained

results confirmed the effectiveness of using a transiogram-based approach for studying the heterogeneity, especially in those environments characterized by a high number of materials with complex transitions like in alluvial plains. The characteristics and the potentialities of spMC, underlined in section 2.4.1, are confirmed even in the WAA, highlighting its helpfulness as tool for building up the geological/hydrogeological conceptual model in heterogeneous areas.

References

Allard D, D'Or D, Froidevaux R. 2011. An efficient maximum entropy approach for categorical variable prediction. European Journal of Soil Science 62 (3): 381–393 DOI: 10.1111/j.1365-2389.2011.01362.x

ARPAV, 2011. INDAGINE AMBIENTALE "AREE AGRICOLE" - macroisola aree agricole – zona ovest, macroisola fusina – aree lungo naviglio brenta - sintesi dei risultati del piano di investigazione iniziale. Report data presentation.

Beretta, G. P., Terrenghi, J., 2017. Groundwater flow in the Venice lagoon and remediation of the Porto Marghera industrial area (Italy). Hydrogeol. J. 25, 847–861. https://doi.org/10.1007/s10040-016-1517-5

Bondesan, A., Primon, S., Bassan, V., Vitturi, A., 2008. Le unità geologiche della provincia di Venezia. Provincia di Venezia, Servizio Geologico e Difesa del Suolo.

Carle SF, Fogg GE. 1996. Transition probability-based indicator geostatistics. Mathematical Geology 28 (4): 453–476 DOI: 10.1007/BF02083656

Fontana A, Mozzi P, Bondesan A (2004) The geomorphological evolution of the Venetian-Friulian plain (in Italian). Whitin the: Bondesan, A., Meneghel, M., 2004. Geomorphology of the Venice Province. Esedra, Padova. 113-138

Mozzi P, Bini C, Zilocchi L, Beccatini R, Mariotti Lippi M (2003) Stratigraphy, palaeopedology and palynology of late Pleistocene and Holocene deposits in the landward sector of the lagoon of Venice (Italy), in relation to Caranto level. Il Quaternario, 16 (1 bis), pag. 193 – 210

R Development Core Team, 2019. R: A Language and Environment for Statistical Computing, Web. https://doi.org/10.1016/0164-1212(87)90019-7

Sartore L, Fabbri P, Gaetan C. 2016. spMC: An R-package for 3D lithological reconstructions based on spatial Markov chains. Computers & Geosciences 94 (July): 40–47 DOI: 10.1016/j.cageo.2016.06.001

Sartore, L., 2013. spMC: Modelling Spatial Random Fields with Continuous Lag Markov Chains. A peer-reviewed, open-access Publ. The R Journal Vol. 5/2, 1–15.

Weissmann, G.S., Carle, S.F., Fogg, G.E. 1999. Three-dimensional hydrofacies modeling based on soil surveys and transition probability geostatistics. Water Resour. Res. 35, 1761–1770. https://doi.org/10.1029/1999WR900048

2.5 Chemical processes definition

2.5.1 Paper 5

Controls of arsenic mobility in the alluvial aquifers near Venice (Italy) elucidated through machine-learning-based mapping and geochemical modeling

Nico Dalla Libera [a], Daniele Pedretti [b], Fabio Tateo [c], Leonardo Mason [d], Leonardo Piccinini [a], Paolo Fabbri [a]

a) Dipartimento di Geoscienze, Università degli Studi di Padova, 35131, Padua, Italy;

b) Dipartimento di Scienze della Terra "A. Desio", Università degli Studi di Milano, 20133 Milan, Italy;

c) Istituto di Geoscienze e Georisorse – CNR – IGG, c/o Dipartimento di Geoscienze, 35131, Padua, Italy;

d) Environmental Protection Agency, 30174, Venice, Italy.

Keywords

Arsenic mobility; Self-Organized Maps; PHREEQC; Redox changes; Venetian Alluvial Plain

Abstract

Naturally occurring high concentrations of arsenic in groundwater are known to mark several young Quaternary aquifers. In the Venetian Alluvial Plain near Venice, Italy, arsenic affects the local shallower aquifers. Several aspects of the physical and geochemical processes controlling arsenic mobility are unclear in the Venetian Alluvial Plain, being complicated by the aquifer heterogeneity, among other factors. The goal of this study was to elucidate what processes have a higher impact on arsenic mobilization in the Venetian Alluvial Plain to obtain a conceptual model that can be used to support decisions by local water authorities for informed groundwater management. An experimental analysis was conducted in the Western Agricultural Areas, a small subset of the Venetian Alluvial Plain containing all key elements to upscale the resulting conceptual model to the whole area. In the Western Agricultural Areas, aqueous and solid phase characterization of the aquifer was performed on sparsely distributed monitoring points. Three piezometers were sampled on a weekly basis to evaluate seasonal dependence of arsenic mobility at different points in the Western Agricultural Areas. The data were analyzed using advanced exploration analysis and reactive transport modeling. The machine-learning-based Self-Organized Maps algorithm allowed for the identification of the main geochemical relationships within the study aquifer and the associated geochemical processes, while reactive transport modeling was used to validate these processes. The results highlighted that redox-controlled dissolution and precipitation of iron hydroxides is the most likely process controlling arsenic mobility in the area. Redox conditions are directly connected to organic matter degradation and rainfall-driven aquifer recharge conditions. The latter influences the amounts of oxidizing species progressively entering the aquifer, leading to oxidized arsenic-free groundwater conditions. Recharge was postulated to be a function of the local stratigraphy and, in particular, of the thickness of the top silty-clay layers of the aquifer. Arsenic mobility, therefore, results from an interaction between processes occurring in the aquifer system and the unsaturated zone. Reductive dissolution is generally active in the system but it might be controlled by local recharge effects.

Introduction

Arsenic (As) contamination in groundwater is a well-known issue that affects several countries worldwide. Elevated As concentrations lead to unhealthy life conditions and potentially shorter life spans, if water is used without proper treatments. It could trigger various diseases such as the “black foot disease”, malignant cancers (Anawar et al., 2001; Appelo, 1994; Choong et al., 2007; Jain and Ali, 2000; Karim, 2000; Nordstrom, 2003; Rango et al., 2013) and cardiovascular diseases even at low chronic dosage (D'Ippoliti et al., 2015). Over the last few decades,

researchers have focused on the assessment of methods to reduce the risk of As contamination in drinking wells in both unconsolidated (Choudhury et al., 2018; Kinniburgh and Smedley, 2001; Dalla Libera et al., 2018; Huang et al., 2018; Jakobsen et al., 2018; Ziegler et al., 2017) and fractured aquifers (Ayotte et al., 2015; Mango and Ryan, 2015; Pedretti et al., 2019). After the pioneering investigation of As contamination in Bangladesh in the early 1990s (Kinniburgh and Smedley, 2001), several studies have evaluated the mechanisms linked to the mobility of As in groundwater, including redox controlled reactions, desorption of As from metal oxides or oxidation of As-bearing sulfides (Smedley and Kinniburgh, 2013). It is currently well understood that each individual mechanism is affected by the local (i.e., site-specific) hydrogeological conditions. Assessing the magnitude and impact of these mechanisms in physically and geochemically heterogeneous systems is highly complicated (Michael and Khan, 2016), posing uncertainty in the determination of As risk for groundwater consumers.

In Italy, the risk of elevated As intake can be a concern for public health (Pompili et al., 2017). Arsenic concentrations exceeding the recommended World Health Organization (WHO) threshold of 10 μg/L are found in several aquifers (Carraro et al., 2013; Dalla Libera et al., 2017; Ducci et al., 2016; Preziosi et al., 2010; Rotiroti et al., 2014). The origin of As differs regionally as a function of the local geological setting. In Central and Southern Italy, As is commonly linked to either volcanic formations or to thermal phenomena and occurs within groundwater because of the water-rock interaction and mixing processes (Ducci et al., 2016; Preziosi et al., 2010). In the alluvial plains of Northern Italy, (Molinari et al., 2012; Rotiroti et al., 2015; Ungaro et al., 2008) high As concentrations result from the geochemical interaction between freshwater and alluvial materials, similar, for instance, to the Southeast Asian alluvial plains (Appelo and Postma, 2005; Bhattacharya et al., 2016; McArthur et al., 2004; Nickson et al., 1998, 2000; Nordstrom, 2003; Postma et al., 2007).

In the Venetian Alluvial Plain (VAP), As-driven contamination represents a major environmental issue affecting groundwater quality and related activities. Arsenic is found both in the solid matrix and in the groundwater (ARPAV, 2011, 2014). Dissolved As is mainly observed within the shallower aquifer systems (Carraro et al., 2015, 2013; Dalla Libera et al., 2018), which are often used as water sources for agricultural activities (e.g., crop irrigation) and yard irrigation. Despite evidence of diffuse As contamination in the VAP, studies considering water-rock interactions based on both solid and liquid data from these groundwater aquifers are recent (Carraro et al., 2015), and no work has been presented to date that has investigated in detail the key physical and geochemical processes linked to As

mobilization in the VAP, especially using model-based reactive transport and systematic field monitoring.

This manuscript presents and analyses the results of a detailed study focused on the understanding and quantification of As mobilization in the Western Agricultural Areas (WAA), a small area (3.8 km^2) within the VAP, located in the proximity of the Venice Lagoon. The WAA is an excellent choice for the assessment of As mobility in the VAP, being easily accessible and suitable for scientific activities. Furthermore, the WAA includes all the important elements (including land use, geographical setting, and key hydrogeochemical behavior) representative of a typical agricultural area of the VAP, as documented in previously reported studies (ARPAV, 2014; Beretta and Terrenghi, 2017; Dalla Libera et al., 2016; Ungaro et al., 2008). Despite the agricultural activities diffused in VAP area, the WAA was chosen even for the lack of anthropogenic influences on aquifer system, as evaluated by the Regional Agency for Environmental Protection and Prevention of Veneto Region (ARPAV) during a preliminary characterization in 2011 (ARPAV, 2011). By analyzing the WAA, the specific goals of this work consist of:

a) developing a conceptual model explaining the occurrence of WHO-limit exceeding As concentrations and characterizing the key geochemical and hydrogeological mechanisms linked to As mobility in the VAP;

b) more generally, further elucidating controlling mechanisms of As mobility that are common to other complex aquifer conditions. In particular, similarities and differences between the VAP and well-studied alluvial aquifers found in the Southeast Asian plain are evaluated and discussed, given their similar geological conditions, as described in the following sections.

c) Demonstrating the combined use of machine learning and process-based geochemical modeling as a useful approach to elucidate As controls.

Material and Methods

The methodology followed in this work consisted of a combination of experimental and model-based analyses. The experimental analysis was based on detailed hydrogeological, geochemical and mineralogical characterizations of the groundwater and soil matrix of the WAA. During a monitoring period of six months, eight piezometers were sampled twice, and three piezometers were sampled on a weekly basis, in an attempt to evaluate seasonality in As response.

Representative soil samples were collected in the proximity of these piezometers. Since the sampling locations were sparsely distributed in the WAA, the surveys were designed expressly to evaluate any potential spatiotemporal variability of As concentrations that could be linked to the response to local hydrogeological conditions, soil matrix heterogeneity or other aspects.

Two model-based analyses were then adopted for the interpretation of the experimental data. The first is an exploratory data analysis (EDA) performed using machine-learning-based mapping based on Self Organizing Maps (SOM; Kohonen, 2013). SOM is a powerful automatic data analysis method generally used for data clustering and exploration. SOM was here combined with Spearman's correlation analysis (Goovaerts, 1997), which offered a widely understood solution to express nonlinear correlation among variables in a simple form. The use of SOM and Spearman's correlation analyses was expected to highlight relationships among variables, providing the initial ingredients to develop the conceptual model and to identify key factors linked to As mobility in the groundwater. While SOM is widely used in industrial, finance, linguistics and environmental studies, especially as an advanced exploratory data analysis and prediction tool (Kalteh et al., 2008; Törönen et al., 1999), no previous applications focused on As mobilization have been documented to date to our best knowledge. The second methodology is a process-based reactive transport modeling analysis using the multicomponent geochemical code PHREEQC (Parkhurst and Appelo, 2013). This code has been adopted in the past to simulate the key mechanisms associated with As release in several alluvial aquifers worldwide (Aiuppa et al., 2003; Flores and Rubio, 2010; Parsons et al., 2013; Postma et al., 2007; Sracek et al., 2004; Wallis et al., 2011). The reactive transport model was used to validate the postulated processes defining the conceptual model and identified using SOM and to obtain a first-cut quantification of the impact of selected geochemical mechanisms assumed to be responsible for As mobility in the WAA and in turn in the VAP.

Study area

From a geological perspective, the VAP results from morphological action of the Brenta River during the last 30000 years (Pleistocene – Holocene; Figure 1A). The alluvial plain is characterized by a strong heterogeneity in grain size distributions due to a past environment shaped by the braided river (Bondesan et al., 2008). In the upper part of the plain, gravelly and sandy alluvial deposits are present, whereas in the distal region, silty-clayey deposits prevail in the alluvial system, according to the typical structure of the Brenta River's mega fan (Fontana et al., 2010, 2008; Mozzi et al., 2013). Specifically, in the distal part of the plain, the subsurface

shows sequences of fine-grained sediments (silt and clay) and coarser materials (fine and silty sand). Peat deposits, with a thickness up to several decimeters and a lateral extension up to several hundred meters, are also present in the floodplain environments. The resulting hydrogeological configuration of the VAP is a sequence of hydrofacies typical of a distal plain, with overlapping sequences of silty-clayed aquitards and aquicludes and fine-grained sandy aquifers. Overall, this sedimentological setting results in a multilayered aquifer system with different degrees of confinement (Fabbri et al., 2011; Fabbri and Piccinini, 2013; Piccinini et al., 2016, 2015; Pola et al., 2016; Trevisani and Fabbri, 2010; Vorlicek et al., 2004).

The WAA (Figure 1B) is located in the distal part of the VAP, toward the Venice Lagoon. Here, the main shallow aquifers are fine and silty sands layers embedded within a clayish-silty matrix. On average, the study area shows a mild-low hydraulic conductivity (5-10 m/d) and a low topographic gradient, from ≈ 5‰ to less than 1‰ approaching the Venice Lagoon. A stratigraphic sketch of the subsurface in the VAP, highlighting the position of the WAA, is shown in Figure 1C. The top shallow aquifer, which is the main target of this work and which comprises on average the first ten meters below the surface, has been hypothesized to be hydraulically confined (ARPAV, 2014), with limited connection to the surface and in turn limited recharge by rainfall events.

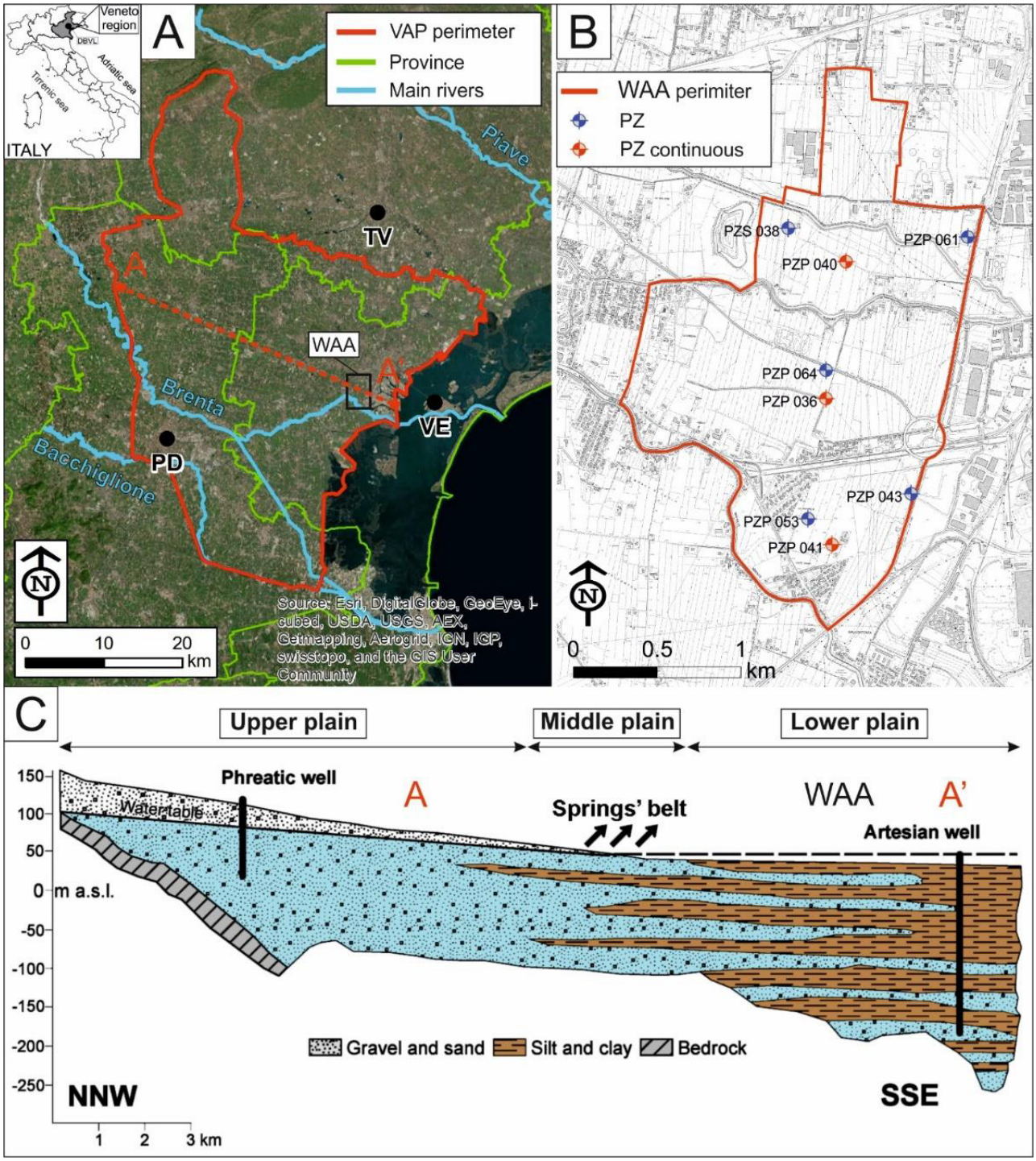

Figure 1 - A) The red line marks the limits of the Venetian Alluvial Plain (VAP), located between Padova (PD), Treviso (TV) and Venice (VE). The VAP is crossed by the Brenta River near its entrance to the Venice Lagoon. The small black square shows the location of the Western Agricultural Area (WAA). B) A topographic map of the WAA, showing the eight piezometers used in this study. The three red piezometers (PZP 036, 040 and 041) have been monitored weekly to highlight short-term variation in As content, related compounds and influencing physical variables. C) The Venetian Plain in the Veneto Region (red area in A), with a schematic cross-section (red dashed line in A; modified from Piccinini et al., 2017).

Experimental database

Eight piezometers located within the WAA were chosen to collect detailed hydrochemical and soil chemistry data, with emphasis on As and other chemical compounds and physical and chemical parameters that could affect its mobility. These piezometers (made of HDPE) used to be part of a more extended monitoring network owned and managed by ARPAV. Monitored for over ten years, this network initially covered the entire WAA and included approximately 40 piezometers. The majority of these points (34) tapped the first shallow aquifer (between 5 and 10 meters below the surface), and a lesser number of them reached the second aquifer (between 15 and 23 meters below the surface). Today, the number of monitored points has decreased to 11 piezometers, eight of which are within the shallower aquifer and three of which are in the deeper aquifer. Since As is mainly present in the shallow aquifer of the VAP (ARPAV, 2011; Dalla Libera et al., 2017), this study targeted exclusively the eight shallower piezometers (Figure 1B).

In each of the eight piezometers, chemical analyses are routinely performed by ARPAV laboratories on groundwater samples. The analysis includes parameters that have been typically associated with As mobility (e.g., NH_4^+, Fe, and Mn concentrations), particularly pH, oxidation-reduction potential (ORP), electrical conductivity (EC), temperature (T) and dissolved oxygen (DO) concentration. Water sampling and analyses followed the standard procedures suggested by the Italian Environmental Protection and Technical Services Agency (APAT, 2006). In situ parameters such as pH, ORP, EC, DO and T were evaluated through a multi-parametric probe YSI Professional Plus. In particular, ORP value was estimated with a platinum electrode and successive automatically corrected to Eh with reference to the standard hydrogen electrode. After that the Eh values were converted in pE for PHREEQC calculations. The main ions and the heavy metals, instead, were evaluated in ARPAV's laboratories using standard protocols (APAT IRSA-CNR, 2003; UNI EN ISO 17294-2:2016).

This study complemented the ARPAV analyses of the eight piezometers with more detailed information that could be relevant to explain As mobility. In particular, the following additional sampling and monitoring activities were performed specifically for this work.

- A detailed mineralogical, geochemical and stratigraphic characterization of the WAA to (a) evaluate the solid-phase content of As-bearing minerals, (b) obtain a detailed assessment of the lithological heterogeneities of the experimental sites, and (c) evaluate the different degrees of aquifer confinement. To this end, the stratigraphic well logs obtained from the drilling of boreholes were observed in detail. Then, manual drilling (from the ground to ≈ 6 m b.g.l.) in the

proximity of each piezometer was completed to collect soil samples and to perform a visual- and grain-size-based stratigraphic description of the subsurface. The soil samples were analyzed through X-ray Powder Diffraction (XRPD), X-ray Fluorescence (XRF) and Inductively Coupled Plasma Optical Emission Spectroscopy (ICP-OES). XRPD identify the main mineralogical composition of the samples, while XRF and ICP-OES identify the chemical composition of the samples. To perform the ICP-OES analysis, the soil samples were previously treated with aqua-regia solution. This pre-treatment was done following a modified ISO 11466:1995 procedure for sample mineralization. Specifically, a gram of soil was treated with a solution composed of 2 ml of water, 2.5 ml of nitric acid (65% in volume) and 7.5 ml of Hydrochloric acid (37% in volume). The mixture of soil and "aqua regia" solution was warmed up to 120 °C for 10 minutes and kept constantly to the same temperature for other 15 minutes, through a controlled-temperature microwaves oven. After that, before the ICP-OES analysis, the mineralized sample was diluted up to 50 ml with a MilliQ water.

- Weekly groundwater monitoring and sampling of three piezometers (PZP 036, PZP 040 and PZP 041; Figure 1B), selected based on their location in the WAA (respectively in the Northern, Central, and Southern parts of the WAA). The purpose of more frequent geochemical analysis was to identify potential variation in As concentrations at a shorter timescale than those measurable through the ARPAV standard monitoring activities. The monitoring of these piezometers lasted between 6th December 2017 and 26th March 2018 (115 days). In addition, on the same three piezometers and in the same time interval, the potentiometric head was acquired with HOBO data loggers to evaluate the potentiometric head responses to recharge events.

The groundwater and soil dataset, gathered through the sampling activities, is provided in Table S1 and S2 of the supplementary materials

Data analysis

Self-Organizing Mapping (SOM)

Self-Organizing Mapping (SOM) is a machine-learning mapping technique based on unsupervised learning artificial neural networks (ANN) and vector quantization. Although SOM has been sometimes referred to as a "k-means clustering" method (Gersho, 1990; Gray and Neuhoff, 1998), the former is based on a distribution of input data items (sample vectors) by means of a finite set of representative weighted vectors (codebook vectors), spatially and

globally ordered (Kohonen, 2013, 2001, 1990). In contrast with other ANN methods, SOM is based on competitive learning, where nodes compete for the *right to respond* to a subset of the input data. SOM is particularly useful when exploring nonlinear correlations among parameters, which is typically the case of geochemical reactions. Detailed explanation of the theory and mathematical construction of SOM can be found in several books, technical documents and reviews (Kohonen, 2013; Obermayer and Sejnowski, 2001; Oja and Kaski, 1999; Simon et al., 2003; Tokutaka et al., 2007; Vesanto et al., 2000).

In SOM, artificial neural networks learn to cluster groups of similar input items from a high dimensional input space in a nonlinear fashion onto a low dimensional discrete lattice of neurons (Kohonen, 2013), for instance, using 2D mapping reflecting the initial toroidal topology of the input data. The basic idea is that simulated *neurons* located close to each other in the SOM's output layer have similar input items, whereas less similar neurons will be situated farther away from each other in the grid (Vesanto et al., 2000). Neurons are located on the nodes of the discrete lattice, which can be rectangular or hexagonal. A conceptual example of the basic structure of a SOM grid is shown in Figure 2. A Euclidean distance (*d*) between input and output nodes is calculated from the result of a *training*, which consists of moving the position of the "weight" vectors (codebook vectors) toward the input data, reducing a distance metric without spoiling the topology induced from the map space.

The results of some is a so-called U-matrix, which expressed the distribution of the *d* statistics over a neurons grid. In this grid, each cell represents a neuron with its associated weight vector, and these cells are colored as function of the average distance *d* between the neuron's weight vector and neighboring neurons. The U-matrix allows to highlight the similarities and the dissimilarities between the input samples. Referring the U-matrix distribution to a specific variable of the input dataset, it is possible to map the samples with respect to the value (high and low) of the interested variable. In this way, correlation of variables is done comparing pairs of SOM maps as follows: the more similar the maps' color patterns, the more directly correlated two variables are. The more opposite the color distribution is, the more inversely correlated two variables are. To quantify the correlation among SOM-generated maps, the well-known Spearman's correlation coefficient, ρ, was adopted. This approach results in $\rho \rightarrow 0$ for uncorrelated variables and $\rho \rightarrow \pm 1$ for positively (+) or negatively (-) correlated variables.

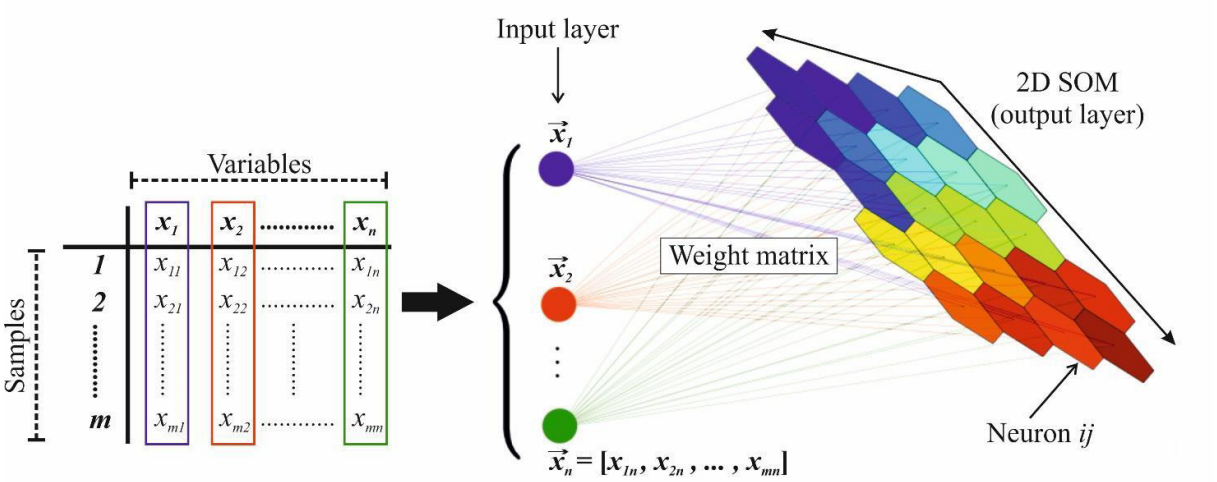

Figure 2 - Basic structure of a 2D SOM with m x n output layer (neuron grid). The input layer represents the item vectors (samples), which will be fitted by the SOM model to create the output organized-map.

In this work, SOM maps were generated for 28 of the groundwater data reported in Table S1 (supplementary materials), obtained during the sampling surveys. We excluded the variables with all values below the limit of quantification (LOQ). For each variable, SOM analysis began with an initial statistical data pretreatment and the selection of an accurate iterative training. Before applying the SOM algorithm, both the removal of missing data and the evaluation of the number of censored values (i.e. values below the LOQ) for chemicals was performed (Davis, 2002). Even though the SOM algorithm is able to manage missing data through model-based reconstruction, this procedure was discarded to avoid error propagation during the SOM analysis. The censored data were considered only when they constituted less than 30% of the total number of values for each given variable. In that case, half of each variable's LOQ was assigned to them. After those modifications, a scaling and centering process was applied (Kohonen et al., 1996; Vesanto et al., 2000). These transformations, which normalized the dataset, are necessary to avoid giving more weight to extreme values than to the other values (Kalteh et al., 2008; Zhang et al., 2009). In the training, the number of times (iterations) that the neural network sees the dataset should be at least 500 times the number of neurons in the output layer (Haykin and Simon, 1994; Kalteh et al., 2008; Kohonen, 2001). Each time that the algorithm explores the dataset, it is able to reduce the distances between the vectors that represent the experimental items and the codebook vectors. During this recursive process, the SOM algorithm attempts to reduce the distance (or "error") associated with the model fit to the within-structure of the dataset. This error is known as the "quantization error" (Q_E) and is a measure of the average distance between the input data vectors and the map nodes (codebook vector) to which they are mapped, with smaller values indicating a better fit (Fraser and

Dickson, 2007). The specific SOM algorithm used in this work is the one implemented within the R environment (R Core Team, 2018) through the Kohonen package (Wehrens, 2007; Wehrens and Kruisselbrink, 2018). This algorithm provides a versatile manner of data input and output organization (as gridded data) and is computationally efficient when dealing with a large number of input variables, as in this study.

PHREEQC modeling

PHREEQC is a well-known and widely adopted multicomponent geochemical modeling tool that can simulate the majority of processes typically linked to the mobility of arsenic in alluvial or fractured aquifers (e.g., reductive dissolution of ferric hydroxides, oxidation of arsenopyrite, and oxidation of organic matter). Table S3 (supplementary materials) summarizes the key equations adopted for this analysis, with corresponding equilibrium constants (k_{eq}) at 25°C, which are based on the thermodynamic database WATEQ4F (Ball and Nordstrom, 1991). In PHREEQC, reactions evolving slowly over the time, often far from equilibrium, can be described through different types of nonlinear kinetics laws. An important kinetic reaction for As mobility is organic matter degradation, which controls the redox condition of the system and can be generally modeled as a Monod kinetics rate (Monod, 1949) describing the degradation of organic matter via aerobic respiration, for instance, as

$$\frac{d[S]}{dt} = R_{Monod} = -k_{max}\frac{[S]}{k_{\frac{1}{2}} + [S]}$$

where S is the concentration of the organic substrate (mol/L) utilized by the microbes for the degradation process, t is the time (s), k_{max} is the maximal rate (mol/L/s), and $k_{1/2}$ is the half-saturation constant (mol/L). Specifically, in this work, this reaction was applied as an additive Monod kinetics model, which considers the concentration of the main terminal electron acceptors (TEAs) in the system (Appelo and Postma, 2005). This model can be expressed as follows:

$$\frac{d[S_{SOC}]}{dt} = -c * [S_{SOC}] * r_{TEAPs}$$

with

$$r_{TEAPs} = \left(\frac{[O_2]}{k_{\frac{1}{2}O_2} + [O_2]} + \frac{[Fe(OH)_3]}{k_{\frac{1}{2}Fe(OH)_3} + [Fe(OH)_3]} + \frac{[NO_3^-]}{k_{\frac{1}{2}NO_3^-} + [NO_3^-]} + \frac{[SO_4^{2-}]}{k_{\frac{1}{2}SO_4^{2-}} + [SO_4^{2-}]} \right)$$

where $[S_{SOC}]$ is the concentration of the organic carbon substrate in the sediment, c is a constant for a first order reaction, and r_{TEAs} represents the electron exchange rate between the oxidants (O_2, $Fe(OH)_3$, NO_3^- and SO_4^{2-}) and the reductant, organic matter (SOC).

PHREEQC can resolve multiphase geochemical reactions, for instance, when gas, water and solids coexist within a representative continuum. The presence of gaseous phases can be important for As release, for instance, if oxygen is present as a regulator of redox conditions. Unlike other codes (Mayer et al., 2002), gas transport in the unsaturated zone is not mechanistically simulated by PHREEQC. As such, either gas transport is implemented through external routines, e.g., using PHREEQCI, (Charlton and Parkhurst, 2011), requiring however a benchmark analysis against known codes, or gas molecules can be added non-mechanistically to a defined reaction. The latter approach can be taken for instance, using the PHREEQC function REACTION under incremental stepwise mode, which reproduces a transient ingress of $O_{2(g)}$ or any other gas molecule. The REACTION function was used in this work to simulate the O_2 ingress linked to recharge events, in order to evaluate its effect on redox potential variation and thus on arsenic mobility.

PHREEQC embeds a variety of surface complexation models (SCMs) that can explicitly consider the electrostatic processes occurring at the molecular scale and that are responsible for the sorption/desorption of both metals and metalloids, including As (Biswas et al., 2014; Jessen et al., 2012; Rawson et al., 2016; Stollenwerk et al., 2007). Although some limitations apply (Rathi et al., 2017), SCMs provide a process-based quantification of As adsorption behavior as a function of the dissolved As concentration and speciation and the solution pH. SCMs also consider the influence of competing ions such as phosphate or bicarbonate as well as the density of adsorption sites on the host minerals, such as Fe-oxides (Rathi et al., 2017). This work adopts a set of surface complexation reactions for arsenic as As(III) and As(V) based on the surface sorption sites defined for HFOs (the primary expected sorption sites for As) in the WATEQ4F database (Table S3, supplementary materials) based on the work by Dzombak and Morel (1990).

Results and discussion

Data exploratory analysis

A summary of the results obtained from the experimental campaigns by ARPAV is provided in Table 1. Recalling that the dataset combines information collected over 115 days from eight piezometers, the statistics of certain parameters and the concentrations of compounds provide initial key elements associated with the geochemical behavior of the system. Mean As concentrations are nearly 10 µg/L, the WHO recommended drinking water concentration threshold. A maximum concentration of 45 µg/L has also been found, indicating the importance of As assessment in the study area. The ORP was found to vary between fairly negative values (-178 mV) and nearly zero. Over time, the aquifers display a variable redox status, from slightly reducing conditions to oxidizing conditions (Figure 3). Water pH is at circumneutral conditions, which is typically the case for the calcite-rich shallow aquifers of the alluvial plains of Northern Italy (Rotiroti et al., 2014). Since As is highly mobile under circumneutral conditions (pH = 6 – 8; Smedley and Kinniburgh, 2013), small variations in pH should not substantially affect As mobility in the studied area.

Table 1 - Summary table of the WAA dataset. The column "head" represents the hydraulic head.

	m a.s.l.	*°C*	*°C*	*mbar*		*mV*	*mg/L*	*µS/cm*	*ppt*	*mg/L*	*mg/L*	*mg/L*	*mg/L*	*mg/L*
	head	**T_air**	**T_gw**	**P_atm**	**pH**	**ORP**	**DO**	**EC**	**SAL**	**HCO3**	**NH4**	**PO4**	**SO4**	**F**
Min	-1.28	-0.60	11.20	998.90	6.68	-173.70	0.09	734.00	0.41	475.00	0.04	0.02	0.50	0.10
1st_Q	-1.03	5.83	12.93	1010.20	6.88	-102.62	0.13	876.80	0.49	522.40	0.14	0.02	20.50	0.18
Median	0.23	8.15	13.95	1018.80	6.95	-84.70	0.17	881.50	0.49	543.40	0.46	0.02	42.00	0.20
Mean	-0.14	9.39	13.66	1019.10	6.96	-83.35	0.26	947.70	0.53	553.70	1.04	0.05	66.61	0.28
3rd_Q	0.44	10.45	14.20	1028.80	7.01	-55.15	0.26	887.50	0.50	565.40	2.07	0.07	73.75	0.29
Max	0.85	23.90	17.00	1035.00	7.23	0.90	1.12	2481.00	1.45	827.00	3.73	0.34	1125.00	1.60
	mg/L	*mg/L*	*mg/L*	*mg/L*	*mg/L*	*mg/L*	*mg/L*	*mg/L*	*µg/L*	*µg/L*	*µg/L*	*µg/L*	*µg/L*	*µg/L*
	Cl	**Na**	**K**	**Mg**	**Ca**	**Si**	**TOC**	**TSS**	**Al**	**As**	**B**	**Cu**	**Fe**	**Mn**
Min	21.00	18.80	0.50	29.00	46.30	3.95	0.60	2.50	0.50	0.50	8.00	0.50	75.00	109.00
1st_Q	24.00	19.73	0.80	34.20	113.80	5.07	1.10	5.00	1.00	2.25	14.25	0.50	487.50	129.00
Median	33.50	26.50	2.00	36.75	123.00	6.81	1.45	9.00	1.00	11.00	64.50	0.50	1248.50	160.00
Mean	36.66	30.78	1.90	43.27	123.40	6.91	1.98	189.60	1.17	11.33	61.50	0.86	1232.00	183.90
3rd_Q	43.00	29.73	2.30	46.95	137.60	8.44	2.70	30.00	1.00	14.75	82.75	1.00	1800.20	198.20
Max	135.00	151.60	7.20	140.80	294.00	10.41	5.90	5925.00	3.00	45.00	266.00	3.00	3222.00	696.00

Figure 3 shows the time series of the measured variation in As and Fe concentrations, potentiometric head and ORP in the three piezometers selected for weekly sampling and monitoring. From an initial qualitative visual assessment of the results, the preliminary ingredients of the conceptual model of As mobility can be inferred. The relationship between

redox conditions and As and Fe concentrations is a key aspect to highlight. Redox conditions are known to control As mobility in both alluvial and fractured aquifers (Ayotte et al., 2015; Mango and Ryan, 2015; Pedretti et al., 2019; Smedley and Kinniburgh, 2013). In iron-rich environments, As tends to adsorb onto hydro ferric oxides (HFOs), which are precipitated during oxidizing conditions and to desorb from HFOs when these oxides dissolve during reducing conditions (Appelo and Postma, 2005). The WAA shows hydrogeological and hydrogeochemical similarities with the alluvial and deltaic aquifers of the Bengal Basin (Kinniburgh and Smedley, 2001), the Mekong Valley and Red River aquifers in Vietnam (Berg et al., 2007; Postma et al., 2007) and the sites in Northern China or Cambodia (Richards et al., 2019), where the reductive dissolution of HFOs has been identified as a primary geochemical process linked to high As concentrations in the groundwater. In the three piezometers (PZP 36, 40 and 41), the trends in the analyzed variables seem to confirm that the reductive dissolution of HFOs may actually be occurring in the studied area, leading to the hypothesis that the fluctuations of ORP in the shallow aquifer could be a key aspect controlling the mobility of As in the VAP.

Sulfide-bearing sediments, which are often assumed to be a source or a sink of As in alluvial aquifers (Carraro et al., 2015; Saunders et al., 2008), are not expected to be predominant in this part of aquifer. While pyrite and other sulfides have been identified by mineralogical analyses on solid samples, the maximum concentrations of sulphate during high ORP stages are far below the expected values when pyrite oxidation occurs, suggesting that the oxidation of As-bearing sediment may not be a primary actor explaining the occurrence of As in the aquifer. These results are in accordance, for instance, with the observations by Harvey et al. (2002) in a Bangladesh site.

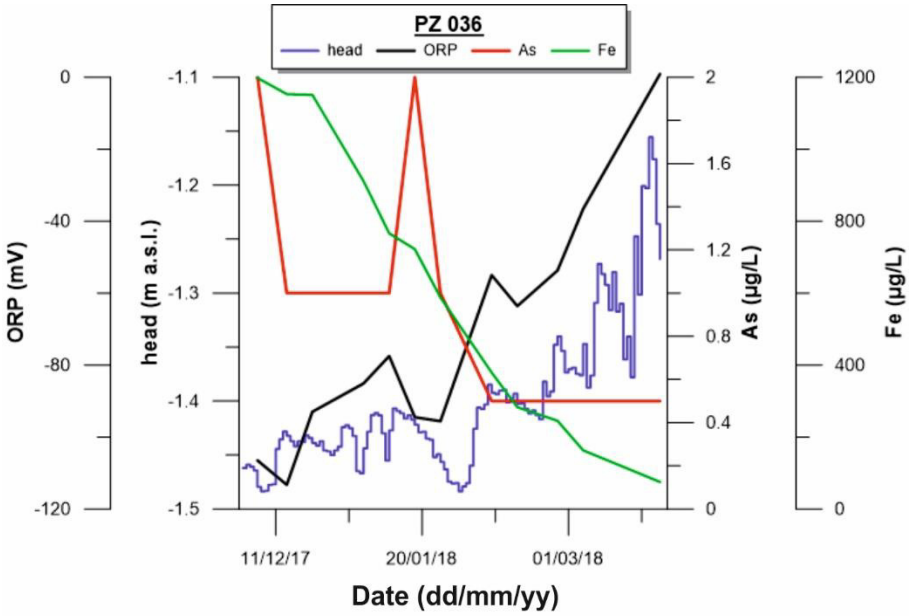
PZ 036
head
ORP
As
Fe
ORP (mV)
head (m a.s.l.)
As (µg/L)
Fe (µg/L)
0
-40
-80
-120
-1.1
-1.2
-1.3
-1.4
-1.5
2
1.6
1.2
0.8
0.4
0
1200
800
400
0
11/12/17
20/01/18
01/03/18
Date (dd/mm/yy)

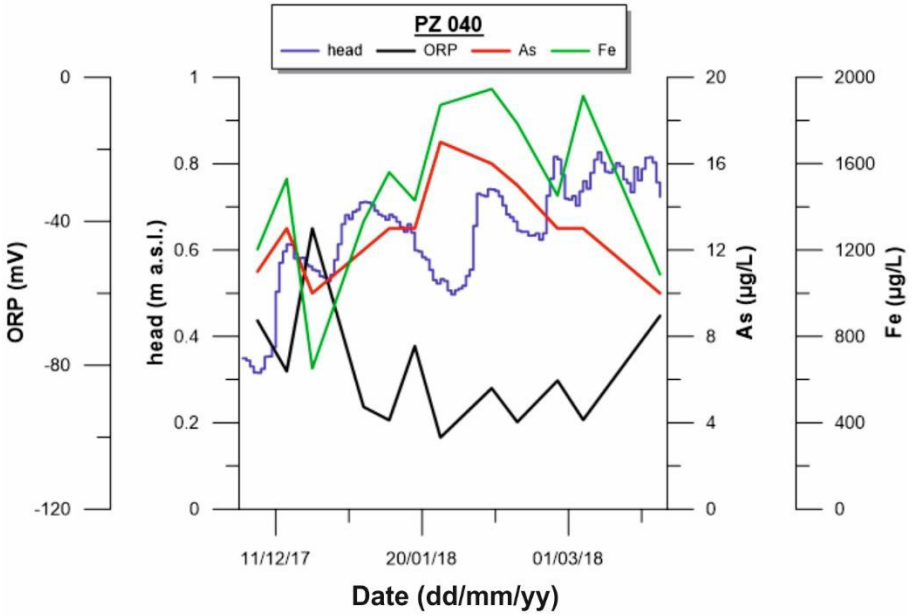
PZ 040
head
ORP
As
Fe
ORP (mV)
head (m a.s.l.)
As (µg/L)
Fe (µg/L)
0
-40
-80
-120
1
0.8
0.6
0.4
0.2
0
20
16
12
8
4
0
2000
1600
1200
800
400
0
11/12/17
20/01/18
01/03/18
Date (dd/mm/yy)

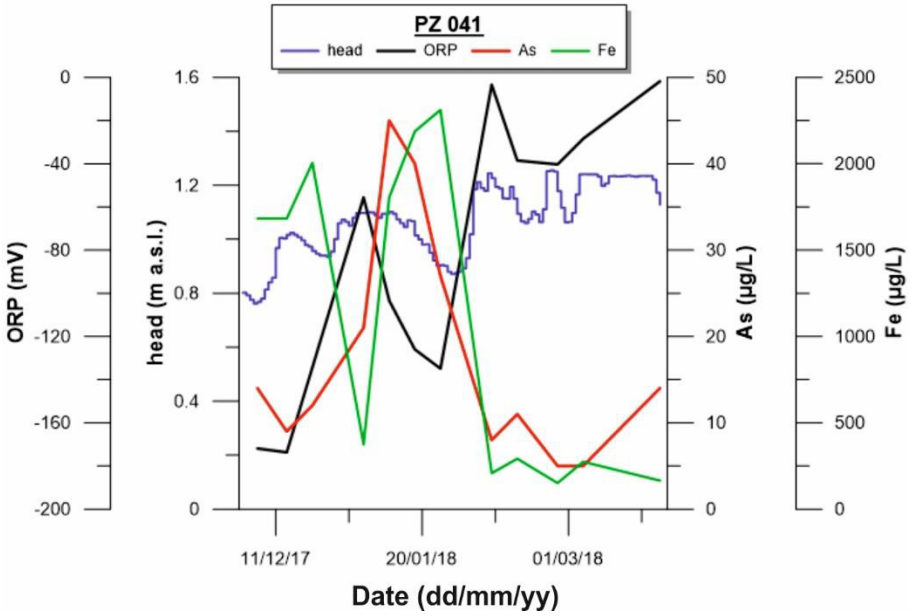
PZ 041
head
ORP
As
Fe
ORP (mV)
head (m a.s.l.)
As (µg/L)
Fe (µg/L)
0
-40
-80
-120
-160
-200
1.6
1.2
0.8
0.4
0
50
40
30
20
10
0
2500
2000
1500
1000
500
0
11/12/17
20/01/18
01/03/18
Date (dd/mm/yy)

Figure 3 - Time series of measured variations of potentiometric head (head), oxy-reduction potential (ORP) and arsenic (As) and iron (Fe) concentrations for the three piezometers monitored weekly, PZP 036, 040 and 041, which embody the physical and chemical behavior of the Northern, Central and Southern parts of the WAA respectively.

The application of SOM helps to obtain a more quantitative estimation of the nonlinear correlation among all the variables and in particular to cluster variables with more affinity from the others. The ANN was trained for 25000 iterations (i.e., 500 times more that the recommended minimum amount). Figure 4 shows the efficiency of the training process over the iterations. The training process reaches a plateau after 20000 iterations at approximately 0.02, suggesting that the neural network obtained the best fit for the experimental vectors.

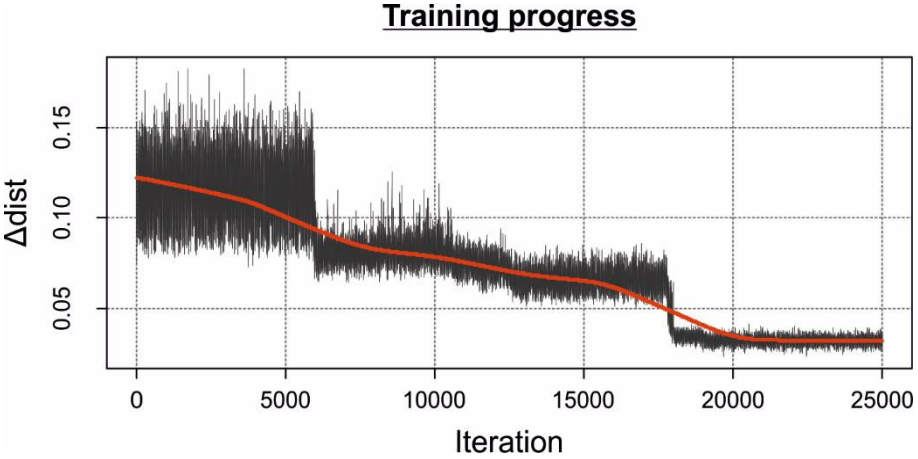

Figure 4 – Progress of the training process of the SOM neural network. The Y-axis shows the variation in the average distance between the closest codebook vector and the sample vectors (input). The red line represents the LOWESS curve coming from LOWESS regression tool (Cleveland, 1981, 1979). The LOWESS curve highlights when the training process stabilizes itself.

In other words, the average distance between the codebook and experimental vectors was no longer changing. A Q_E = 1.44 was found, which is an acceptable error below the recommended error thresholds. The maps resulting from the use of SOM analysis for each individual variable of the experimental database are shown in Figure 5. A normalization was applied to each map to rescale the *d* values for each hexagonal cell, to highlight more clearly similarities and dissimilarities among the variables. The visual analysis of Figure 5 helps to recognize important relations between As and other variables. The Spearman's correlation analysis allows a more quantitative assessment of the most meaningful visual correlations. The resulting correlation coefficients ρ are reported within each box in Figure 5.

The As SOM map shows lower values in the left and bottom parts of the map than in the top and right parts of it and higher values in the mid-right position. The arsenic map is used as a

reference for evaluating the correlation between the As concentration and other variables. The maps of NH_4 and Fe show similar color patterns and results respectively of ρ=0.58 and ρ=0.66 when correlated with As, suggesting that As is directly related to these elements. Low ORP values are probably controlled by the degradation of organic matter concentrated within peat horizons and dispersed in other sediments, a process that has been already hypothesized to be associated with dissolved As concentrations in other Italian aquifers (Carraro et al., 2015, 2013; Rotiroti et al., 2014) and elsewhere in the world (McArthur et al., 2001) and is likely the cause of reduced conditions. The correlation of NH_4^+ and TOC concentrations (ρ = 0.55, visible from comparison of their SOM maps) supports the degradation of organic matter and its role as redox driver in the system. The degradation of organic components may thus be involved in the control of the redox conditions of the subsurface, which favors the dissolution of HFOs.

In the VAP, potentiometric head changes are mainly driven by rainfall-driven recharge (Beretta and Terrenghi, 2017), which typically occur from October to May and occasionally from June to September. Recharge could drive the ingress of oxidants into the aquifer, which would explain the progressive increase in ORP within the aquifer as the experimental time elapses (Figure 3 – PZP 36 and PZP 41). Nonetheless, it is likely influenced by the heterogeneity of soil permeability of the study area, which would limit the rate of infiltration toward the aquifer leading to more reduced condition. The As map is also positively correlated with Cl (ρ=0.54), which is a conservative element that can also be introduced into the system during recharge events (e.g., salts accumulating on the surface and quickly leached into the aquifer during rainfall events)

Maps of TOC and SO_4 also show similar patterns compared to the As map, corresponding correlation coefficients of ρ = 0.3 and ρ = -0.71. TOC is expected to be more abundant under reducing conditions (low ORP). Indeed, the ORP maps are negatively correlated with As (ρ = -0.42), confirming that the degradation of the organic matter (peat) could be an important driver of reducing conditions in the system and thus an important mechanism to consider in the geochemical model. The inverse correlation between As and sulphates confirms the decoupled geochemistry of As and S under oscillatory redox conditions. A poor correlation was found between the As and pH SOM maps, consistent with the low variation of pH in the systems, corroborating that pH conditions are not expected to affect the mobility of As in the studied area.

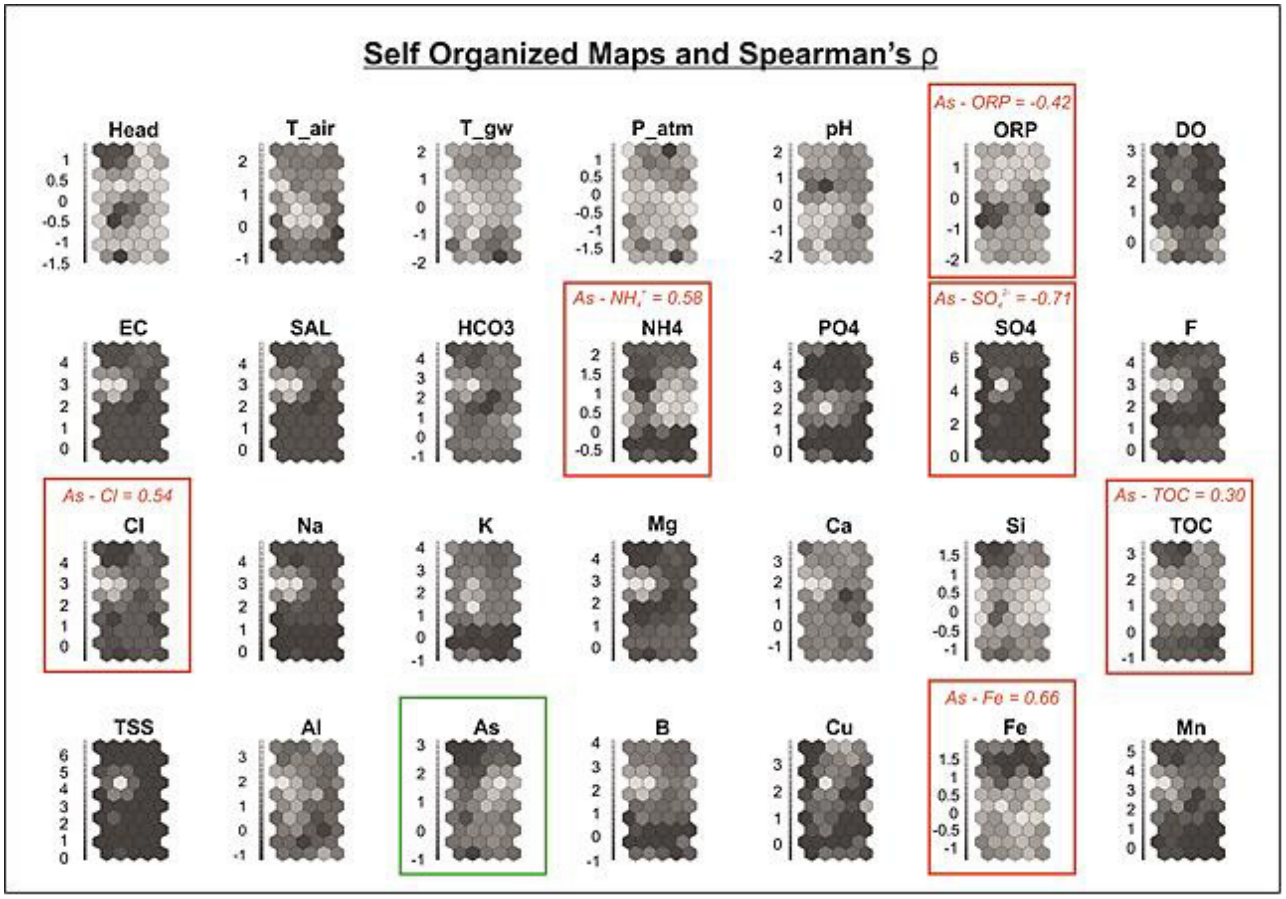

Figure 5 - Self organized maps for each input variable. The vector space of the SOM is represented through a toroidal lattice (5x10) made of hexagonal cells. The maps show the normalized values of variables with a grayscale. The dark colors represent lower values and the light colors higher values. The green box highlights the SOM pattern of arsenic, whereas the red boxes plus the respective Spearman's rho value emphasizes the chemicals involved in the described relationships with arsenic.

Conceptual model

The results of the visual assessment of the time series and the correlation evidenced by the SOM analysis provide the basis to propose a conceptual model explaining the mobility of As in the study area. The key elements to highlight are:

a) Similar to well-studied young aquifers of Southeast Asia and elsewhere in the world, the reductive dissolution of iron hydro-oxides (HFOs) could be the most likely process controlling As mobility in the VAP.

b) Degradation of organic matter has a key role in determining reduced conditions. Consistent with other parts of Northern Italy, peat layers are common in distal alluvial environments. In the VAP, the hypothesis of degradation of peat layers is reinforced by the relationship

between As, NH_4 and TOC concentrations. A progressive increase in ORP occurs as the potentiometric heads increase. At the beginning of the rainy season, the shallower aquifer of the WAA shows a reduced environment with ORP values between -150 mV and -50 mV. With time, some piezometers show an increase in ORP toward oxidized condition (~ 3 mV) after the beginning of the rainy season.

c) Sulfide oxidation has a poor influence on the release of As. While oxidants enter the aquifer during the rainy season, the experimental analysis suggests that sulfide oxidation is unlikely to occur in the system, and thus this mechanism is supposed to be influencing As less than is the redox control of As-bearing HFOs.

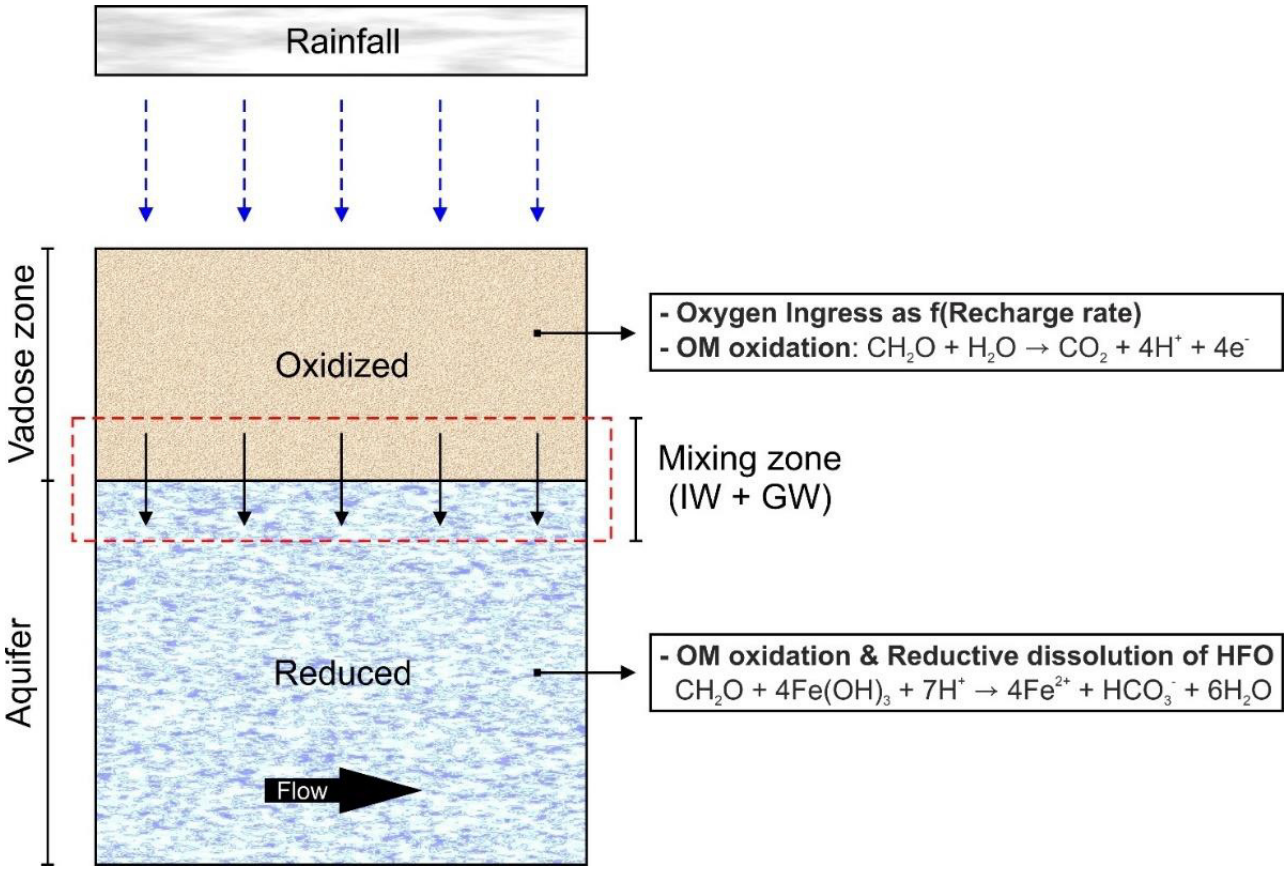

Figure 6 - Conceptual model that explains the main processes able to control arsenic mobility in the WAA groundwater.

Based on the aspects presented above, a possible hydrochemical conceptual model explaining the mobility of As in the studied area is depicted in Figure 6 and explained as follows:

a) At a given initial time prior to the beginning of the rainy season, the aquifer is under reducing conditions (Initial time of ORP time series in Figure 3). This redox status is likely due to the degradation of organic matter found in the studied area and in the VAP as peaty

materials or dispersed in other sediment types (Carraro et al., 2015). In a reduced system, iron is mobile, and Fe-bearing minerals are dissolved, resulting in high mobility of As. The difference in As concentrations observed in the sampled piezometers may be due to the heterogeneous abundance of the local As source (e.g., variability in the abundance of previously existing As-bearing HFOs prior to dissolution).

b) As precipitation occurs, the aquifer is recharged (potentiometric head rises). During recharge, oxidizing species (e.g., oxygen and sulphate) enter the aquifer, ORP increases, and iron is precipitated forming, among other minerals, highly reactive HFOs, on which As is adsorbed and immobilized. The ingress of oxidizing species may be progressive, as observed by the smooth decrease in As concentration and increase in ORP, probably linked to the transient aquifer recharge driven by precipitation events of different intensities.

Arsenic concentrations are therefore assumed to be controlled directly by aquifer recharge. To test this hypothesis, it is important to assess how oxidizing species enter the aquifer during the rainfall-controlled recharge stages. Three main processes related to the ingress of oxidizing conditions are hypothesized to occur in the VAP:

a) transport of $O_{2(aq)}$ and SO_4 by infiltration of oxidized rainfall water;

b) diffusion of $O_{2(g)}$ from the ground;

c) transport of trapped $O_{2(g)}$ and $O_{2(aq)}$ in the vadose zone being "pushed" downward by the propagation of the wetting front.

The gas transport modality of the third case (c) was already proposed by others (Healy and Cook, 2002) and is motivated by the empirical relation between potentiometric head and As concentration (Figure 3 for PZP 036). Because potentiometric head in the area is expected to be driven by rainfall-driven recharge (Beretta and Terrenghi, 2017), rainfall events could be the key triggers of oxidizing conditions in the system, creating a series of pulses that determine a progressive increase in ORP and a subsequent reduction in Fe and, in turn, As.

Model-based verification

To verify the validity of the postulated processes controlling As mobility and to assess which transport modality dominates the redox conditions, a reactive transport model using PHREEQC

was developed. The basic idea was to reproduce the time series of the three weekly monitored piezometers (PZP 036, PZP 040, and PZP 041) by simulating three scenarios corresponding to the three transport mechanisms of oxidizing compounds (a, b and c) described above. A simplified geochemical setup has been chosen explicitly to reduce the model complexity compared to reality and to maximize the interpretation of the processes. The selected geochemical systems maintain all the hypothesized expected dominant factors linked to As mobility as controlled by reductive dissolution of HFOs.

Initially, the aquifer is simulated under reducing conditions. The first day corresponds to 6th December 2017. The simulated time is 115 days, covering the entire experimental monitoring activities with progressively increasing oxidizing conditions (Figure 3). The initial mineralogical phases were estimated from the experimental characterization of the solid matrix and the general knowledge of the system from previous studies (ARPAV, 2014). The simulated minerals in the aquifer were calcite, organic matter (OM) and ferrihydrite. The input parameters of the model are reported in Table 2. Calcite and ferrihydrite were assumed to be in equilibrium in the system, while OM had kinetic rates far from equilibrium (Nordstrom and Campbell, 2013) and was simulated as a rate-limited degradation process following Monod kinetic law (Section 2). An initial sensitivity analysis (not reported) was performed to find suitable OM kinetic rates that enable ORP reduction according to the observed results during the monitoring time (115 days), based on scenario (c) reported below.

Table 2 - Chemical composition of both groundwater samples and rainfall used as input for the geochemical model.

Parameter	**PZP 036**	**PZP 040**	**PZP 041**	**Rainfall (Pieri et al., 2012)**
T [°C]	14.200	15.000	14.300	14.2
pH	7.220	7.140	7.100	6.55
pe	-1.870	-1.180	-3.010	4 (function of O_2 atm)
Chemicals	*[mg/L]*	*[mg/L]*	*[mg/L]*	*[µmol/L]*
Al	0.001	0.002	0.001	\
Alkalinity (as HCO_3^-)	533.600	555.600	572.700	\
As	0.002	0.011	0.014	\
B	0.083	0.013	0.077	\
Ca	136.700	123.700	117.900	105.22
Cl	23.000	32.000	45.000	63.3
F	0.180	0.280	0.160	\
Fe	1.198	1.203	1.682	\
H(1)	\	\	\	0.3
Mg	33.700	46.000	34.900	37.95
Mn	0.160	0.139	0.194	\
N(+5)	\	\	\	62.25
N(-3)	0.770	0.150	3.730	\
Na	27.800	18.800	31.700	97.8
P	0.030	0.015	0.030	\
S(6)	80.000	24.000	17.000	41.95
Si	5.190	7.330	10.410	\

Keeping an identical reference model setup, three scenarios (a, b, c) were generated as follows. In scenario (a), ingress of oxidizing species was assumed to be solely controlled by aquifer recharge, without any further contribution of gaseous phases. Dissolved oxygen $O_{2(aq)}$ was assumed to be in equilibrium with atmospheric gas composition at the ground level. A typical composition of rainfall for the study area was considered (Table 3). Using the function MIX in PHREEQC, the proportion of infiltration and native groundwater was fixed through trial-and-error. The assumption considers that during a recharge event, the groundwater in this model remains composed mainly of the native groundwater in the system, with only a few % of the newly infiltrating waters. An initial 94:6 ratio between native and infiltrating water was assumed for each model, similar to the estimate 6% of groundwater recharge found by Beretta and Terrenghi (2017) for the WAA. In scenario (b), a steady ingress of $O_{2(g)}$ was simulated using the REACTION function. Oxygen gas molecules at a partial pressure of 0.21 atm entered the aquifer without rate-limiting effects, simulating a perfect connection between the atmosphere and the aquifer. In scenario (c), rainfall-controlled transient ingress of $O_{2(g)}$ and $O_{2(aq)}$ were

simulated. Using the step-by-step function REACTION in PHREEQC, a specific number of moles of oxygen for each discretized time step of the simulation were added. This amount of oxygen was calibrated manually (trial and error) to best-fit the observed ORP. This third scenario is the one that more closely represents the influence of rainfall-controlled recharge conditions on the redox response of the aquifer. The results of PZP 036 were used for the description of the analysis, while the comparison of results among piezometers is provided in the following section. From Figure 7 (black dashed line), it is possible to observe that without the explicit simulation of gas transport, the simulated ORP remained at steady negative values; i.e., the system was under reducing conditions for the entire simulated time. The model outputs underestimated the observed ORP, suggesting that the ingress of oxidizing species in dissolved form without the presence of gaseous phases is not enough to progressively increase the ORP to oxidizing conditions, likely due to the limited solubility of oxygen in water, which is quickly consumed by the OM. Analyzing Figure 7 (blue dashed line), the steady ingress of $O_{2(g)}$ with perfect equilibrium with the atmosphere increases the ORP with time, with final oxidizing conditions exceeding the observed values. The model was insensitive to different OM kinetic rates, likely because a constant number of oxygen molecules was added for each simulated time step, resulting in a linearly increasing trend of ORP. Figure 7 (red line) shows that a transient increase in $O_{2(g)}$ based on a best-fitted function, shown in Figure 8, results in a much better fit to the observed data than the previous scenarios (a and b). The shape of the resulting function, with values ranging 10^{-3} -10^{-5} mol/L, is consistent with the observed precipitation events in the study area, corroborating the hypothesis that recharge events are strongly linked to As mobility. In particular, pulses of oxygen entering the aquifers cause increasing amounts of Fe to precipitate in the form of HFOs, onto which As is adsorbed.

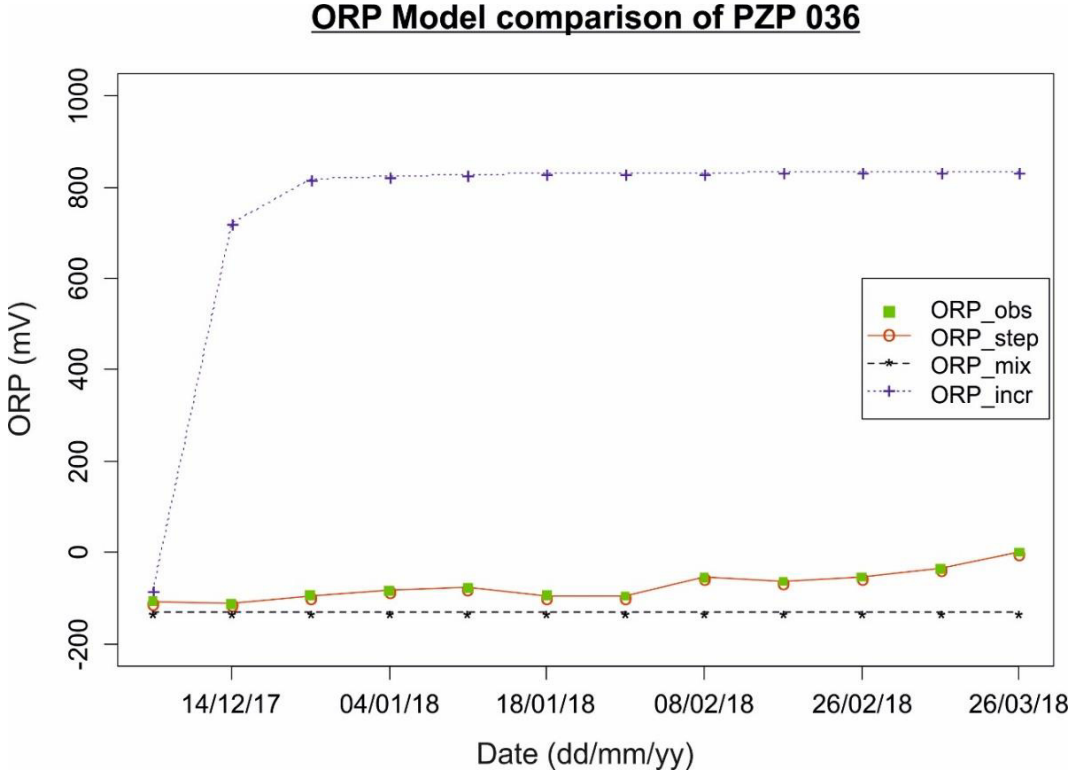

Figure 7 – Comparison among the Eh models obtained from the three described scenarios, a, b and c, for PZP 036, which was used as an example of the effect of the different settings. The black dashed, blue dashed and red lines refer to scenarios a, b and c, respectively.

In summary, an important conclusion is that aquifer recharge could be a key control of the As in the studied WAA area. This result could have multiple implications for decision makers as it indicates that As is controlled by the hydraulic response of the aquifer. An hydrological control of As mobility agrees with previous studies focusing on young sedimentary aquifers in Southeast Asia (Acharyya et al., 1999; Harvey et al., 2006; Michael and Khan, 2016; Postma et al., 2007; Richards et al., 2019). One aspect that requires further investigation is how crop irrigation could affect natural recharge. The VAP aquifers are affected by irrigation during the dry season. Irrigation-related processes could also have other implications for As mobility. In a Bangladesh site, Harvey et al. (2006) indicated that irrigation water tends to pond over the low-permeable layers, thereby changing both the hydrologic budget and the biogeochemistry of recharge water. Although our study lacks sufficient data to quantify the influence of irrigation on aquifer recharge, irrigation is not expected to be a fundamental trigger of As mobility in the VAP at least for what concerns sulfide oxidation, as postulated for instance by Acharyya et al. (1999). Indeed, sulfide oxidation is not expected to be a main As trigger in the studied area.

Implication of aquifer heterogeneity and model limitations

Using an identical modeling approach, the setup of the model adopted for PZP 036 was applied to reproduce the experimental results from the other two piezometers with weekly geochemical monitoring, PZP 040 and PZP 041. By comparing the model outputs and the resulting fitted functions, resulting deviation can be noted and discussed that could be related to local processes affecting the release of As in different parts of the site and related to its heterogeneity.

The results for PZP 036, located in the central zone of the WAA (Figure 8), suggest that few sources of As may be present in the proximity of this piezometer, given that As concentrations range between 1 and 3 μg/L when the aquifer is under reducing conditions. Along the central part of the WAA, the top layer is principally formed of sandy silt of limited thickness compared with that of the other locations (see supplementary materials Figure S4). According to our conceptual model, the aquifer requires an ingress of oxygen during recharge events to increase the redox potential to oxidizing conditions. To receive some rainfall-driven recharge over short time scales, the aquifer should behave hydraulically as a semiconfined system rather than as a confined aquifer, in contrast with previous hypotheses (ARPAV, 2011).

The results from PZP 040 (Figure 8), located in the northern part of the site, display a different behavior compared to PZP 036. At the beginning of the experimental activity, the As concentration ranged between 12 μg/L and 20 μg/L. These values are higher than those found near PZP36, representative of the central zone of the WAA, and exceed the WHO recommended threshold. In contrast with PZP 036, throughout the monitoring period, PZP 040 shows a generally stable trend in ORP between -40 and -100 mV, with a slightly decrease in the central part of the time series. According to our conceptual model, this behavior should be linked to a lower effective recharge of oxidizing waters within the aquifer near PZPZ40. Indeed, the amount of oxygen in the REACTION function required to fit the observed ORP data is approximately 10^{-5} mol/L, i.e., approximately one order of magnitude lower than the amount of oxygen required to fit PZP 036. This observation is consistent with the different stratigraphy of PZP040 compared to PZP36. Figure A (see supplementary material) shows a fine-grained layer topping the main aquifer that is thicker than the one observed at PZP 036. This thicker layer could significantly reduce aquifer recharge and the amounts of oxidizing species entering the aquifer. For instance, a delayed response was observed for ORP at PZP 040 compared with PZP 036 (of approximately 15 days) for identical rainfall events. PZP 040 possibly represents a more confined aquifer condition than around PZP 036, further supporting the hypothesis that recharge is a key factor controlling As mobility in the studied area.

The behavior of PZP 041 (Figure 8) is different from the other observed points and provides further support to corroborate the validity of the proposed conceptual model. At this piezometer, the highest As concentrations among the three points were found, with values exceeding 40 µg/L. Over time, an increasing trend in ORP similar to that at PZP 036 is observed. However, the increase is less smooth than at PZP036, showing well-defined peaks with a rapid increase and decrease in ORP. The amount of oxygen ingress needed to model these peaks is approximately 10^{-3} mol/L. The stratigraphy (supplementary materials Figure S4) shows a thick layer of clayish material on the top of the sequence, which should further limit natural recharge compared to PZP 040 and thus contrast with the conceptual model presented so far. It is however plausible that PZP 041 is strongly influenced by a quick external perturbation that unnaturally drives oxygen or oxidizing water directly in the system. This seems to be confirmed by the rapid response of the potentiometric head to rainfall events. While preferential flow could exist at the site, allowing rapid flow bypassing the clay layer, in situ visual observations of the piezometer during rainfall events suggest that water tended to pond around the PZP 041 wellhead, resulting in the direct flow of the surface runoff water into the piezometer. While this anomalous perturbation of PZP 041 renders it invalid to explore the natural aquifer response around this piezometer, the good match between the model and the observations at PZP 041 corroborates the hypothesis that the ingress of oxidizing species and the subsequent sequestration of As by HFOs precipitation could explain As mobility in the system, thus confirming the strong redox control on the fate of As in the studied area.

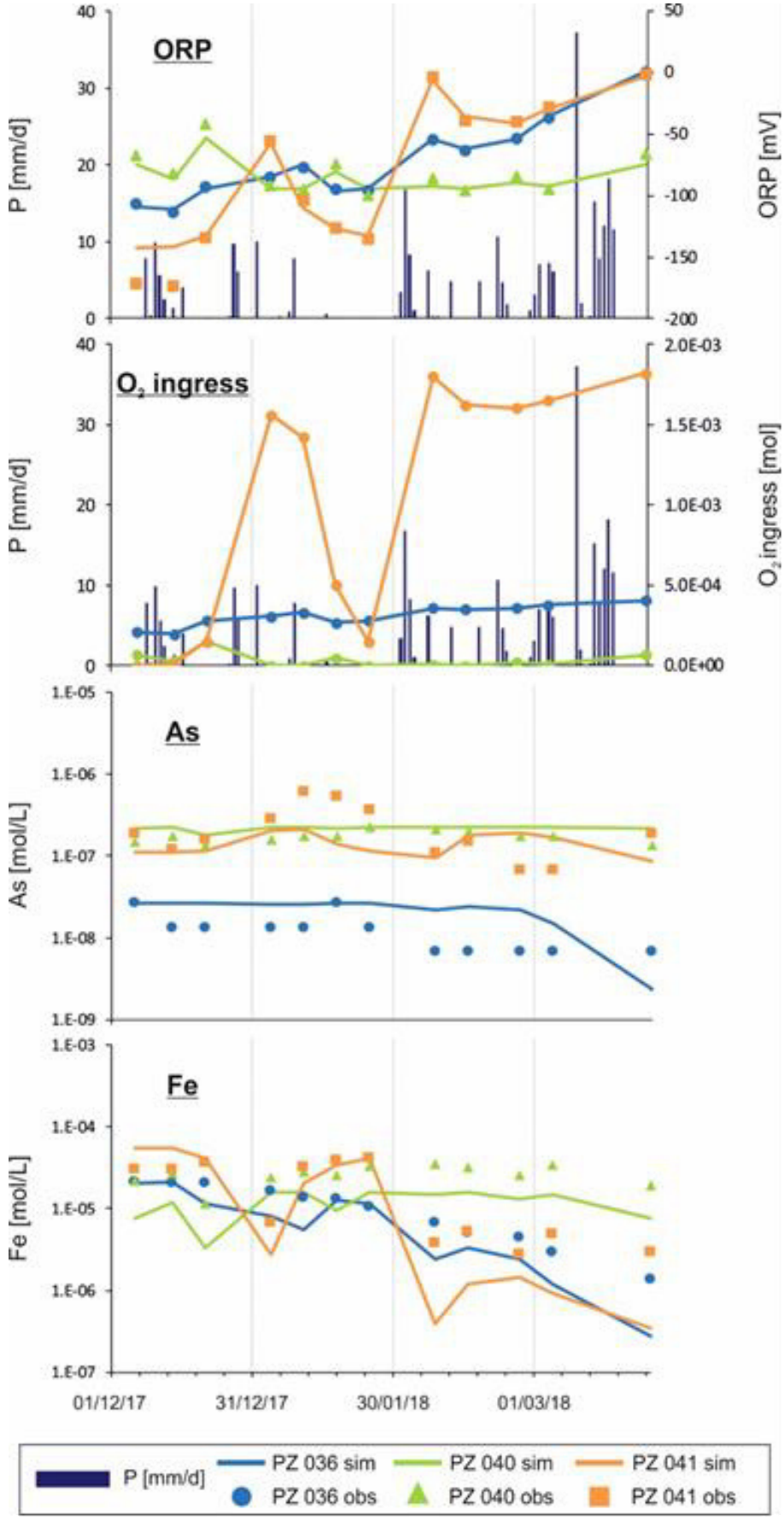

Figure 8 - Results of the batch-like model for PZ 036, 040, and 041. The first box from the top shows the comparison between the observed ORP trend (symbols) and the simulated trend (lines). The second box highlights the simulated

amount of O_2 (g) for reproducing the observed ORP and the correspondence with rainfall (P). The third and fourth boxes report the simulated concentrations of As and Fe (lines) with respect to the experimental values (symbols).

Notably, the model adopted in this work was expressly designed to capture and identify the processes that are more likely to explain the behavior of As at the site as proof of the reliability of the proposed conceptual model. The model has some limitations that hamper its use as a predictive tool to quantify the actual risk of As in the whole VAP. Primarily, the model is set up as batch-like reactor while a multidimensional, multicomponent reactive transport model (Prommer et al., 2003) represents a closer approximation to reality. In particular, such a multidimensional model should be able to evaluate the impact of the spatial variability of the key parameters, such as peat distribution and recharge rates, to quantify the magnitude of the As release more accurately. Such models are currently under development by the authors.

Conclusion

Excess As intake from groundwater consumption represents a major risk to human health in several countries in the world. Interpreting the dominant processes controlling As mobility can be complicated by the number of nonlinearly related variables and the presence of aquifer heterogeneities. This paper presents the results of an experimental and model-based analysis that aimed to evaluate the main processes controlling As mobility within the Western Agricultural Area (WAA), a small area within the Venetia Alluvial Plain in Italy, where As concentrations exceeding the WHO recommended thresholds have been measured.

Our analysis demonstrates that the interpretation of the key controls of As mobility in the WAA benefitted from the combined used of advanced exploratory analysis based on SOM (a machine learning-based model) and PHREQQC (a multicomponent reactive transport model). The use of SOM is particularly innovative for As mobility assessment in aquifer and allowed the evaluation of nonlinear relationships among the multiple variables emerging from a hydrogeological and geochemical assessment of the WAA. The PHREEQC model served to corroborate the validity of the model and to give preliminary semiquantitative indications of the magnitude of the processes controlling As mobility.

For what concerns As mobility in the WAA, the following main conclusions of this analysis were achieved:

a) According to the proposed conceptual model, redox-controlled reductive dissolution and precipitation of HFOs is the most likely and important process controlling As mobility in

the VAP. This is consistent with other studies evaluating geologically young alluvial deposits, such as in Southeast Asia or Northern China, and it is corroborated by the correlation between As and Fe concentrations and ORP.

b) Reduced conditions are likely controlled by organic matter and, in particular, the degradation of peat layers, sparsely found in the aquifer. Aquifer recharge is a key mechanism controlling redox conditions and in turn As mobility. The increase of potentiometric heads during rainfall events is positively correlated with the increase in ORP, showing similar pulse-like responses to rainfall events

c) Recharge drives oxidizing species to enter the aquifer, precipitating HFOs and, in turn, As. However, aquifer heterogeneities determine a distinct response of the different piezometers observed during the experiments. One piezometer (PZP 036), characterized by a reduced amount of fine-grained sediments at the top of the stratigraphic sequences, shows a more direct impact of recharge-driven oxidation than another piezometer (PZP 040) that is less sensitive to recharge and topped by a thicker fine-grained layer.

Acknowledgements

This study was conducted under a collaboration agreement between University of Padua and Veneto Region Environmental Protection Agency (ARPAV). The authors thank the ARPAV laboratories for the chemical analysis performed on groundwater and soil samples. Experimental data are available in the supporting information.

References

Aiuppa, A., D'Alessandro, W., Federico, C., Palumbo, B., Valenza, M., 2003. The aquatic geochemistry of arsenic in volcanic groundwaters from southern Italy. Appl. Geochemistry 18, 1283–1296. https://doi.org/10.1016/S0883-2927(03)00051-9

Anawar, H.M., Akai, J., Mostofa, K.M.G., Safiullah, S., Tareq, S.M., 2001. Arsenic poisoning in groundwater: Health risk and geochemical sources in Bangladesh. Environ. Int. 27, 597–604. https://doi.org/10.1016/S0160-4120(01)00116-7

APAT (2006) Handbook for environmental investigation upon con- taminated sites. Handbooks and guidelines (in Italian). I.G.E.R. srl, Roma.

APAT IRSA – CNR, 2003. Water analytical methods. Handbooks and guidelines (in Italian). I.G.E.R. srl, Roma.

ARPAV, 2011. INDAGINE AMBIENTALE "AREE AGRICOLE" - macroisola aree agricole – zona ovest, macroisola fusina – aree lungo naviglio brenta - sintesi dei risultati del piano di investigazione iniziale. Report data presentation.

ARPAV, 2014. ALiNa – Analysis of the Natural Background Level for Some Compounds Within the Groundwater of the Shallow Aquifer in the Drainage Basin to the Venice Lagoon (Brenta River Alluvial System) – Report and Data Presentation

Appelo, C.A.J., 1994. Postma. Geochemistry Groundw. Pollution, Rotterdamm.

Appelo, C.A.J., Postma, D., 2005. Geochemistry, groundwater and pollution. 2nd. Ed. Balkema, Rotterdam.

Ayotte, J.D., Belaval, M., Olson, S.A., Burow, K.R., Flanagan, S.M., Hinkle, S.R., Lindsey, B.D., 2015. Factors affecting temporal variability of arsenic in groundwater used for drinking water supply in the United States. Sci. Total Environ. 505, 1370–1379. https://doi.org/10.1016/J.SCITOTENV.2014.02.057

Ball, J.W., Nordstrom, D.K., 1991. User's manual for WATEQ4F, with revised thermodynamic data base and test cases for calculating speciation of major, trace, and redox elements in natural waters.

Beretta, G. P., Terrenghi, J., 2017. Groundwater flow in the Venice lagoon and remediation of the Porto Marghera industrial area (Italy). Hydrogeol. J. 25, 847–861. https://doi.org/10.1007/s10040-016-1517-5

Berg, M., Stengel, C., Trang, P.T.K., Hung Viet, P., Sampson, M.L., Leng, M., Samreth, S., Fredericks, D., 2007. Magnitude of arsenic pollution in the Mekong and Red River Deltas — Cambodia and Vietnam. Sci. Total Environ. 372, 413–425. https://doi.org/10.1016/J.SCITOTENV.2006.09.010

Bhattacharya, P., Hossain, M., Jacks, G., Ahmed, K., Hasan, M., von Brömssen, M., Frape, S., 2016. Hydrogeochemical contrasts across the multi-level aquifers of Bengal basin in Matlab, Bangladesh: Implications for arsenic free and low -manganese drinking water sources 45–46. https://doi.org/10.1201/b20466-22

Biswas, A., Gustafsson, J.P., Neidhardt, H., Halder, D., Kundu, A.K., Chatterjee, D., Berner, Z., Bhattacharya, P., 2014. Role of competing ions in the mobilization of arsenic in groundwater of Bengal Basin: Insight from surface complexation modelling. Water Res. 55, 30–39. https://doi.org/10.1016/j.watres.2014.02.002

Bondesan, A., Primon, S., Bassan, V., Vitturi, A., 2008. Le unità geologiche della provincia di Venezia. Provincia di Venezia, Servizio Geologico e Difesa del Suolo.

Carraro, A., Fabbri, P., Giaretta, A., Peruzzo, L., Tateo, F., Tellini, F., 2015. Effects of redox conditions on the control of arsenic mobility in shallow alluvial aquifers on the Venetian Plain (Italy). Sci. Total Environ. 532, 581–594. https://doi.org/10.1016/j.scitotenv.2015.06.003

Carraro, A., Fabbri, P., Giaretta, A., Peruzzo, L., Tateo, F., Tellini, F., 2013. Arsenic anomalies in shallow Venetian Plain (Northeast Italy) groundwater. Environ. Earth Sci. 70, 3067–3084. https://doi.org/10.1007/s12665-013-2367-2

Charlton, S.R., Parkhurst, D.L., 2011. Modules based on the geochemical model PHREEQC for use in scripting and programming languages. Comput. Geosci. 37, 1653–1663. https://doi.org/10.1016/J.CAGEO.2011.02.005

Choong, T.S.Y., Chuah, T.G., Robiah, Y., Gregory Koay, F.L., Azni, I., 2007. Arsenic toxicity, health hazards and removal techniques from water: an overview. Desalination 217, 139–166. https://doi.org/10.1016/j.desal.2007.01.015

Choudhury, R., Nath, B., Khan, M.R., Mahanta, C., Ellis, T., Geen, A., 2018. The Impact of Aquifer Flushing on Groundwater Arsenic Across a 35-km Transect Perpendicular to the Upper Brahmaputra River in Assam, India. Water Resour. Res. 54, 8160–8173. https://doi.org/10.1029/2017WR022485

Acharyya S. K., Chakraborty P., Lahiri S., Raymahashay B. C., Saumyen Guha, Amitava Bhowmik, 1999. Arsenic poisoning in the Ganges delta. Nature 401, 545–546. https://doi.org/10.1038/44056

Cleveland, W.S., 1981. Scatterplots by Robust LOWESS: A Program for Smoothing Locally Weighted Regression Lattice Designs: Analysis of Variance and Randomized Layouts. Am. Nat. 35, 829–836. https://doi.org/10.2307/2683591

Cleveland, W.S., 1979. Robust Locally Weighted Regression and Smoothing Scatterplots. J. Am. Stat. Assoc. 74, 829–836. https://doi.org/10.2307/2286407

Kinniburgh, D.G., Smedley, P.L., 2001. Arsenic contamination of groundwater in Bangladesh. Br. Geol. Surv. Tech. Rep. WC/00/19 1, 1–21.

Dalla Libera, N., Fabbri, P., Mason, L., Piccinini, L., Pola, M., 2018. A local natural background level concept to improve the natural background level: a case study on the drainage basin of the Venetian Lagoon in North-eastern Italy. Environ. Earth Sci. 77, 487. https://doi.org/10.1007/s12665-018-7672-3

Dalla Libera, N., Fabbri, P., Mason, L., Piccinini, L., Pola, M., 2017. Geostatistics as a tool to improve the natural background level definition: An application in groundwater. Sci. Total Environ. 598, 330–340. https://doi.org/10.1016/j.scitotenv.2017.04.018

Dalla Libera, N., Fabbri, P., Piccinini, L., Pola, M., Leonardo Mason, L., 2016. Natural Arsenic in groundwater in the drainage basin to the Venice lagoon (Brenta Plain, NE Italy): the organic matter's role. Rend. Online della Soc. Geol. Ital. 41, 30–33. https://doi.org/10.3301/ROL.2016.85

Davis, J.C., 2002. Statistics and data analysis in geology. J. Wiley.

D'Ippoliti, D., Santelli, E., De Sario, M., Scortichini, M., Davoli, M., Michelozzi, P., 2015. Arsenic in Drinking Water and Mortality for Cancer and Chronic Diseases in Central Italy, 1990-2010. PLoS One10, e0138182. https://doi.org/10.1371/journal.pone.0138182

Ducci, D., Condesso, M.T., Melo, D., Preziosi, E., Sellerino, M., Parrone, D., Ribeiro, L., 2016. Science of the Total Environment Combining natural background levels (NBLs) assessment with indicator kriging analysis to improve groundwater quality data interpretation and management. Sci. Total Environ. 569–570, 569–584. https://doi.org/10.1016/j.scitotenv.2016.06.184

Dzombak, D.A., Morel, F., 1990. Surface complexation modelling: hydrous ferric oxide. Wiley.

Fabbri, P., Gaetan, C., Zangheri, P., 2011. Transfer function-noise modelling of an aquifer system in NE Italy. Hydrol. Process. 25, 194–206. https://doi.org/10.1002/hyp.7832

Fabbri, P., Piccinini, L., 2013. Assessing transmissivity from specific capacity in an alluvial aquifer in the middle Venetian plain (NE Italy). Water Sci. Technol. 67, 2000–2008. https://doi.org/10.2166/wst.2013.074

Flores, A.N., Rubio, L.M.D., 2010. Arsenic and metal mobility from Au mine tailings in Rodalquilar (Almería, SE Spain). Environ. Earth Sci. 60, 121–138. https://doi.org/10.1007/s12665-009-0174-6

Fontana, A., Mozzi, P., Bondesan, A., 2010. Late pleistocene evolution of the Venetian–Friulian Plain. Rend. LINCEI 21, 181–196. https://doi.org/10.1007/s12210-010-0093-1

Fontana, A., Mozzi, P., Bondesan, A., 2008. Alluvial megafans in the Venetian-Friulian Plain (north-eastern Italy): Evidence of sedimentary and erosive phases during Late Pleistocene and Holocene. Quat. Int. 189, 71–90.

Fraser, S.J., Dickson, B.L., 2007. A New Method for Data Integration and Integrated Data Interpretation: Self-Organising Maps. Procedings Explor. 07 Fifth Decenn. Int. Conf. Miner. Explor. 907–910.

Gersho, A., 1990. Optimal nonlinear interpolative vector quantization. IEEE Trans. Commun. 38, 1285–1287. https://doi.org/10.1109/26.61363

Goovaerts, P., 1997. Geostatistics for natural resources evaluation. Oxford University Press.

Gray, R.M., Neuhoff, D.L., 1998. Quantization. IEEE Trans. Inf. Theory 44, 2325–2383. https://doi.org/10.1109/18.720541

Harvey, C.F., Ashfaque, K.N., Yu, W., Badruzzaman, A.B.M., Ali, M.A., Oates, P.M., Michael, H.A., Neumann, R.B., Beckie, R., Islam, S., Ahmed, M.F., 2006. Groundwater dynamics and arsenic contamination in Bangladesh. Chem. Geol. 228, 112–136. https://doi.org/10.1016/J.CHEMGEO.2005.11.025

Harvey, C.F., Swartz, C.H., Badruzzaman, A.B.M., Keon-Blute, N., Yu, W., Ali, M.A., Jay, J., Beckie, R., Niedan, V., Brabander, D., Oates, P.M., Ashfaque, K.N., Islam, S., Hemond, H.F., Ahmed, M.F., 2002. Arsenic Mobility and Groundwater Extraction in Bangladesh. Science (80). 298, 1602–1606. https://doi.org/10.1126/science.1076978

Haykin, S.S., Simon, 1994. Neural networks: a comprehensive foundation. Macmillan.

Healy, R.W., Cook, P.G., 2002. Using groundwater levels to estimate recharge. Hydrogeol. J. 10, 91–109. https://doi.org/10.1007/s10040-001-0178-0

Huang, K., Liu, Y., Yang, C., Duan, Y., Yang, X., Liu, C., 2018. Identification of Hydro-biogeochemical Processes Controlling Seasonal Variations in Arsenic Concentrations Within a Riverbank Aquifer at Jianghan Plain, China. Water Resour. Res. 54, 4294–4308. https://doi.org/10.1029/2017WR022170

International Organization for Standardization, 1995. Soil quality -- Extraction of trace elements soluble in aqua regia (standard n. 11466). Retrieved from https://www.iso.org/standard/19418.html

Jain, C.K., Ali, I., 2000. Arsenic: Occurrence, toxicity and speciation techniques. Water Res. 34, 4304–4312. https://doi.org/10.1016/S0043-1354(00)00182-2

Jakobsen, R., Kazmierczak, J., Sø, H.U., Postma, D., 2018. Spatial variability of groundwater arsenic concentration as controlled by hydrogeology; Conceptual analysis using 2-D reactive transport modelling. Water Resour. Res. https://doi.org/10.1029/2018WR023685

Jessen, S., Postma, D., Larsen, F., Nhan, P.Q., Hoa, L.Q., Trang, P.T.K., Long, T.V., Viet, P.H., Jakobsen, R., 2012. Surface complexation modelling of groundwater arsenic mobility: Results of a forced gradient experiment in a Red River flood plain aquifer, Vietnam. Geochim. Cosmochim. Acta 98, 186–201. https://doi.org/10.1016/J.GCA.2012.07.014

Kalteh, A.M., Hjorth, P., Berndtsson, R., 2008. Review of the self-organizing map (SOM) approach in water resources: Analysis, modelling and application. Environ. Model. Softw. 23, 835–845. https://doi.org/10.1016/j.envsoft.2007.10.001

Karim, M.M., 2000. Arsenic in groundwater and health problems in Bangladesh. Water Res. 34, 304–310. https://doi.org/10.1016/S0043-1354(99)00128-1

Kinniburgh, D.G., Smedley, P.L., 2001. BGS Technical Report WC/00/19. Br. Geol. Surv. Keyworth, UK.

Kohonen, T., 2013. Essentials of the self-organizing map. Neural Networks 37, 52–65. https://doi.org/10.1016/j.neunet.2012.09.018

Kohonen, T., 2001. Self-Organizing Maps. Springer Berlin Heidelberg.

Kohonen, T., 1990. The self-organizing map. Proc. IEEE 78, 1464–1480. https://doi.org/10.1109/5.58325

Kohonen, T., Hynninen, J., Kangas, J., Laaksonen, J., 1996. The Self-Organizing Map Program Package. Univ. Technol. Comput. Inf. Sci. Helsinki, Finl. https://doi.org/10.1074/jbc.M115.652156

Mango, H., Ryan, P., 2015. Source of arsenic-bearing pyrite in southwestern Vermont, USA: Sulfur isotope evidence. Sci. Total Environ. 505, 1331–1339. https://doi.org/10.1016/J.SCITOTENV.2014.03.072

Mayer, K.U., Frind, E.O., Blowes, D.W., 2002. Multicomponent reactive transport modeling in variably saturated porous media using a generalized formulation for kinetically controlled reactions. Water Resour. Res. 38, 13-1-13–21. https://doi.org/10.1029/2001WR000862

McArthur, J.M., Banerjee, D.M., Hudson-Edwards, K.A., Mishra, R., Purohit, R., Ravenscroft, P., Cronin, A., Howarth, R.J., Chatterjee, A., Talukder, T., Lowry, D., Houghton, S., Chadha, D.K., 2004. Natural organic matter in sedimentary basins and its relation to arsenic in anoxic ground water: The example of West Bengal and its worldwide implications. Appl. Geochemistry 19, 1255–1293. https://doi.org/10.1016/j.apgeochem.2004.02.001

McArthur, J.M., Ravenscroft, P., Safiulla, S., Thirlwall, M.F., 2001. Arsenic in groundwater: Testing pollution mechanisms for sedimentary aquifers in Bangladesh. Water Resour. Res. 37, 109–117. https://doi.org/10.1029/2000WR900270

Michael, H.A., Khan, M.R., 2016. Impacts of physical and chemical aquifer heterogeneity on basin-scale solute transport: Vulnerability of deep groundwater to arsenic contamination in Bangladesh. Adv. Water Resour. 98, 147–158. https://doi.org/10.1016/J.ADVWATRES.2016.10.010

Molinari, A., Guadagnini, L., Marcaccio, M., Guadagnini, A., 2012. Natural background levels and threshold values of chemical species in three large-scale groundwater bodies in Northern Italy. Sci. Total Environ. 425, 9–19. https://doi.org/10.1016/j.scitotenv.2012.03.015

Monod, J., 1949. The Growth of Bacterial Cultures. Annu. Rev. Microbiol. 3, 371–394. https://doi.org/10.1146/annurev.mi.03.100149.002103

Mozzi, P., Ferrarese, F., Fontana, A., 2013. Integrating Digital Elevation Models and stratigraphic data for the reconstruction of the post-lgm unconformity in the Brenta alluvial megafan (north-eastern Italy. Alp. Mediterr. Quat. 26, 41–54.

Nickson, R., McArthur, J., Burgess, W., Ahmed, K.M., Ravenscroft, P., Rahman, M., 1998. Arsenic poisoning of Bangladesh groundwater. Nature 395, 338. https://doi.org/10.1038/26387

Nickson, R.T., Mcarthur, J.M., Ravenscroft, P., Burgess, W.G., Ahmed, K.M., 2000. Mechanism of arsenic release to groundwater, Bangladesh and West Bengal. Appl. Geochemistry 15, 403–413. https://doi.org/10.1016/S0883-2927(99)00086-4

Nordstrom, D.K., 2003. Arsenic in Ground Water, Science Mag. Springer US, Boston, MA. https://doi.org/10.1007/b101867

Nordstrom, D.K., Campbell, K.M., 2013. Modelling Low-Temperature Geochemical Processes, 2nd ed, Treatise on Geochemistry: Second Edition. Published by Elsevier Inc. https://doi.org/10.1016/B978-0-08-095975-7.00502-7

Obermayer, K., Sejnowski, T.J. (Terrence J., 2001. Self-organizing map formation: foundations of neural computation. MIT Press.

Oja, E., Kaski, S., 1999. Kohonen maps. Elsevier.

Parkhurst, D.L., Appelo, C.A.J., 2013. Description of input and examples for PHREEQC Version 3 — A computer program for speciation, batch-reaction, one-dimensional transport, and inverse geochemical calculations. U.S. Geol. Surv. Tech. Methods, B. 6, chapter A43 6-43A. https://doi.org/10.1016/0029-6554(94)90020-5

Parsons, C.T., Couture, R.M., Omoregie, E.O., Bardelli, F., Greneche, J.M., Roman-Ross, G., Charlet, L., 2013. The impact of oscillating redox conditions: Arsenic immobilisation in contaminated calcareous floodplain soils. Environ. Pollut. 178, 254–263. https://doi.org/10.1016/j.envpol.2013.02.028

Pedretti, D., Luoma, S., Ruskeeniemi, T., Backman, B., 2019. A geologically-based approach to map arsenic risk in crystalline aquifers: Analysis of the Tampere region, Finland. Geosci. Front. https://doi.org/10.1016/J.GSF.2018.12.004

Piccinini, L., Fabbri, P., Pola, M., Marcolongo, E. (2017) An example of aquifer heterogeneity simulation to modeling well-head protection areas. Ital J Eng Geol Environ 2017:103–115. https://doi.org/10.4408/IJEGE.2017-01.S-10

Piccinini, L., Fabbri, P., Pola, M., 2016. Point dilution tests to calculate groundwater velocity, an example in a porous aquifer in NE Italy. Hydrol. Sci. J. In Press. https://doi.org/10.1080/02626667.2015.1036756

Piccinini, L., Fabbri, P., Pola, M., Marcolongo, E., Rosignoli, A., 2015. Numerical modelling to well-head protection area delineation, an example in Veneto Region (NE Italy). Rend. online della Soc. Geol. Ital. 35, 232–235. https://doi.org/10.3301/ROL.2015.108

Pieri, L., Dinelli, G., Pisa, P.R., 2012. Study of the quality of precipitation at two sites in the province of Bologna: trend of the last decade. Ital. J. Agrometeorol. 17, 5–14.

Pola, M., Fabbri, P., Piccinini, L., Dalla, N., Zampieri, D., Roghel, A., Onisto, S., Zampieri, E., Bianchi, A., Rossi, C., Pennazzato, A., 2016. Mapping the variation of the potentiometric level of the Euganean thermal aquifer and relationship with the exploitation. Rend. online della Soc. Geol. Ital. 41, 284–287. https://doi.org/10.3301/ROL.2016.149

Pompili, M., Vichi, M., Dinelli, E., Erbuto, D., Pycha, R., Serafini, G., Giordano, G., Valera, P., Albanese, S., Lima, A., De Vivo, B., Cicchella, D., Rihmer, Z., Fiorillo, A., Amore, M., Girardi, P., Baldessarini, R.J., 2017. Arsenic: Association of regional concentrations in drinking water with suicide and natural causes of death in Italy. Psychiatry Res. 249, 311–317. https://doi.org/10.1016/J.PSYCHRES.2017.01.041

Postma, D., Larsen, F., Minh Hue, N.T., Duc, M.T., Viet, P.H., Nhan, P.Q., Jessen, S., 2007. Arsenic in groundwater of the Red River floodplain, Vietnam: Controlling geochemical processes and reactive transport modelling. Geochim. Cosmochim. Acta 71, 5054–5071. https://doi.org/10.1016/j.gca.2007.08.020

Preziosi, E., Giuliano, G., Vivona, R., 2010. Natural background levels and threshold values derivation for naturally As, V and F rich groundwater bodies: a methodological case study in Central Italy. Environ. Earth Sci. 61, 885–897. https://doi.org/10.1007/s12665-009-0404-y

Prommer, H., Barry, D.A., Zheng, C., 2003. PHT3D-A MODFLOW/MT3DMS based reactive multi-component transport model. Groundwater.

R Core Team, 2018. R: A language and environment for statistical computing. R Foundation for Statistical Computing, Vienna, Austria. URL https://www.R-project.org/.

Rango, T., Vengosh, A., Dwyer, G., Bianchini, G., 2013. Mobilization of arsenic and other naturally occurring contaminants in groundwater of the main Ethiopian rift aquifers. Water Res. 47, 5801–5818. https://doi.org/10.1016/j.watres.2013.07.002

Rathi, B., Neidhardt, H., Berg, M., Siade, A., Prommer, H., 2017. Processes governing arsenic retardation on Pleistocene sediments: Adsorption experiments and model-based analysis. Water Resour. Res. 53, 4344–4360. https://doi.org/10.1002/2017WR020551

Rawson, J., Prommer, H., Siade, A., Carr, J., Berg, M., Davis, J.A., Fendorf, S., 2016. Numerical Modeling of Arsenic Mobility during Reductive Iron-Mineral Transformations. Environ. Sci. Technol. 50, 2459–2467. https://doi.org/10.1021/acs.est.5b05956

Richards, L.A., Magnone, D., Sültenfuß, J., Chambers, L., Bryant, C., Boyce, A.J., van Dongen, B.E., Ballentine, C.J., Sovann, C., Uhlemann, S., Kuras, O., Gooddy, D.C., Polya, D.A., 2019. Dual in-aquifer and near surface processes drive arsenic mobilization in Cambodian groundwaters. Sci. Total Environ. 659, 699–714. https://doi.org/10.1016/J.SCITOTENV.2018.12.437

Rotiroti, M., Jakobsen, R., Fumagalli, L., Bonomi, T., 2015. Arsenic release and attenuation in a multilayer aquifer in the Po Plain (northern Italy): Reactive transport modelling. Appl. Geochemistry 63, 599–609. https://doi.org/10.1016/j.apgeochem.2015.07.001

Rotiroti, M., Sacchi, E., Fumagalli, L., Bonomi, T., 2014. Origin of Arsenic in Groundwater from the Multilayer Aquifer in Cremona (Northern Italy). Environ. Sci. Technol. 48, 5395–5403. https://doi.org/10.1021/es405805v

Saunders, J.A., Lee, M.-K., Shamsudduha, M., Dhakal, P., Uddin, A., Chowdury, M.T., Ahmed, K.M., 2008. Geochemistry and mineralogy of arsenic in (natural) anaerobic groundwaters. Appl. Geochemistry 23, 3205–3214. https://doi.org/10.1016/J.APGEOCHEM.2008.07.002

Simon, G., Lendasse, A., Cottrell, M., Verleysen, M., 2003. Long-Term Time Series Forecasting using Self-Organizing Maps: the Double Vector Quantization Method. Proc. Conf. ANNPR Florence 8–14.

Smedley, P.L., Kinniburgh, D.G., 2013. Arsenic in Groundwater and the Environment, in: Essentials of Medical Geology. Springer Netherlands, Dordrecht, pp. 279–310. https://doi.org/10.1007/978-94-007-4375-5_12

Sracek, O., Bhattacharya, P., Jacks, G., Gustafsson, J.P., Von Brömssen, M., 2004. Behavior of arsenic and geochemical modeling of arsenic enrichment in aqueous environments. Appl. Geochemistry 19, 169–180. https://doi.org/10.1016/j.apgeochem.2003.09.005

Stollenwerk, K.G., Breit, G.N., Welch, A.H., Yount, J.C., Whitney, J.W., Foster, A.L., Uddin, M.N., Majumder, R.K., Ahmed, N., 2007. Arsenic attenuation by oxidized aquifer sediments in Bangladesh. Sci. Total Environ. 379, 133–150. https://doi.org/10.1016/j.scitotenv.2006.11.029

Tokutaka, H., Ohkita, M., Fujimura, K., 2007. Self-organizing maps and its application.

Törönen, P., Kolehmainen, M., Wong, G., Castrén, E., 1999. Analysis of gene expression data using self-organizing maps. FEBS Lett. 451, 142–146. https://doi.org/10.1016/S0014-5793(99)00524-4

Trevisani, S., Fabbri, P., 2010. Geostatistical modeling of a heterogeneous site bordering the Venice lagoon, Italy. Ground Water 48, 614–623. https://doi.org/10.1111/j.1745-6584.2009.00632.x

Ungaro, F., Ragazzi, F., Cappellin, R., Giandon, P., 2008. Arsenic concentration in the soils of the Brenta Plain (Northern Italy): Mapping the probability of exceeding contamination thresholds. J. Geochemical Explor. 96, 117–131. https://doi.org/10.1016/j.gexplo.2007.03.006

UNI EN ISO 17294-2:2016, 2016. Water quality -- Application of inductively coupled plasma mass spectrometry (ICP-MS) -- Part 2: Determination of selected elements including uranium isotopes. https://www.iso.org/standard/62962.html

Vesanto, J., Himberg, J., Alhoniemi, E., Parhankangas, J., 2000. Self-Organizing Map in Matlab: the SOM Toolbox. Matlab DSP Conf. 35–40. https://doi.org/10.1.1.25.9495

Vorlicek, P.A., Antonelli, R., Fabbri, P., Rausch, R., 2004. Quantitative hydrogeological studies of the Treviso alluvial plain, NE Italy. Q. J. Eng. Geol. Hydrogeol. 37, 23–29. https://doi.org/10.1144/0036-9276/02-006

Wallis, I., Prommer, H., Pichler, T., Post, V., B. Norton, S., Annable, M.D., Simmons, C.T., 2011. Process-based reactive transport model to quantify arsenic mobility during aquifer storage and recovery of potable water. Environ. Sci. Technol. 45, 6924–6931. https://doi.org/10.1021/es201286c

Wehrens, R., Buydens, L.M.C., 2007. Self-and super-organizing maps in R: the Kohonen package. J. Stat. Softw. 21, 1–19.

Wehrens, R., Kruisselbrink, J., 2018. Flexible Self-Organizing Maps in kohonen 3.0. J. Stat. Softw. 87. https://doi.org/10.18637/jss.v087.i07

Zhang, L., Scholz, M., Mustafa, A., Harrington, R., 2009. Application of the self-organizing map as a prediction tool for an integrated constructed wetland agroecosystem treating agricultural runoff. Bioresour. Technol. 100, 559–565. https://doi.org/10.1016/j.biortech.2008.06.042

Ziegler, B.A., Schreiber, M.E., Cozzarelli, I.M., 2017. The role of alluvial aquifer sediments in attenuating a dissolved arsenic plume. J. Contam. Hydrol. 204, 90–101. https://doi.org/10.1016/J.JCONHYD.2017.04.009

2.6 Future development: 3D reactive transport model

2.6.1 Introduction

The analyses presented so far identified key processes that are likely controlling As mobility in the WAA. From a decision-making perspective, the stakeholders are interested in understanding the arsenic mobility mechanism to plan a more occulated environmental management strategy in the Venetian Alluvial Plain (VAP). 3D reactive transport models are suitable tools to upscale local-scale information to the regional scale assessment. The results described in the remaining of this section present and discuss preliminary results obtained from the initial development of a 3D REACTIVE TRANSPORT MODEL focusing on the WAA and based on code PHAST (Parkhurst et al., 2010). While the model is expected to be concluded within a few months (and published on an international journal in 2020), the initial results provide preliminary elements to assess and confirm the effectiveness of the supposed hydrochemical processes working in the WAA (described in section 2.5), in particular the ingress of oxygen linked to the recharge process. In turn, this model will set the basis for a more extended model representing As dynamics at the scale of the VAP. Starting from a local-scale

model provides a fundamental test to verify, among others aspects, whether such complex modeling approach is computationally feasible, given the strong nonlinearity of the three-dimensional equations describing the physical and geochemical processes involved in the problem. Computational limitations could explain why very few 3D REACTIVE TRANSPORT MODEL analyzing As mobility in heterogeneous systems have been documented so far in the literature, rendering the present study a breakthrough, innovative study in this field. Beyond the research impact, this study provides new awareness and knowledges about the processes controlling arsenic mobility in the VAP, so that a more suitable environmental management can be adopted with respect to arsenic contamination.

2.6.2 Materials and Methods

Background information

The 3D reactive transport model is based on a physical and geochemical model that inherits all the hypothesized processes and conclusions obtained during the PhD. Important elements to recall are:

- The spMC subsurface heterogeneity reconstruction of the lithological facies in the WAA can be assumed as the reference spatial distribution of the 3D model parameters.

- The main geochemical process controlling As distribution is the redox-sensitive dissolution and oxidation of iron hydroxides (HFOs), on which As molecules are, respectively, detaching from or attaching to. When the aquifer experiences reduced conditions, As is liberated and aqueous As concentrations increase, in some cases exceeding the WHO-recommended limits for drinking purposes (10 μg/L). During oxidizing stages, HFOs form and trap, by means of surface reactions, dissolved As, reducing aqueous concentrations in some case to <10 μg/L.

- Aquifer redox conditions are supposed to be controlled by organic matter degradation, which generates reduced aquifer conditions.

- Rainfall-driven recharge events increase the concentrations of oxidants (particularly O2) in the deeper parts of the aquifer. The effectiveness of the latter process is assumed to be controlled by the dynamic interaction between the aquifer system and the unsaturated zone. Variations of ORP value observed through the field data are consistent with the simulated amount of oxygen entering the aquifer by means of a batch-like PHREEQC-based geochemical

model (section 2.5). The ingress of oxygen from the surface to the aquifer, supposed for ORP shift toward oxidized conditions during the monitoring period, varies around the WAA being influenced by the presence and the thickness of fine materials on top of the aquifer.

Given that recharge dynamics are strongly nonlinear processes from a mathematical perspective, and given that the aquifer is heterogeneous, particularly for what concerns the distribution of fine-grained materials topping the shallow aquifer, it is difficult to compute the local recharge rate in space and time at the scale of the WAA. In this sense, the 3D reactive transport model was structured to evaluate the impact of recharge-driven oxidizing conditions of the aquifer during rainfall events and study the occurrence of As at the scale of the entire domain.

PHAST

The 3D reactive transport model was setup using PHAST, a code that embed all the information acquired during the PhD project, such as the subsurface heterogeneity reproduced by means of spMC results (Section 2.4.2), the hydraulic information came from field aquifer test (slug tests), and the chemical processes by the calibrated batch-like model (Section 2.5). PHAST combines a geochemical model, PHREEQC (Parkhurst and Appelo, 2013), and a flow and transport node-centered finite difference model, HST3D (Kipp, 1987), to simulate multicomponent reactive transport in three-dimensional saturated groundwater flow systems. Flow and advective-dispersive transport assume constant fluid density and constant temperature, a limitation which does not affect the results of the modeling analysis presented here. While PHAST is not formulated to reproduce unsaturated flow, free-surface boundary conditions (BC) can simulate partial saturation in the top layer and groundwater table oscillation. With the free-surface BC active, the code inactivated all those cells with hydraulic head lower than the bottom of the cell, but it allows for rewetting once the hydraulic head becomes higher. In this way, one can simulate the groundwater table variation as in a free aquifer without solving the vadose zone equations. Together with the free-surface BC, a variety of BC are available in PHAST to simulate flow and transport, including specified-head, flux (specified-flux), and leaky (head-dependent) conditions, as well as the special cases of rivers, drains, and wells (Kipp, 1987, 1997). Being based on PHREEQC, PHAST can embed a wide range of equilibrium and kinetic reactions, either from existing databases or allowing user-defined reactions, spanning from homogeneous equilibria using an ion-association or Pitzer specific interaction thermodynamic model to heterogeneous equilibria between the aqueous solution and minerals, ion exchange sites,

surface complexation sites, solid solutions, and gases. Kinetic reactions rates can be defined as a function of the solution composition. PHAST can resolve three-dimensional multicomponent reactive transport models. 3D reactive transport models require a large amount of memory and long-time use of CPU. To ease the computational burden PHAST is parallelized and runs on a multiprocessor computer or on a collection of clustered computers (Parkhurst et al., 2010). In this work, the model was run on an eight cores workstation.

Data involved in the model

- *Lithology heterogeneity*

The spatial material distribution characterizing the subsurface heterogeneity in the WAA was introduced in the model by geostatistical simulations of spMC code (section 2.4.2). The material distribution resulting from spMC are compatible for PHAST software as both are based on the same node-centered grid. The using of a regular node-centered grid allows to directly upload the 3D subsurface heterogeneity of lithologies in the PHAST grid, without any issues with spatial references. Specifically, the spMC grid has 84788 nodes subdivided in 44 along X, 47 along Y and 41 along Z. The materials distributed in the spMC grid (Figure 1) are four and represented by sand, silt, clay and peat, where peat is referred to both silty/clayey materials rich in organic matter and peat itself.

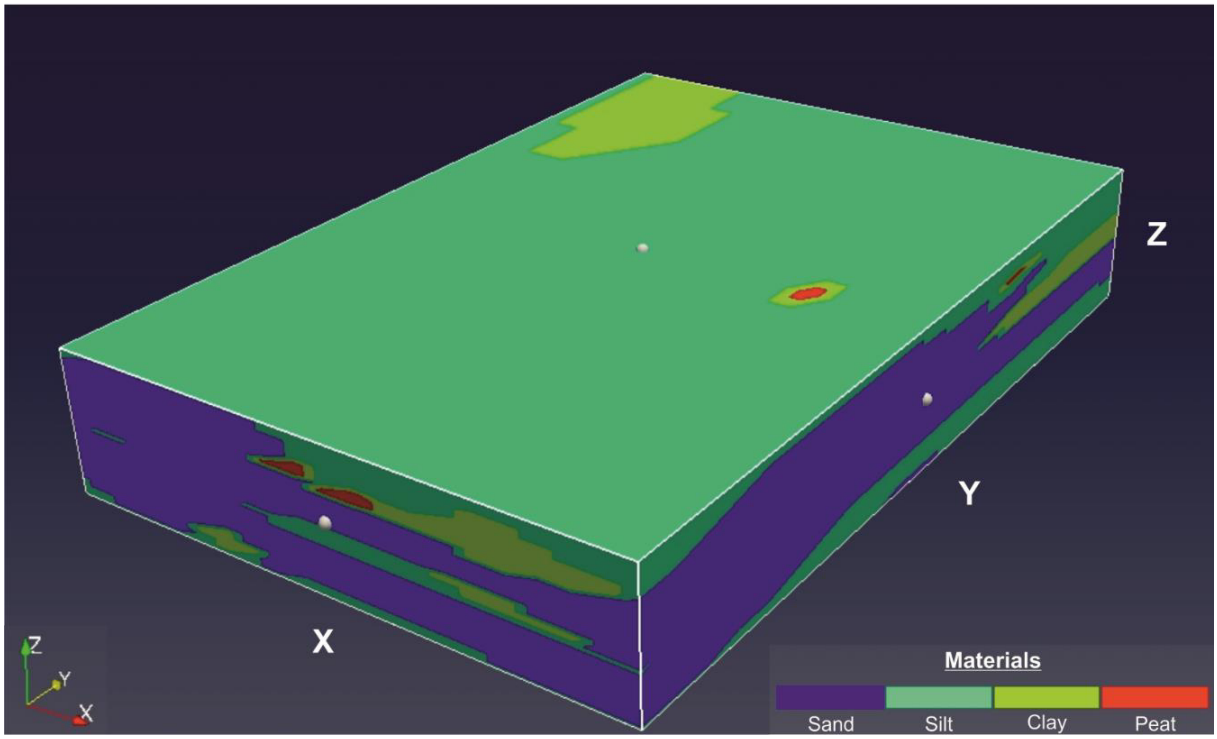

Figure 1 – Subsurface heterogeneity model obtained by geostatistical simulation described in section 2.4.2.

- *Hydraulic parameters*

The hydraulic parameters necessary for implementing the 3D reactive transport model were collected through in situ tests and literature references. The hydraulic conductivity (K) for aquifer sands was obtained by slug tests performed on the eight piezometers available in WAA (Figure 2).

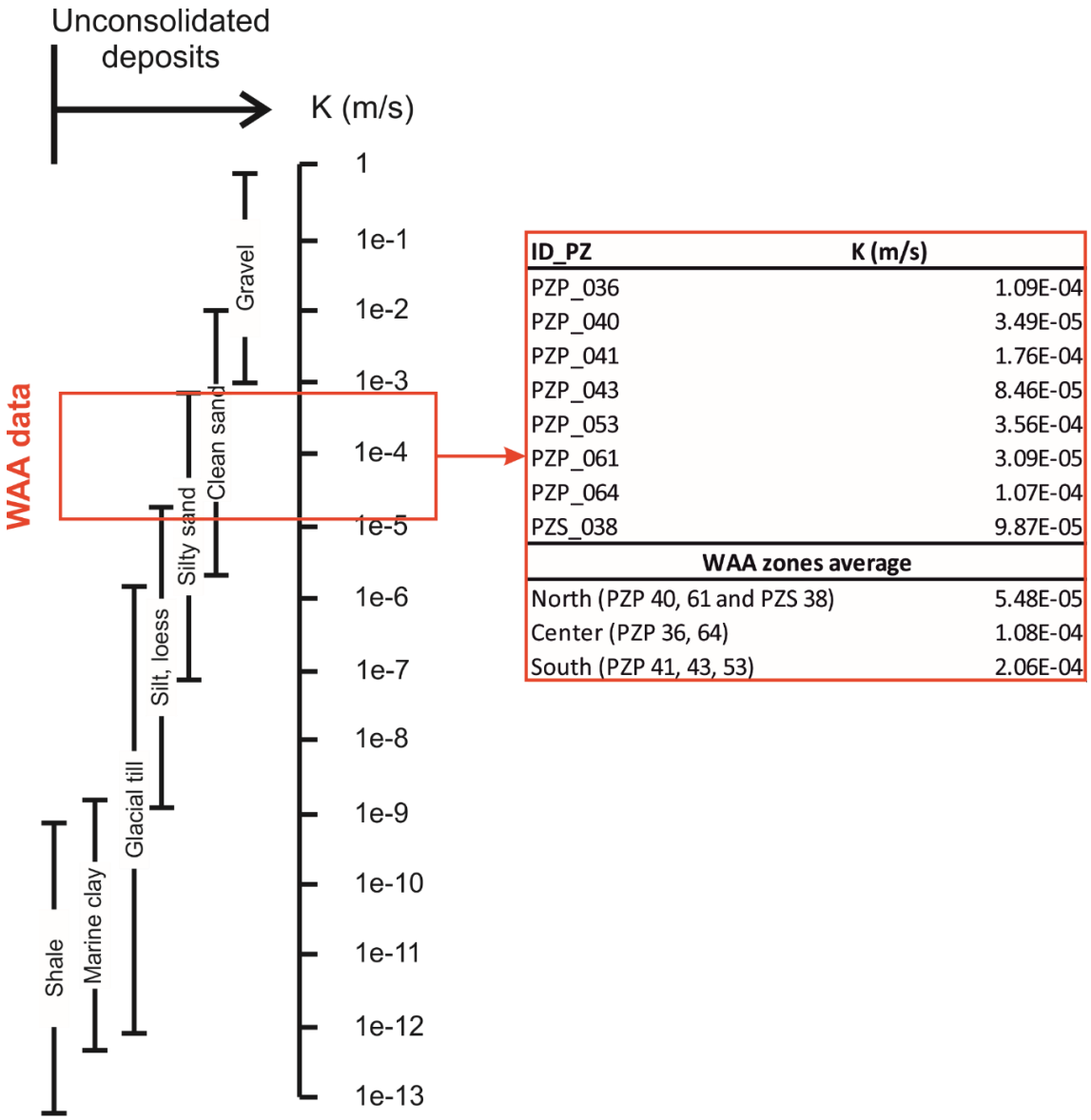

ID_PZ	K (m/s)
PZP_036	1.09E-04
PZP_040	3.49E-05
PZP_041	1.76E-04
PZP_043	8.46E-05
PZP_053	3.56E-04
PZP_061	3.09E-05
PZP_064	1.07E-04
PZS_038	9.87E-05
WAA zones average	
North (PZP 40, 61 and PZS 38)	5.48E-05
Center (PZP 36, 64)	1.08E-04
South (PZP 41, 43, 53)	2.06E-04

Figure 2 – Hydraulic conductivity values estimated for WAA through slug test methods. The average values reported in the red box represent the average hydraulic conductivity for the northern, central and southern part of WAA. The hydraulic conductivity scale is modified from Freeze and Cherry, 1997.

Slug tests were carried out in agree with ASTM D4044-96 technical guide, and thy were repeated several times for each piezometer to get a statistically significant value. The data collected during the slug tests were interpreted with AQTSolve software (Duffield, 2007) and

the water-level displacement curves were fitted applying the type curve methods of Cooper, Bredehoeft and Papadopulos (Cooper et al., 1967) for overdamped slug test (fine sediments aquifer, Figure 3). The interpretations of slug tests performed with AQTSolve are reported as graphs in supplementary materials (supplementary files S5 – S12). The hydraulic conductivity (K) and storage parameters (Ss, Sy) for silt, clay and peat were obtained from data already available in those areas (ARPAV, 2011; Beretta et al., 2017). Despite the lack of direct investigation of fine materials, their hydraulic characteristics were fixed using literature values as function of boreholes stratigraphic information.

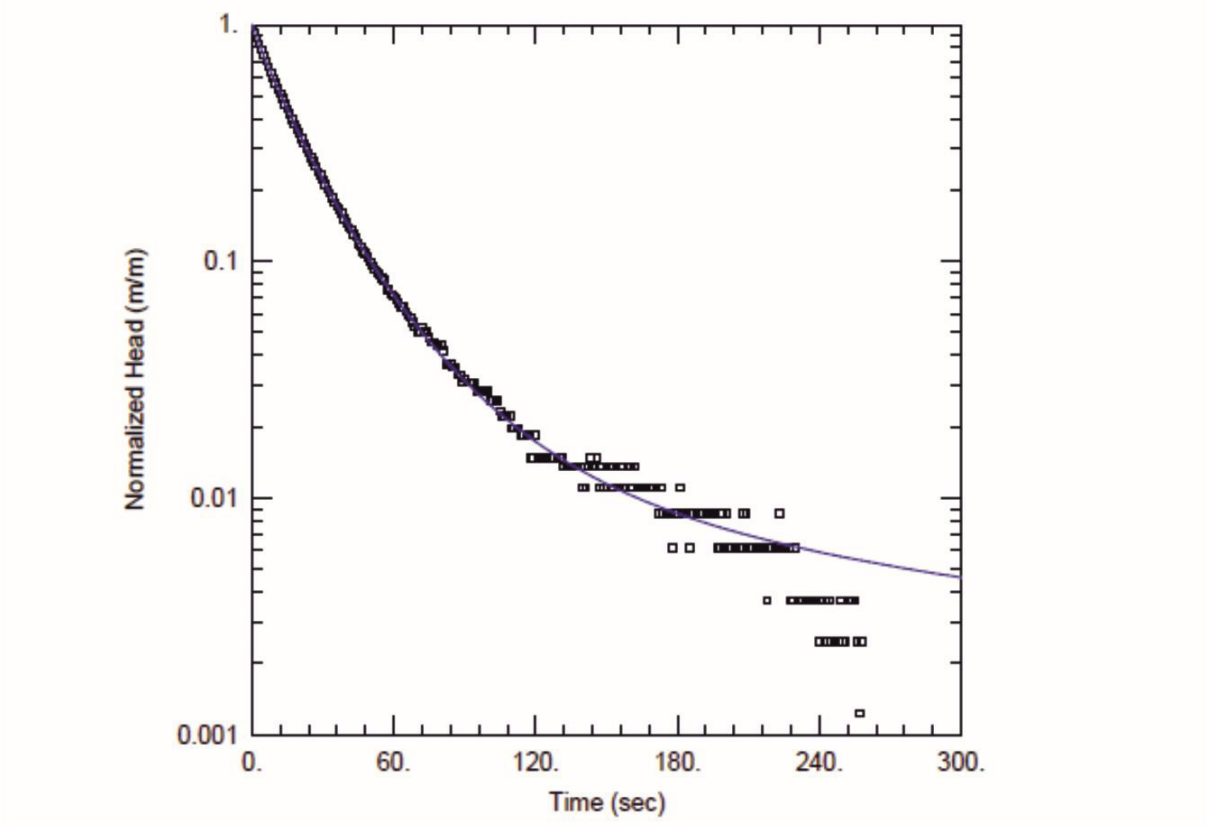

WELL TEST ANALYSIS

Data Set: C:\Users\Utente\Desktop\TESI\pzp_041_slug\pzp_041_slug.aqt
Date: 04/04/18 Time: 16:19:04

PROJECT INFORMATION

Company: tesi magistrale
Test Well: pzp_041
Test Date: 23/11/2017

AQUIFER DATA

Saturated Thickness: 3. m Anisotropy Ratio (Kz/Kr): 0.1

WELL DATA (pzp_041)

Initial Displacement: -0.814 m
Total Well Penetration Depth: 3. m
Casing Radius: 0.055 m
Static Water Column Height: 4.757 m
Screen Length: 3. m
Well Radius: 0.076 m

SOLUTION

Aquifer Model: Confined
Solution Method: Cooper-Bredehoeft-Papadopulos
T = 0.0006239 m^2/sec
S = 6.64E-7

Figure 3 - Example of slug test interpretation by AQTSolve software. The blue line, fitting the experimental hydraulic head data, represents the solution method of Cooper, Bredehoeft and Papadopulos (Cooper et al., 1967). The example is referring on a slug test performed in the PZP 41 borehole located in southern zone of WAA.

- *Potentiometric time series*

The data were collected in three piezometers (PZP36, PZP40 and PZP41) along a 115 days period (from 6th December 2017 to 23rd March 2018), monitored by an hourly acquisition system (Figure 4). The monitoring system is composed of three HOBO devices monitoring groundwater level, and a HOBO device recording atmospheric pressure. The atmospheric pressure is necessary to compensate groundwater level recorded. The potentiometric time series were used as target during the numerical flow model calibration procedure.

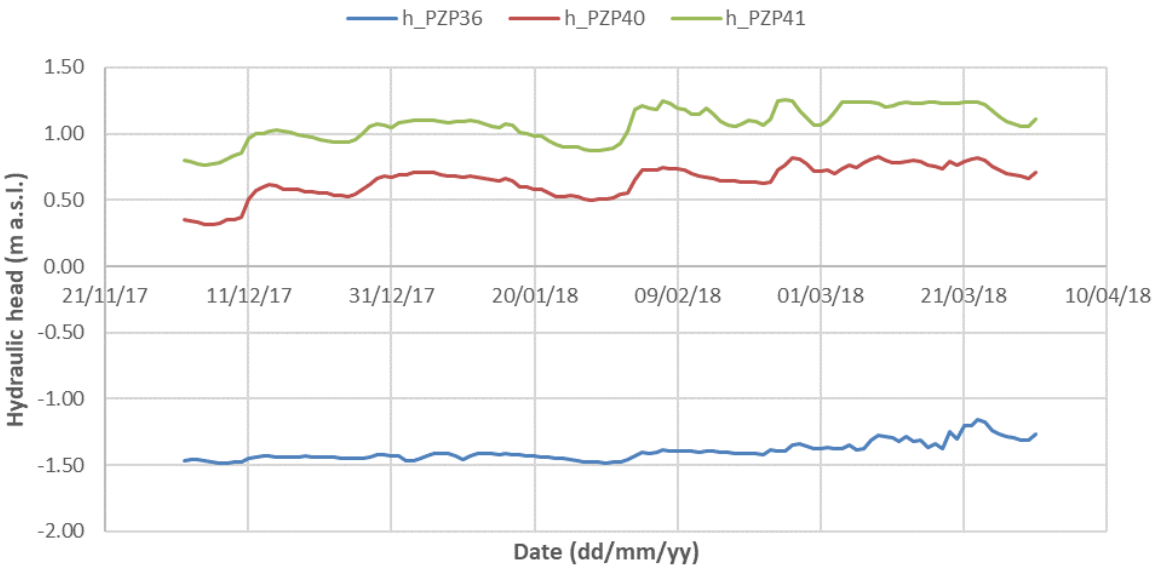

Figure 4 – hydraulic head time series for the three weekly monitored piezometers PZP36, PZP40 and PZP 41, located in the middle, northern and southern zone of WAA respectively. The acquired time series consider a time lag of an hour.

- *Rainfall time series*

The recharge component is one of the main features for a flow model and it gets relevance even for the reactive transport affecting arsenic mobility within the WAA. Then, modeling the groundwater flow and its chemical evolution in time requires input information on recharge rate. The recharge can be estimated using the rainfall amount falling in the study area during a defined period, for instance following the well-known SCS method (USDA,1986). In this study, the Environmental Protection Agency of Veneto Region supplied rainfall data, with a monitoring interval comparable with the head level measurements (Figure 5). The reference weather station used for rainfall measurement is located 7 km far from the WAA, which is deemed close enough for providing representative rainfall rates for modelled domain.

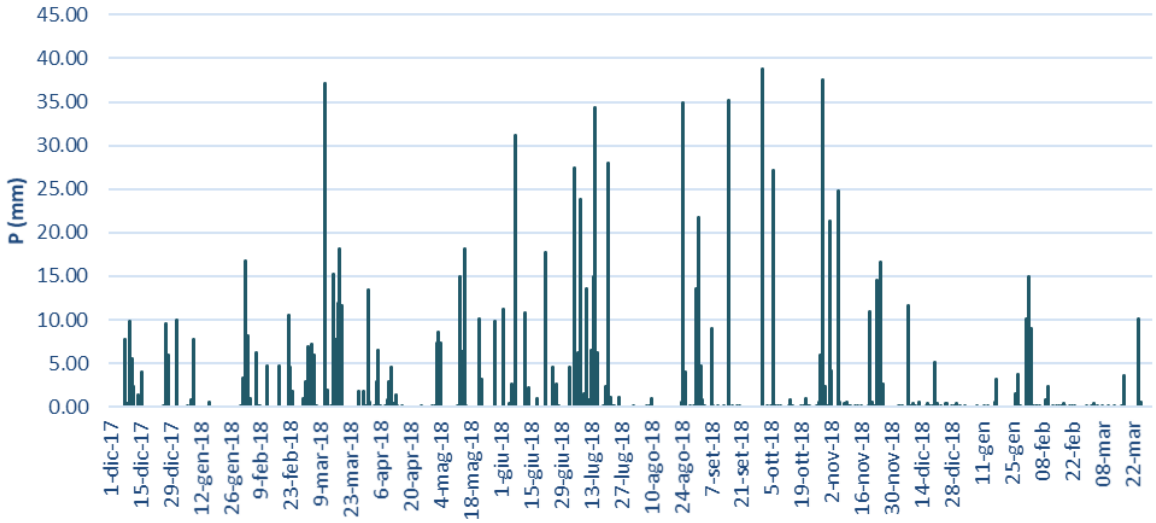

Figure 5 – Daily rainfall time series supplied by Environmental protection Agency of Veneto Region (ARPAV, Italian acronym). The time series was acquired using a weather station located in Mira (VE) (7 km far from the WAA).

- *Chemical data and related processes: (0D model)*

Data used to perform chemical part of the reactive transport model are the same used for the batch-like model explained in section 2.5. Detailed description of sampling methods and data values are reported in section 2.5 ("material and methods" sub-section) and in the supplementary materials of that thesis.

3D multicomponent reactive transport model implementation

The implementation of the 3D reactive transport model, aiming to evaluate the effects of ingress of oxygen on arsenic mobility, can be divided in two part. The first part describes the implementation of the 3D transient flow model and the second one explaining the coupled geochemical model.

Flow model implementation

The numerical flow model implementation can be resumed as following:

- Discretization of modeling domain

The flow model was developed on a regular grid composed of rectangular cells with 45 x 60 x 0.3 m in X, Y and Z direction respectively. The modeling grid is 1935 m large (X), 2760 m long (Y) and 12 m deep (Z). In such a grid was transferred the subsoil heterogeneity coming from geostatistical simulation obtained by spMC code. The heterogeneity of subsoil is reproduced by

the spatial distribution of materials (i.e.: sand, silt, clay and peat), considering that each material has its hydraulic and chemical properties. The top of the model was at 3 m above sea level (max height of ground surface), and it was kept constant in all the domain.

- Subsurface material parameterization

Once the grid is defined and the material distribution is defined, the material parameters (i.e.: K, Ss, Sy) were assigned to each node considering the material present. The construction of input xyz files containing the parameters was performed within the R environment (R Core Team, 2018). Considering that each material has its parameters, and that spMC output grid contains spatial material distribution, such an output grid was modified assigning the hydraulic parameter values for each material in each xyz position. The resulting xyz files are for K, Ss and Sy. Table 1 reports the input parameters for the 3D flow model.

Table 6 – Calibrated hydraulic parameter assigned to each material involved in the 3D flow and reactive transport model.

	m/s	*1/m*	
Material	**K**	**Ss**	**Sy**
Sand	1.25E-04	1.00E-07	0.2
Silt	5.00E-06	1.00E-04	0.01
Clay	1.00E-08	5.00E-04	0.005
Peat	1.00E-08	5.00E-04	0.005

- Boundary conditions

In order to simulate the hydraulic head condition occurring in the WAA, two types of boundary condition (BC) were used. The types and location of these BCs are shown in Figure 6. As visible in Figure 6, along the WAA edges were assigned four General Head Boundary (GHB, third type BC). Along the Western and Northern edges, the GHB is suitable for simulating the contribution of the upstream aquifer, which is directly connected and supplies water from the regional recharge zones. The GHB assigned along the Southern edge aims to simulate the interaction between the study aquifer and the Naviglio Brenta River present in that area. The last GHB, located on the Eastern edge, reproduces the hydraulic interaction between WAA aquifer and the Venice Lagoon. On the entire WAA a Recharge BC (RCH, second type) was applied to the uppermost active cells in order to simulate the local recharge effect due to rainfall infiltration rate. The RCH was split in two BCs because the recharge rate in the system varies from North to South, being linked to the different amount of less permeable materials present on the top of

the aquifer. Finally, a DRAIN BC was in the central zone of the WAA, in order to simulate the behavior of an existing drain lowering groundwater head in that zone. The simulation of this anthropic element is necessary as its action could foster the oxygen ingress in the aquifer portions close to it. The defined BCs were set as transient BCs when the transient model was run, at exclusion of DRAIN no time-dependent.

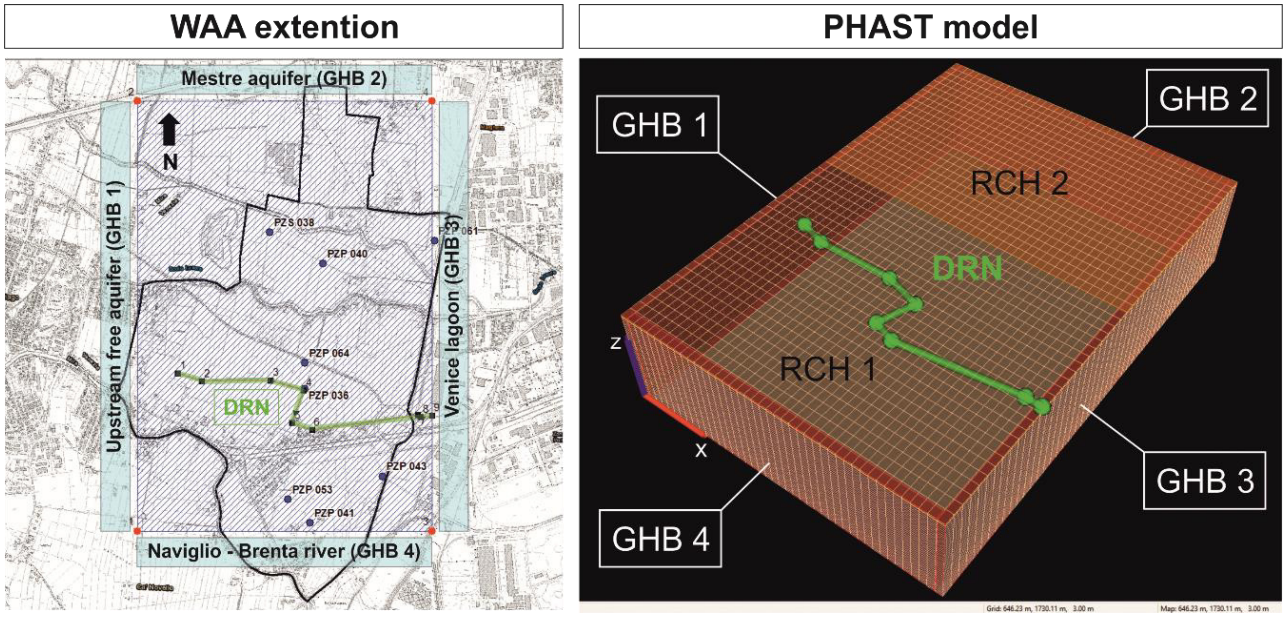

Figure 6 – 3D model set up showing boundary conditions of numerical reactive-transport flow model.

- Initial condition

In numerical modelling it is common practice to consider e results of the steady-state model as initial head condition. This is the strategy adopted for this 3D reactive transport model. Once the grid and the BCs were set, the model in steady-state conditions was run and the hydraulic head distribution resulting were saved and used as initial hydraulic head condition of the 3D transient flow of the WAA. Passing from a steady-state model to a transient one, the simulation time was defined equal to 115 day and the duration of the time steps in which it was divided were set to one day.

Reactive transport model

Required parameters for the reactive transport modeling analysis are divided in two groups, the physical parameters required for the advective and dispersive transport mechanisms and chemical parameters required for the diffusive and reactive mechanisms.

The key physical parameters for the reactive transport modeling analysis are porosity and coefficient of local dispersivity (α). Since α is a 3D tensor, α must be defined for each direction x,y,z. Since the mean flow direction is parallel to the x direction, only the three component αl αth and αtv (respectively, longitudinal dispersion, horizontal transverse dispersion and vertical transverse dispersion) must be set. Lacking of direct measurements from tracer tests, we used a classic rule-of-thumb in line with the compilation of results by Gelhar et al., 1992 and set αl as 100m (about 1/10 the domain size), and a ratio αth = 0.1αl and αtv = 0.1αth. The choice satisfies Peclet's number for numerical stability (Fletcher, 1991), as the transport solution was based on an upstream-weighted algorithm.

To perform the 3D reactive transport model, the transient flow model has to be coupled with a chemical model able to reproduce chemical processes observed in filed data and evaluated by PHREEQC model reported in section 2.5. The reaction model was developed using the main chemical processes pointed out by the batch-like model. That model highlighted the occurrence of reductive dissolution of iron hydroxides jointly with the ingress of oxygen as effect of the local recharge rate. In this direction, the chemical model introduced in PHAST algorithm considers three main features, which are able to reproduce the abovementioned processes keeping into account the heterogeneity of the subsurface. The chemical file, used as input for reactions, has the same structure of the PHREEQC input file but it requires some indexes for referring the chemical block commands to each material or BC. The BCs, anyway, could have only associated solution and no chemical reaction (i.e.: equilibria, kinetics, sorption, etc.). In this line, the input chemical file could be resumed as follow:

- Solution definition

The first part of the file defines the chemical composition of all solutions used for reactive transport model. The model considers three solutions (Table 2) characterizing respectively the initial solution filling the aquifer at t = 0 (Solution 1), the groundwater entering the system from the GHB BCs (Solution 2), and the Rainfall water assigned to the RCH BCs (Solution 3).

Table 2 - Solutions composition used in 3D REACTIVE TRANSPORT MODEL.

Solution 1 - initial solution				Solution 2 - GHB		Solution 3 - RCH	
	average	min	max				
T (°C)	14.43	13.40	14.20	**T (°C)**	14.43	**T (°C)**	14.20
pH	6.98	6.97	6.85	**pH**	6.98	**pH**	6.55
pe	-1.71	-1.26	-1.81	**pe**	-1.50	**pe**	f(O2 atm)
	Chemicals [mg/L]			*Chemicals [mg/L]*		*Chemicals [µg/L]*	
HCO3-	550.320	517.000	556.600	**HCO3-**	550.320	**Ca**	105.220
As	0.027	0.001	0.045	**Ca**	112.010	**Cl**	63.300
B	0.076	0.087	0.082	**Cl**	42.440	**Mg**	37.950
Ca	112.010	56.900	125.500	**K**	3.160	**Na**	97.800
Cl	42.440	22.000	43.000	**Mg**	33.700	**NO2**	65.250
F	0.360	0.190	0.150	**Na**	42.290	**SO4-2**	41.950
Fe	1.648	0.633	1.805	**Si**	8.060		
K	3.160	2.300	2.000				
Mg	33.700	35.700	37.000				
Mn	48.160	0.163	0.247				
NH4+	1.610	0.380	2.550				
Na	42.290	28.600	30.100				
PO4-3	0.090	0.040	0.030				
SO4-2	93.090	70.000	0.220				
Si	8.060	4.590	7.810				

- Equilibrium phases

The second part of the file defines the chemical concentration of the mineral phases reacting in equilibrium with groundwater. The mineral phases considered for the model are the same used in the batch-like model (PHREEQC 0D model), thus, calcite and Ferrihydrite (amorphous Hfo). The "equilibrium phases" (as call in PHREEQC code) data block was defined for each material included in the spMC heterogeneity model. The minerals concentration was assigned using the mineralogical data obtained by XRD and XRF analyses for each material. As for the solution, even the "equilibrium phases" blocks were indexed, in order to assign them to each material in the PHAST grid. The indexes are 2, 3, 4, 5, which represents sand, silt, clay and peat respectively.

- Sorption surfaces

The same philosophy used for the equilibrium phases was adopted defining the sorption surfaces. The reactive surfaces were referred to the iron concentration in the solid matrix, following the procedure suggested in Appello and Postma, 2005. The concentration and the

proportions between strong binding sites and weak binding sites are the same described in section 3.5. In order to refer them to each material in the model, even the "Surface" data blocks were indexed and their indexes are the same for the previously described "equilibrium phases".

2.6.3 Preliminary results and discussion

Parameter calibration

The head levels collected through the three piezometers indicated in the previous chapters (PZP 36, PZP 40 and PZP 41) with a continuous hourly acquisition system were used as reference information for the model calibration. The flow model was calibrated through a trial and error method, in order to find out the best set of input parameters allowing for the reproduction of the hydraulic head distribution during the monitoring period. The calibration involved the hydraulic parameters of the sandy aquifer and the recharge rates associated to the RCH boundary conditions. The calibration for the fine materials was not considered because no data of hydraulic head within them are available, thus the parameters were set using literature values consistent with the system settings (see Table 1 in Flow model implementation). The recharge rate, assigned to each RCH boundary condition, was calibrated in order to reproduce the variations of the hydraulic head measurements collected during the weekly monitoring. The variation observed from the field data required a time-depended recharge rate, which decreases over the time as function of the progressively saturation of system due to rainfall infiltration. In the northern part of WAA, the recharge rate associated to RCH2 BC starts from an initial value of 10% of the total rainfall and decreases up to 1% after 97 days. In the southern and in the middle zones, instead, the assigned recharge rate varies from 10% (as initial condition) to 3% after 60 days, remaining on this stage till the end simulated period. The different recharge rate calibrated for the two areas is linked to the different degree of confinement and the degree of saturation of system. The calibrated recharge rates are in line with the value of 6% found out by Beretta et al., 2017.

Flow model

The developed numerical model of the groundwater flow results realistic and able to reproduce the hydraulic head distribution occurring in the study area during the evaluated period. The model output (Figure 7) shows how the WAA is characterized by anomalous hydraulic head distribution, mainly controlled by the mechanical drainage system running in its central part (described by the DRN boundary condition). The occurrence of this man-made elements, act to

preserve the agricultural setting of that area, creates a depressed hydraulic zone influencing the natural groundwater flow. In this setting the groundwater is forced to flow toward the central part of the WWA rather than flowing toward the venetian lagoon.

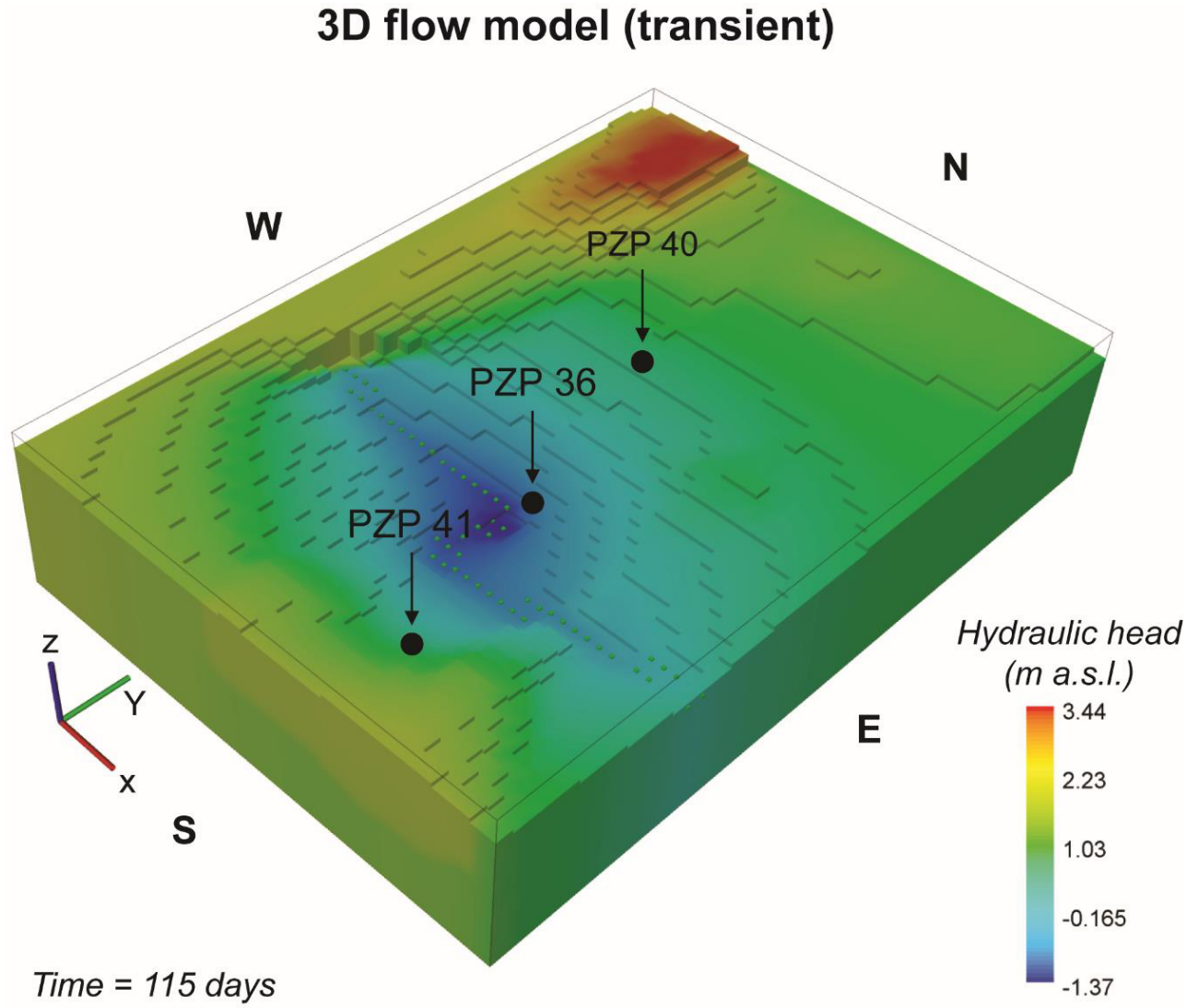

Figure 7 – Simulated hydraulic head distribution within the WAA. The result refers to the end of the transient simulation after 115 days. The central zone is characterized by a depressed potentiometric level due to the mechanical drainage system (green dots).

The recharge of system is due to both the regional contribute of the main aquifer bodies surrounding the WAA and the local infiltration of the rainfall. The effects of the latter process are relevant during the considered time period as the regional upstream recharge acts in longer time than the rainfall-based one. The groundwater velocity outlined by the numerical model, indeed, range between 0.3 m/d and 0.1 m/d, in accordance with the hydrogeological setting of the study area. The overall increasing/decreasing trend of hydraulic head is controlled by the regional water flow, but the faster oscillations are due to the effect of rainfall infiltration as

application of different recharge rates results in different simulated hydraulic head time series. The accuracy of the flow model was evaluated comparing analysis between the simulated hydraulic head time series and the observed ones. The observed time series refer to the three weekly monitored piezometer PZP36, PZP40 and PZP41, respectively located in the middle, northern and southern zones of WAA. The obtained results are shown in Figure 8.

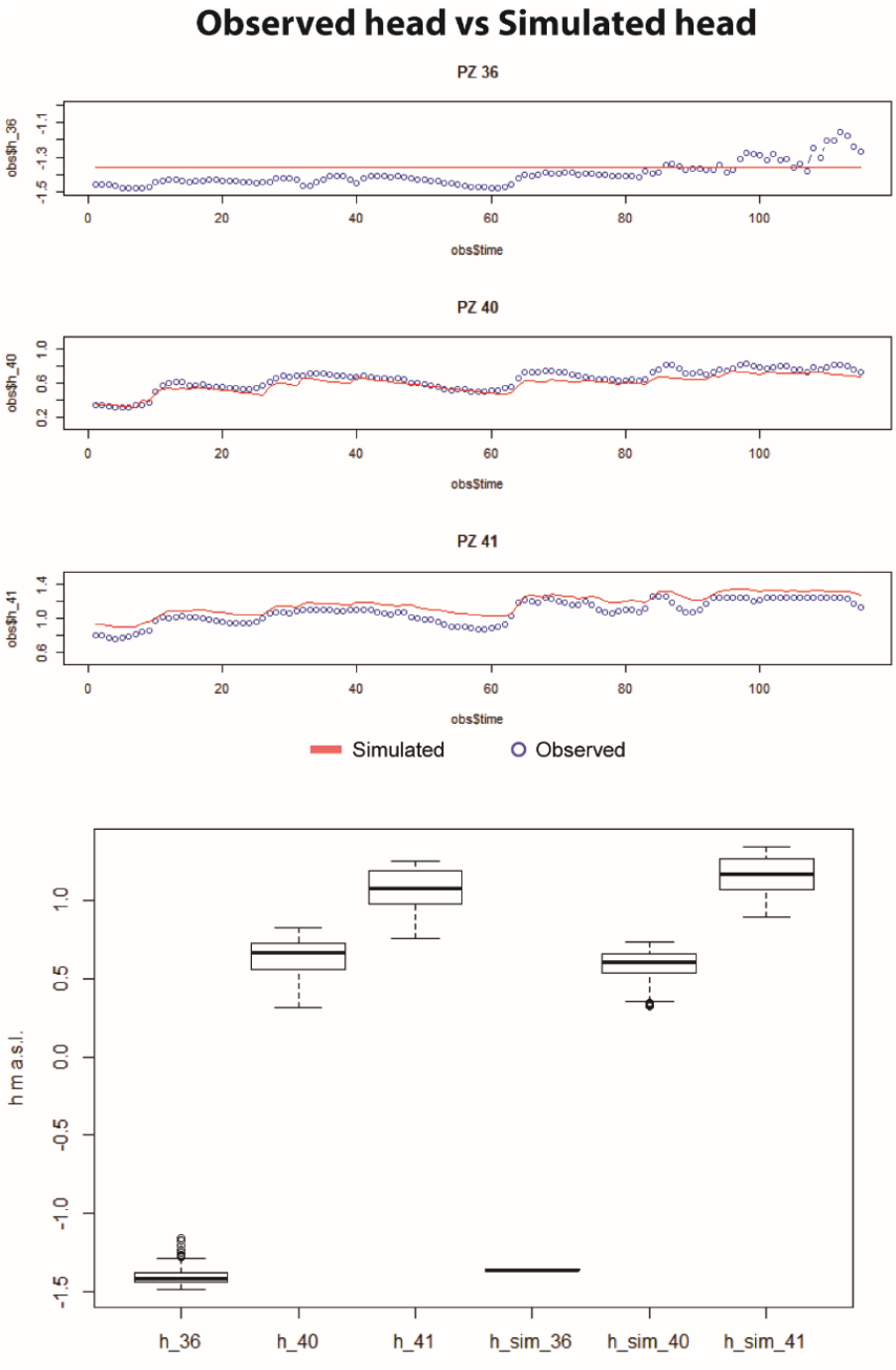

Figure 8 – Model accuracy evaluation. Comparison between the observed data collected through the weekly monitoring and the simulated data obtained by the 3D flow model. Both datasets are expressed using a daily lag time.

Observing graphs (Figure 8), the implemented numerical model is able to fit the main hydrogeological behavior of the study aquifer system. The associated average efficiency index, evaluated through the Nash-Sutcliffe method (Moriasi et al., 2007; Ritter and Munoz-Carpena, 2013), is equal to 0.33, confirming the reliability of the model. The middle part of WAA, represented by the results of PZP36, is the less accurate and it is due to the proximity to the DRN boundary. The problem might be solved applying a grid refinement around the PZP36 location. Unfortunately, this expedient was not applicable in this kind of model because of the integration of the stochastic subsurface heterogeneity model. If a grid refinement was applied the information of the material distribution, applied to each node, would be distorted. Thus, in order to preserve the integrity of the subsurface model and the effectiveness of the numerical flow model, the numerical model was set to reproduce the overall behavior of the system accurately (Figure 9). It seems to be a good tradeoff for achieving the purpose of the 3D reactive transport model.

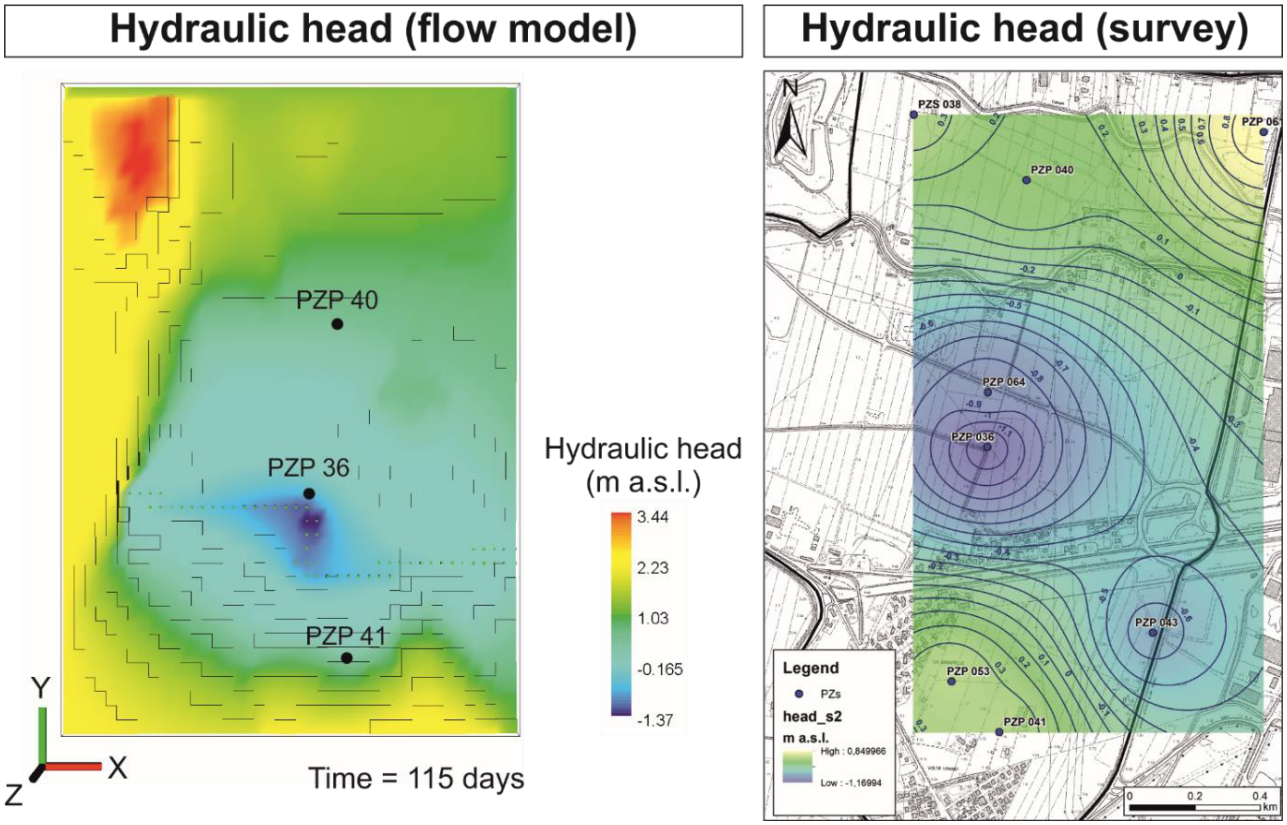

Figure 9 – Comparison between the hydraulic head distribution simulated through the 3D flow model in PHAST and the hydraulic head map obtained from the interpolation of the data collected during the surveys. The extension of the model is larger than the experimental map.

Reactive transport model

The reactive transport model was developed to evaluate the effectiveness of the chemical processes defined in section 2.5, in particular, the oxygen ingress mechanism. It is supposed to be one of the main actors driving toward different hydrochemical behaviors of the study aquifer, thus toward the patchy arsenic distribution of WAA. In order to achieve the aforementioned purpose, the reactive transport model was test under average chemical condition (using Solution 1 – average in Table 2). The average condition refers to the use of an initial solution characterized by an arsenic concentration representing the mean of the experimental data collected in the WAA during the monitoring period. This configuration allows to evaluate the response of the system under an average condition that could be used as proxy for further tests under different conditions (i.e. maximum and minimum scenarios). The Figure 10 shows the results obtained for the reactive transport model. The considered variables are the three main variables describing the processes supposed for the batch-like model in section 3.5. Just to remind, they are the reduced condition due to organic matter degradation, reductive dissolution of Hfo and the ingress of oxygen as function of recharge process. As visible in figure 10, the ingress of oxidized water is working forming an oxidized front that goes down toward the deeper part of the aquifer system as function of the recharge process. This behavior occurs in the whole area and it is visible in the three representative piezometers. Anyway, comparing the ORP profiles of the three piezometers, it is possible to observe the ingress of oxidized water varying at different depths of the sampling point. The PZP36, indeed, shows a more linear trend of pE in depth rather than the PZP40 and PZP41. This different behavior is due to the subsurface heterogeneity characterizing the WAA. The middle part of the study area, represented by PZP36, is characterized by a lesser amount of fine materials resulting in a semi-confined setting with an effective recharge process. This aquifer behavior was already observed in the results of the batch-like model reported in section 3.5. The sampling points, PZP40 and PZP41, show a similar behavior of ORP value (expressed as pE) with its sharp increase in the upper part of the system and a lesser variation downward toward the aquifer. This behavior is linked to the stratigraphic setting of both northern and southern part of WAA. The occurrence of thicker fine sediments layers on top of the sandy aquifer avoids an effective propagation of the oxidizing front due to the recharge process, in agree with a confined aquifer structure. Considering the iron and arsenic variables, their decrease in time and depth are in accordance with the increase of pE, as result of the sequestration of arsenic on the reactive surfaces of the precipitated Hfo (Figure 10). Considering the iron and arsenic trend, the central part has a different behavior with respect to the northern and southern ones. The behavior of arsenic and iron outlined the central role of ingress of oxygen in arsenic mobility, influencing the redox

condition of the aquifer system and the reductive dissolution of iron hydroxides. In the central part of WAA, the presence of a mechanical drainage system (simulated by the DRN boundary) could influence the mobility of oxygen and oxygenated water from surface to the aquifer. The drawdown of the water level desaturates the upper part of the system, enhancing both the movement of oxidized infiltration water front and, at the same times, the oxygen trapped within the pores. The wet front, coming from the surface, works like a “piston” that pushes down the air occurring in the unsaturated zone between itself and the water table. This mechanism could contribute to enhance the increase of pE in the aquifer located in the middle part of WAA. This is a hypothesis that required further investigations in the future.

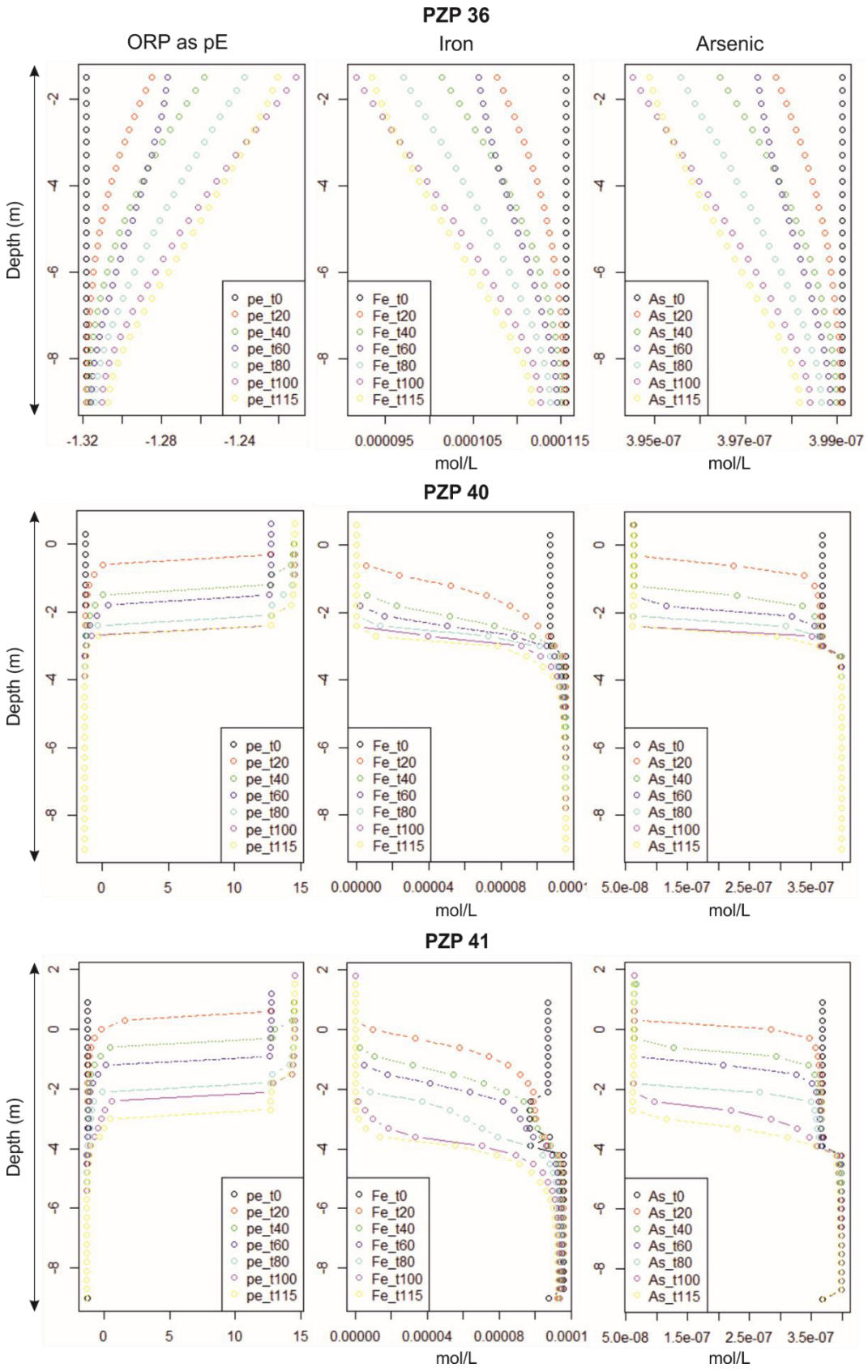

Figure 10 – Results of the reactive transport model performed under average system conditions. The colors represent the model output for a specific time step (black t = 0, red t = 20, green t = 40, blue t = 60, cyan t = 80, purple t = 100 and yellow t = 115 days).

The numerical model was also tested under minima (using Solution 1 – Min, Table 2) and maxima (using Solution 1 – Max, Table 2) conditions in As. The different chemical settings for the filling water composition were chose to reproduce the magnitude of arsenic occurrence observed in field data. These conditions were considered to evaluate the response of the system when it is under limit conditions. Figure 11 and Figure 12 show the results of these two models. As visible in diagrams of pE, Fe and As, the behavior of the aquifer system is quite similar to that obtained in the average condition. Some differences exist in the range of variation for the iron and arsenic concentrations, and they are in agree with the initial condition applied for the model. These evidences suggest that the initial chemical conditions, defined by the initial solution that fill the model, influences the output chemicals concentrations being the starting point for the hydrochemical evolution in time. The performed models were not able to reproduce the heterogeneous distribution of the arsenic because the initial conditions are homogeneous around the area. The future models should consider an initial condition fitting realistic distribution of arsenic as described in sections 2.3.1, 2.3.2 and 2.3.3.

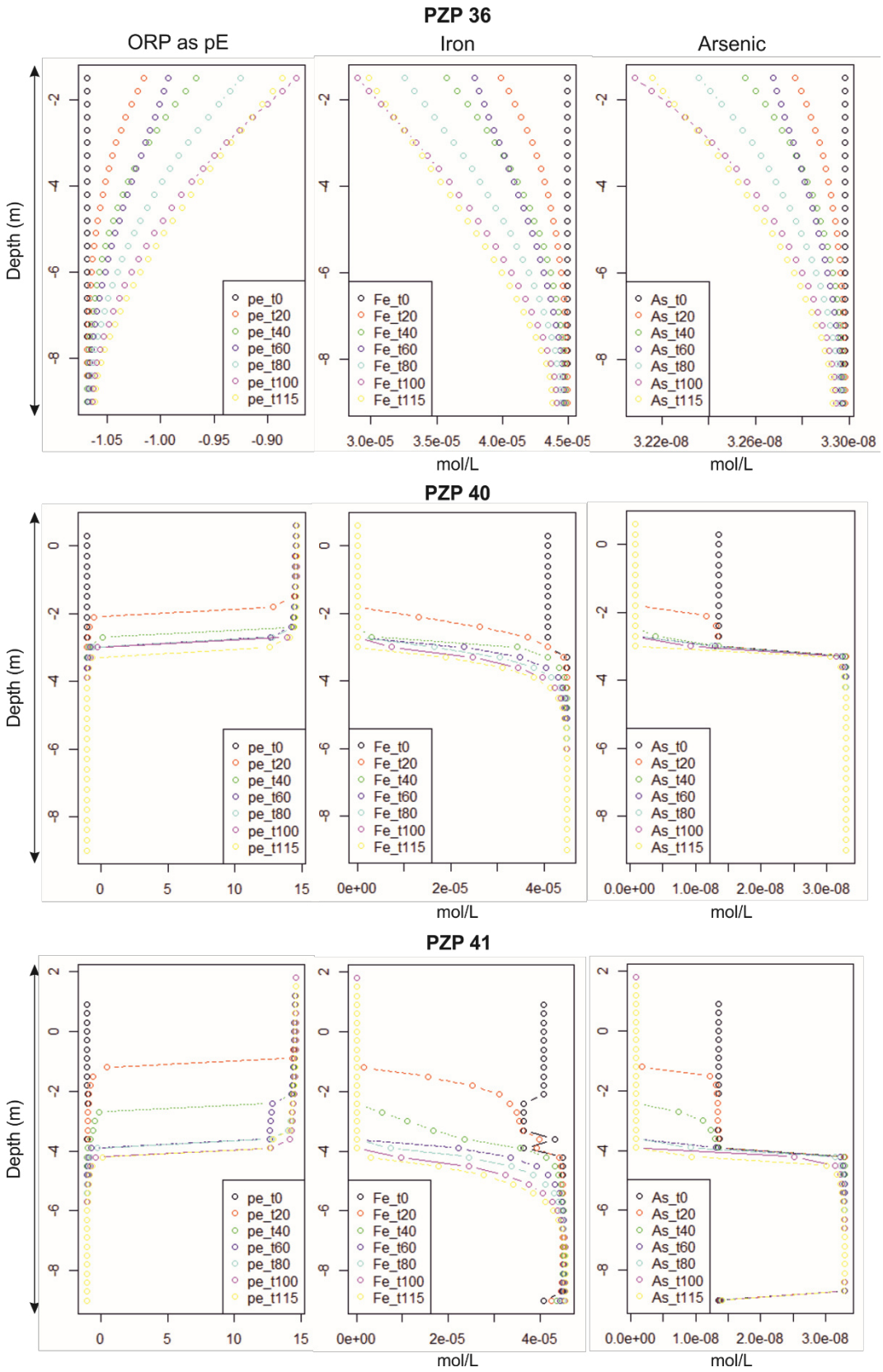

Figure 11 - Results of the reactive transport model performed under minima system conditions. The colors represent the model output for a specific time step (black t = 0, red t = 20, green t = 40, blue t = 60, cyan t = 80, purple t = 100 and yellow t = 115 days).

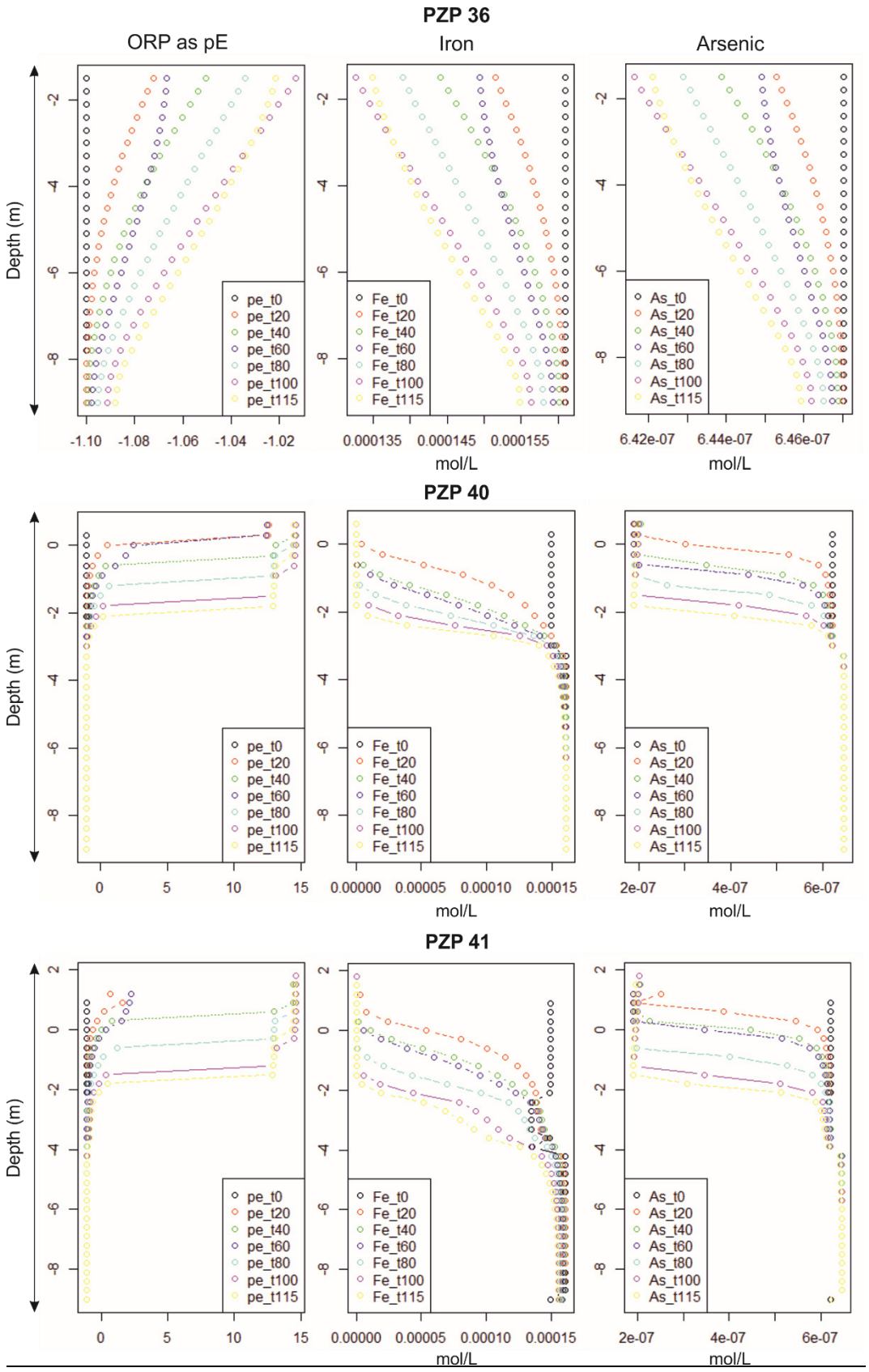

Figure 12 - Results of the reactive transport model performed under maxima system conditions. The colors represent the model output for a specific time step (black t = 0, red t = 20, green t = 40, blue t = 60, cyan t = 80, purple t = 100 and yellow t = 115 days).

2.6.4 Preliminary conclusions

The results obtained from the 3D reactive model confirm the effectiveness of the supposed chemical processes for arsenic mobility. The organic matter degradation together with the ingress of oxygen mainly control the redox variations of the study aquifer, influencing the reductive dissolution of iron hydroxides, thus arsenic mobility. As already supposed in the section 2.5, the heterogeneity of the subsurface plays an import role in controlling the hydrochemical processes involved in arsenic mobility. The fine material distribution, especially as cover layer, controls the ingress of oxygen linked to the local recharge events. This is an import result because it gives a clearer picture of the system behavior and evolution. The obtained information, although preliminary, lead toward a wider awareness about the arsenic contamination in the shallower aquifer of WAA, allowing for a more occulated environmental management by the stakeholders operating on that area. Nonetheless, the 3D reactive transport model development pointed out some murky aspects that give food for future thoughts. The construction of more realistic 3D reactive model is still a work in progress, but the right pathway seems to be marked for future developments.

References

Appelo, C.A.J., Postma, D., 2005. Geochemistry, groundwater and pollution. 2nd. Ed. Balkema, Rotterdam.

Beretta, G.P., Terrenghi, J., 2017. Groundwater flow in the Venice lagoon and remediation of the Porto Marghera industrial area (Italy). Hydrogeol. J., 25, 847–861.

Cooper, H.H., J.D. Bredehoeft and S.S. Papadopulos, 1967. Response of a finite-diameter well to an instantaneous charge of water, Water Resources Research, vol. 3, no. 1, pp. 263-269.

Duffield, G.M., 2007 AQTESOLV for Windows User's Guide. Version 4.5, HydroSOLVE, Inc., Reston.

Fletcher, C.A.J., 1991. Computational techniques for fluid dynamics, volume 1, 2d ed.: New York, Springer-Verlag, 401 p.

Gelhar, L.W., Welty, C., Rehfeldt, K.R., 1992. A critical review of data on field-scale dispersion in aquifers. Water Resour. Res. 28, 1955–1974. https://doi.org/10.1029/92WR00607

Kipp, K.L., 1987. HST3D—A computer code for simulation of heat and solute transport in three-dimensional ground-water flow systems: U.S. Geological Survey Water-Resources Investigations Report 86–4095, 517 p.

Kipp, K.L., 1997. Guide to the revised heat and solute transport simulator HST3D—Version 2: U.S. Geological Survey Water-Resources Investigations Report 97–4157, 149 p.

Moriasi, D.N., Arnold, J.G., Van Liew, M.W., Bingner, R.L., Harmel, R.D. and Veith, T.L., 2007. Model evaluation guidelines for systematic quantification of accuracy in watershed simulations. Transactions of the ASABE, 50(3), pp.885-900.

Parkhurst, D., Kipp, K., Charlton, S., 2010. PHAST Version 2 - A program for simulating groundwater flow, solute transport, and multicomponent geochemical reactions. Model. Tech. B. 6 1–181.

Parkhurst, D.L., Appelo, C.A.J., 2013. Description of input and examples for PHREEQC Version 3 — A computer program for speciation, batch-reaction, one-dimensional transport, and inverse geochemical calculations. U.S. Geol. Surv. Tech. Methods, B. 6, chapter A43 6-43A. https://doi.org/10.1016/0029-6554(94)90020-5

R Core Team, 2018. R: A language and environment for statistical computing. R Foundation for Statistical Computing, Vienna, Austria. URL https://www.R-project.org/.

Ritter, A., Muñoz-Carpena, R., 2013. Performance evaluation of hydrological models: Statistical significance for reducing subjectivity in goodness-of-fit assessments. J. Hydrol. 480, 33–45. https://doi.org/10.1016/j.jhydrol.2012.12.004

USDA, 1986. Urban hydrology for small watersheds. 210 - VI – TR – 55, Second edition.

3. General conclusions

The presented PhD project allowed to get several detailed information about a current topic as the arsenic groundwater contamination in the Venetian Alluvial Plain (VAP). The stakeholders' need for a more occulated environmental management and water quality preservation fed the will of improving the knowledge on arsenic release mechanism and the related processes influencing itself. So far, general studies on the VAP and WAA were performed, but they never reached details on the chemical processes behind the anomalous observed distributions of arsenic. They always focused on investigating the spatial distribution of arsenic and the chemical relationship between it and others dissolved chemicals. On the contrary, none of them posed their attention in evaluating the water-rock interaction processes that could be the base of arsenic occurrence in those areas. In this sense, the PhD work increases knowledge on the main chemical processes influencing arsenic mobility, as it developed a detailed analysis considering all the geological, hydrogeological and chemical aspects occurring in the study site. Furthermore, the strength of this study lies in the rational combination of these unavoidable aspects and the ability of involving them into the understanding process. Thanks to the application of advance methodologies in the main phases of the project and the innovative idea of coupling themselves for enhancing the investigation capabilities, this study allowed for obtaining detailed results useful for both groundwater and environmental management and further investigations. The performed geostatistical subsurface reconstruction defined a detail heterogeneity model, describing the overall stratigraphical setting of the area and, at the same time, providing sufficient detail on specific zones. The chemical model, instead, elucidated the main characteristics of the hydrochemical environment persisting into WAA, and more likely into VAP. The evaluation and the outlining of the main hydrochemical processes governing arsenic contamination shed light on the central role of the reductive dissolution of iron hydroxides as the main arsenic release process in that area. This process, as outlined through the chemical model, is strictly connected with the occurrence of organic matter in subsoil, whose degradation leads toward reduced conditions, favorable for arsenic release. Another important factor, which was never considered for affecting the system behavior, is represented by the ingress of oxygen through the vadose zone. The performed analysis gave clear hints about the oxygen main contribute in arsenic dynamics in presence of semi-confined or unconfined aquifers. As demonstrated by the chemical model and the 3D reactive transport model, the ingress of oxygen, as function of the local recharge rate, can avoid the arsenic mobilization, especially in those area characterized by semi-confined or unconfined setting.

Under those conditions, hydrogeological system is more susceptible to the infiltration of oxidizing rainfall, due to the downward transport of oxygen. Thus, the interaction between oxygen from the vadose zone and the underlyng aquifer shifts the redox condition to an oxidized environment, which allows for arsenic sequestration. Moreover, the applied methodologies (i.e.: PHREEQC chemical model and 3D reactive transport one) allowed to highlight the subsurface heterogeneity influence on arsenic mobilization. The study proved how the chemical factors are strongly linked to the heterogeneity of the subsoil, confirming the importance of heterogeneity in contaminant behavior. The spatial occurrence of both orgenic matter and fine materials, thus the variability of such linked chemical mechanisms pointed out in this thesis (i.e.: reductive dissolution of HFOs, ingress of oxygen as function of local recharge), are clear examples of how and how much the heterogeneity is important in environmental studies. Information about the heterogeneity is often neglected because difficult to manage, nonetheless its role is quite evident, especially in so heterogeneous systems like alluvial aquifer ones. In conclusion, the hydrochemical features, outlined in this PhD project, increase the knowledge in arsenic groundwater contamination affecting WAA, thus VAP alluvial plain, but they could be further enhanced especially about a 3D reactive transport model approach. The 3D advective-reactive transport modeling, indeed, is an advanced tool that has huge potentialities for helping the environmental management and the related decisions. The chemical model (PHREEQC model) by itself can give lot of information about the contaminant behavior, but the real improvement comes out when these chemical evidences are coupled with a transport model able to describe contaminat's fate over both the space and time. Furthermore, the potentiality of a 3D reactive transport modeling lies in its capability of involving the subsurface heterogeneity information, a substantial improvement respect to the sole chemical model. In this direction, the PhD project doesn't want to be conclusive, rather, it aims to be a starting point for future pioneering investigations able to dig out new hidden knowledge on arsenic behavior and a more realistic and more detailed 3D reactive transport model as well.

Acknowledgements

The list of people that are worthy of gratitude for teaching and supporting me during my PhD career is very long. First of all, I would like to express my special thanks of gratitude to my Supervisor Paolo Fabbri, who give me the golden opportunity to do this important experience, both from the professional and personal perspective. Another great thanks to my Co-supervisor Fabio Tateo for helping me during field and laboratory activities. Many thanks go to Daniele Pedretti (GTK Finland and University of Milan) to support and teach me during my research period in Helsinki. Thanks to Prof. Kirsti Korkka-Niemi, who gave me the opportunity to spend an amazing period at University of Helsinki, during which I learnt lots of things and I met lots of capable people. I would like to say "thank you" to Leonardo Piccinini for helping me during the modeling sessions. Thanks to Filippo Torresan, who shared with me ideas and gave me a different point of view on modeling troubleshooting. A great thanks to anyone who encouraged me, supported me and drove me to do my best for achieve this objective.

Supplementary materials

- Table S1 - Physic and chemical parameters for WAA's groundwater;
- Table S2 – Mineralogical and chemical analyses for WAA's soil samples;
- Table S3 - List of geochemical reactions considered for the WAA aquifer model. The model is based on WATEQ4F database (Ball and Nordstrom, 1991).
- Figure S4 – Location of PZP 036, PZP 040, PZP 041 and stratigraphic logs. 1) Log of PZP 036, 2) Log of PZP 040 and 3) Log of PZP 041.
- Figure S5 – Slug test interpretation diagrams for PZP 36.
- Figure S6 - Slug test interpretation diagrams for PZS 38.
- Figure S7 - Slug test interpretation diagrams for PZP 40.
- Figure S8 - Slug test interpretation diagrams for PZP 41.
- Figure S9 - Slug test interpretation diagrams for PZP 43.
- Figure S10 - Slug test interpretation diagrams for PZP 53.
- Figure S11 - Slug test interpretation diagrams for PZP 61.
- Figure S12 - Slug test interpretation diagrams for PZP 64.

Table S1

Seasonal surveys

ID_PZ	Date_survey	n_survey	T_ext_air	T_H2O	P_atm	pH	ORP	EC	HCO3	NH4	NO2	NO3	PO4	SO4	F	Cl	Na	K	Mg	Ca	Si	S	TOC	TSS	TDS	Al	As	B	Be	Cd	Co	Cu	Cr	Fe	Hg	Mn	Ni	Pb	Sb	Zn
			°C	°C	mbars		mV	µS/cm	mg/L	mg/L	mg/L	mg/L	mg/L	mg/L	mg/L	mg/L	mg/L	mg/L	mg/L	mg/L	mg/L	mg/L	mg/L	mg/L	mg/L	µg/L	µg/L	µg/L	µg/L	µg/L	µg/L	µg/L	µg/L	µg/L	µg/L	µg/L	µg/L	µg/L	µg/L
PZP 036	2017-10-10	1S	22.50	14.20	1019.00	7.16	-161.00	855.00	539.00	0.91	<0.01	<1	0.10	71.00	0.16	21.00	26.50	2.10	31.60	135.60	5.15	<0.1	3.00	608.00	572.85	2.00	3.00	78.00	<1	<0.1	<0.5	1.00	<0.5	1257.00	<0.2	162.00	<1	<0.4	<1	<5
PZP 040	2017-10-12	1S	20.40	17.00	1024.30	7.07	-110.40	886.00	530.90	0.15	<0.01	<1	<0.03	31.00	0.27	34.00	18.90	0.80	45.10	119.70	7.45	<0.1	1.50	9.00	593.62	1.00	17.00	14.00	<1	<0.1	<0.5	1.00	<0.5	1464.00	<0.2	168.00	<1	<0.4	<1	<5
PZP 041	2017-10-11	1S	21.50	14.30	1022.70	7.02	-141.20	881.00	539.00	3.67	<0.01	<1	0.14	12.00	0.13	45.00	33.90	2.40	34.10	118.60	10.40	<0.1	3.40	8.00	590.27	1.00	16.00	77.00	<1	<0.1	<0.5	<1	<0.5	2245.00	<0.2	195.00	<1	<0.4	<1	<5
PZP 043	2017-10-11	1S	18.50	15.10	1023.70	7.10	-100.30	737.00	477.00	3.44	0.04	<1	0.12	<1	0.19	33.00	30.20	2.40	31.20	92.40	8.80	<0.1	3.70	8.00	493.79	1.00	29.00	48.00	<1	<0.1	<0.5	1.00	<0.5	1391.00	<0.2	119.00	<1	<0.4	<1	<5
PZP 053	2017-12-06	1S	4.50	13.90	1032.70	7.27	-137.20	611.00	438.70	2.50	<0.01	<1	<0.03	<3	0.25	15.00	9.80	7.50	23.70	91.40	10.82	<0.1	2.00	46.00	409.37	1.00	126.00	21.00	<1	<0.1	<0.5	<1	<0.5	1441.00	<0.2	153.00	<1	<0.4	<1	<5
PZP 061	2017-10-11	1S	22.00	15.80	1022.90	6.78	-78.90	2432.00	688.00	0.12	<0.01	<1	0.05	<1	1.50	135.00	151.60	2.70	137.00	294.00	8.50	<0.1	5.00	900.00	1629.44	3.00	8.00	251.00	<1	<0.1	1.10	<1	<0.5	1240.00	<0.2	696.00	2.00	<0.4	<1	<5
PZP 064	2017-10-10	1S	23.90	16.20	1018.60	7.18	-151.30	894.00	498.00	0.79	<0.01	<1	0.34	56.00	0.19	48.00	35.80	7.20	29.00	128.60	5.03	<0.1	2.60	21.00	598.98	2.00	14.00	65.00	<1	<0.1	0.50	1.00	<0.5	2779.00	<0.2	370.00	1.00	<0.4	<1	<5
PZS 038	2017-10-12	1S	23.40	14.30	1024.40	6.90	-48.30	904.00	636.50	2.30	<0.01	<1	<0.03	<1	0.10	26.00	28.20	2.50	42.20	129.20	9.00	<0.1	2.90	219.00	605.68	<1	11.00	28.00	<1	<0.1	<0.5	<1	<0.5	3222.00	<0.2	159.00	<1	<0.4	<1	<5
PZP 036	2018-01-29	2S	7.80	13.40	1031.50	6.97	-71.80	883.00	517.00	0.38	<0.01	<1	0.04	78.00	0.19	22.00	28.60	2.30	35.70	56.90	4.59	<0.1	1.30	44.00	591.61	1.00	1.00	87.00	<1	<0.1	<0.5	<1	<0.5	633.00	<0.2	163.00	<1	<0.4	<1	<5
PZP 040	2018-01-30	2S	6.90	12.20	1029.70	6.96	-78.10	883.00	535.00	0.12	<0.01	<1	<0.03	41.00	0.29	34.00	19.70	0.70	50.30	73.80	6.95	<0.1	1.00	13.00	591.61	1.00	17.00	11.00	<1	<0.1	<0.5	<1	<0.5	1998.00	<0.2	126.00	<1	<0.4	<1	<5
PZP 041	2018-01-29	2S	5.30	14.00	1033.50	6.88	-136.30	883.00	545.00	3.06	<0.01	<1	0.10	18.00	0.14	43.00	33.50	2.40	36.50	51.80	10.41	<0.1	2.70	4.00	591.61	1.00	23.00	82.00	<1	<0.1	<0.5	<1	<0.5	2097.00	<0.2	227.00	<1	<0.4	<1	<5
PZP 043	2018-01-29	2S	8.50	14.00	1032.60	6.95	-83.20	734.00	475.00	3.40	<0.01	<1	0.10	<1	0.20	32.00	31.80	2.50	33.00	46.30	9.10	<0.1	3.30	10.00	491.78	2.00	30.00	55.00	<1	<0.1	<0.5	<1	<0.5	1443.00	<0.2	117.00	<1	<0.4	<1	<5
PZP 053	2018-01-29	2S	6.70	13.70	1033.30	7.00	-123.00	612.00	417.00	2.21	<0.01	<1	0.21	<1	0.20	15.00	10.40	2.40	25.50	47.10	11.58	<0.1	1.90	13.00	410.04	1.00	111.00	22.00	<1	<0.1	<0.5	<1	<0.5	1859.00	<0.2	108.00	<1	<0.4	<1	<5
PZP 061	2018-01-30	2S	8.50	14.40	1029.10	6.68	-9.80	2481.00	827.00	0.04	<0.01	<1	<0.03	1125.00	1.60	110.00	148.00	5.20	140.80	269.00	7.14	<0.1	5.90	5925.00	1662.27	2.00	5.00	266.00	<1	<0.1	1.30	3.00	<0.5	454.00	<0.2	363.00	3.00	<0.4	<1	10.00
PZP 064	2018-01-30	2S	7.80	14.30	1029.60	7.04	-42.60	888.00	484.00	0.34	0.04	1.00	0.15	53.00	0.31	44.00	42.20	5.00	30.90	67.70	4.91	<0.1	1.50	9.00	594.96	2.00	5.00	83.00	<1	<0.1	0.80	<1	<0.5	385.00	<0.2	199.00	1.00	<0.4	<1	<5
PZS 038	2018-01-30	2S	5.90	14.00	1029.60	6.78	-87.40	881.00	658.00	2.37	<0.01	<1	0.03	<1	0.11	22.00	27.60	2.40	44.00	70.10	9.08	<0.1	2.30	62.00	590.27	1.00	9.00	34.00	<1	<0.1	<0.5	<1	<0.5	2460.00	<0.2	144.00	<1	<0.4	<1	<5

Weekly surveys

ID_PZ	Date_survey	n_survey	T_ext_air	T_H2O	P_atm	pH	ORP	EC	HCO3	NH4	NO2	NO3	PO4	SO4	F	Cl	Na	K	Mg	Ca	Si	S	TOC	TSS	TDS	Al	As	B	Be	Cd	Co	Cu	Cr	Fe	Hg	Mn	Ni	Pb	Sb	Zn
			°C	°C	mbars		mV	µS/cm	mg/L	mg/L	mg/L	mg/L	mg/L	mg/L	mg/L	mg/L	mg/L	mg/L	mg/L	mg/L	mg/L	mg/L	mg/L	mg/L	mg/L	µg/L	µg/L	µg/L	µg/L	µg/L	µg/L	µg/L	µg/L	µg/L	µg/L	µg/L	µg/L	µg/L	µg/L
PZP 036	2017-12-06	1M	10.00	14.20	1031.80	7.22	-106.50	885.00	533.60	0.77	<0.01	<1	0.03	80.00	0.18	23.00	27.80	2.20	33.70	136.70	5.19	<0.1	1.20	934.00	592.95	1.00	2.00	83.00	<1	<0.1	<0.5	1.00	<0.5	1198.00	<0.2	160.00	<1	<0.4	<1	<5
PZP 036	2017-12-14	2M	6.70	14.10	1007.80	7.23	-113.30	880.00	533.30	0.65	<0.01	<1	0.14	73.00	0.18	24.00	27.50	2.20	33.70	135.00	5.04	<0.1	1.10	152.00	589.60	1.00	1.00	87.00	<1	<0.1	<0.5	1.00	<0.5	1153.00	<0.2	141.00	<1	<0.4	<1	<5
PZP 036	2017-12-21	3M	5.20	14.10	1034.10	6.97	-93.00	884.00	513.00	0.59	<0.01	<0.5	0.09	72.00	0.18	24.00	27.30	2.30	34.10	139.20	5.21	<0.1	1.20	58.00	592.28	1.00	1.00	79.00	<1	<0.1	<0.5	<1	<0.5	1151.00	<0.2	146.00	<1	<0.4	<1	<5
PZP 036	2018-01-04	4M	6.80	13.80	1008.70	6.97	-85.10	875.00	521.20	0.52	<0.01	<1	0.11	82.00	0.18	23.00	26.10	2.10	33.80	138.60	4.62	<0.1	1.10	8.00	586.25	1.00	1.00	67.00	<1	<0.1	<0.5	<1	<0.5	911.00	<0.2	153.00	<1	<0.4	<1	<5
PZP 036	2018-01-11	5M	10.50	13.90	1012.80	6.96	-77.50	880.00	523.70	0.50	<0.01	1.00	0.05	91.00	0.16	23.00	26.50	2.20	34.20	140.50	3.95	<0.1	1.10	60.00	589.60	1.00	1.00	92.00	<1	<0.1	<0.5	<1	<0.5	766.00	<0.2	159.00	<1	<0.4	<1	<5
PZP 036	2018-01-18	6M	9.60	13.50	1013.50	6.97	-94.50	876.00	503.00	0.42	<0.01	1.00	<0.03	89.00	0.19	23.00	27.50	2.10	34.50	135.00	4.65	<0.1	0.70	113.00	586.92	1.00	2.00	95.00	<1	<0.1	<0.5	2.00	<0.5	722.00	<0.2	171.00	<1	<0.4	<1	<5
PZP 036	2018-01-25	7M	8.20	13.20	1027.00	6.96	-95.60	883.00	509.00	0.37	<0.01	<1	0.03	80.00	0.21	23.00	28.10	2.20	35.70	70.30	4.55	<0.1	1.30	16.00	591.61	1.00	1.00	84.00	<1	<0.1	<0.5	1.00	<0.5	588.00	<0.2	172.00	1.00	<0.4	<1	<5
PZP 036	2018-02-08	8M	11.00	13.20	1014.10	6.96	-55.00	866.00	515.00	0.36	0.02	<1	<0.03	80.00	0.20	21.00	26.10	2.10	34.20	137.90	4.59	<0.1	1.30	8.00	580.22	1.00	<1	88.00	<1	<0.1	<0.5	<1	<0.5	379.00	<0.2	171.00	1.00	<0.04	<1	<5
PZP 036	2018-02-15	9M	7.50	12.90	1024.20	6.98	-63.60	870.00	541.80	0.38	0.01	1.00	<0.03	77.00	0.18	22.00	25.10	2.10	34.30	141.20	4.82	<0.1	1.20	8.00	582.90	1.00	<1	76.00	<1	<0.1	<0.5	<1	<0.5	283.00	<0.2	160.00	1.00	<0.04	<1	<5
PZP 036	2018-02-26	10M	1.00	13.10	1010.80	7.03	-53.70	864.00	498.00	0.36	<0.01	1.00	0.03	74.00	0.20	21.00	24.00	2.00	34.30	138.20	4.48	<0.1	0.90	15.00	578.88	1.00	<1	90.00	<1	<0.1	<0.5	1.00	<0.5	245.00	<0.2	152.00	1.00	<0.4	<1	<5
PZP 036	2018-03-05	11M	10.30	12.70	1000.20	6.99	-36.60	852.00	508.89	0.35	<0.01	33.00	<0.03	72.00	0.38	22.00	24.00	2.00	34.10	138.00	4.69	<0.1	0.90	<5	570.84	2.00	<1	74.00	<1	<0.1	<0.5	1.00	<0.5	163.00	<0.2	139.00	2.00	<0.4	<1	<5
PZP 036	2018-03-26	12M	12.60	12.90	1010.00	6.95	0.90	853.00	522.00	0.27	<0.01	<1	0.03	67.00	0.18	24.00	21.60	2.00	33.90	112.50	4.77	<0.1	1.10	<5	571.51	1.00	<1	66.00	<1	<0.1	0.70	1.00	<0.5	75.00	<0.2	127.00	4.00	<0.4	<1	<5
PZP 040	2017-12-06	1M	8.00	15.00	1031.40	7.14	-67.60	882.00	555.60	0.15	<0.01	<1	<0.03	24.00	0.28	32.00	18.80	0.80	46.00	123.70	7.33	<0.1	1.40	32.00	590.94	2.00	11.00	13.00	<1	<0.1	<0.5	1.00	<0.5	1203.00	<0.2	139.00	<1	<0.4	<1	<5
PZP 040	2017-12-14	2M	7.10	14.50	1006.90	7.17	-81.70	882.00	565.80	0.14	<0.01	<1	<0.03	28.00	0.25	31.00	19.10	0.70	47.00	123.40	6.99	<0.1	1.20	12.00	590.94	1.00	13.00	12.00	<1	<0.1	<0.5	<1	<0.5	1530.00	<0.2	153.00	<1	<0.4	<1	<5
PZP 040	2017-12-21	3M	2.90	14.10	1035.00	6.89	-42.00	881.00	551.00	0.12	<0.01	<0.5	<0.03	28.00	0.28	31.00	18.80	0.70	46.80	124.50	7.01	<0.1	1.10	14.00	590.27	1.00	10.00	11.00	<1	<0.1	<0.5	<1	<0.5	651.00	<0.2	132.00	<1	<0.4	<1	<5
PZP 040	2018-01-04	4M	2.60	13.30	1009.00	6.91	-91.60	880.00	620.50	0.14	<0.01	<1	<0.03	35.00	0.28	32.00	18.90	0.60	47.60	123.00	6.44	<0.1	1.10	6.00	589.60	1.00	12.00	9.00	<1	<0.1	<0.5	<1	<0.5	1332.00	<0.2	124.00	<1	<0.4	<1	<5
PZP 040	2018-01-11	5M	8.90	13.00	1013.40	6.91	-95.30	879.00	574.80	0.13	0.01	1.00	<0.03	37.00	0.30	33.00	19.00	0.50	48.20	122.20	5.61	<0.1	1.10	<5	588.93	<1	13.00	14.00	<1	<0.1	<0.5	<1	<0.5	1560.00	<0.2	124.00	<1	<0.4	<1	<5
PZP 040	2018-01-18	6M	4.70	12.80	1014.70	6.91	-74.70	881.00	578.70	0.13	0.02	1.00	<0.03	42.00	0.30	37.00	19.00	0.60	48.20	120.00	6.82	<0.1	0.60	9.00	590.27	1.00	13.00	64.00	<1	<0.1	<0.5	1.00	<0.5	1429.00	<0.2	128.00	<1	<0.4	<1	<5
PZP 040	2018-01-25	7M	5.70	12.50	1028.00	6.89	-100.10	883.00	550.00	0.13	<0.01	<1	<0.03	38.00	0.28	33.00	19.80	0.60	49.80	67.50	6.79	<0.1	1.00	<5	591.61	<1	17.00	15.00	<1	<0.1	<0.5	<1	<0.5	1872.00	<0.2	126.00	<1	<0.4	<1	<5
PZP 040	2018-02-08	8M	10.00	12.30	1013.70	6.90	-86.40	886.00	571.00	0.12	0.01	<1	<0.03	38.00	0.28	33.00	18.90	0.50	48.30	122.60	6.69	<0.1	1.10	5.00	593.62	<1	16.00	11.00	<1	<0.1	<0.5	<1	<0.5	1946.00	<0.2	125.00	<1	<0.4	<1	<5
PZP 040	2018-02-15	9M	4.60	11.90	1024.10	6.90	-95.80	883.00	594.80	0.12	0.02	1.00	<0.03	43.00	0.29	35.00	19.00	0.50	49.20	123.10	6.61	<0.1	1.10	5.00	591.61	1.00	15.00	10.00	<1	<0.1	<0.5	<1	<0.5	1786.00	<0.2	124.00	<1	<0.4	<1	<5
PZP 040	2018-02-26	10M	-0.60	11.40	1011.20	6.97	-84.30	879.00	552.00	0.13	<0.1	1.00	<0.03	42.00	0.29	35.00	19.40	0.50	49.30	121.80	6.73	<0.1	1.50	7.00	588.93	1.00	13.00	10.00	<1	<0.1	<0.5	<1	<0.5	1452.00	<0.2	118.00	<1	<0.4	<1	<5
PZP 040	2018-03-05	11M	6.30	11.30	1000.90	6.89	-95.20	881.00	539.00	0.14	<0.01	1.00	<0.03	43.00	0.30	35.00	19.10	0.50	49.30	122.20	6.83	<0.1	1.00	<5	590.27	2.00	13.00	10.00	<1	<0.1	<0.5	1.00	<0.5	1914.00	<0.2	120.00	<1	<0.4	<1	<5
PZP 040	2018-03-26	12M	10.30	11.20	1010.00	6.86	-66.30	879.00	538.00	0.10	0.01	1.00	<0.03	43.00	0.26	35.00	19.00	0.50	49.70	95.20	6.88	<0.1	0.90	<5	588.93	1.00	10.00	9.00	<1	<0.1	<0.5	<1	<0.5	1087.00	<0.2	109.00	<1	<0.4	<1	<5
PZP 041	2017-12-06	1M	5.80	14.30	1033.40	7.10	-171.90	870.00	572.70	3.73	<0.01	<1	0.03	17.00	0.16	45.00	31.70	2.50	34.90	117.90	10.41	<0.1	2.70	17.00	582.90	1.00	14.00	77.00	<1	<0.1	<0.5	2.00	<0.5	1682.00	<0.2	194.00	<1	<0.4	<1	<5
PZP 041	2017-12-14	2M	5.20	14.30	1009.40	7.12	-173.70	841.00	589.10	2.52	<0.01	<1	0.09	16.00	0.13	36.00	24.60	1.90	35.20	120.80	9.89	<0.1	2.30	73.00	563.47	1.00	9.00	8.00	<1	<0.1	<0.5	<1	<0.5	1682.00	<0.2	238.00	<1	<0.4	<1	<5
PZP 041	2017-12-21	3M	5.20	14.20	1033.40	6.86	-134.40	873.00	530.00	2.79	<0.01	<0.5	0.10	20.00	0.15	39.00	28.40	2.00	36.10	122.70	10.13	<0.1	2.40	24.00	584.91	1.00	12.00	61.00	<1	<0.1	<0.5	<1	<0.5	2005.00	<0.2	220.00	<1	<0.4	<1	<5
PZP 041	2018-01-04	4M	8.10	14.00	1007.50	6.87	-55.60	881.00	551.30	1.72	<0.01	2.00	<0.03	30.00	0.20	37.00	24.60	1.70	37.40	131.40	8.24	<0.1	2.60	<5	590.27	1.00	21.00	46.00	<1	<0.1	<0.5	<1	<0.5	375.00	<0.2	195.00	1.00	<0.4	<1	13.00
PZP 041	2018-01-11	5M	10.00	14.20	1012.50	6.85	-103.40	897.00	556.60	2.55	<0.01	<1	0.03	22.00	0.15	43.00	30.10	2.00	37.00	125.50	7.81	<0.1	2.60	12.00	600.99	1.00	45.00	82.00	<1	<0.1	<0.5	<1	<0.5	1805.00	<0.2	247.00	1.00	<0.4	<1	11.00
PZP 041	2018-01-18	6M	10.50	14.20	1012.00	6.87	-126.00	894.00	547.70	2.73	<0.01	<1	<0.03	20.00	0.17	42.00	30.40	2.00	36.60	122.00	9.85	<0.1	1.90	6.00	598.98	1.00	40.00	86.00	<1	<0.1	<0.5	1.00	<0.5	2187.00	<0.2	243.00	<1	<0.4	<1	<5
PZP 041	2018-01-25	7M	7.80	14.10	1025.70	6.87	-134.90	889.00	535.00	2.99	<0.01	<1	0.07	19.00	0.15	44.00	33.10	2.30	36.90	58.10	10.14	<0.1	2.70	13.00	595.63	<1	27.00	83.00	<1	<0.1	<0.5	<1	<0.5	2312.00	<0.2	231.00	<1	<0.4	<1	<5
PZP 041	2018-02-08	8M	10.90	13.10	1013.90	6.83	-3.40	1050.00	603.00	0.55	0.28	30.00	<0.03	92.00	0.35	43.00	25.10	1.10	41.60	171.40	5.99	<0.1	3.40	<5	703.50	1.00	8.00	48.00	<1	<0.1	0.50	2.00	<0.5	208.00	<0.2	180.00	2.00	<0.4	2.00	79.00
PZP 041	2018-02-15	9M	8.70	13.60	1023.40	6.88	-38.50	979.00	564.00	0.84	0.30	10.00	<0.03	61.00	0.36	45.00	28.60	1.50	39.30	157.10	7.13	<0.1	2.90	<5	655.93	1.00	11.00	57.00	<1	<0.1	0.50	2.00	<0.5	292.00	<0.2	203.00	2.00	<0.4	2.00	82.00
PZP 041	2018-02-26	10M	1.30	12.90	1009.90	6.88	-40.30	1033.00	558.00	0.53	0.45	6.00	<0.03	75.00	0.34	44.00	26.70	1.30	40.50	166.80	6.43	<0.1	3.20	<5	692.11	1.00	5.00	54.00	<1	<0.1	<0.5	1.00	<0.5	151.00	<0.2	207.00	2.00	<0.4	2.00	82.00
PZP 041	2018-03-05	11M	10.10	12.60	998.90	6.83	-28.40	1019.00	550.00	0.49	0.30	1.00	<0.03	74.00	0.20	46.00	25.70	1.20	40.90	165.40	6.59	<0.1	3.40	<5	682.73	2.00	5.00	47.00	<1	<0.1	0.50	2.00	<0.5	274.00	<0.2	196.00	2.00	<0.4	1.00	82.00
PZP 041	2018-03-26	12M	13.30	13.50	1009.90	6.85	-1.80	892.00	563.00	2.18	<0.01	<1	<0.03	19.00	0.27	45.00	32.90	2.50	35.60	105.30	9.04	<0.1	2.40	5.00	597.64	1.00	14.00	78.00	<1	<0.1	0.70	1.00	<0.5	165.00	<0.2	260.00	2.00	<0.4	1.00	68.00

Table S2

materials legend: c = clay; fs = fine sand; oc = organic clay; occ = over-consolidated clay; osi = organic silt; si = silt; ssi = sandy silt

				XRPD								
	m b.g.l.			*g/kg*								
ID_PZP	**depth**	**zone**	**material**	**Qtz**	**Dol**	**Cc**	**K-fd**	**Plg**	**Chl**	**Ill**	**Goe**	**Py**
36 A	1.20-1.30	vadose	ssi	352.000	247.000	148.000	33.000	90.000	41.000	88.000	0.000	0.000
36 B	1.80-1.90	aquifer	fs	372.000	181.000	171.000	26.000	107.000	45.000	98.000	0.000	0.394
38 A	1.60-1.70	vadose	ssi	485.000	143.000	13.000	26.000	154.000	47.000	131.000	0.000	0.790
38 B	2.25-2.35	vadose	oc	242.000	157.000	217.000	9.000	92.000	59.000	218.000	0.000	2.059
38 C	2.50-3.00	aquifer	fs	320.000	222.000	145.000	15.000	94.000	91.000	93.000	0.000	1.028
40 A	1.50-1.60	vadose	c	138.000	136.000	444.000	2.000	55.000	36.000	178.000	0.000	0.949
40 B	2.10-2.20	vadose	oc	296.000	151.000	187.000	8.000	86.000	55.000	213.000	0.000	0.473
40 C	2.40-2.50	vadose	oc	318.000	150.000	123.000	25.000	111.000	70.000	202.000	0.000	0.870
40 D	3.50-3.60	aquifer	fs	333.000	158.000	228.000	10.000	98.000	56.000	115.000	0.000	1.187
41 A	1.00-1.10	vadose	si	229.000	214.000	195.000	8.000	82.000	58.000	214.000	0.000	0.235
41 B	3.50-3.60	vadose	c	179.000	233.000	321.000	22.000	59.000	47.000	134.000	0.000	0.632
41 C	5.10-5.30	aquifer	fs	292.000	153.000	261.000	8.000	77.000	55.000	152.000	0.000	1.187
43 A	1.20-1.30	vadose	occ	211.000	118.000	330.000	3.000	73.000	41.000	208.000	15.000	1.028
43 B	1.60-1.70	vadose	si	346.000	229.000	113.000	26.000	118.000	57.000	109.000	0.000	1.425
43 C	1.90-2.45	aquifer	fs	342.000	221.000	109.000	26.000	114.000	65.000	122.000	0.000	0.394
53 A	1.40-1.85	vadose	oc	443.000	1.000	0.000	26.000	135.000	50.000	343.000	0.000	0.000
53 B	2.50-3.00	vadose	occ	202.000	162.000	270.000	4.000	81.000	58.000	220.000	0.000	0.949
53 C	3.75-5.80	vadose	c	135.000	141.000	452.000	1.000	46.000	46.000	175.000	0.000	1.662
53 D	5.80-5.85	aquifer	fs	364.000	164.000	175.000	31.000	131.000	54.000	76.000	0.000	3.169
61 A	1.15 - 1.65	vadose	osi	524.000	22.000	0.000	30.000	155.000	38.000	230.000	0.000	0.315
61 B	2.74 -3.50	vadose	c	195.000	133.000	370.000	7.000	68.000	58.000	166.000	0.000	0.552
61 C	4.15 - 4.60	vadose	ssi	398.000	149.000	212.000	23.000	102.000	53.000	62.000	0.000	1.425
61 D	4.60 - 5.40	aquifer	fs	327.000	137.000	218.000	30.000	124.000	57.000	106.000	0.000	1.187
64 A	1.40-1.80	vadose	ssi	423.000	67.000	85.000	25.000	130.000	36.000	219.000	10.000	0.870
64 B	1.80-2.30	vadose	ssi	333.000	131.000	148.000	13.000	118.000	50.000	198.000	6.000	0.711
64 C	2.30-2.85	aquifer	fs	430.000	133.000	121.000	46.000	111.000	52.000	102.000	0.000	0.394

				ICP-OES											
	m b.g.l.			*g/kg*											
ID_PZP	**depth**	**zone**	**material**	**As**	**Be**	**Co**	**Cr**	**Ni**	**Pb**	**Cu**	**Sn**	**V**	**Zn**	**TOC**
36 A	1.20-1.30	vadose	ssi	0.010	0.000	0.006	0.013	0.015	0.012	0.013	0.001	0.015	0.046	0.800
36 B	1.80-1.90	aquifer	fs	0.003	0.000	0.006	0.010	0.013	0.020	0.012	0.008	0.015	0.041	0.800
38 A	1.60-1.70	vadose	ssi	0.021	0.001	0.006	0.012	0.014	0.012	0.016	0.001	0.020	0.050	0.800
38 B	2.25-2.35	vadose	oc	0.019	0.001	0.010	0.022	0.026	0.019	0.020	0.002	0.029	0.069	20.000
38 C	2.50-3.00	aquifer	fs	0.007	0.001	0.008	0.015	0.018	0.013	0.014	0.003	0.021	0.046	1.700
40 A	1.50-1.60	vadose	c	0.025	0.001	0.009	0.017	0.023	0.019	0.019	0.001	0.021	0.063	0.800
40 B	2.10-2.20	vadose	oc	0.003	0.001	0.010	0.022	0.030	0.018	0.023	0.001	0.025	0.074	6.000
40 C	2.40-2.50	vadose	oc	0.005	0.001	0.009	0.016	0.023	0.014	0.018	0.001	0.020	0.055	0.800
40 D	3.50-3.60	aquifer	fs	0.006	0.000	0.005	0.010	0.013	0.009	0.012	0.001	0.014	0.037	0.800
41 A	1.00-1.10	vadose	si	0.014	0.001	0.009	0.019	0.021	0.019	0.021	0.001	0.025	0.066	3.000
41 B	3.50-3.60	vadose	c	0.012	0.001	0.009	0.015	0.021	0.014	0.018	0.001	0.022	0.052	0.800
41 C	5.10-5.30	aquifer	fs	0.009	0.001	0.008	0.015	0.022	0.013	0.016	0.001	0.019	0.045	3.000
43 A	1.20-1.30	vadose	occ	0.038	0.001	0.011	0.017	0.022	0.020	0.020	0.001	0.023	0.063	0.800
43 B	1.60-1.70	vadose	si	0.003	0.001	0.009	0.016	0.021	0.016	0.021	0.001	0.020	0.064	0.800
43 C	1.90-2.45	aquifer	fs	0.003	0.000	0.006	0.010	0.012	0.011	0.012	0.001	0.013	0.042	0.800
53 A	1.40-1.85	vadose	oc	0.011	0.001	0.010	0.025	0.023	0.028	0.018	0.001	0.033	0.099	26.000
53 B	2.50-3.00	vadose	occ	0.021	0.001	0.011	0.017	0.021	0.022	0.025	0.001	0.023	0.073	4.200
53 C	3.75-5.80	vadose	c	0.016	0.001	0.010	0.018	0.027	0.016	0.019	0.001	0.020	0.058	5.100
53 D	5.80-5.85	aquifer	fs	0.015	0.000	0.005	0.009	0.010	0.009	0.010	0.001	0.012	0.034	0.800
61 A	1.15 - 1.65	vadose	osi	0.016	0.001	0.011	0.019	0.020	0.038	0.020	0.001	0.025	0.077	6.500
61 B	2.74 -3.50	vadose	c	0.006	0.001	0.009	0.016	0.022	0.014	0.018	0.001	0.022	0.055	0.800
61 C	4.15 - 4.60	vadose	ssi	0.008	0.000	0.005	0.009	0.011	0.008	0.010	0.001	0.013	0.032	0.800
61 D	4.60 - 5.40	aquifer	fs	0.008	0.000	0.006	0.010	0.013	0.010	0.011	0.001	0.015	0.039	0.800
64 A	1.40-1.80	vadose	ssi	0.057	0.001	0.010	0.023	0.024	0.021	0.027	0.001	0.030	0.080	1.800
64 B	1.80-2.30	vadose	ssi	0.013	0.001	0.008	0.015	0.018	0.016	0.020	0.001	0.019	0.063	0.800
64 C	2.30-2.85	aquifer	fs	0.005	0.000	0.006	0.009	0.012	0.010	0.011	0.001	0.013	0.041	0.800

				XRF																								
	m b.g.l.			*g/kg*																								
ID_PZP	**depth**	**zone**	**material**	**Si**	**Ti**	**Al**	**Fe**	**Mn**	**Mg**	**Ca**	**Na**	**K**	**P**	**S**	**V**	**Cr**	**Co**	**Ni**	**Cu**	**Zn**	**Rb**	**Sr**	**Y**	**Zr**	**Nb**	**Ba**	**La**	**Ce**	**Nd**	**Pb**
36 A	1.20-1.30	vadose	ssi	189.523	2.528	40.812	20.464	0.481	37.947	126.862	8.481	14.344	0.363	0.208	0.040	0.049	0.007	0.025	0.020	0.052	0.080	0.146	0.021	0.136	0.009	0.264	0.013	0.046	0.000	0.012
36 B	1.80-1.90	aquifer	fs	190.673	2.295	37.240	15.653	0.369	35.715	134.794	8.470	13.468	0.325	0.207	0.035	0.031	0.005	0.027	0.016	0.049	0.078	0.154	0.017	0.125	0.012	0.236	0.021	0.042	0.011	0.020
38 A	1.60-1.70	vadose	ssi	251.601	3.610	47.962	19.419	0.464	34.052	69.383	10.869	17.580	0.557	0.148	0.043	0.055	0.009	0.039	0.026	0.061	0.083	0.095	0.022	0.189	0.006	0.313	0.018	0.052	0.019	0.019
38 B	2.25-2.35	vadose	oc	163.916	2.650	53.076	24.584	0.462	30.987	123.668	5.855	19.234	0.420	2.835	0.067	0.076	0.013	0.044	0.029	0.084	0.121	0.173	0.025	0.125	0.018	0.326	0.026	0.049	0.014	0.020
38 C	2.50-3.00	aquifer	fs	165.558	2.269	40.578	20.138	0.575	32.264	152.855	6.709	14.909	0.387	0.736	0.046	0.053	0.008	0.034	0.022	0.057	0.085	0.199	0.021	0.113	0.011	0.269	0.024	0.047	0.013	0.014
40 A	1.50-1.60	vadose	c	126.134	2.186	51.901	27.030	0.606	26.238	179.172	4.296	17.200	0.269	0.164	0.065	0.055	0.009	0.030	0.034	0.076	0.105	0.213	0.023	0.084	0.007	0.385	0.035	0.049	0.012	0.018
40 B	2.10-2.20	vadose	oc	179.084	3.029	58.360	23.402	0.424	33.355	116.061	6.142	18.795	0.436	0.530	0.075	0.077	0.010	0.043	0.031	0.087	0.114	0.160	0.026	0.143	0.009	0.377	0.024	0.056	0.016	0.022
40 C	2.40-2.50	vadose	oc	132.300	2.240	47.453	26.209	0.556	30.693	173.993	4.652	16.355	0.375	0.191	0.060	0.057	0.010	0.035	0.027	0.070	0.094	0.249	0.023	0.104	0.006	0.322	0.020	0.027	0.014	0.014
40 D	3.50-3.60	aquifer	fs	176.804	2.160	35.479	15.129	0.362	35.357	150.460	7.489	12.432	0.355	1.262	0.035	0.033	0.006	0.015	0.019	0.046	0.067	0.183	0.018	0.116	0.005	0.231	0.012	0.032	0.015	0.006
41 A	1.00-1.10	vadose	si	167.728	2.403	58.496	27.364	0.696	36.623	125.161	6.367	18.974	0.394	0.304	0.067	0.064	0.011	0.034	0.031	0.080	0.116	0.148	0.025	0.107	0.009	0.378	0.028	0.047	0.009	0.023
41 B	3.50-3.60	vadose	c	129.463	2.214	44.102	26.372	0.498	36.368	173.328	4.487	15.123	0.405	0.218	0.058	0.061	0.010	0.036	0.025	0.066	0.087	0.226	0.023	0.101	0.007	0.299	0.030	0.046	0.017	0.012
41 C	5.10-5.30	aquifer	fs	156.200	2.413	42.325	20.934	0.513	35.900	156.831	6.047	14.260	0.382	1.160	0.053	0.057	0.011	0.034	0.027	0.056	0.082	0.219	0.022	0.117	0.008	0.287	0.035	0.034	0.015	0.017
43 A	1.20-1.30	vadose	occ	155.124	2.472	60.720	30.760	0.580	30.071	139.731	6.136	20.872	0.355	0.310	0.067	0.068	0.015	0.032	0.031	0.088	0.125	0.175	0.024	0.115	0.008	0.438	0.035	0.059	0.008	0.025
43 B	1.60-1.70	vadose	si	204.124	3.008	54.465	21.952	0.383	33.750	105.250	8.620	19.215	0.492	0.238	0.056	0.065	0.010	0.029	0.025	0.073	0.111	0.145	0.025	0.167	0.014	0.358	0.029	0.058	0.014	0.016
43 C	1.90-2.45	aquifer	fs	206.857	2.898	50.196	19.220	0.381	35.438	108.551	8.885	17.617	0.451	0.245	0.048	0.054	0.009	0.024	0.017	0.063	0.110	0.136	0.022	0.141	0.022	0.320	0.021	0.057	0.014	0.015
53 A	1.40-1.85	vadose	oc	274.200	4.795	88.371	29.812	0.351	10.108	8.286	9.903	28.059	0.282	0.363	0.093	0.094	0.017	0.036	0.025	0.119	0.181	0.090	0.034	0.215	0.011	0.557	0.048	0.088	0.019	0.039
53 B	2.50-3.00	vadose	occ	156.263	2.483	61.535	30.787	0.583	30.302	140.191	5.988	20.901	0.356	0.290	0.068	0.067	0.015	0.032	0.032	0.088	0.123	0.176	0.025	0.114	0.009	0.441	0.025	0.059	0.016	0.026
53 C	3.75-5.80	vadose	c	120.620	2.060	47.406	22.178	0.594	27.691	192.172	4.050	16.386	0.332	1.703	0.063	0.067	0.011	0.044	0.027	0.073	0.097	0.291	0.022	0.080	0.008	0.350	0.031	0.033	0.013	0.014
53 D	5.80-5.85	aquifer	fs	185.819	2.369	35.395	14.303	0.366	38.571	142.011	8.464	12.579	0.323	2.788	0.031	0.040	0.008	0.021	0.017	0.043	0.068	0.168	0.017	0.118	0.008	0.228	0.021	0.036	0.010	0.012
61 A	1.15 - 1.65	vadose	osi	316.972	4.315	73.377	30.255	0.572	8.518	6.885	12.193	22.600	0.343	0.106	0.070	0.075	0.015	0.034	0.028	0.091	0.134	0.082	0.029	0.214	0.011	0.472	0.039	0.071	0.022	0.046
61 B	2.74 -3.50	vadose	c	136.014	2.202	46.281	26.585	0.558	29.391	176.308	4.998	16.143	0.376	0.301	0.058	0.063	0.012	0.033	0.027	0.069	0.092	0.237	0.023	0.108	0.007	0.321	0.030	0.049	0.014	0.013
61 C	4.15 - 4.60	vadose	ssi	189.244	2.231	33.320	13.460	0.366	35.667	146.084	8.224	11.397	0.323	1.715	0.028	0.039	0.007	0.019	0.018	0.042	0.072	0.178	0.016	0.115	0.019	0.210	0.016	0.031	0.012	0.010
61 D	4.60 - 5.40	aquifer	fs	189.547	2.296	37.431	18.253	0.481	32.918	136.755	8.177	13.080	0.362	1.391	0.035	0.049	0.009	0.022	0.019	0.053	0.074	0.178	0.018	0.120	0.009	0.259	0.033	0.042	0.017	0.013
64 A	1.40-1.80	vadose	ssi	263.030	3.428	68.984	35.021	0.607	13.649	49.982	10.320	21.274	0.452	0.310	0.068	0.071	0.013	0.036	0.040	0.097	0.125	0.097	0.030	0.166	0.007	0.435	0.037	0.072	0.018	0.027
64 B	1.80-2.30	vadose	ssi	207.496	3.001	59.051	29.904	0.566	25.869	99.298	8.549	19.894	0.460	0.234	0.060	0.066	0.011	0.029	0.031	0.081	0.121	0.130	0.027	0.168	0.017	0.398	0.025	0.055	0.014	0.023
64 C	2.30-2.85	aquifer	fs	210.359	2.459	39.105	16.762	0.380	32.289	120.602	9.093	14.418	0.335	0.133	0.036	0.046	0.007	0.023	0.016	0.055	0.074	0.145	0.019	0.133	0.003	0.249	0.021	0.045	0.018	0.014

Table S3

Geochemical reactions	Reference	Log(K) at 25°C
Phases		
$CH_2O + H_2O = CO_2 + 4H^+ + 4e^-$	(Appelo & Postma, 2005)	4.80
$FeAsS + 3.25O_2 + 1.5H_2O = Fe^{2+} + SO_4^{2-} + H_3AsO_4$	(modified from Craw et al., 2002)	198.17
$FeOO_2H_3 + 3H^+ = Fe^{3+} + 3H_2O$	(Appelo & Postma, 2005)	2.00
$CO_2 = CO_2$	(Ball & Nordstrom, 1991)	-1.47
$CaCO_3 = Ca^{2+} + CO_3^{2-}$	(Ball & Nordstrom, 1991)	-8.48
Ion exchange		
$X^- = X^-$	(Appelo & Postma, 2005)	0.00
Surface complexation	(All from Dzomback & Morel, 1990)	
Strong binding sites - Hfo_s		
Hfo_sOH = Hfo_sOH		0.00
$Hfo\_sOH + H^+ = Hfo\_sOH_2^+$		7.29
$Hfo\_sOH = Hfo\_sO^- + H^+$		-8.93
Weak binding sites -Hfo_w		
Hfo_wOH = Hfo_wOH		0.00
$Hfo\_wOH + H^+ = Hfo\_wOH_2^+$		7.29
$Hfo\_wOH = Hfo\_wO^- + H^+$		-8.93

Figure S4

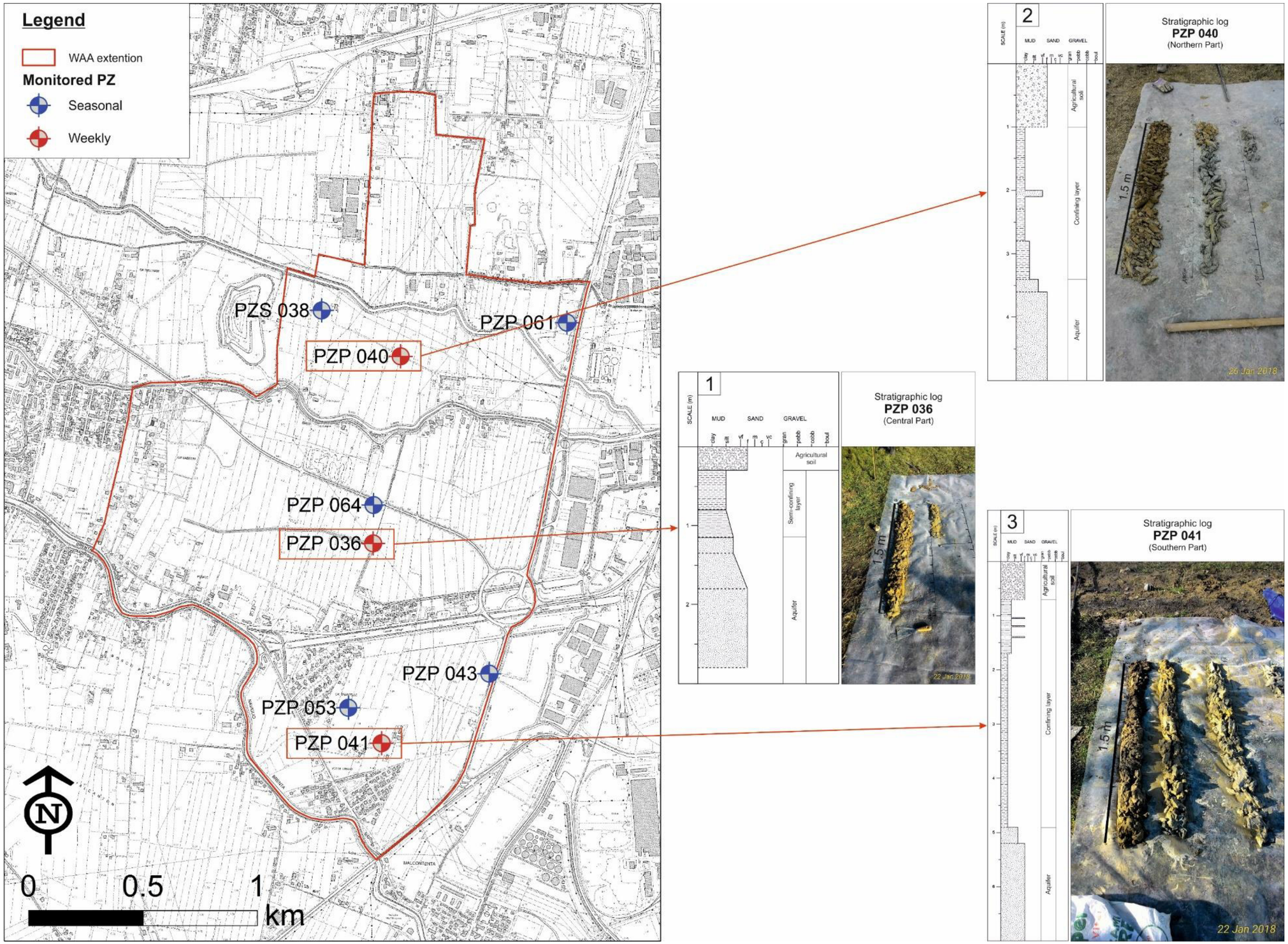
Legend
WAA extention
Monitored PZ
Seasonal
Weekly
PZS 038
PZP 061
PZP 040
PZP 064
PZP 036
PZP 043
PZP 053
PZP 041
N
0
0.5
1
km
1
SCALE (m)
MUD
SAND
GRAVEL
clay
silt
vf
f
m
c
vc
gran
pebb
cobb
boul
Agricultural soil
Semi-confining layer
Aquifer
Stratigraphic log
PZP 036
(Central Part)
1.5 m
22 Jan 2018
2
Confining layer
Stratigraphic log
PZP 040
(Northern Part)
3
Stratigraphic log
PZP 041
(Southern Part)

Figure S5

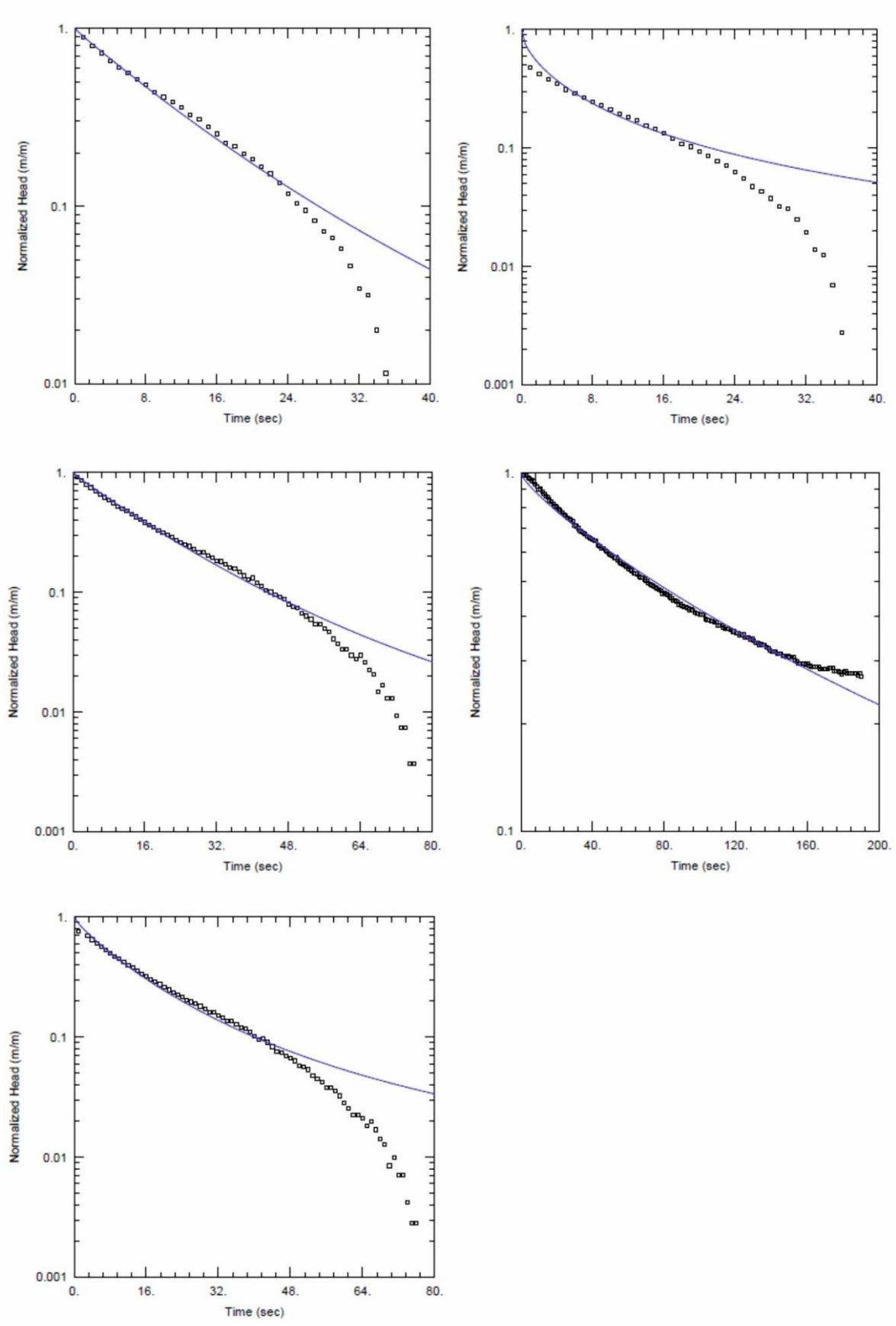
Normalized Head (m/m)
Time (sec)
1.
0.1
0.01
0.001
0.
8.
16.
24.
32.
40.
48.
64.
80.
120.
160.
200.

Figure S6

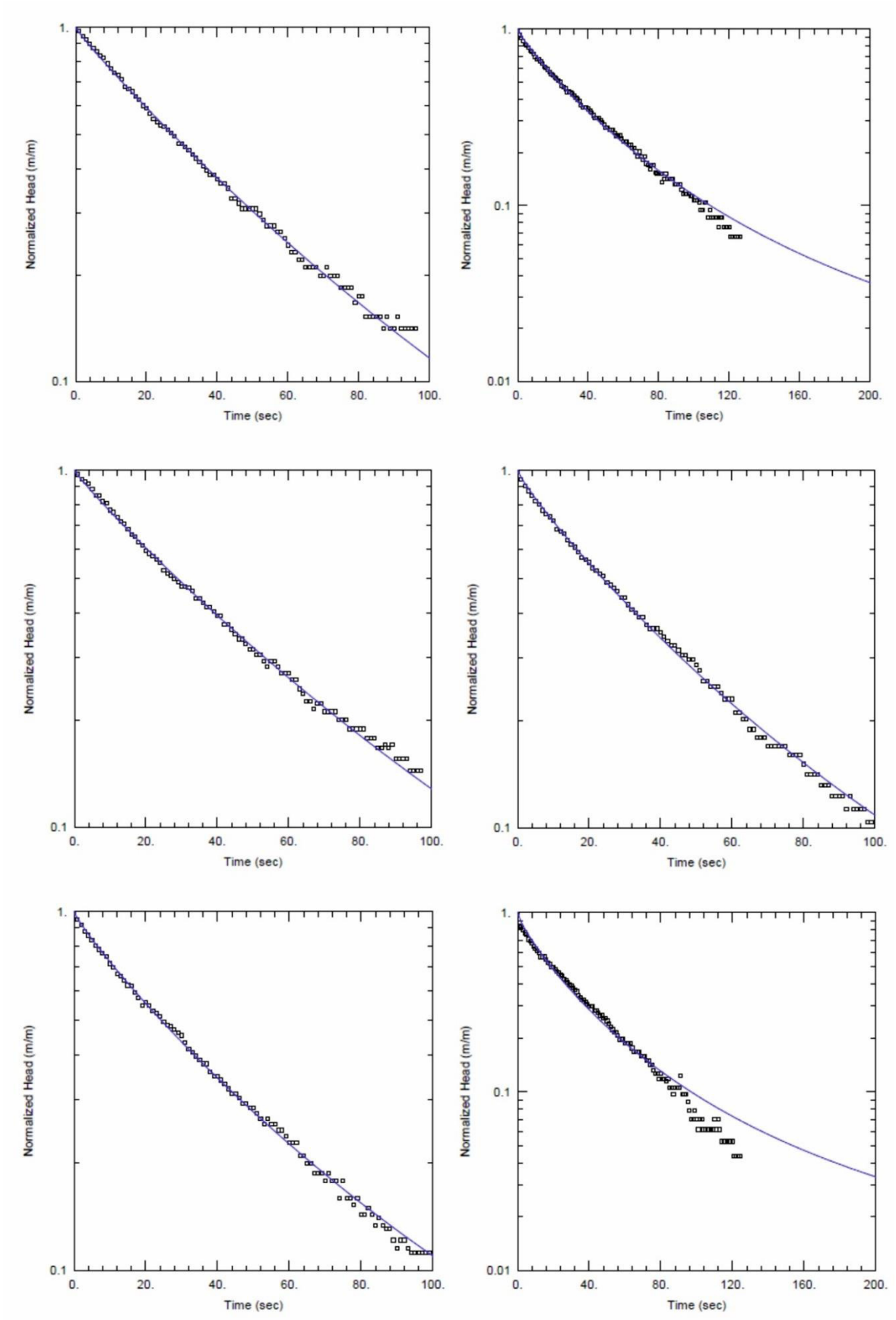
Normalized Head (m/m)
Time (sec)
1.
0.1
0.01
0.
20.
40.
60.
80.
100.
120.
160.
200.

Figure S7

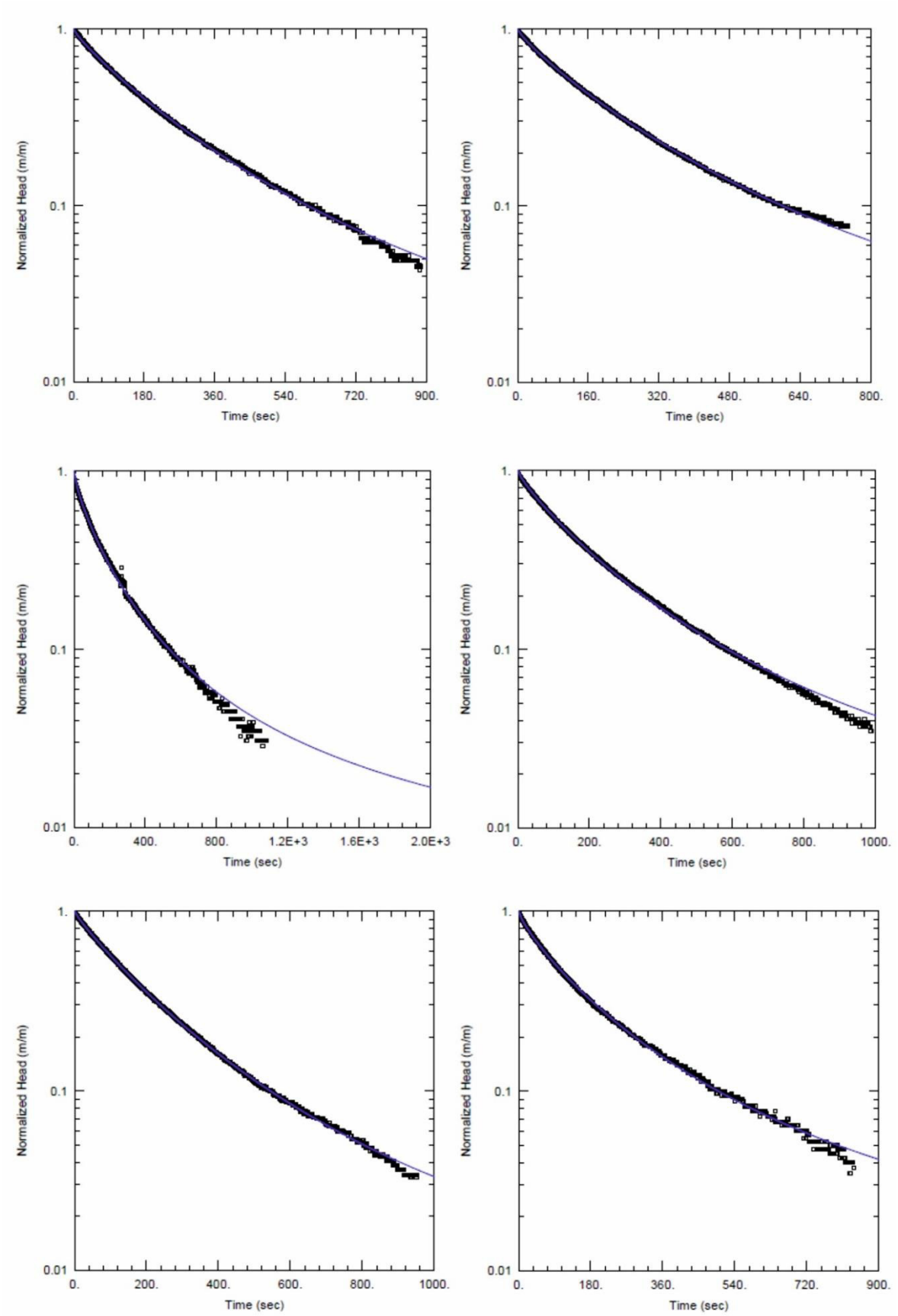
Normalized Head (m/m)
Time (sec)
1.
0.1
0.01
0.
180.
360.
540.
720.
900.
160.
320.
480.
640.
800.
400.
800.
1.2E+3
1.6E+3
2.0E+3
200.
400.
600.
800.
1000.

Figure S8

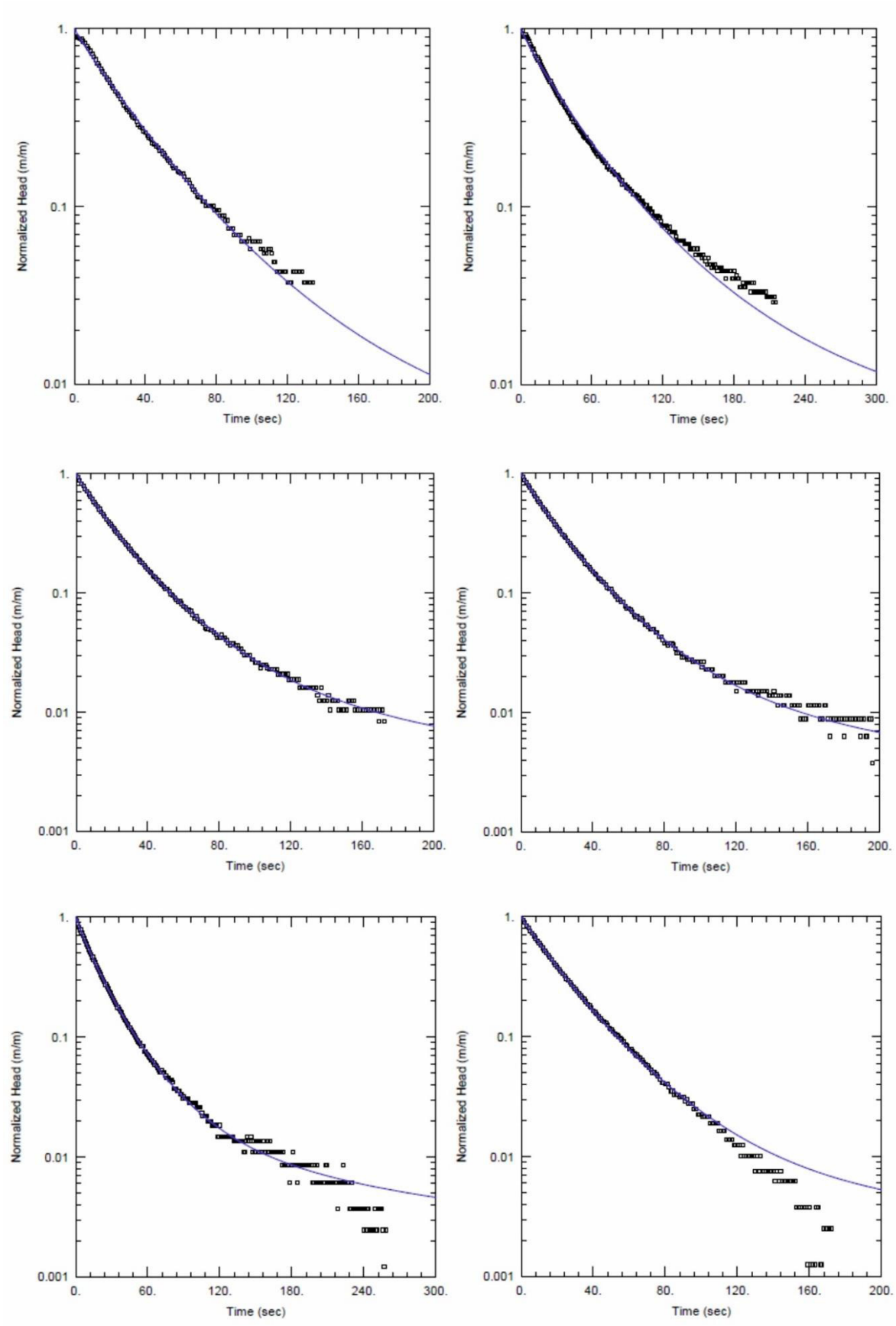
Normalized Head (m/m)
Time (sec)
1.
0.1
0.01
0.001
0.
40.
60.
80.
120.
160.
180.
200.
240.
300.

Figure S9

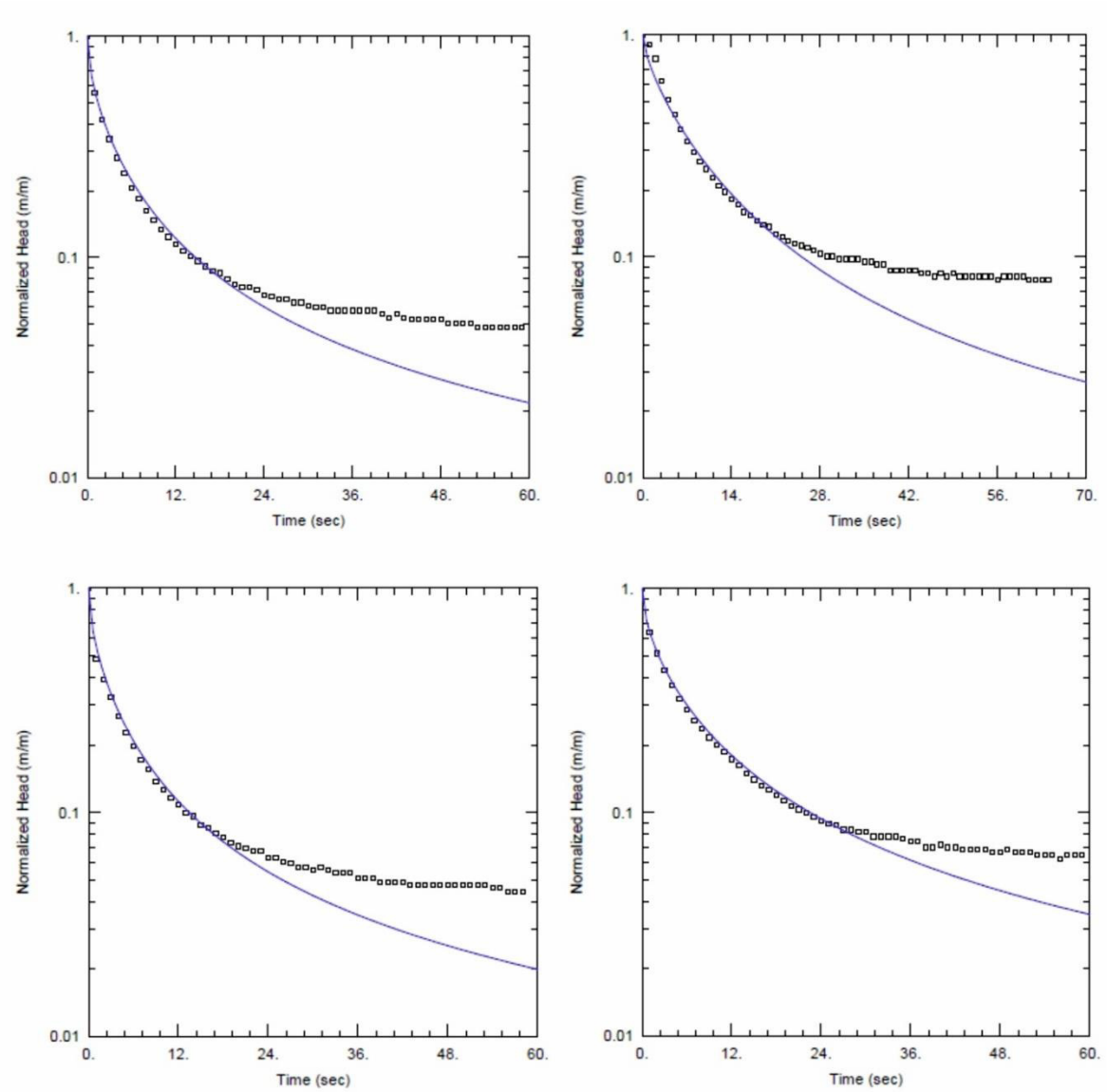
Normalized Head (m/m)
1.
0.1
0.01
0.
12.
24.
36.
48.
60.
Time (sec)
Normalized Head (m/m)
1.
0.1
0.01
0.
14.
28.
42.
56.
70.
Time (sec)
Normalized Head (m/m)
1.
0.1
0.01
0.
12.
24.
36.
48.
60.
Time (sec)
Normalized Head (m/m)
1.
0.1
0.01
0.
12.
24.
36.
48.
60.
Time (sec)

Figure S10

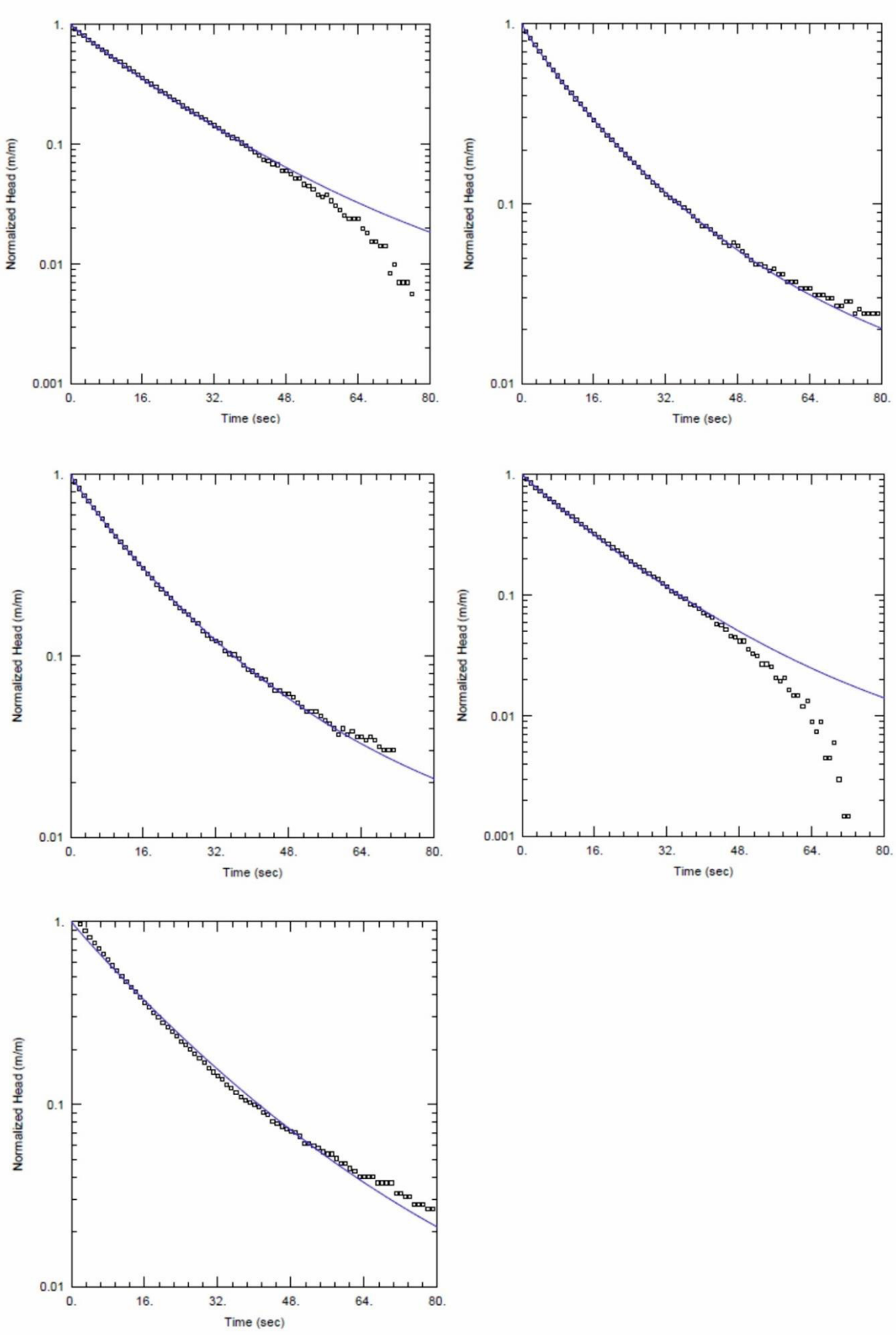

Figure S11

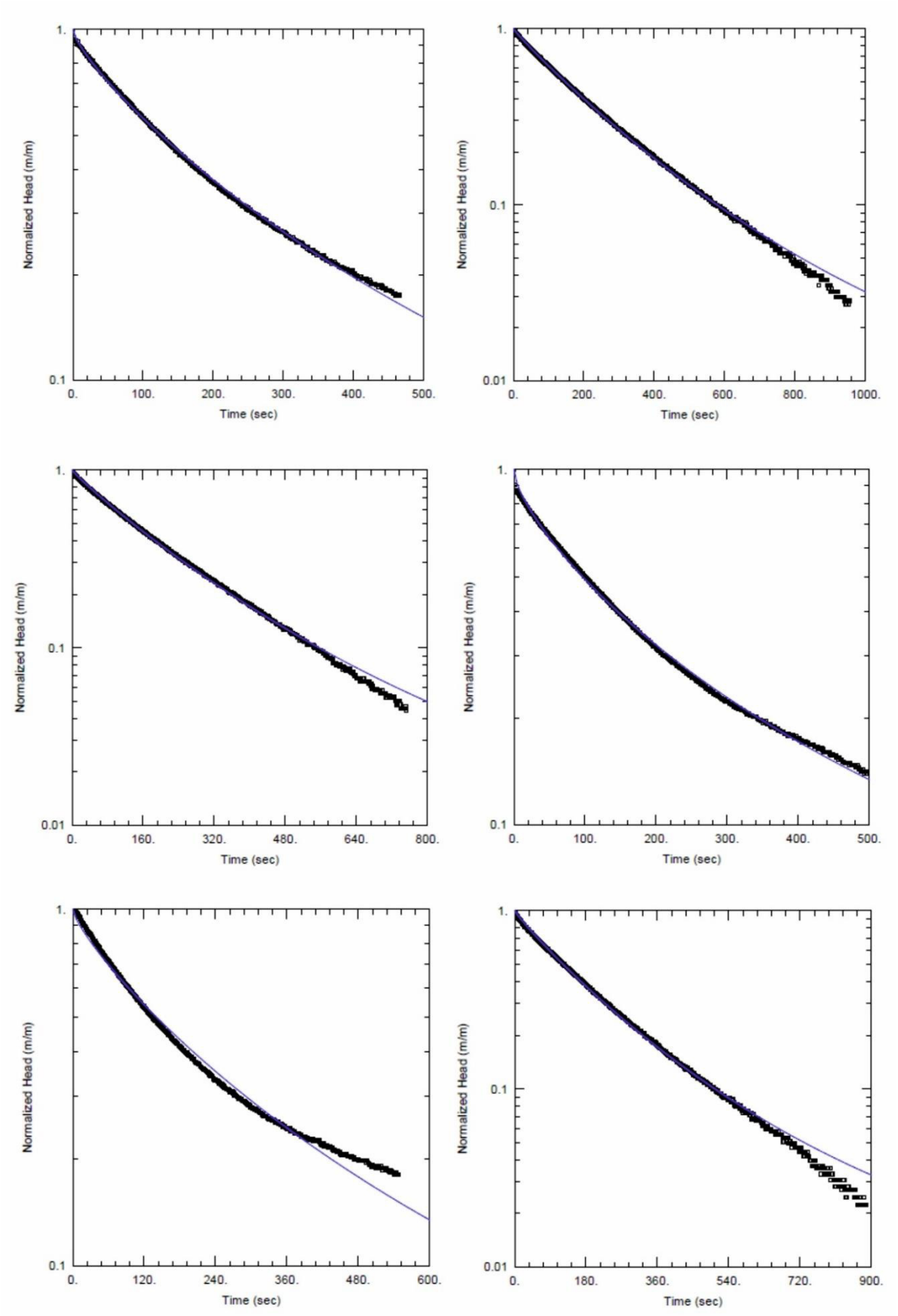
Normalized Head (m/m)
Time (sec)
1.
0.1
0.01
0.
100.
200.
300.
400.
500.
600.
800.
900.
1000.
120.
160.
180.
240.
320.
360.
480.
540.
640.
720.

Figure S12

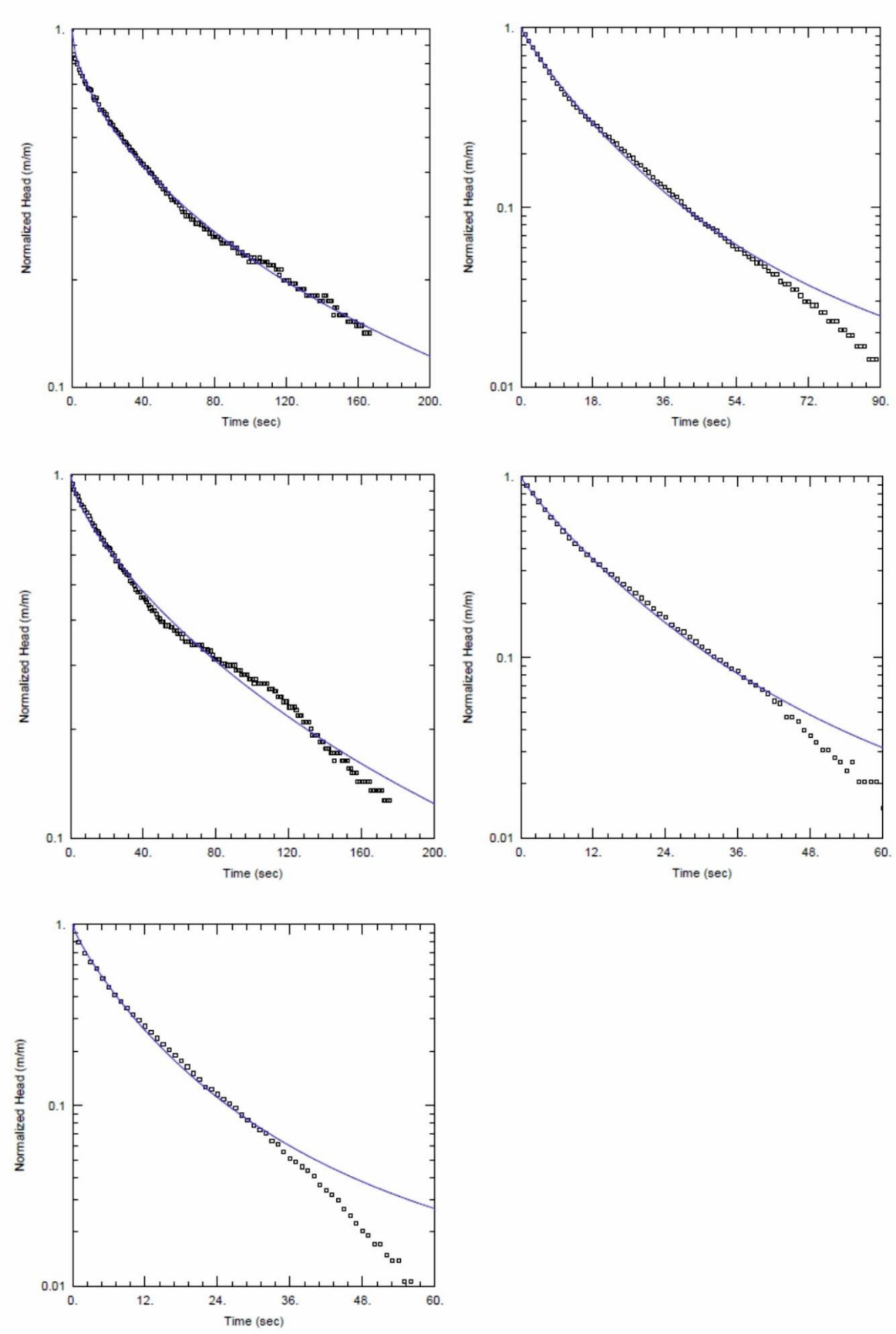
Normalized Head (m/m)
Time (sec)
1.
0.1
0.01
0.
40.
80.
120.
160.
200.
18.
36.
54.
72.
90.
12.
24.
48.
60.